PROTON DONOR AND MEDIUM EFFECTS IN ELECTROCHEMICAL PROTON DISCHARGE

by

DAVID P WILKINSON

A Thesis Submitted in Partial Fulfillment of
the Requirements for the Degree of
Doctor of Philosophy
in the
Department of Chemistry
University of Ottawa
Ottawa, Canada
September 1986

B.E. Conway
Professor of Chemistry
Research Supervisor

David P Wilkinson
Ph.D Candidate

PREFACE

Historically, the electrochemical hydrogen evolution reaction (h.e.r.) has been taken as a model in the treatment of double-layer effects and for the kinetic study of simple and other complex multistep electrode reactions. While the h.e.r has lost some of its predominance in electrode kinetics since the development of new techniques and instrumentation which allow the study of faster but simpler ionic redox reactions, it nevertheless remains a reaction of fundamental importance for the study of coupled atom/electron transfer reactions Also, in recent years, the practical study of the h.e.r. has become of major technical importance in energy related fields.

Despite much work which has been published on certain aspects of the h.e.r. kinetics, such as elucidation of the rate-controlling steps and relation to metal properties, the mechanism and molecular mechanics of the initial electrochemical proton discharge step is still not understood well. The experimentally determined Tafel slope, b, which characterizes the effect of potential on electrochemical reaction rates and is a quantity central to the understanding of the molecular mechanism of activation, is rarely represented correctly as a function of temperature, T, by the commonly assumed relation, $b=2.3RT/\alpha F$. Current treatments of the activation process (cf. Dogonadze, Kuznetsov and Levich treatment) do not take into account these deviations of

electrochemical kinetic behaviour from that expected conventionally These treatments neglect specific solvational and solvent structure aspects of the activation process but emphasize long range outer-shell reorganization in the system. While such treatments may be applicable to ionic redox reactions, where a state of solvation is maintained in the electron transfer process, and no atom transfer and complete charge elimination is involved, they are certainly less applicable to atom/electron transfer reactions where the ionic charge is extinguished in the electrode reaction, and the corresponding solvation of the initial state is eliminated.

At Hg, the electrochemical proton discharge step is generally accepted as being rate-determining so that evaluation of the kinetics of the overall h.e.r. at this metal gives information on the initial proton discharge step. In the present work, the kinetics of the h.e.r. at Hg from a selection of proton sources in various solvent media was investigated over a wide range of temperatures. This study provides a basis for characterizing the unconventional temperature-dependence of the Tafel slope and transfer coefficient or symmetry factor, and leads to a better understanding of the nature of the activation process in the elementary act of complex electron and atom transfer. Also, the work leads to valuable practical information on the h.e.r. in nonaqueous solvent media, e.g. factors which lead to optimization in kinetic parameters which determine the rates of the H_2 evolution reaction under various

conditions.

Most of the work described in this Thesis has been submitted for publication or is in preparation as follows:

1) Comparison of "True" Kinetic Parameters for H_2 Evolution from Various Proton Donors in Water, Acetonitrile and N,N - Dimethylformamide, D.P. Wilkinson, Energy Research Summer Fellowship Report, J. Electrochem. Soc., 132, 479C (1985).

2) Experimental Evidence for the Potential-Dependence of Entropy of Activation in Electrochemical Reactions in Relation to the Temperature-Dependence of Tafel Slopes, B.E. Conway, D.F. Tessier and D.P. Wilkinson, J. Electroanal. Chem., 199(2), 249 (1986).

3) Kinetic Behaviour of Electrochemical Proton Discharge in Relation to the Proton Source and its Environment, B.E. Conway, D.F. Tessier and D.P. Wilkinson, J. Electroanal. Chem., 204(1-2), 111 (1986).

4) Conditions Enabling Determination of Entropy and Enthalpy of Activation of Electrode Reactions at Zero Metal-Solution Potential Difference, B.E. Conway and D.P. Wilkinson, J. Electroanal. Chem., 201(1), 167 (1986).

5) Electrocatalysis in the H_2 Evolution Reaction, B.E. Conway, L. Bai, D.F. Tessier and D. Wilkinson, Extended Abstract No. 636, Electrochemical Society Symposium, Toronto, May 12-17, 1985.

6) Proton Donor and Medium Effects on Potential-Dependence of Entropy of Activation in Proton Discharge, B.E. Conway and D.P. Wilkinson, Extended Abstract No. 511, Electrochemical Society Symposium, Boston, May 4-9, 1986.

7) Potential Dependence of the Entropy Component of the Free-Energy of Activation in Linear Free-Energy Relations for Electrode Processes, B.E. Conway, D.F. Tessier and D.P. Wilkinson, Chem. Phys. Lett., 125(5-6), 589 (1986).

8) Entropic and Enthalpic Components of the Symmetry Factor for Electrochemical Proton Transfer From Various Proton Donors Over a Wide Temperature Range, B.E. Conway and D.P. Wilkinson, J. Electroanal. Chem., 214(1), 633 (1986).

9) Effects of Potential, External and Internal to the Metal, on Electrochemical Reaction Rates, B.E. Conway and D.P. Wilkinson, J. Chem. Phys., 85(7), 4197 (1986).

10) Evaluation of Entropies of the H^+/H_2, AgCl/Ag and Ag^+/Ag Reactions in Various Solvents by Thermocell EMF Measurements, B.E. Conway and D.P. Wilkinson, in preparation.

11) Brønsted Relations for Heterogeneous Proton Transfer at Electrode Interfaces, B.E. Conway and D.P. Wilkinson, in preparation.

ACKNOWLEDGEMENTS

I wish to express my gratitude to Professor B.E. Conway for his help and guidance during this work.

I also wish to thank my colleagues for their support and discussions, especially David Harrington, David Tessier and Jan Wojtowicz who were very helpful and always prepared to give freely of their time.

Also, sincere thanks to the members of the support staff who were most helpful on many occasions.

Grateful acknowledgement is made to the University of Ottawa, the province of Ontario and the Natural Sciences and Engineering Research Council Canada for post-graduate scholarships and to the Electrochemical Society for the Energy Research Summer Fellowship.

I am grateful for the support and interest given by Dr. G. Ballard, P. Howard and Dr. K. Prater of Ballard Research Incorporated.

I wish to thank my parents for their continued guidance and encouragement.

Finally, I am indebted to my wife Susan for her unfailing support and inspiration throughout this endeavour.

TABLE OF CONTENTS

CHAPTER 2

Page No.

Page No

CHAPTER 5

RESULTS AND DISCUSSION

Page No.

Page No.

LIST OF FIGURES

Figure | Page No

Figure | Page No

Figure | Page No.

Figure — Page No

Figure — Page No

LIST OF TABLES

ABSTRACT

The theory of charge transfer in electrode kinetics, especially for coupled atom/electron transfer processes such as the hydrogen evolution reaction, is still not well understood, particularly with respect to the temperature dependence of the kinetics and the nature of the effects of potential on the energy and entropy of activation.

By means of steady-state polarization measurements the kinetics of the hydrogen evolution reaction at Hg from several proton sources (H_3O^+, ROH_2^+, $DMFH^+$, $EtNH_3^+$, Et_3NH^+, H_2O, CH_3COOH, CF_3COOH) in aqueous and nonaqueous media (CH_3OH, 1 propanol, 2-propanol, isobutanol, $HCONH_2$, DMF and AN) were investigated over a wide range of temperature. In all cases proton discharge was from well defined states and was the rate-controlling step at Hg at which coverage by the H intermediate is negligible (<0.03%). Kinetic activation parameters were determined at a constant metal-solution potential rather than at constant overpotential (giving only the apparent activation parameters), by means of isothermal and non-isothermal reference electrode cell measurements which allowed corrections to be made for variation of the reference electrode potential with temperature and solution composition.

Comparison of these chemically significant activation parameters allows medium and proton source effects to be distinguished in the activation process Current theories

about electron and proton transfer in the electrochemical hydrogen evolution reaction place little emphasis on the specific nature of the solvated proton source in solution but only emphasize long-range fluctuations in solvent dielectric polarization in the activation process. However, the present results indicate that specific as well as general medium effects have to be included in any interpretation of the mechanism of proton discharge, and probably in other electrode processes too. Also, a linear free energy relationship, i.e., Brønsted relation, between the rate of electrochemical proton transfer and the acid/base strength of proton donors in several solvents in clearly demonstrated in the present work, indicating the importance of specific bond effects in the activation process.

It is shown that the entropy of activation or the corresponding frequency factor for proton discharge is substantially dependent on electrode potential and not constant as usually assumed. These results show that the effect of electrode potential on electrochemical rates for a simple discharge process must now be considered as a combination of two effects: i) an "inner" effect on the Fermi level of electrons in the metal relative to their energy in vacuum, and ii) an "outer" effect on the solvent structure and state of reactant ion and solvated transition state in the double-layer at the electrode interphase. Previous theories of electron and atom transfer at electrodes have not treated this important

entropy effect, but have been concerned mainly with quantal and solvation reorganization aspects of the energy of activation with little reference to the structural aspects of the process in the interphase.

Consideration of the effect of electrode potential on both the enthalpy and entropy of activation results in a symmetry factor of the form, $\beta = \beta_H + T\beta_S$ where β_H and $T\beta_S$ are the enthalpic and entropic components of the overall symmetry factor β. Contrary to conventional assumptions, the Tafel slope b is not given by the usual relation $b = \pm 2.3RT/\beta F$ but rather by $b = \pm 2\ 3RT/(\beta_H + T\beta_S)F$ which can now account for the often observed "anomalous" temperature dependence of the Tafel slope.

A variety of behaviour is found from cases where β is dominated by the β_H term giving rise to conventional behaviour of b as a f(T), to cases where β is determined mainly by the $T\beta_S$ term, giving b almost independent of T. An important compensation effect between values of β_H and $T\beta_S$ is demonstrated that makes β approximately constant and near 0.5 at 298 K, even though β_H and $T\beta_S$ vary considerably The enthalpy and entropy of activation also vary together in a systematic and compensatory way.

CHAPTER 1

INTRODUCTION

A. Theories of Proton and Electron Transfer in the Hydrogen Evolution Reaction

1. Introduction

The electrochemical hydrogen evolution reaction (h.e.r) is a prototype electrochemical atom transfer reaction which has often been used as a basis for the discussion of the kinetic treatment of more complex multistep electrode reactions (1,2) The mechanism of proton transfer at electrodes is still controversial but is fundamental to the understanding of the elementary process in the cathodic h.e.r. and is related to homogeneous acid-base proton transfer processes (3,4,5). In the case of electrochemical proton transfer, there is a coupled electron and H-particle transfer with neutralization of the proton charge and elimination of the proton's solvation. Other examples of electron charge-transfer processes at electrodes that also involve a coupled transfer of a neutralized atom are the anodic evolution of halogens and metal deposition reactions While the same general principles apply both to bond-breaking/forming charge-transfer processes and to ionic redox reactions, an important distinction can be made in the latter case, since both the initial and final states of the electron transfer reaction are solvated or ligand-complexed ions, i e , the state of solvation or ligand shell interaction is maintained or only

somewhat modified in the electron transfer process while in atom transfer processes the state of solvation and ionic charge is eliminated in the electrode reaction.

The "electrochemical proton transfer step with chemisorption" is represented by

$$H_3O^+ \text{ (or } H_2O) + \underset{1-\theta_H}{M} + e \rightarrow \underset{\theta_H}{M\text{-}H_{ads}} + H_2O \text{ (or } OH^-) \qquad [1]$$

and is a necessary primary step in the h.e.r. but is usually followed by an "electrochemical desorption" process

$$\underset{\theta_H}{M\text{-}H_{ads}} + H_3O^+ \text{ (or } H_2O) + M + e \rightarrow \underset{1-\theta_H}{M} + H_2O \text{ (or } OH^-) + H_2 \qquad [2]$$

or an "heterogeneous chemical recombination desorption" process

$$\underset{\theta_H}{M\text{-}H_{ads}} + \underset{\theta_H}{M\text{-}H_{ads}} \rightarrow \underset{1-\theta_H}{2M} + H_2 \qquad [3]$$

where θ_H is the fraction of the metal surface covered by adsorbed H and $1-\theta_H$ is the corresponding fraction of unoccupied metal (M) sites. H_{ads} is a state of chemisorbed H, the energy of which is usually dependent on coverage and the nature of the metal M. At Hg, almost all authors, with the exception of Horiuti (6), agree that proton discharge is the rate-controlling step, i.e., eqn.[1], and consequently coverage by the H intermediate is negligible ($\theta_H < 0.03\%$) so that evaluation of the kinetics of the overall h.e.r. at this metal gives information on the rate constant of the proton discharge step.

The temperature and potential dependence of H adsorption can be approximated by an electrochemical Langmuir isotherm (7) or a

Temkin isotherm (8) for metals where H adsorption is important Depending on the particular electrode metal used, the rate of the h.e.r. (characterized, e.g., by the exchange current density, i_o) can vary over about ten orders of magnitude. Since the electrochemical free energy of activation, $\Delta\bar{G}^{\ddagger}_{\phi}$, at electrode potential ϕ is independent of the metal work function, Φ_m, the observed correlation between the rate (expressed as i_o) of the h.e.r. and Φ_m (9, 10) must arise mainly from an indirect effect on the heat of adsorption of H. Another indirect but usually weak effect of Φ_m on the rate of the h.e.r. may occur through a shift of the potential of zero charge and the associated change in the structure of the electrode double-layer. The formation of solvated electrons in relation to Φ_m and their role as a reaction intermediate in the h.e.r. has been considered (11, 12), but Conway and MacKinnon (13) have shown that the solvated electron is unlikely to be important under ordinary polarization conditions. Much work has been published on the characterization of the kinetics of electrochemical reactions with regard to elucidation of rate-controlling steps and relation to metal properties, and can be found in most electrochemical monographs.

2. Representations of Rates of Electrode Processes

The empirical equation due to Tafel (14), which represents the potential dependence of electrochemical reaction rates according to

$$\eta = a + b \log i \qquad [4]$$

(where i is the current density, b is the Tafel slope, a is a

constant and η is the overpotential defined as the difference between the applied electrode potential V and the corresponding reversible potential V_R when the electrode process is at equilibrium, i.e., $\eta = V-V_R$) has provided the basis for empirical and theoretical treatments of electrochemical reaction rates.

At equilibrium, i.e., $\eta = 0$, both the forward and backward current components of the electrode reaction are equal to each other, i.e. $\vec{i} = \overleftarrow{i} = i_o$ (the equilibrium exchange-current density), so that there is no net current across the metal solution interface. This leads to an alternative form of the Tafel equation, written exponentially as

$$i = i_o \exp [2.3\eta/b] \qquad [5]$$

so that $a = -b \log i_o$ in eqn.[4].

The first attempts at deriving a theoretical rate equation for a heterogeneous electrochemical process involving only electron transfer were given by Gurney (15) and Gurney and Fowler (16). Up to Gurney's time the phenomenon of overpotential was often associated with generation of a gaseous film or a layer of oriented solvent dipoles (17). Gurney's pioneer paper (15) was an attempt to rationalize experimental results obtained for the h.e.r. by Bowden (18) in cases where the electron transfer step is rate-determining, by recognizing the essential quantum-mechanical aspects of electron transfer at electrodes.

Radiationless quantum-mechanical tunneling of an electron through a potential-energy barrier can occur only if the energy of the electron to be transferred from (or to) the metal is equal

to the energy of the lowest unoccupied (or highest occupied) electronic level (orbital) of the reactant ion. Gurney's models for electron transfer from a metal to an ion in vacuum and to an ion in solution are shown in Figs. 1a and 1b, respectively. For these cases Gurney assumed that there is no interaction of either the ion or atom with the metal or the atom with the solvent. The effect of applied potential is to change the Fermi level of the electrons in the metal ($\Phi_V = \Phi_{V=0} \pm eV$) so as to bring the energy levels on both sides of the barrier to equal values so that radiationless tunneling can proceed with maximum probability. The basic condition for electron-tunneling in vacuum, e.g., from an H atom to the metal, is given by

$$\Phi \pm eV \leq I \qquad [6]$$

where I is the ionization energy of the H atom and $\Phi \pm eV$ is the energy of the Fermi level as modified by applied potential. In solution a loss of electrostatic solvation energy, L, upon neutralization causes an increase in potential energy of the final state so that the electron-tunneling condition in solution is given by

$$\Phi \pm eV \leq I + L \qquad [7]$$

The electron transfer rate was calculated in terms of the integral of the product of probabilities of electron states in the metal according to Fermi Dirac statistics and acceptor states of the reacting ion according to a Boltzmann distribution of rotation-vibration levels (in the case of a molecular reactant) Later Gurney took into account the solvent-atom interaction,

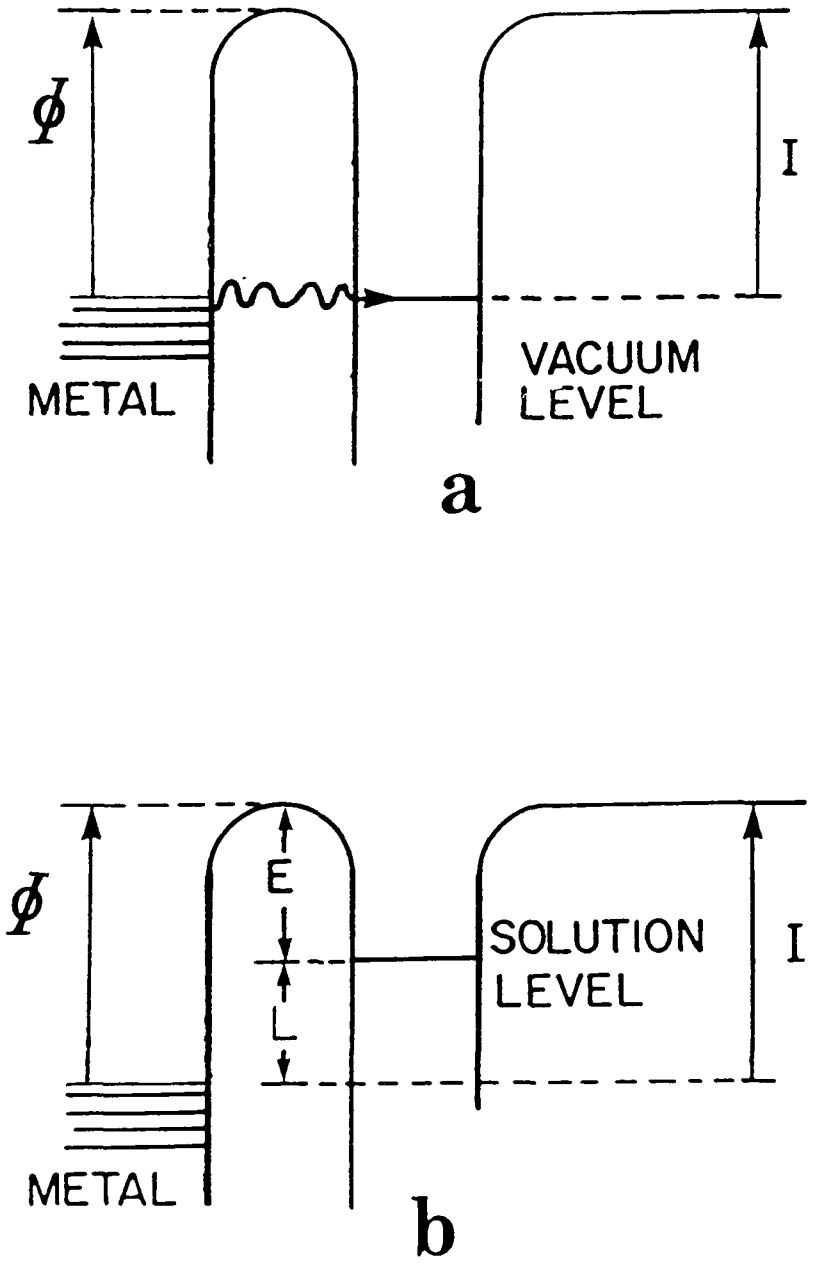

Fig. 1 Models for ion neutralization at an electrode surface according to Gurney (ref. 15) : a) ion in vacuum, b) ion in solution.

i.e., the repulsive energy, R, so that the electron-tunneling condition is then given by

$$\Phi \pm eV \leq I + L \quad R \qquad [8]$$

as shown schematically in Fig 2. Curve ABC represents the potential energy of the H/H_20 repulsion interaction and curve DEFG the potential energy of the H^+/H_20 solvation interaction. It is seen that when the solvation energy, L, increases (from EF to DG) the repulsion, R, decreases (from B to C), so that the change in L-R is greater than the change in L. In the absence of definite information concerning the dependence of R and L on internuclear separation, Gurney used the empirical relation $dL = \beta d(L-R)$ where $0< \beta <1$, and β depends on the value of relative slopes of the curves FG and BC which is taken as a constant for the energy range under consideration. Gurney omitted the work function, Φ, of the metal, probably because it is invariant with respect to nuclear separation, but inclusion of it by Butler (19) who replotted Gurney's graphical representation raises the curve ABC yielding the familiar representation of intersecting initial and final state energy curves.

While Gurney's theory gave a correct qualitative account of the potential-dependence of the rates of reaction, (i.e , it resulted in an equation of the form of the empirical Tafel relation), it predicted activation energies that were much larger than those observed experimentally This was a result of assuming the final state of H atom as free in solution near the metal surface rather than adsorbed on the metal, an aspect

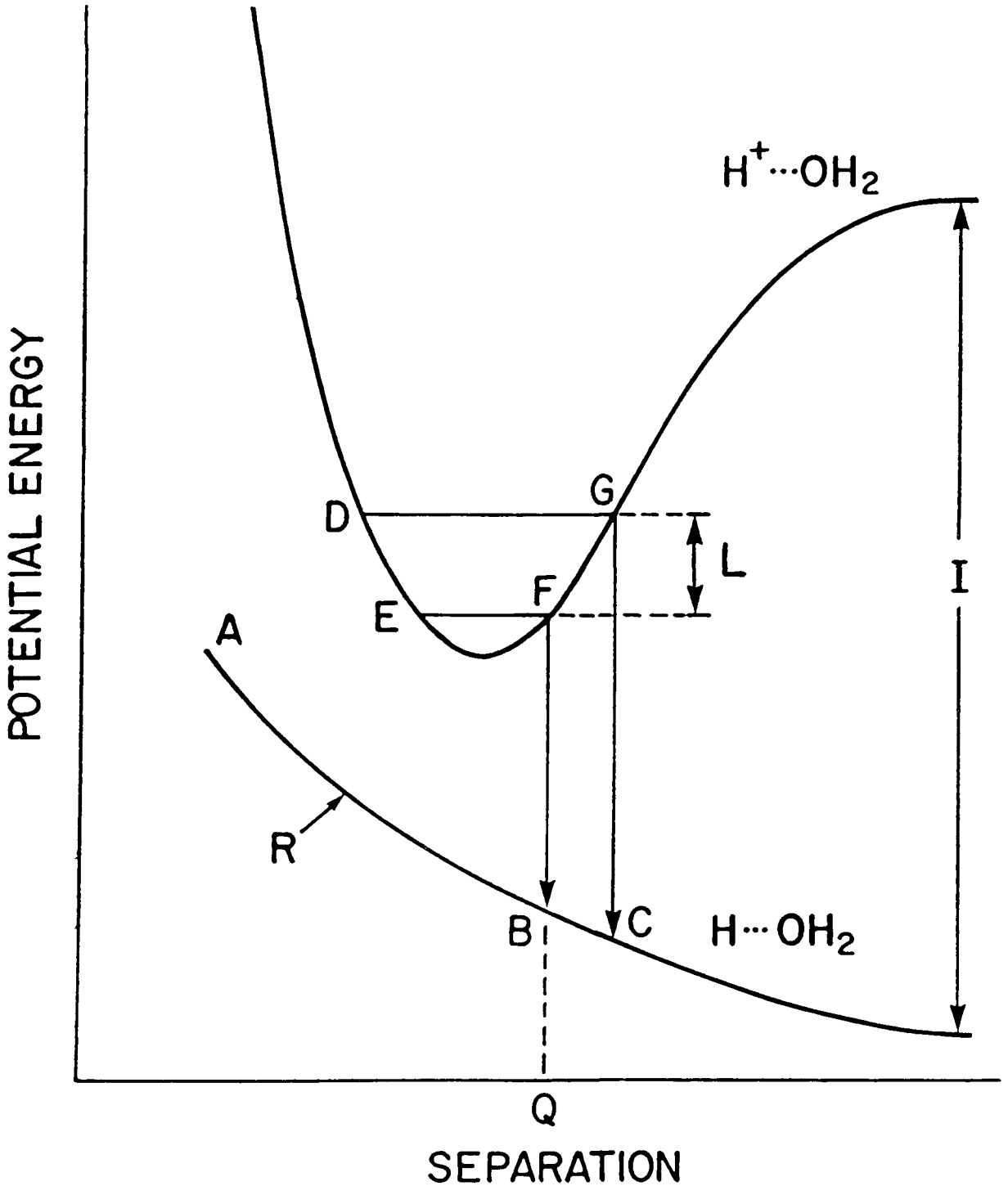

Fig. 2 Gurney model for proton transfer according to Butler (ref 19)

treated by Butler. Also, the symmetry factor β has its essential origin with the theory of Gurney and although implicit, it is the coefficient relating the energy difference in the metal and in the H atom at the electrode-solution interface to the thermal energy required by the ion in order to fulfill the electron-tunneling condition given by eqn.[8].

At about the same time as Gurney's seminal paper, Erdey-Gruz and Volmer (20), and Butler (21), wrote a general kinetic equation for a one-electron transfer process given by

$$i = i_0\{\exp(-\alpha\eta F/RT) - \exp[(1-\alpha)\eta F/RT]\} \qquad [9]$$

which explicitly took into account the exponential potential-dependence of the forward and backward current components through the charge-transfer coefficients α* and $1-\alpha$, respectively. For appreciable polarizations, i.e., $|\eta| > 0.1$V, eqn.[9] reduces to the Tafel equation in the form of eqn.[5], so that the Tafel slope, b, can be defined as $2.3RT/\alpha F$. This is the essential origin of the conventional representation of b in terms of a charge-transfer coefficient α.

The use of potential-energy profiles or surface diagrams to

---

* The symbol α was originally used by Erdey-Gruz and Volmer as the Brønsted factor for the discharge reaction. However, this factor is usually designated now by the symbol, β, the "barrier symmetry factor", which refers to the potential dependence of the rate of the electron transfer step itself while the symbol, α, the "charge transfer coefficient", corresponds to the potential dependence of the rate of the overall reaction. When the initial electron transfer step is rate-determining $\alpha \equiv \beta$, e.g., for the h e.r. at Hg, but for reactions involving more than one step with a discharge process as the primary step, α is usually greater than β if a subsequent step is rate-determining, e g , for the h e r , $\alpha = 2$ when recombination of two adsorbed H atoms is rate-determining.

represent the symmetry factor, β, and the energy course of the h.e.r. discharge step with distance along a reaction coordinate originated with the work of Horiuti and Polyani (22). These surface diagrams are usually two-dimensional representations (or cross-sections) of a multi-dimensional potential energy surface in which the reaction coordinate is not necessarily linear. In principle, "free energy profiles" should be considered rather than "potential-energy profiles" but they require evaluation of the entropy change along the reaction coordinate which is very difficult to calculate, especially for reactions involving solvated ions where entropy effects are quite large in the activation process; in fact, the entropy effects in electrode processes have been rather neglected but will form an important aspect of the present work.

Horiuti and Polyani (22) assumed the H atom to be adsorbed on the electrode and were the first authors to point out that the state of adsorption of the H atom would affect the rate of proton discharge. Transfer of H_3O^+ to an adsorbed state on the electrode surface was viewed in terms of a gradual breaking of the H_2O-H^+ bond and formation of a M-H bond. Neutralization of the ion was assumed implicitly to occur at the "crossing point" of the H_2O-H^+ and M-H energy curves, i.e., in the activated state, corresponding to neutralization by transfer of an electron to a proton in an excited rotation-vibration level of the H_3O^+ ion, as proposed by Gurney.

More quantitative calculations based on the approaches of

Gurney (15) and Horiuti and Polanyi (22) were first given by Butler (19), who recognized the importance of the metal to H adsorption energy as well as solvational interactions in the kinetics of the h.e.r. Butler considered the H atom formed by the discharge of the H_3O^+ ion to be adsorbed at the metal surface, i.e., M-H_{ads}, rather than in solution near the metal surface as was implicit in the Gurney theory. Consideration of the M-H interaction energy, A, results in an electron tunneling condition given by

$$\Phi + eV \leq I + L \quad R + A \qquad [10]$$

as shown schematically in Fig. 3 Curve BB is a replot of Gurney's representation of the final state, $H|H_2O$, which includes the electronic work function of the metal, which he omitted. Curve CC includes the M-H interaction energy in the final state energy profile and this results in a lowering of the intersection point, i.e., from X to X', and consequently a lower energy of activation in better agreement with experiment. Butler's work provided the foundation for understanding the wide range of rates of the h.e.r at different electrode metals, i.e., a basis for electrochemical catalysis, through the role of H adsorption energy and the metal electron work function. More detailed treatments of the solvational interaction and M-H adsorption energy were given by Parsons and Bockris (23) who calculated the activation energy for the discharge step of the h.e.r. at Hg and Ni, and by Conway and Bockris (24) in a theoretical study of the electrochemical desorption step, i.e., eqn.[2], on Cu, Ni, W and

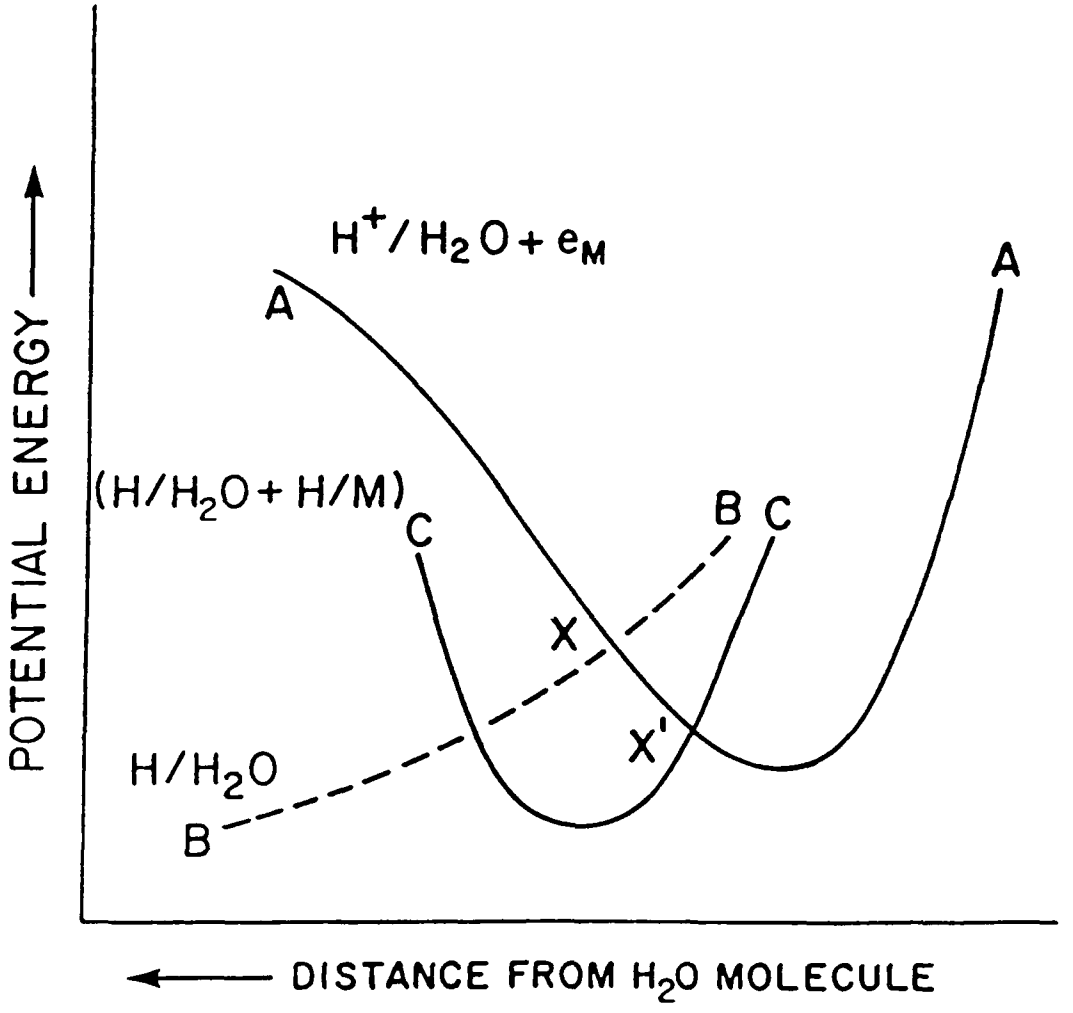

Fig. 3 Model for proton transfer according to Butler (ref. 19)

Hg.

The effect of applied potential is shown schematically in Fig. 4, according to the representation of Horiuti and Polanyi (22) and Butler (19), in which the effect of potential is to shift the initial state energy curve, e.g., $H_3O^+ + e + M$, by an amount VF, which changes the relative energy of the activated state by $(1-\beta)VF$, with a consequent change of activation energy of βVF for the forward reaction. A simplifying linearization of the anharmonic potential-energy profiles, e.g., Morse curves, near the point of intersection allows a simple approximate geometric interpretation of β in terms of the relative slopes m_1 and m_2 of the linearized curves for the reactant and product species, near the intersection point of these curves, viz.

$$\beta = \frac{m_1}{m_1 + m_2} \qquad [11]$$

For a symmetrical energy barrier it is obvious that $\beta \approx 0\ 5$, as was shown by Essin and Kozheurov (25) and by Parsons and Bockris (23) using a similar model. In these treatments the effect of potential is considered only to change the Fermi level of the electrons in the metal, i.e., $\Phi_V = \Phi_{V=0} + eV$, and not the behaviour of the reactant ion, so that the form of the energy profile remains unchanged with modulation of the potential. However, later Despić and Bockris (26) extended the potential energy profile method for calculating the symmetry factor to include cases where potential energy profiles intersect in a non-linear harmonic region, e.g., near the zero-point energy level(s), so that β becomes dependent on electrode potential

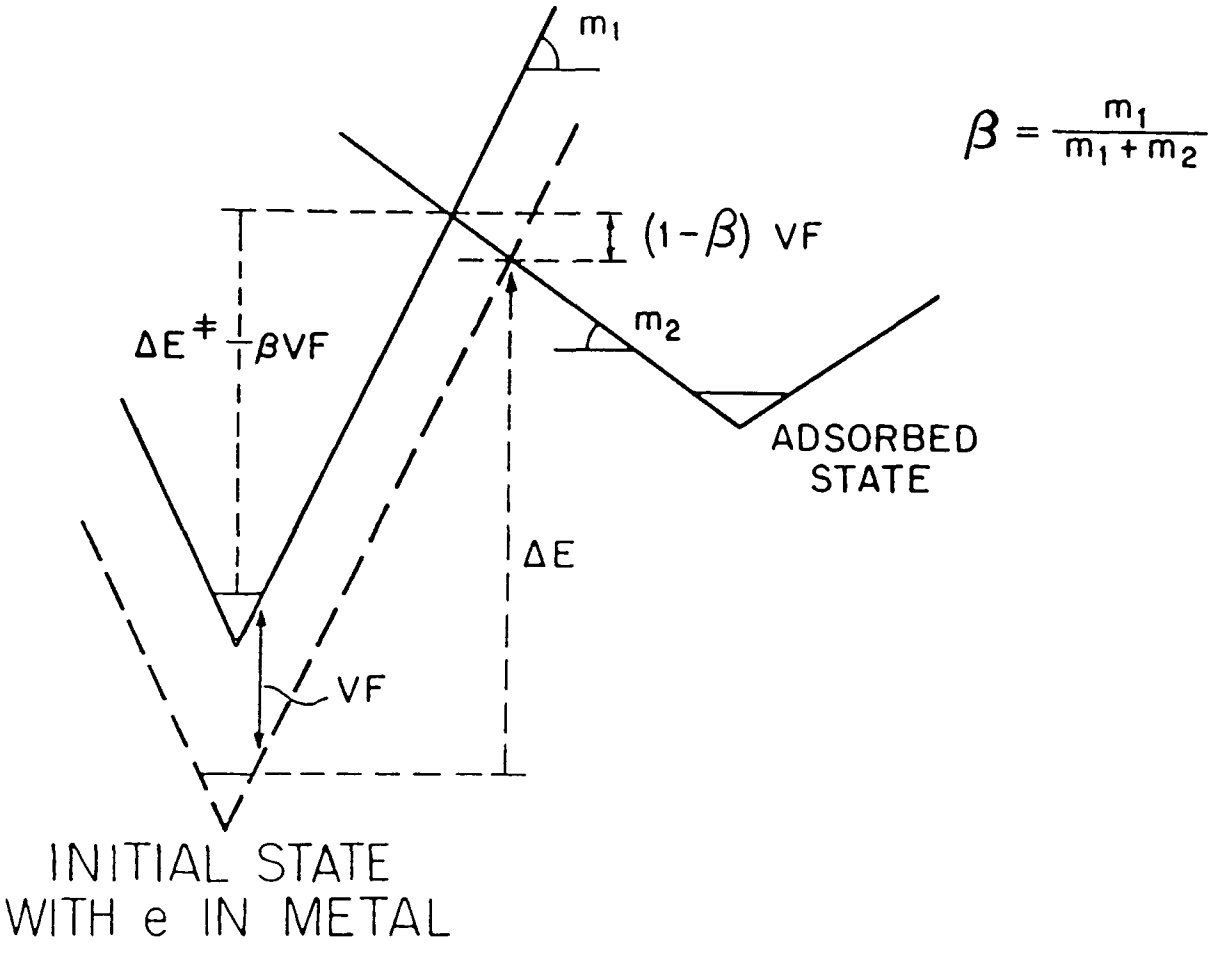

Fig. 4 Schematic representation of the effect of applied potential on the energy of activation of a charge transfer process

They also identified how β could alternatively be represented in terms of the position of the activated state, i.e., point of intersection of potential-energy profiles, with respect to the potential energy minima; then

$$\beta = \frac{\text{Distance along reaction coordinate between initial and activated states}}{\text{Distance along reaction coordinate between initial and final states}} \qquad [12]$$

This basis of expressing β was first used by Bockris and Parsons (23, 27) who ascribed the observed temperature-dependence of α or β to a change in the double-layer thickness with temperature which changes the relative positions of the potential-energy profiles along the reaction coordinate, but this effect was found to be of insufficient magnitude to account for the experimental behaviour. Changes of relative position on the energy axis with potential produce changes in β similar to those arising from changes of position on the reaction coordinate. However, for many electrode processes, β is found to be <u>constant</u> over an appreciable range of potential; e.g., Nürnberg (28) found experimentally that β for the h.e.r. at Hg is almost constant over 1.2 V or 10 decades of change of rate, so that eqn.[12] is not a satisfactory representation of β for these cases. For ionic migration in films, e.g., oxide films (29), eqn.[12] is probably satisfactory since the charged particle can be regarded as passing down a field to the activated state. Since β or α is usually about 0.5, the distance to the activated state is sometimes called the "half-jump" distance because it is considered to be half-way between the initial and final states.

While the two representations of β, i.e., eqn.[11] and eqn.[12], normally predict $\beta \approx 0.5$, it is clear that they will not necessarily give identical results since they depend on the geometry assumed for the potential energy curves and the magnitude of the activation energy relative to the overall energy change in the process.

3. Proton Tunneling in the H.E.R.

For the h.e.r. the possibility that the proton itself tunnels to the electrode rather than being transferred by chemical activation must be considered. Possible quantum-mechanical effects arising from proton tunneling, e.g., an H|D isotope effect in addition to that due to differences in zero-point energies, were recognized by Wigner (30) and Bell (31). In particular, Bell calculated the effect of tunneling for a hypothetical proton transfer reaction using an Eckart (32) activation energy barrier (i.e., the potential energy profiles are based on curves like Morse functions) and concluded that the heat of activation would be temperature dependent. This results in deviation from a linear Arrhenius plot as shown schematically in Fig. 5, particularly at low temperatures where the current approaches a constant value. Following the work of Bell for homogeneous proton transfer, Bawn and Ogden (33) and Appelby and Ogden (34) discussed the possibility of proton tunneling in the proton discharge step of the h.e.r. The use of too wide an energy barrier and neglect of zero-point energy differences led to high values of the H|D separation factor, S, defined by

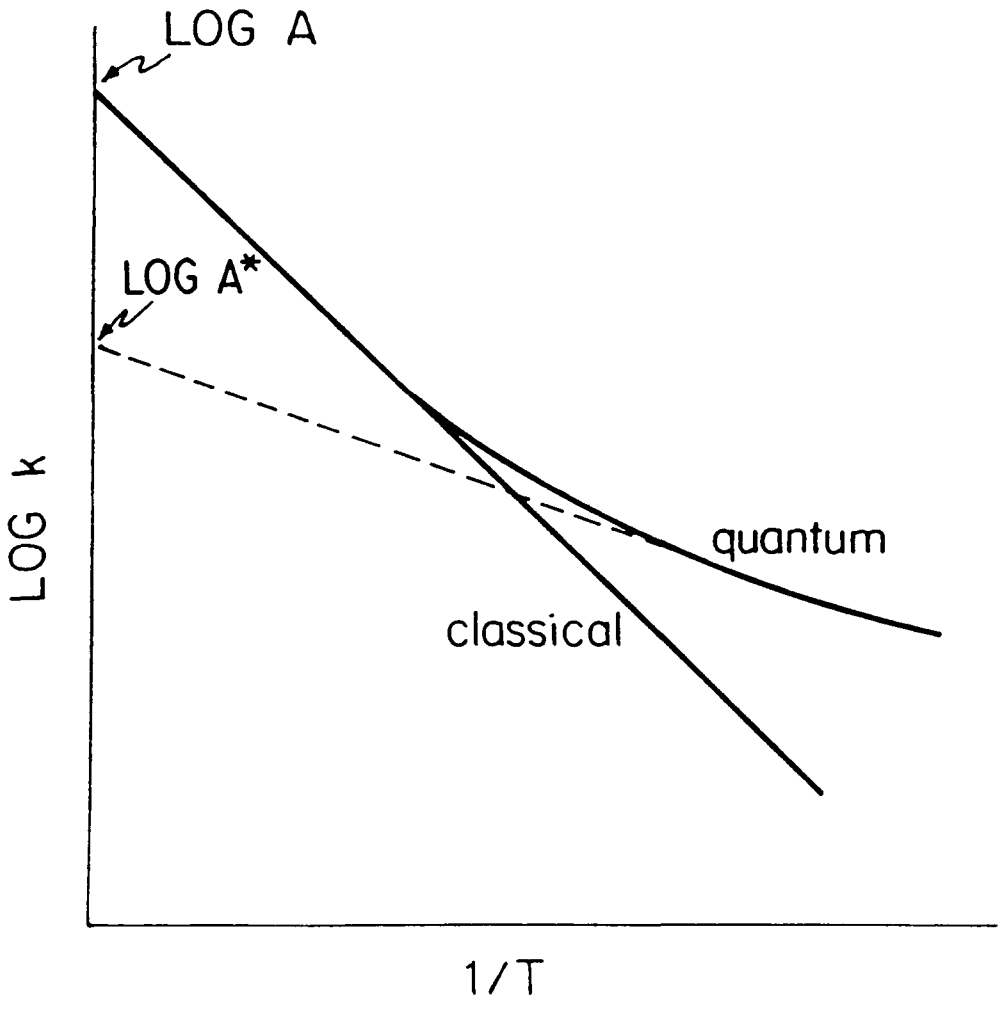

Fig. 5 Arrhenius plot showing the effect of proton tunneling according to Bell (ref. 31)

$$S_{H,D} = (C_H|C_D)_{gas} / (C_H|C_D)_{soln.} \quad [13]$$

which have not been confirmed experimentally. Later, more detailed theoretical calculations of the effect of proton tunneling on Tafel parameters and H|D kinetic isotope effects were given by Christov (35), Conway (36) and Conway and Salomon (37, 38), who predicted appreciable proton tunneling rates and a potential-dependent H|D separation factor. Christov used both Eckart and parabolic energy barriers in his analysis and divided the total current associated with proton discharge into two components: one for classical passage over the barrier and the other for tunneling through the barrier, i.e., i_T = i(quantum) + i(classical). For a parabolic barrier, at low temperatures where tunnel effects are larger, the Tafel slope was found to be greater than the classical value $b \approx 2.3RT/0.5F$ and approximately independent of temperature but, for an Eckart barrier, the Tafel slope was less effected and had a classical temperature-dependence. Although Christov (35) was the first to show the relation between Tafel parameters and proton tunneling, Conway (36) was the first to take into account the zero-point energy differences in the initial and activated states, in the evaluation of the mass dependence of the Tafel slope for pure tunneling control. This behaviour is shown in Fig 6, where the electrode potential is plotted as a function of the logarithm of the integral of tunneling probability which is proportional to the electrochemical proton or deuteron transfer rate (the current) An appreciable difference in the Tafel slope is

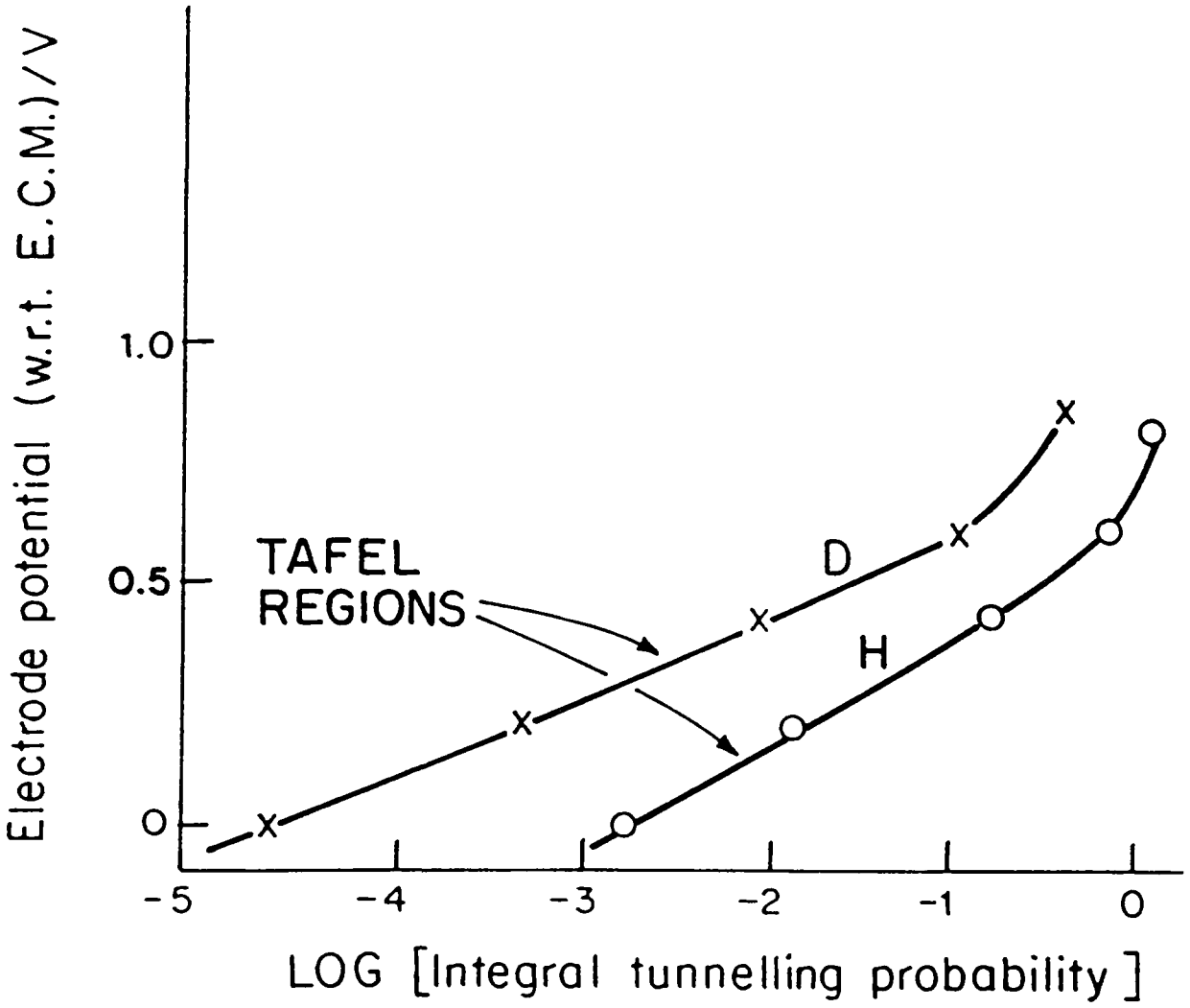

Fig. 6 Tafel relation arising from complete tunneling control in the h.e.r according to Conway (ref. 36).

predicted for proton discharge (≈0 25 V) and for deuteron discharge (≈0.17 V) for pure tunneling transfer In practice, both classical and nonclassical transfer occur in parallel, the relative extent of which is dependent on temperature and deuteron transfer will tend to occur with a relatively greater classical transfer probability. The calculations of Conway were based on Bell's method of integrating tunneling probability over the height of an Eckart barrier, allowing for a quantized Boltzmann distribution of initial H_2O-H^+ states.

Experimentally, appreciably greater Tafel slopes for H transfer than for D transfer have not been observed in the h.e.r. In experimental studies down to 163 K in cooled alcoholic solutions, Conway and Salomon (37, 38) were unable to find any deviations from linearity in Arrhenius plots or anomalies in the Tafel plots and concluded that isotope effects found in the h.e.r. could be explained satisfactorily from a consideration of zero-point energy difference effects. Later, Bockris and Matthews (39) reexamined the question of proton tunneling in the h.e.r. using an unsymmetrical Eckart barrier with allowances for zero-point energies and found that the Tafel slope dependence on mass and temperature, and the dependence of rates on temperature, are not sensitive enough tests for proton tunneling. However, the potential dependence of the separation factor ($S_{H,D}$ and $S_{H,T}$ decrease with increasing potential, the effect being more pronounced for $S_{H,T}$) was attributed to an appreciable degree of proton tunneling, i.e., 69% proton tunneling at a cathodic

potential of ~1.0 V at Hg in acid solution. The potential dependence of S has been regarded as a useful test for proton tunneling.

4. Relation of Solvation Effects and Electrode Potential to the Brønsted Theory of Homogeneous Proton Transfer

The so-called Brønsted relation was first proposed by Brønsted and Pedersen (40) as a result of their experimental work on the decomposition of nitramide It relates the effectiveness of an "acid catalyst" to its acid-base strength by the relations

$$k_A = G_A K^{\alpha} \quad , \quad k_B = G_B (1/K)^{\beta} \qquad [14]$$

where k_A and k_B are the catalytic rate constants for acid and base catalysis, K is the dissociation equilibrium constant for the acid, and G_A, G_B, α and β are constants for a series of similar catalysts but depend on the nature of the reaction, the solvent and the temperature. The Brønsted factors α and β are usually positive, less than unity, and commonly near 0.5. Since the main step in acid-base catalysis always involves the transfer of a proton between the catalyst and the substrate, the Brønsted relation applies to direct proton transfer reactions of the type

$$AH^+ + B = A + HB^+ \qquad [15]$$

The Brønsted relation was the first example of a "linear free energy relationship" between rates and equilibrium constants since taking logarithms of eqn.[14] and substituting, $\ln K = -\Delta G^\circ/RT$, gives

$$\ln k_A = \alpha \Delta G^\circ/RT + \ln G_A \qquad [16]$$

for acid catalysis and

$$\ln k_B = \beta \Delta G^\circ / RT + \ln G_B \qquad [17]$$

for base catalysis.

Catalytic studies do not normally cover a wide range of acid or base strengths but Eigen et al. (41), using temperature-jump studies on the reaction of the keto form of acetylacetone with bases, was able to cover a range of approximately 16 pK units. The linear Brønsted relations of eqns.[16] and [17] do not hold over such a large range of acid or base strength and the slopes, α and β, decrease with increasing reaction velocity even when the rates do not approach the diffusion-controlled limits. However, the Brønsted relation for acid-base reactions usually covers a wider range of structural variation than most linear free energy relations, e.g., aromatic and aliphatic species are often covered by the same relation.

A molecular interpretation of the Brønsted relation in terms of potential energy curves was given by Horiuti and Polanyi (22) and by Bell (42), and is shown schematically in Fig. 7a In this figure a change in base strength associated with a change in free energy of $\Delta RT \ln K$ shifts curve B_1 to curve B_2 with a reduction in the free energy of activation of $G_1^{\ddagger} \quad G_2^{\ddagger} = \alpha \Delta RT \ln K$, where the Brønsted factor, α, is determined by the relative slopes of the curves at the point of intersection. In this type of treatment, a change in acid or base strength is simply represented by a vertical shift of the energy curves without any change in shape. However, in reality changes in bond strength are usually accompanied by a change in the shape and relative

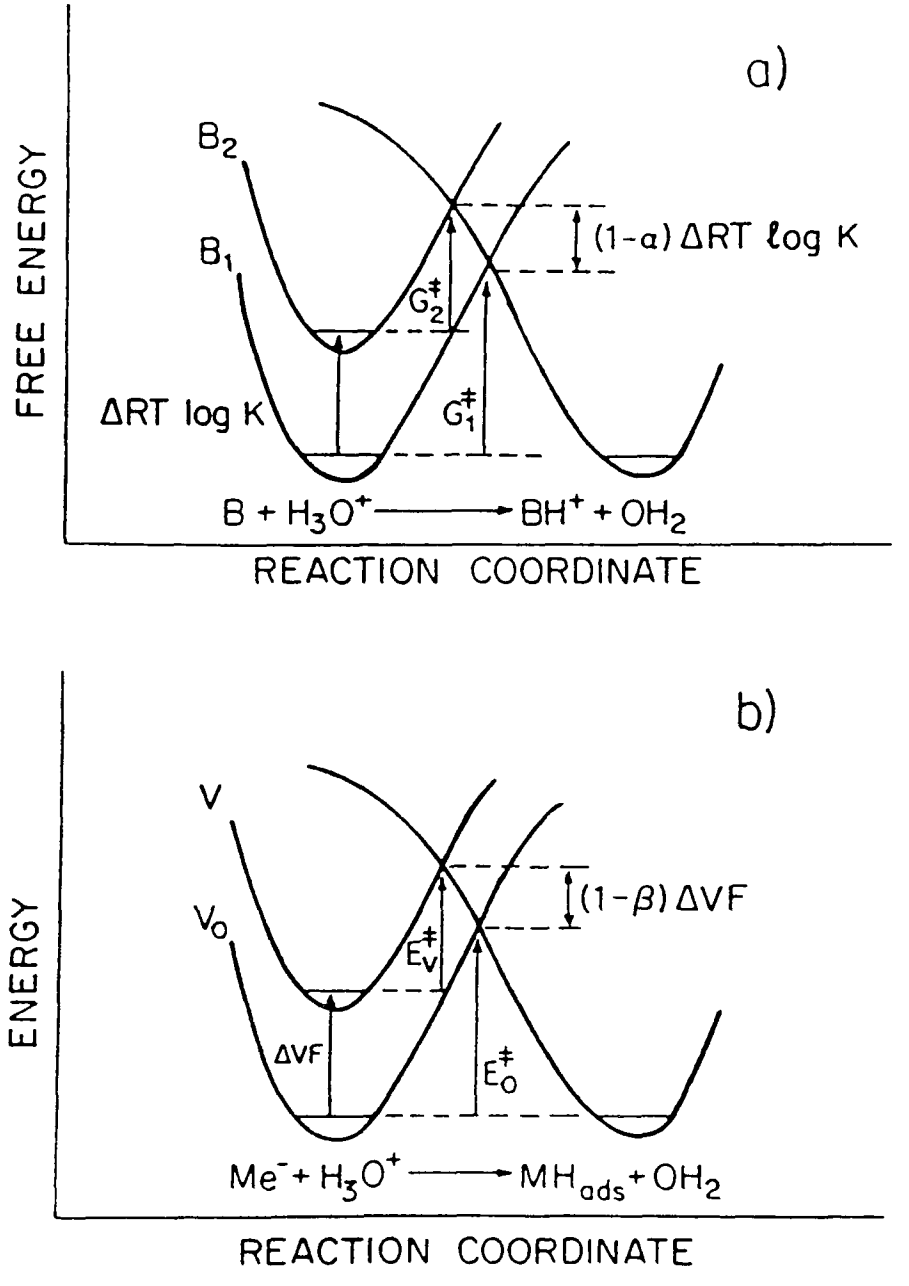

Fig. 7 Potential energy diagrams showing the relation between the symmetry factor β in electrochemical kinetics and the α coefficient in Brønsted's relation: a) the effect of a change of base strength; b) the effect of a change of electrode potential

position of the whole energy curve since force constants for bonds change approximately linearly with bond strengths, e.g., as represented by Badger's rule. Changes in shape and position of the energy curve for acid-base systems of widely differing structure and bond energy can account for the observed deviations from the linear Brønsted relation.

The parallelism between the kinetics of electrochemical proton transfer and the Brønsted relation was first pointed out by Brønsted and Ross-Kane (43) and treated further by Frumkin (4). Salomon and Conway (37) proposed an alternative representation of the discharge step in the h.e.r. in which the activated complex was regarded as analogous to that in homogenous acid-base proton transfer processes with the electrode acting as a base of variable strength depending on the electron surface charge density.

The effect of a change in electrode potential on the free energy of activation for heterogeneous proton transfer is also shown schematically in Fig. 7b for comparison with the homogeneous proton transfer case of Fig. 7a. For a change in applied potential of ΔVF, curve V_o is shifted to curve V with a reduction in the free energy of activation of $E_o^{\ddagger} \quad E_V^{\ddagger} = \beta \Delta VF$, where the symmetry factor is seen to have a significance analogous to that of the Brønsted factor, α. Since the main effect of applied potential as represented in this model is on the Fermi level of electrons in the metal, the linear free energy relation for electrode processes, i.e., the Tafel relation, is

usually linear over a wider range of energy change than for the Brønsted relation for acid-base reactions over a comparable range of bond strength change or pK. Although changes in potential do not significantly change the shape or relative position of the energy curves, they may have some effect on solvent orientation and ion adsorption at the electrode surface and thus have some effect on the state of solvation of the ion being discharged. This point will be discussed later in chapter 5.

The effect of a change of solvent on the kinetics of electrochemical proton transfer is shown schematically in Fig. 8, for which solvation effects are regarded as changing only the initial state energy curve ($M + e + DH_s^+$) and indirectly the activated state, but do not affect the final state ($MH_{ads} + D_s$). For a decrease in solvation energy, i.e. $+\Delta G_s$, there is a reduction in the free energy of activation of $-\beta\Delta G_s$, and vice versa. Solvent effects in electrochemical proton transfer are exactly analogous to the Brønsted relation for changes in acid-base strength, and changes in solvation energy will usually also modify both the shape and relative position of the initial energy curve. Usually, weaker solvation would correspond to a flatter energy curve, so that the energy of the transition state changes less than that shown in Fig. 8, resulting in a larger Brønsted coefficient, β.

Solvation effects in ionic redox reactions ($M_s^{z+} + e \rightarrow M_s^{(z\ 1)+}$) are different from those in atom/electron transfer reactions because the energy curves of <u>both</u> the reactant and

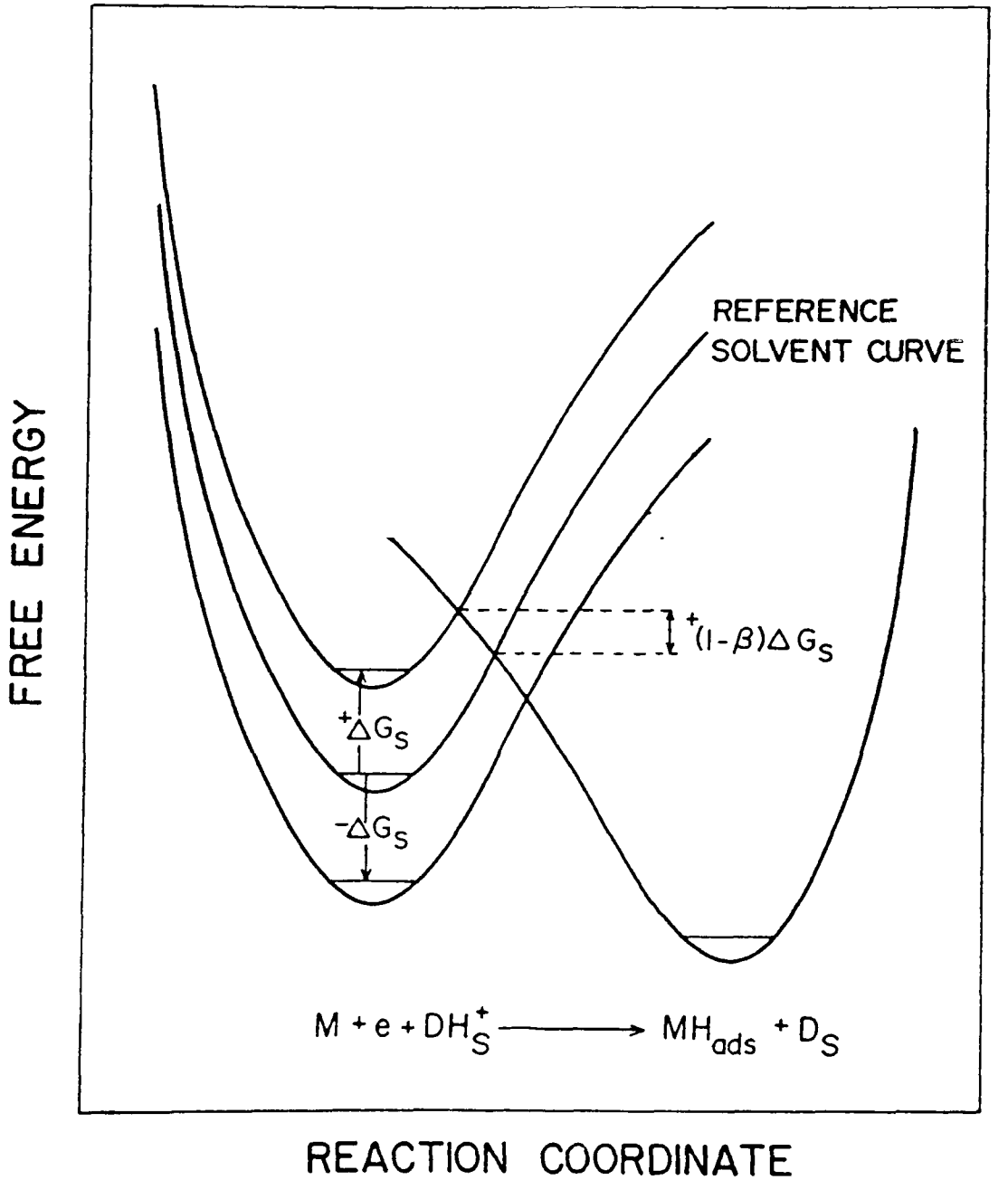

Fig. 8 Schematic representation of solvation effects in an electrochemical proton/electron transfer reaction

product species are modified in the former case, i e. both the initial and final states are solvated, or ligand-complexed, ions. If the solvation energy of the reactant and product ions are changed equally with a change of solvent, as shown schematically in Fig. 9, then no change of activation energy will occur. However, usually the solvation energy of the more highly charged species (M_s^{z+}) is changed more than that of the less charged species ($M_s^{(z-1)+}$), and the shape of the energy curves may also be different, so that some change in activation energy would be expected.

5. Modern Treatments of Charge Transfer

Modern treatment of charge transfer have developed from the theories of Hush (44) and (R.A.) Marcus (45, 46, 47) for electron transfer in redox reactions, both in solution and at electrodes. For such processes, no bonds are broken or formed in the reaction in the conventional sense so that only pure electron transfer occurs but with some "reorganization" of the solvational environment of the ions. In solution, "outer-sphere" redox reactions are defined as those processes for which the conjugate pair of ions do not share an electron-transfer facilitating ligand in the collision complex; for the analogous case of a redox reaction at an electrode, there is correspondingly no specific adsorption of the reactant ions or molecule In contrast to the earlier treatments of charge transfer, the activation process has been treated by Marcus (47) and by

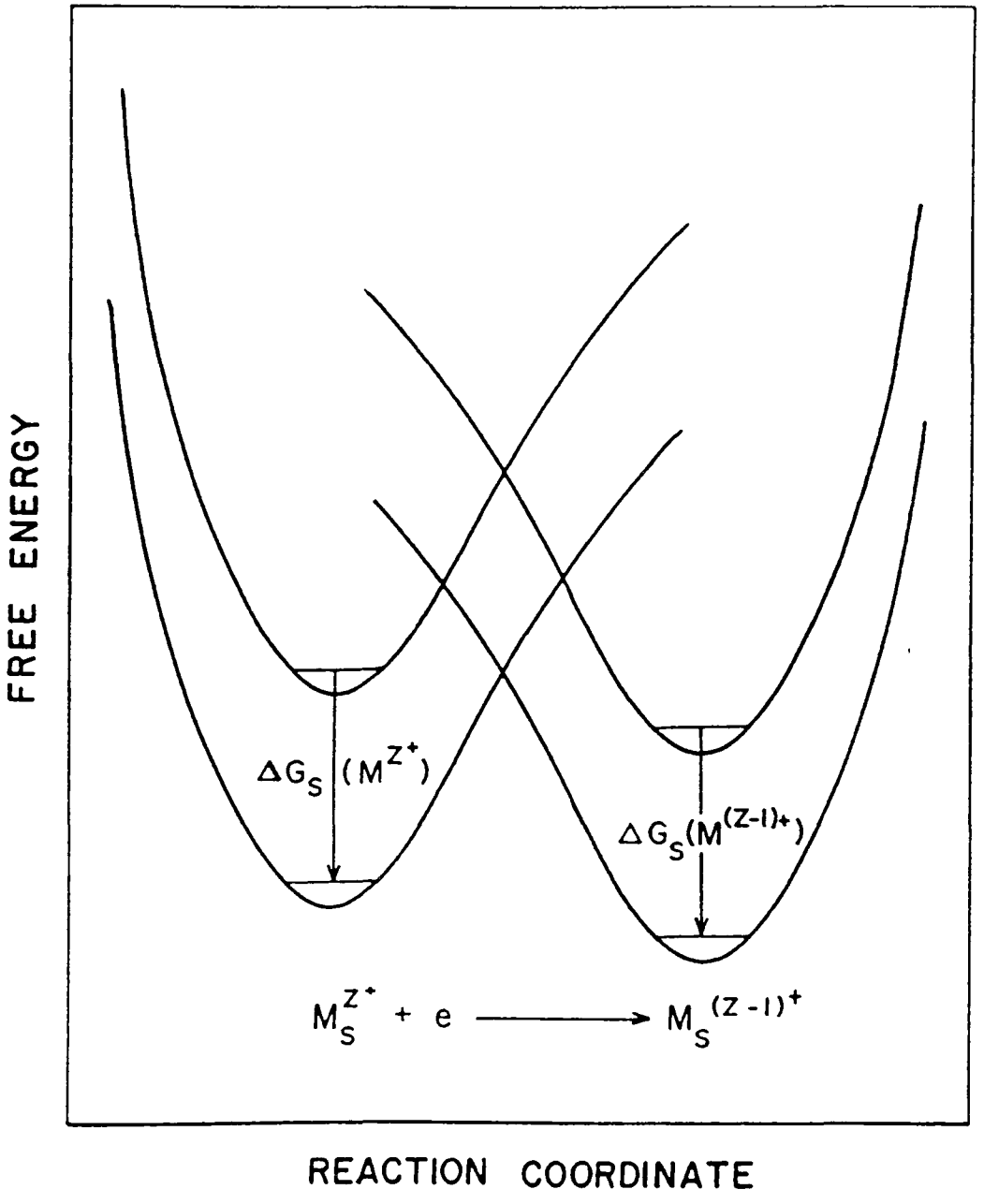

Fig 9 Schematic representation of solvation effects in an ionic redox reaction where the solvent effect is the same on both ions of the redox pair.

Dogonadze et al (48) in terms of long-range, nonspecific fluctuations of solvent dielectric polarization according to Born's equation, i.e , the "reorganization energy". This approach was based on analogies with polaron theory for the creation of charges in a solid medium and had its origin in Hush's treatment.

The unique aspect of Hush's theory is the description of the redox reaction in terms of variation of electron charge density along the reaction coordinate, i.e., electrostatic "equilibrium" between the average charge on the ion in the activated complex and its environment is envisaged. The symmetry factor, β, is considered by Hush to correspond to the fraction of a unit charge transferred to the activated state as it is formed from the initial state, e g., for a symmetrical redox reaction, $\beta = 0.5$. It should be noted that such a representation of β could not be combined with one involving the fraction of the potential across the Helmholtz larger from the initial to the activated state since then β would be ≈ 0.25, which is not experimentally found!

The theory of (R.A.) Marcus for homogeneous electron transfer reactions developed from the work of Weiss (49), Libby (50), and (R.J.) Marcus et al. (51) and was later applied to electrode redox reactions (52). Generally, in the Marcus treatments, the central solvated ion is treated as a rigid sphere inside which no changes in interatomic distances occur during the reaction and the solvation cosphere is treated as an unsaturated dielectric continuum. When the reactant(s) are near to each other (or the

electrode) a suitable solvent fluctuation can result in formation of the activated state in some atomic configuration; then electron transfer takes place coupled with solvent relaxation resulting in formation of the products. Nonequilibrium states were considered in the reaction scheme in which the atomic and dipole orientation polarizations are not in equilibrium with the charge on the activated complex since the solvent molecules and atomic configuration do not have time to adjust during the fast electron transfer (cf. the Frank-Condon principle). In a later theory of electrode redox reactions (53), Marcus apparently took into account the ion-solvent intermolecular bond stretching energy in addition to the solvent reorganization energy. In the Marcus treatments the solvent polarization fluctuations are given by harmonic potential energy functions so that a quadratic dependence of log i on overpotential arises, i.e., a potential-dependent Tafel slope or symmetry factor is expected. According to the Marcus theory the symmetry factor is given by

$$\beta = 0.5 + \eta F/2\lambda \qquad [18]$$

where λ is the reorganization energy for the particle undergoing electron transfer, and is defined as the energy change on going from the initial-state energy surface to the final-state one, in an unchanged configuration on the reaction coordinate. The above relation could give rise to a temperature-dependent β because, in most solvents, the reorganization energy λ, will be temperature-dependent but such an effect would only arise for processes which exhibit a quadratic dependence of log i on overpotential

The most developed recent treatment of electrochemical proton discharge has been given by Dogonadze, Kuznetzov, and Levich (48), i.e., the DKL model, who have combined the solvation-shell reorganization treatments of Marcus and Hush with quantum-mechanical tunneling of H^+ from a solvationally activated state. A reorganization energy similar to that in an ionic redox reaction was considered in the activation process with the energy of the proton particle treated in terms of the Born polarization energy of the surrounding dielectric. In principle, the DKL model does not differ from the earlier quantum-mechanical treatments of the rate of H transfer evaluated by Bell's method (31). That treatment took into account vibrational activation with H tunneling from various excited vibrational states according to a Boltzmann distribution of energies. However, in the DKL model, thermal activation of the bond between O and H (in H_3O^+ or H_2O) was considered not to be significant at ordinary temperatures because the large vibrational quanta (about 42 kJ mole ^{1} for OH^+ vibrations in a gas phase H_3O^+ ion and 17 kJmole ^{1} for the vibration of adsorbed M-H) are >> kT, so that it was concluded that H exists only in the ground vibrational state in both the initial and final states.

Although much as been made of this point, the following objections have been raised (54,55): (1) vibrational states of energy >> kT can always arise because there is a Boltzmann distribution of states each with a probability of exp($h\nu/kT$), and (2) the high partial molar heat capacity for the hydrated

proton in aqueous solution (56) indicates there must be a range of lower frequency hydration "lattice modes" from which thermal activation can arise.

A potential energy diagram for proton discharge according to the treatment of Dogonadze, Kuznetzov and Levich is shown in Fig. 10, for which two energy barriers result from consideration of the electron, proton and solvent as three subsystems. Long-range fluctuations in solvent polarization along a multi dimensional solvent coordinate, q, produce a continuum of energy levels which provide energy from which activation of the initial state arises, while the proton coordinate, R, corresponding to the ground vibrational state of the initial state, remains fixed. Proton tunneling occurs from the (solvationally) activated state to an adsorbed state on the metal of equal energy but in the ground vibrational state; subsequent relaxation of the solvent yields the equilibrium final state.

Krishtalik (57) has discussed cases where $\beta = 1$ (barrierless discharge) or $\beta = 0$ (activationless discharge) which result from the DKL theory. These cases are shown in Fig. 11, and depend on whether the initial-state potential-energy profile intersects the final state profile at or below* its zero-point energy level, or vice versa. The possibility of experimentally attaining these situations arises because the barrier height can be modified by electrode potential, so that three Tafel regions are

---

* The physical significance of this situation is not altogether clear

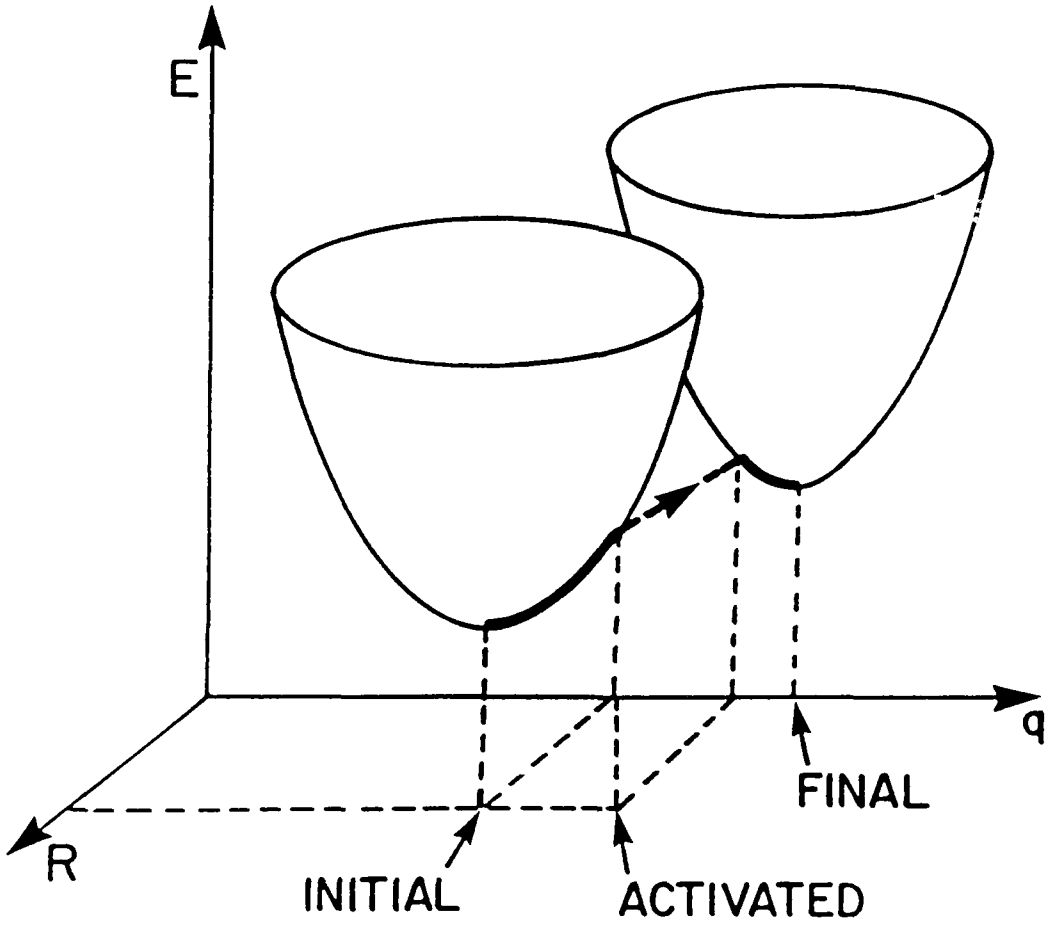

Fig. 10 Model for proton transfer according to Dogonadze, Kuznetsov and Levich (ref 48)

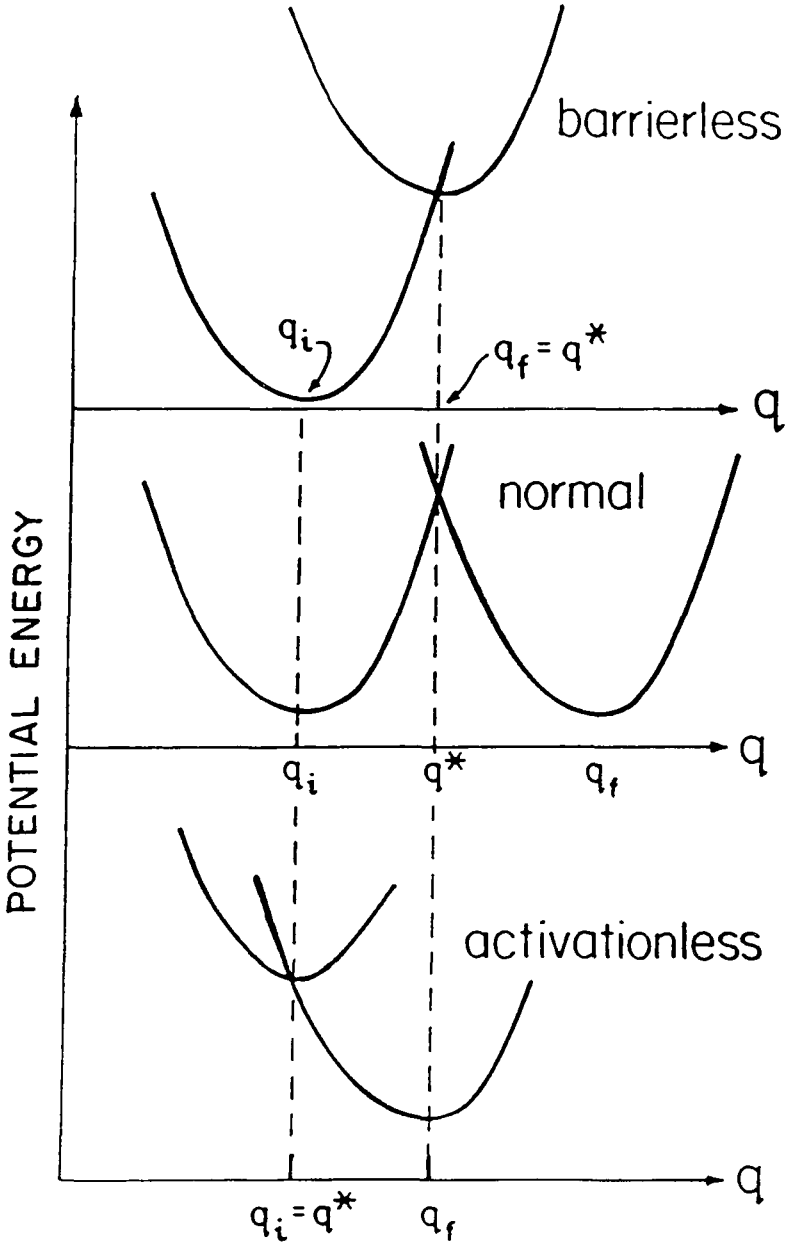

Fig. 11 Limiting activation behaviour along the solvent coordinate for low (barrierless), moderate (normal) and high (activationless) overpotential according to Krishtalik (ref. 57)

theoretically expected as shown in Fig 12 where, at very low overpotentials, $\beta = 1$, at intermediate values $\beta \approx 1/2$ and at high values $\beta = 0$. It should be noted that barrierless and activationless discharge are not unique to the DKL treatment but can arise in other treatments, e.g., Butler's representation (19)

Although behaviour corresponding to activationless discharge has not been observed, Krishtalik (57) has argued that barrierless discharge can be detected experimentally, e g., in the h.e r. at Hg at very low current densities, but experimental results are ambiguous because of double-layer corrections and anion adsorption effects near the potential of zero charge A potential-dependent Tafel slope or symmetry factor predicted on the basis of a harmonic model of solvent polarization has only been detected in a few systems, e g., oxidation in the Cr^{+3}/Cr^{+2} system (58) and reduction of some nitro compounds (59) The most common kinetic behaviour is usually a constant α or β over quite a large range of potential, e.g , for the h.e r at Hg, β is constant over about 1 0 V Hence, a number of factors have been examined within the DKL model in order to extend the predicted region of potential exhibiting linear Tafel behaviour

Kharkats and Ulstrup (60) have observed a linear Tafel relation (b = 0 106 V) over 1 V in potential for the h.e.r by including anharmonicity effects and excited vibrational levels in the central ion, $H_9O_4^+$, but treating its solvent cosphere as a dielectric continuum Kutznetsov (61) has attributed linear

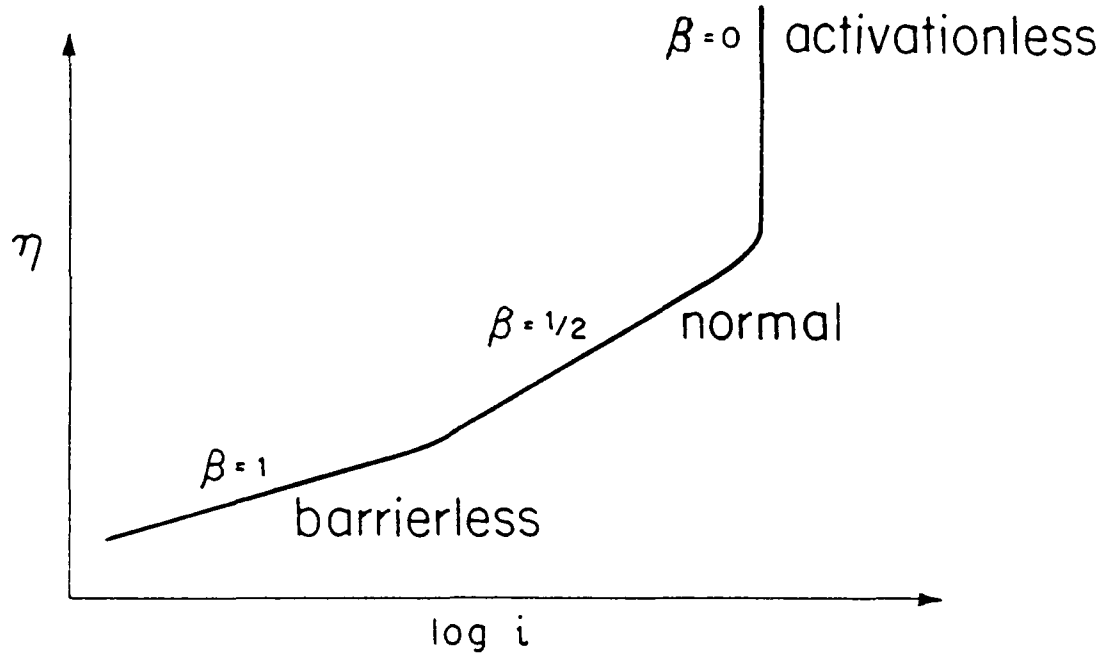

Fig 12 Schematic representation of the range of Tafel behaviour according to the DKL model

Tafel behaviour, i e , constant α or β, to variations of residual charge on the adsorbed atom resulting from fluctuations of the medium molecules, which changes the shape of the energy surface of the final state Also, within the DKL framework, the temperature-dependence of the symmetry factor (62, 63) has been attributed to a number of factors: a) the temperature-dependence of the contribution of the excited vibration states of the proton to the transition probability, b) the temperature-dependence of the transfer distance, c) the temperature-dependence of the shape of the energy surfaces and d) the temperature-dependence of the dielectric properties of the medium. However, these factors lead to a weak temperature-dependence of β under normal conditions, i.e., β varies $\leq$ 5% in the temperature range of 150 to 300 K, which is often much too small in relation to experiment where β typically varies by $\approx$40% over the same temperature range.

6 Concluding Remarks

Current treatments of charge transfer (cf. Marcus and DKL treatments) neglect specific solvational and solvent structure aspects of the activation process but emphasize long-range outer-shell reorganization in the system. There are major differences between this type of model and the bond-stretching models involving thermal activation. Clearly, tests are required to distinguish between these models especially for atom/electron transfer reactions such as the h.e.r. where the initial state of solvation and ionic charge is eliminated in the electrode reaction. These models of charge transfer can only account for a

very small variation of the symmetry factor with temperature, but the experimental variation is usually much larger, indicating the importance of other effects such as possibly field-dependent solvent orientation in the inner region of the double-layer Therefore quantitative evaluation of the entropy of activation as a function of potential is required to determine the temperature-dependence of the symmetry factor and its correct form. Reliable measurements need to be made on the kinetics of the proton discharge step in the h.e.r. for various proton sources in various solvent media in order to provide a basis for characterizing the temperature-dependence of the symmetry factor and the nature of the activation process in the elementary act of complex electron and atom transfer.

These fundamental aspects of electrode kinetics are the subject of the work described in this thesis.

CHAPTER 2

EXPERIMENTAL

1 Introduction

The aim of this research project was i) to make a systematic study of solvent and proton donor effects on the kinetics of the cathodic hydrogen evolution reaction (h.e.r.) at mercury and ii) to investigate the temperature-dependence of the Tafel slope b and the activation barrier symmetry factor β. This requires the temperature and potential dependence of the electrochemical reaction rates in the different media to be determined. The h.e r. can be studied at the Hg electrode without the complication of a potential-dependent coverage of the electrode by adsorbed H such as arises at Pt or Ni (64). A Hg electrode offers the further advantage of freezing at 234.16 K, so that in some nonaqueous media the kinetics of the h.e.r can be studied at both liquid and solid Hg.

The electrochemical reaction kinetics were studied by the potentiostatic method, in which the steady-state current density is measured at various applied potential differences across the electrode interface. In addition to steady-state polarization measurements, complimentary open-circuit potential decay measurements at various temperatures were made for some of the systems in order i) to investigate the double-layer capacitance behaviour at liquid and solid Hg and ii) to provide another method for determination of the Tafel slope

2. Choice of Systems

The h.e.r at Hg was the reaction principally studied in the present work but a parallel electrode-kinetic examination was also made of the anodic bromine evolution reaction (b.e r.) from 0.4M $(n\text{-}C_3H_7)_4NBr$/0.2M Br_2 in acetonitrile (AN) at vitreous carbon electrodes. This system was chosen in order to provide comparative information on the behaviour of an anodic reaction from a relatively unstructured but polar aprotic solvent. The use of acetonitrile also eliminates the difficulty encountered in the aqueous medium that the reaction product Br_2 has a limited solubility in water.

The impedance behaviour of the b.e.r. at vitreous carbon was investigated by means of a Solartron 1172 frequency response analyzer over the frequency range 10 mHz to 10 kHz. Only one semicircle was found in the plot of the real and imaginary components of impedance in the complex plane over an overpotential range of 0.01 to ca. 0.1 V (See Fig. 13), indicating that there is no potential-dependent pseudocapacitance in this range. Like the h.e.r. at Hg, it is of interest that the b.e.r. at vitreous carbon evidently does not involve any significant potential-dependent changes in surface coverage ($Br^{\bullet}$ in the b.e r. case) in the overpotential range studied. This matter will be referred to in more detail later (see chapter 5-B).

The electrolyte systems chosen for the work on the

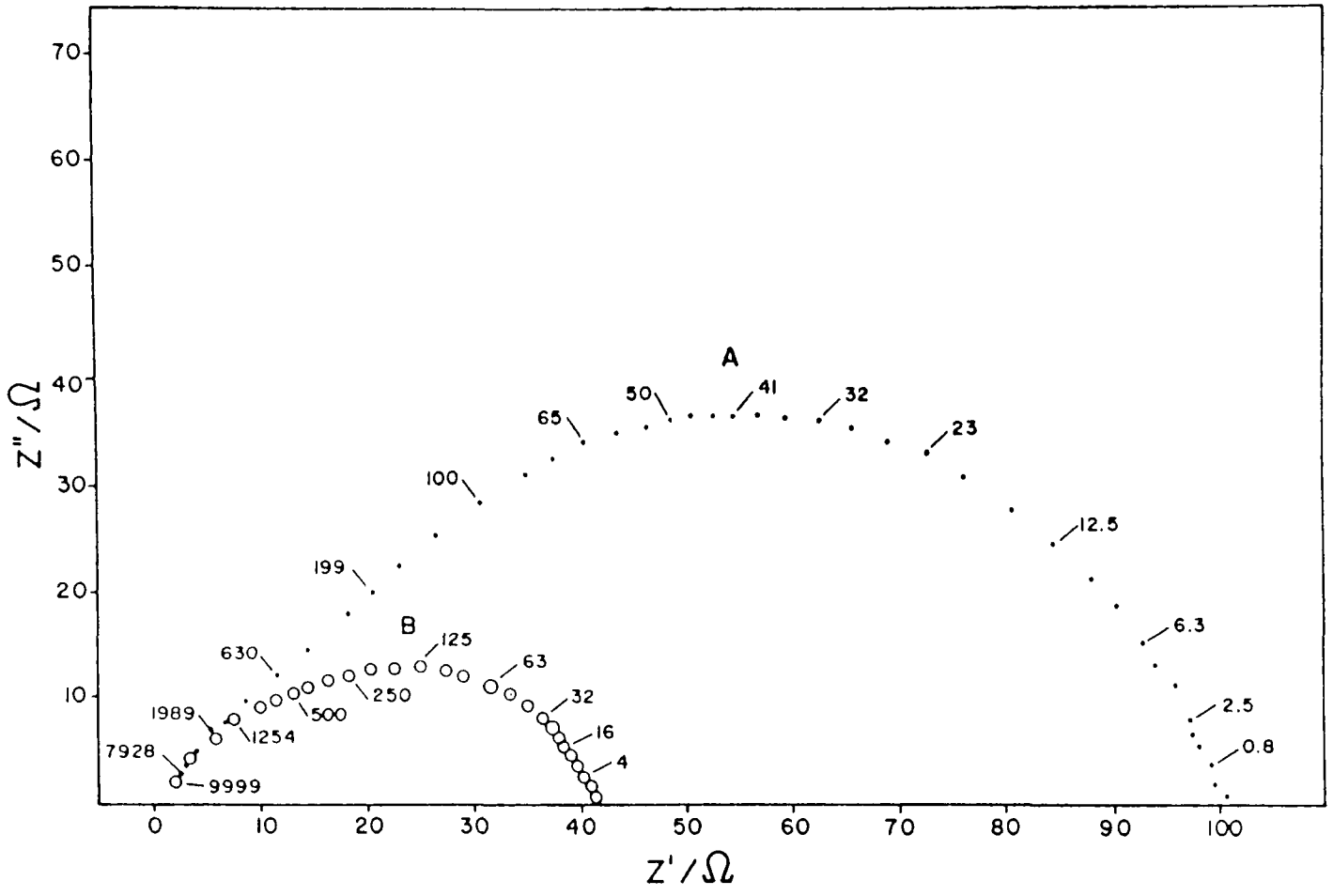

Fig 13 Complex plane impedance plots for the b.e.r. from 0.4M $(C_3H_7)_4NBr|0.2M\ Br_2$ in CH_3CN at vitreous carbon at 295K: A) η=0 08 V B) η=0.120 V. Frequency in Hz.

h.e.r. are listed in Table 1, together with some relevant data. In choosing the systems, several factors had to be considered: solubility, dissociation constants of the acids and salts used, electrolytic conductivity, electrochemical inertness of the solvent and supporting electrolyte, thermal stability and chemical inertness of the electrolyte system, double-layer effects, choice of reference electrodes compatible with the chemistry of the systems used and finally ease of preparation and purification of the materials.

The use of nonaqueous solvents allows a variety of properties to be changed and enables the temperature range over which the kinetics of the h.e.r. are studied to be extended beyond those accessible in water. In aqueous systems, low temperatures can only be reached in concentrated acid and salt solutions where the dependence of the kinetics (e.g., Tafel slope) on concentration and temperature is unconventional (65), probably on account of specific adsorption of ions.

a) Supporting Electrolyte

A supporting electrolyte was used only for the proton sources which had small dissociation constants: Et_4NCl for H_2O (pK_{H_2O} = 14.00) and Et_4NClO_4 for CH_3COOH in acetonitrile (pK_{CH_3COOH} = 22.4) and Et_4NClO_4 for CF_3COOH in acetonitrile (pK_{CF_3COOH} = 14.2). These supporting electrolytes are completely dissociated in their respective solvents (66) and are especially suited for cathodic reduction experiments because of their electrochemical stability. The cathodic potential range is limited, however, by the reduction of the quaternary ammonium

TABLE 1

Electrolyte Systems for the Study of the H.E.R. from Various Proton Sources

Electrolyte (0.1M)	Solvent	K_A / M^{-1} (298 K) [a,b]	Λ_o^+/$cm^2\Omega^{-1}mole^{-1}$ (298 K) [a,b]	Λ_o/$cm^2\Omega^{-1}mole^{-1}$ (298 K) [a,b]
HCl	H_2O	*	349 8	76.4
$EtNH_3Cl$	H_2O	*	32.6-73.4	76.4
Et_3NHCl	H_2O	*	32.6-73.4	76.4
Et_4NCl	H_2O	*	32.6	76.4
$EtNH_3Cl$	$HCONH_2$	*	11.0-15.6**	17.1
Et_3NHCl	$HCONH_2$	*	11.0-15.6**	17.1
$EtNH_3Cl$	CH_3OH	*	57.8-60.5**	52.3
Et_3NHCl	CH_3OH	*	57.8-60.5**	52.3
HCl	CH_3OH	17	146.2	52.3
HCl	1 Propanol	170	19.35	10.5
HCl	2-Propanol	466(ii),(iv)	17.3(i)	10.6
HCl	Isobutanol	1430(ii)	10.8(i)	≈ 6.2(vi),f
CF_3SO_3H	DMF	*d	34.7c	43.6d
$Et_3NHCF_3SO_3$	DMF	*c,d	35.1c	43.6d
$Et_3NHCF_3SO_3$	AN	≤1c,d	≈85	96.3d
$H_3OCF_3SO_3$	AN	<2.6d	--	96.3d
CH_3COOH	AN	≈10 22e	--	--
(0.1M Et_4NClO_4)		(7)d	(85.1)	(103.8)
CF_3COOH	AN	≈10 14(v)		-
(0.1M Et_4NClO_4)		(7)d	(85.1)	(103.8)
0.4M Pr_4NBr| 0.2M Br_2***	AN	≈2	70.3	101

* Completely dissociated
** Range Based on Λ_o^+ for NH_4^+ and Et_4N^+
*** B.E.R.
(i) Walden's Rule; Λ_o^{HCl} (Solvent) = Λ_o^{HCl}(1 Propanol) η_o(1 Propanol)/η_o(Solvent)
(ii) $K_A = (1-\alpha)/\alpha^2 c y_{\pm}^2$; Values of $y_{\pm}$ from Table 6.
(iii) $\alpha = \Lambda_i/\Lambda_o$; values of Λ_i for 0.1M HCl from Ref. 95; $\Lambda_o = \Lambda_o^+ + \Lambda_o^-$.
(iv) α (2 Propanol) = [Λ_o^{HCl}(2-Propanol)/Λ_o^{HCl}(1 Propanol)] (0.480) = 0.448.
(v) pK(AN) - pK(H_2O) ≈ 14 (ref. 5); $pK_{CF_3COOH}(H_2O)$ = 0.25.
(vi) $\Lambda_o^{Br^-}$ = 6.2

[a] ref. 82; [b] ref. 66; [c] ref. 92; [d] ref. 68; [e] ref. 93; [f] ref. 94.

ion (≈ -2.6 V vs S.C.E. for 0.1M Et_4NClO_4 in H_2O and ≈ 2 8 V vs S.C.E. for 0.1M Et_4NClO_4 in acetonitrile). Reduction of the quaternary ammonium ion at Hg leads to formation of an unstable amalgam in H_2O, but a stable grey, solid amalgam in acetonitrile (67). The cathodic potential ranges used for studies of the h.e.r. from the selected proton sources were well below the reduction potential limit of the supporting electrolyte and no change in the colour of the Hg or the polarization behaviour was noticed. A supporting electrolyte was not necessary for the other systems used as most of the acids and salts were strongly dissociated in their respective solvents at the low concentration (0.1M) used. Those systems that were only partially dissociated provided, however, enough electrolyte conductivity to cover at least 1.5 decades of linear-Tafel behaviour.

b) Choice of Anion

With the exception of Et_4NClO_4, the trifluoromethane-sulfonate anion ($CF_3SO_3^-$) was chosen as the anion for the salts and acid used in the aprotic solvents acetonitrile and N,N-dimethylformamide. Salts of this anion have excellent solubilities in nonaqueous solvents and dissociate to give solutions of very high conductivity comparable or better than that of salts of perchlorates and tetrafluoroborates. Trifluoromethane sulfonic acid (CF_3SO_3H) is completely dissociated in DMF and is a strong acid in the less basic solvent AN (pK_{HA}=2.60), (68). Also, the anion $CF_3SO_3^-$ has superior thermal stability, oxidative and reductive stability, and resistance to hydrolysis; also its salts

and acid are simple to prepare, purify and dehydrate Specific adsorption of the $CF_3SO_3^-$ anion on Hg in DMF and AN is similar to that for perchlorates (69) and is quite similar in aqueous solutions to that of perchlorate and nitrate anions (70, 71).

The choice of the chloride anion for the salts and acid used in the protic solvents (H_2O, alcohols, formamide) was dictated by the chemistry of the systems and the use of the Ag|AgCl reference electrode which could be employed without liquid junction in isothermal polarization measurements. Ideally, one would prefer to use salts and the acid of the $CF_3SO_3^-$ anion but trifluoromethanesulphonic acid is a powerful esterifying agent and would tend to esterify the alcohols. The choice of HCl as an acid for the alcohols was an obvious one, because it can be easily obtained in a dry, gaseous state and has been used in such media in previous work (13). In dilute protic media, Cl^- ions should not be appreciably adsorbed, especially at the high overpotentials which obtain at appreciable rates ($> 10^{-6}$ A/cm^2) of H_2 evolution (71, 72, 73).

c) Electrolyte Inertness

Potentials were always kept cathodic to the oxidation potential of Hg and the solvent windows were wide enough that the proton sources could be discharged before the reduction potential of the solvent was reached. Electrolyte systems were chosen which were thermally stable and chemically inert over the temperature range and time period studied. Formamide is thermally unstable at high temperature (b.p. = 473 K, decomposes), decomposing to carbon

monoxide and ammonia, and this limits the useful temperature range with this solvent to < 333 K. Of course, anhydrous conditions are essential to prevent hydrolysis of formamide, DMF and AN to ammonia and their respective carboxylic acids, which will occur under acidic conditions in the presence of H_2O

Polarographic studies of the electrochemical reduction of chlorine-containing acetic acids in the aprotic solvent DMF (75) indicate that one-electron transfer can occur with subsequent C-Cl bond breaking. Preliminary polarization measurements on a trichloroacetic acid solution in AN (0.1M CCl_3COOH, 0.1M Et_4NClO_4 in AN) gave erratic results. No H_2 bubble formation was observed over the potential range studied and addition of 5 cm^3 of the electrolyzed trichloroacetic acid solution to a solution of silver nitrate in H_2O gave a precipitate of AgCl, indicating that free Cl ion had been generated. Although the h.e.r. could not therefore be unambiguously studied from trichloroacetic acid in AN, no problems were indicated in the study of the h.e.r. from trifluoroacetic acid in AN. Polarography of the electrochemical reduction of trifluoroacetic acid in DMF (75) gives only one polarographic wave due to the solvated proton and no fluoride ions are detected in the electrolyzed solutions

An alcohol can interact with a hydrogen halide to form an alkylhalide and H_2O (76). Although HCl is the least reactive of the hydrogen halides, the rate of the reaction increases with increasing temperature and depends on the reactivity of the alcohol (allyl, benzyl > tertiary > secondary > primary < CH_3)

Samples of the alcoholic hydrochloride solutions used in this study were checked before and after temperature cycling for the presence of alkyl halides with a Perkin-Elmer 283 infrared spectrophotometer. No absorption bands were found in the infrared region of 800 cm^{-1} to 550 cm^{1} where absorption due to the C-Cl stretching mode is strong. Preliminary polarization measurements on a solution of HCl in tertiary butanol gave erratic results and the solution showed very strong absorption at 750 cm^{-1} indicating appreciable alkyl halide formation . This system is therefore also unsatisfactory.

3. Experimental Method

Polarization measurements were conducted with a reference electrode at the same but varied temperature as that of the working electrode (isothermal measurement). Corrections were then made to the potential scale used by means of separate measurements of non-isothermal reference cell potentials where the thermal junction potential was minimized. This approach has also been adopted by Weaver and coworkers (77, 78) in their studies of complex ion redox reactions and will be discussed in detail in the next section.

The steady-state polarization measurements were made by holding the potential constant for about 30 seconds by means of a potentiostat before recording the current and at least 10 points were taken per decade of current change. This rapid procedure of current measurement has been shown to be preferable to the slow

procedure (79) partly because time-dependent electrolytic deposition of trace impurities at Hg is minimized or residual reduction processes are avoided.

The uncompensated solution resistance and the open-circuit potential decay measurements were made at the same time as the polarization measurements, also to minimize any time-dependent effects. In order to determine the reproducibility or hysteresis behaviour of the steady-state polarization measurements i) the temperature program was repeated at least twice for each electrolyte system and ii) at each temperature, current measurements were taken for directions of increasing and decreasing potential change.

4. Preparation and Purification of Solutions and Gases

a) Solvents

Preliminary experiments indicated no difference in polarization behaviour between experiments conducted with pyrodistilled H_2O (80) and doubly distilled H_2O, so that the latter was used for the aqueous solution experiments Spectroscopic grade methanol and 2-propanol were further purified by refluxing over dried CaO (12 hours), followed by double distillation in an atmosphere of dried purified nitrogen. Karl Fischer analysis of the middle fractions indicated a higher concentration of H_2O in the distilled solvents than in the solvents directly from the bottle. Therefore, the following Burdick and Jackson spectroscopically pure solvents (with their

water content determined by Karl Fischer analysis) were used directly: methanol (<0.015% H_2O), 1-propanol (<0.029% H_2O), 2-propanol (<0.052% H_2O), isobutanol (<0.005% H_2O), DMF (<0.008% H_2O) and AN (<0.006% H_2O). Formamide (Fluka, purity >99%) which is known to decompose in time, was refluxed over dried CaO (12 hours) in a dried purified nitrogen atmosphere and then vacuum distilled twice (342 K, <1 torr). Conductivity measurements on the collected middle fraction using a Sybron/Barnstead conductivity meter (PM-70CB) gave a specific conductance of ca. $13.8 \times 10^{-6} \Omega^{-1} cm^{-1}$ at 298 K, well within the range of (900 to 1500)$10^{-8} \Omega^{-1} cm^{-1}$ for pure formamide cited in the literature (81, 82, 66). The formamide was used immediately after purification because it is difficult to keep in a high state of purity for extended periods of time

b) Salts and Acids

The alcoholic HCl solutions were prepared by bubbling dry electronic grade HCl (purity >99.99%) through the respective alcohols at a slow rate to minimize heating The concentrations of the solutions were determined by titration on separate samples The gas transfer system was flushed out with HCl gas for about 30 minutes before bubbling, to remove any traces of moisture Preliminary experiments indicated no difference in polarization behaviour between aqueous HCl prepared as above, and solutions prepared directly from high purity Aristar hydrochloric acid.

Trifluoromethanesulfonic acid (3M Company) was purified by double distillation at atmospheric pressure (b p 435 K) in a

nitrogen stream with trifluoromethanesulfonic anhydride added before the second distillation to remove any traces of H_2O The anhydride (b.p. 357 K) was prepared by distillation of the acid in a nitrogen stream from P_2O_5 (84). The monohydrate, $CF_3SO_3^-H_3O^+$, was prepared and purified as described previously (85). A stoichiometric quantity of pyrodistilled water was added to the purified acid and the monohydrate formed was vacuum distilled twice (355 K, <1 torr) in an all-glass apparatus. The distilled fractions were collected in Pyrex collection ampoules which were immediately sealed under vacuum for subsequent use. The Aldrich Gold Label grade acids, CH_3COOH and CF_3COOH were used directly without further purification. For the electrolyte systems containing the acids CH_3COOH, CF_3COOH or CF_3SO_3H a small amount of the acid anhydride (≈0.01 M) was added to react with any residual H_2O as a "getter" to attain ultra-dry conditions.

The triethylamine trifluoromethanesulphonate salt, $(C_2H_5)_3NHCF_3SO_3$, was prepared by adding the purified acid, CF_3SO_3H slowly to a large excess of $(C_2H_5)_3N$ (Fluka, purity >99.5%, H_2O<0.05%) kept at 233 K. The salt (m.p. 314 K) was recrystallized several times from reagent grade diethyl ether and then vacuum dried at ca. 298 K for several days. The high purity Fluka salts $(C_2H_5)_3NHCl$, $(C_2H_5)NH_3Cl$, $C_2H_5)_4NCl$ and $(C_2H_7)_4NBr$ were recrystallized twice from spectroscopic grade methanol and vacuum dried at 333K for several days. High purity tetraethylammonium perchlorate (Eastman Kodak Co.,) was recrystallized twice from doubly distilled H_2O and vacuum dried at

343 K for several days. The melting points of the salts were used as a criterion of purity Weighing and transfer of the very hygroscopic solutes, CF_3SO_3H, $CF_3SO_3H_3O^+$ and $(C_2H_5)_3NHCF_3SO_3$ was done in a Vacuum Atmospheres glove box under a positive pressure of dry nitrogen.

c) Gases

Ultra high purity (purity >99.999%) hydrogen and nitrogen gases for use in the polarization and reference electrode cells were subjected to a further purification operation before use, mainly to remove traces of O_2 that may be incidently introduced from the air. Hydrogen gas was passed through a conventional purification train consisting of the drying agent magnesium perchlorate, a molecular sieve, an oven containing palladized asbestos and Cu turning at 632 K and finally two activated charcoal traps maintained at liquid nitrogen temperature. Nitrogen gas was passed through an identical purification train with the exception that only Cu turnings were used in the oven. The Cu turnings were regenerated periodically by passing hydrogen through the oven until the Cu turnings were in a bright metallic state

5 Electrochemical Cells

a) Main Cell

The main cell used for the steady-state polarization and transient experiments is shown in Fig 14. The separate counter and reference electrode compartments, working electrode,

temperature probe, and bubbler were inserted into the working electrode compartment through the cell top. The use of these insertable components into one cylindrical compartment (diameter = 5.6 cm) i) allowed the cell to be conveniently placed in a Dewar flask for temperature control and ii) prevented contact between any ground-glass joints and Teflon seals of the cell with the temperature bath. The use of Teflon seals allowed the positions of the counter electrode compartment, reference electrode Luggin capillary and working electrode to be adjusted relative to each other. Adjustment was made to give a well defined symmetrical current field between the working and counter electrodes, and to minimize the solution potential drop between the working electrode and reference Luggin capillary. The integrity of the Teflon seals and ground glass joints was sufficient to reduce oxygen diffusion (cathode depolarizer) to very low values ($<10^{-6}$ A/cm^2) after hydrogen bubbling. The cell was effectively isolated from the atmosphere by passage of H_2 for the h.e.r. and N_2 for the b.e.r. through a presaturator directly into the cell and out of the cell through bubblers.

b) Counter Electrode Compartment

The counter electrode compartment was isolated from the working electrode compartment by means of a specially designed ground glass disk (See Fig. 14) approximately 1-2 mm in thickness. This design was used to reduce resistance in the circuit so that higher overpotentials (extended Tafel region) could be obtained before reaching the limiting maximum output voltage of the

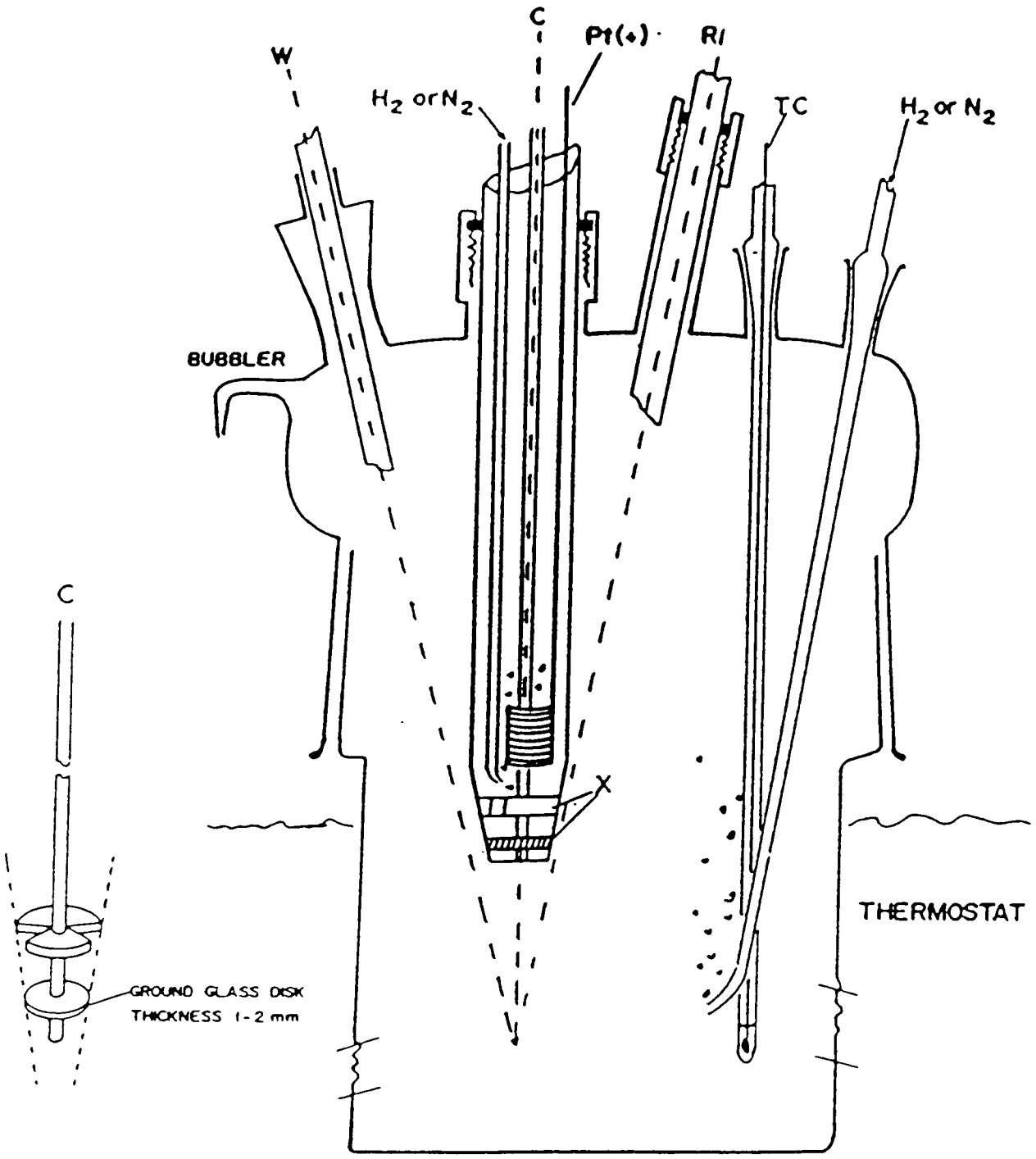

Fig. 14 Schematic diagram of the main electrochemical cell and the specially designed ground glass disk for use in the counter electrode compartment

potentiostat. Each disk was checked in the counter electrode compartment to see if it held a vacuum (<1 torr). In order to further reduce migration of oxidation products from the counter electrode compartment to the working electrode compartment i) the counter-electrode solution was replaced regularly and ii) the solution level in the working-electrode compartment was always kept higher than in the counter electrode compartment.

c) Reference Electrode Cell

Non-isothermal and isothermal reference electrode measurements were made using the cell shown in Fig. 15. A thermostated fluid (water or ethanol) was circulated through each jacket. The salt bridge compartment was filled through a side arm which could accommodate volume expansion and contraction of the solution during temperature cycling. For non-isothermal measurements, the jacketed compartment next to the side arm was kept at 298 K and the thermal liquid junction was established in the 1 cm x 0.8 cm i.d. tube between the jacketed compartments. The short distance between the compartments ensured only a negligible development of concentration polarization due to thermal diffusion (Soret effect). The plugs were removed by placing the cell in hot water in an ultrasonic bath.

d) Temperature Control

For the low temperature experiments (173 K < T < 298 K) the polarization cell was placed in a large Dewar flask containing technical grade 99% ethanol (f.p. 158.5 K) which was agitated using a nitrogen gas stream. A CC-100 Neslab Cryo Cool immersion

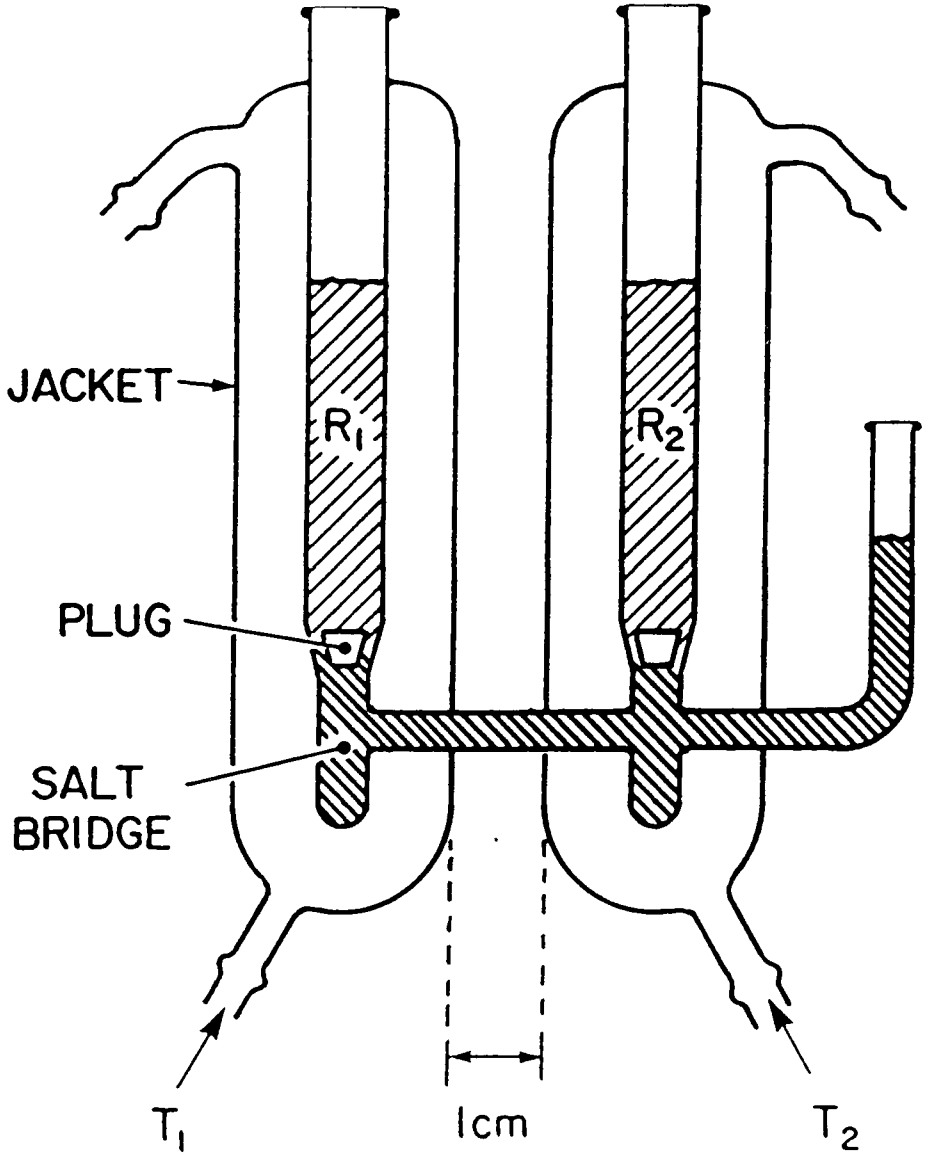

Fig. 15 Jacketed non-isothermal reference electrode cell with provision for a salt bridge in the region of the thermal liquid junction.

cooler with a flexible cooling probe could maintain the temperature, at low temperatures, to within ± 0.5 K. For experiments above room temperature (T<358 K) a thermostated water bath (±0.1 K) was used. The level of the electrolyte in the cell was always kept below that of the thermostated fluid. Chromel alumel thermocouples (reference junction at 273 K) were used to measure the temperature inside the cell and in the surrounding thermostated fluid, and electrochemical measurements were only started when these temperatures were equal.

e) Cleaning and Preparation

Prior to each experiment, the cell and its glass component parts were immersed in fresh concentrated chromic-sulfuric acid solution for about 12 hours, then rinsed many times with doubly distilled water and finally soaked in doubly distilled water for at least 24 hours to remove any chromate ions. For the experiments in nonaqueous media, the cell and component parts were dried in an oven at 413 K for about 12 hours in order to remove any residual water. The cell was assembled a few minutes after removal from the oven and then flushed out with dry, purified hydrogen or nitrogen for about 30 minutes before the electrolyte was transferred.

6. Electrodes

a) Reference Electrodes

Non-isothermal cell measurements, in which the potential of a temperature-invariant reference electrode (298 K) was compared to the potential of another temperature-varied reference electrode,

were used to determine the reversibility and reproducibility of the reference electrodes. Electrodes which are not behaving reversibly do not give steady, time-independent values of potential and only rarely give identical potentials. Satisfactory performance of the reference electrodes was indicated by i) time-independent reproducibility of the non-isothermal cell measurements over the temperature range of study; ii) agreement to within 1 mV of the isothermal potential taken at several different temperatures and iii) immediate recovery of the initial relative potential of a pair of hydrogen reference electrodes when nitrogen bubbling was replaced by hydrogen bubbling.

i) Hydrogen Reference Electrode

The hydrogen reference electrodes were prepared according to the procedure given by Ives and Janz (86) and were used in the cell without liquid junction (see Fig. 16). Lead acetate was not used in the platinizing solution (2% H_2PtCl_6 in 2N HCl) because of the possibility of introducing undesirable impurities into the working electrode electrolyte. Thick deposits of platinum black were avoided because they lead to sluggish, erratic behaviour and pieces of the deposit could fall off and contact the Hg electrode Freshly prepared hydrogen reference electrodes were thoroughly washed with distilled water and kept in the appropriate solvent until required. In preliminary experiments it was found that the hydrogen reference electrode was not suitable for use in solutions containing $(C_2H_5)_3NH^+$ and $(C_2H_5)NH_3^+$(> 20 mV variations) probably because, in neutral solutions (pH ≈7) in the absence of buffers

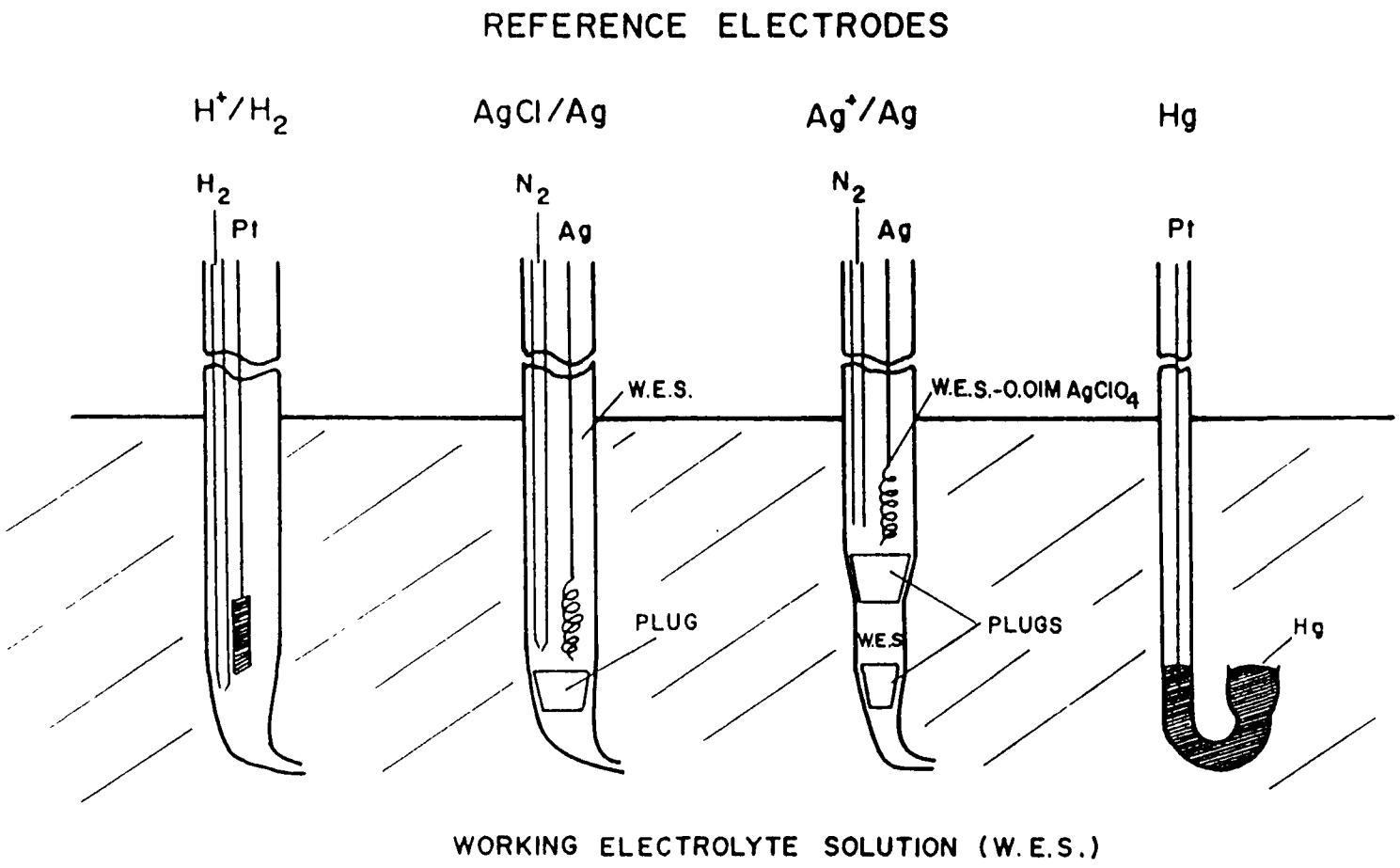

Fig. 16 Schematic diagram of the electrodes used in the main electrochemical cell.

the solutions are extremely susceptible to disturbances of pH.

ii) Silver-Silver Chloride Reference Electrode

Silver-silver chloride reference electrodes were prepared electrolytically in pairs using pure silver wire according to the procedure given by Ives and Janz (86) and could be used in the cell with negligible liquid-junction potential (See Fig. 16). Freshly prepared electrodes were thoroughly washed with distilled water and kept in the appropriate solvent for at least 2 days before use. A ground glass plug was used to separate the reference from the working electrode compartment to minimize the diffusion of Ag^+ and anionic complexes (e.g. $AgCl_2^-$) to the Hg electrode. The reference electrode compartment was bubbled out with dry nitrogen to remove dissolved air in the solution which can cause poor electrode behaviour due to the slow oxidation reaction.

$$2\ Ag + 2\ HCl + 1/2\ O_2 \rightarrow 2\ AgCl + H_2O \qquad [19]$$

From the point of view of forming an effective Ag|AgCl reference electrode without an appreciable liquid-junction potential the equilibrium constant K_f for the reaction

$$AgCl_{(S)} + Cl^- = AgCl_2^- \qquad [20]$$

is more important than the solubility product K_s for AgCl. These constants are given at 298 K for the solvents used (87) as follows: H_2O, $\log K_s = -9.42$, $\log K_f = -4.70$; methanol, $\log K_s = 13.0$, $\log K_f = 5.0$; formamide, $\log K_s = -8.28$, $\log K_f = 2.12$. The equilibrium constants indicate that the concentrations of Ag^+ and $AgCl_2^-$ are very small compared to the electrolyte concentration

and would lead to only a negligible liquid-junction potential.

iii) Silver-Silver Ion Reference Electrode

The silver-silver ion electrode is reversible in most aprotic solvents but there is some doubt about its stability in DMF because Ag^+ may oxidize the solvent. However, many authors have used the $Ag|Ag^+$ electrode in DMF successfully and the Nernst relation has been verified (87). In this study, the electrode was found to be very stable in both DMF and AN.

The electrode was easily made by putting a silver wire in a solution containing 0.01M $AgClO_4$. The pure silver wire was cleaned in 3M nitric acid, washed thoroughly with distilled water and kept in the appropriate solvent until required. The reference electrode compartment shown in Fig. 16, was separated from the working electrode compartment by two ground glass plugs in order to minimize diffusion of Ag^+ to the Hg electrode. This was verified by the reproducibility of polarization measurements over a period of 96 hours, using the same Hg electrode.

The liquid-junction potential of the $Ag|Ag^+$ reference electrode half cell

$Ag|0.01M\ AgClO_4, 0.1M\ M^+,B^-||0.1M\ M^+,B^-||0.1M\ M^+,B^-....$

should be negligible because the concentration of the electrolyte is almost tenfold that of Ag^+ and ClO_4^- and will "swamp out" the effect of these ions. Also, based on the limiting ionic conductivities of Ag^+ and ClO_4^- in DMF ($\Lambda_o^+ = 35.2\ cm^2\Omega^{-1}mole^{-1}$, $\Lambda_o^- = 52.4\ cm^2\Omega^{-1}mole^{-1}$) and in AN ($\Lambda_o^+ = 86.2\ cm^2\Omega^{-1}\ mole^{-1}$, $\Lambda_o^- = 103.8\ cm^2\Omega^{-1}mole^{-1}$) the transference numbers are probably similar

for the cation and anion, one of the conditions desirable for minimization of liquid junction potential

iv) Bromine Reference Electrode

For the anodic oxidation of Br^- at vitreous carbon in AN, a rod of ultra "F" purity graphite (total metallic impurity < 5 ppm, Union Carbide Corp.) which had previously been cleaned and soaked in AN was used as the reference electrode. The electrode was used in the cell without liquid junction and gave a relative potential less than 1 mV when compared to the vitreous carbon working electrode in the same solution.

b) Working Electrodes

i) Mercury

Preliminary experiments using a hanging mercury drop electrode (Metrohm EA 290 HMDE) were unsatisfactory because of solution creep along the capillary walls which led to interruption of the Hg thread at high potentials. A Hg pool electrode (see Fig. 16) was therefore constructed and was used successfully It consisted of a silanized pyrex glass cup containing pure liquid Hg (Aldrich Gold Label, 99.99999%) giving an area of about 0 393 cm^2 The change in the surface area upon solidification of the Hg is less than 10% according to Ksenfontov et al (88) Electrical connection was made by contact of a Pt wire with the Hg at the backside of the pool, furthest away from the working electrode's surface.

The most serious difficulty with the Hg electrode was creeping of the electrolyte solution between the Hg and glass

This changes the accessible surface area of the electrode and can result in poor reproducibility of measurements and frequency-dependent double-layer capacitance results. Creeping of the electrolyte was minimized by ensuring a clear, smooth glass surface (89) and covering it with a hydrophobic silicone coating (90). The following silanisation procedure was used with success:

a) Immersion in 65% nitric acid to remove Hg residues.

b) A rinse with distilled H_2O.

c) Immersion in a 50/50 HF|HCl solution for ca. 30 seconds

d) A rinse with distilled H_2O.

e) Drying for 2 hours at 403 K 413 K.

f) Repeated dipping in a solution of 6% $(CH_3)_2SiCl_2$ in toluene

g) Drying for 2-3 hours at 403 K 413 K.

The Hg pool electrode was resilanized regularly to prevent solvent creep, and the Hg was replaced regularly to prevent any accumulation of impurities at the Hg surface.

ii) Vitreous Carbon

Vitreous carbon electrodes (Vitrecarb Co) for use in the bromine evolution reaction were prepared by heat-shrinking a Teflon sleeve onto a rod of vitreous carbon. This formed a leakproof seal without contamination by any sealing compounds and Hg was used within the insulating sleeve in order to make electrical contact with the C rod. The geometrical area of the smooth, non-porous electrode surface (ca. 0 8 cm^2) was used to

compute the real current densities.

c) The Counter Electrode

A platinized platinum gauze having a very large surface area was used as the counter electrode. The large surface area minimizes the reaction resistance and the polarization of the electrode which also reduces any dissolution of Pt (26).

7 Electrical Circuit

The electrical circuit used for the polarization and potential decay measurements is shown schematically in Fig. 17. The potential of the working electrode was controlled to within 1 mV using a Wenking HP72 potentiostat (small signal rise time, <10 μsec). The potential between the working and reference electrodes was applied through a high-impedance Tektronix AM501 operational amplifier in cathode follower configuration to a multimeter and oscilloscope. The current was measured by means of a Racal Dana 4002 digital multimeter (range 0.01 μA to 2000 μA) in the counter electrode circuit and was checked periodically with a precision Leeds and Northrup resistance box. A Hg-wetted relay in the counter electrode circuit was used to interrupt the steady-state current and the resulting potential decay was followed by means of a Nicolet 2090 digital oscilloscope (4096 data points, maximum speed 0.5 μsec per point).

8. Solution Resistance Compensation

Generally, ohmic solution potential drop corrections are specially important at low temperatures and for non-aqueous

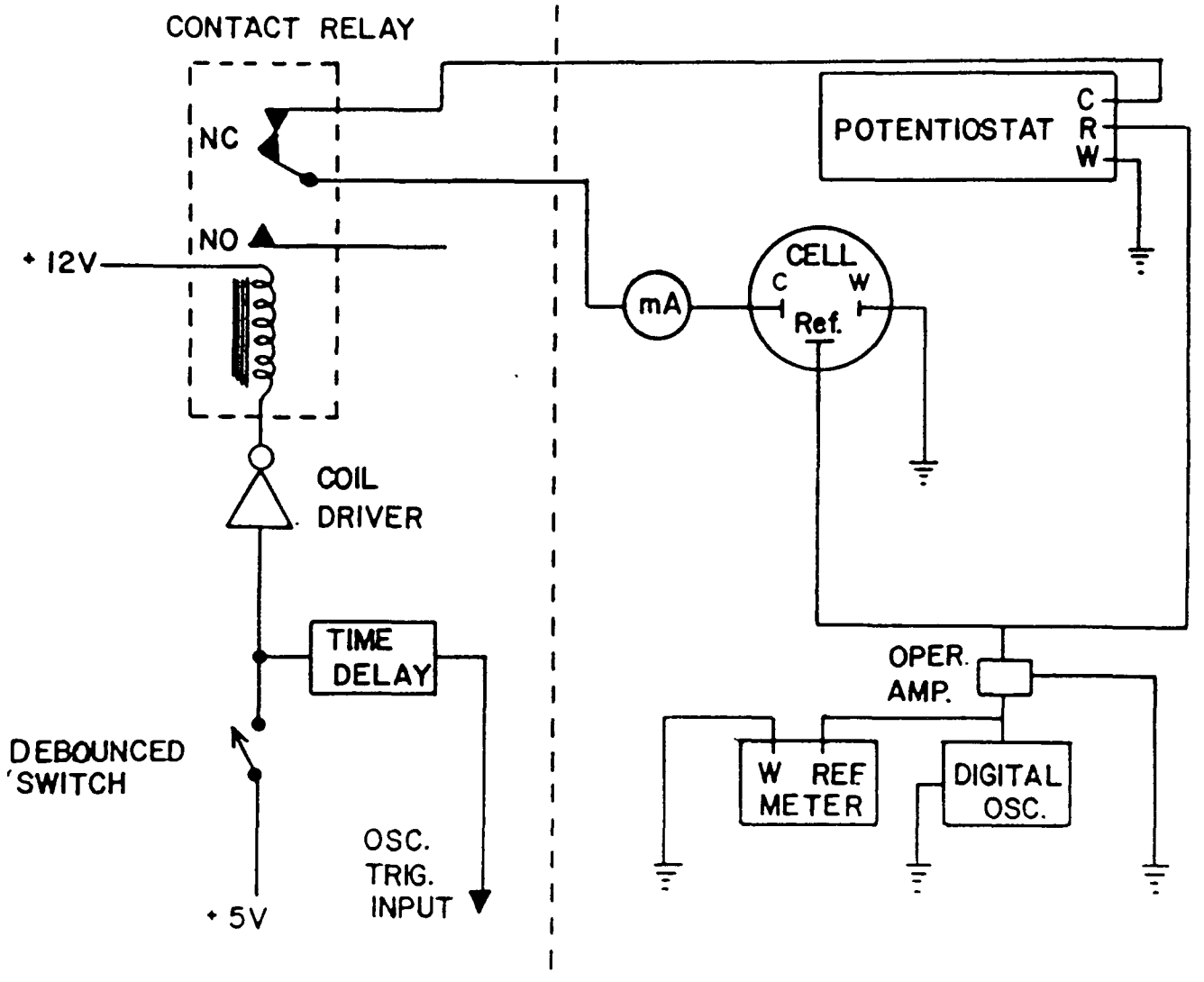

Fig. 17 Electrical circuit for steady-state polarization and potential decay measurements

systems because of lower electrolyte conductivity When a net current is passed across an electrode interface, the reference electrode Luggin capillary measures a finite potential drop, iR_s, in the solution as well as the interfacial potential difference, ΔV.

$$V_{observed} = \Delta V + iR_s \qquad [21]$$

This situation can be represented by the equivalent circuit shown in Fig. 18 which, for the electrodes used here, does not require a potential-dependent pseudocapacitance to be included. For Tafel behaviour

$$V_{observed} = b \log(i/i_o) + iR_s \qquad [22]$$

so that the solution potential drop is more strongly dependent on i than the overpotential component which is only logarithmic in i, and thus will eventually be dominated by the iR_s

The solution potential drop was determined for several different currents at each temperature by means of current interruption. The resulting potential decays were practically instantaneous across the solution resistance but usually much slower across the interfacial impedance Plots of the solution potential drop versus the current were linear, passed through the origin, and the slope of the plot gave a unique value of the solution resistance, R_s, which was used to correct the polarization data. The potential decays on the fast time scale (0 5 μsec per point) of the digital oscilloscope usually showed some sort of initial downward spike (<50 μsec) probably due to an instrumental effect, before recovering and decaying normally

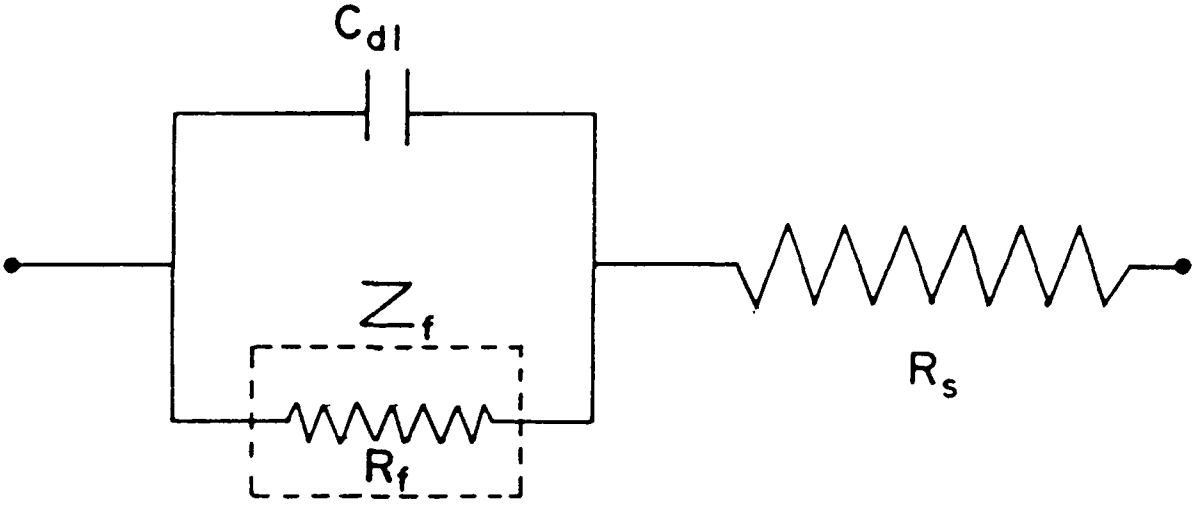

Fig 18 Equivalent circuit for the electrode interface and solution resistance.

Extrapolation of the potential decays back to zero time gave values of the solution resistance that, when used to correct the polarization data, were consistent with linear Tafel behaviour. For the anodic b.e.r., values of the solution resistance determined by the interruption method were in agreement with those determined by a.c impedance measurements.

CHAPTER 3

EXPERIMENTAL RESULTS

1 Cathodic and Anodic Polarization Curves

Log (current)-potential relations were obtained for proton discharge at Hg from several proton sources (H_3O^+, ROH^+_2, $DMFH^+$, $EtNH_3^+$, Et_3NH^+, H_2O, CH_3COOH, CF_3COOH) in aqueous and nonaqueous media (CH_3OH, 1-propanol, 2-propanol, isobutanol, $HCONH_2$, DMF and AN) over a wide range of temperature and are shown in Figs. 19-36. In some cases polarization data were also obtained at solid Hg (F.P. = 234.2 K) Log (current)-potential relations were also obtained for bromide discharge at vitreous carbon from 0 4M Pr_4NBr, 0.2M Br_2 in AN as function of temperature and are shown in Fig. 37.

All polarization measurements were conducted with the reference electrode at the same but varied temperature as that of the working electrode (isothermal measurement). The reference electrode electrolytes were the same as that in the working electrode compartment with the exception of the $Ag^+|Ag$ reference electrode electrolyte which contained 0.01M $AgClO_4$ in addition to the working electrolyte solution.

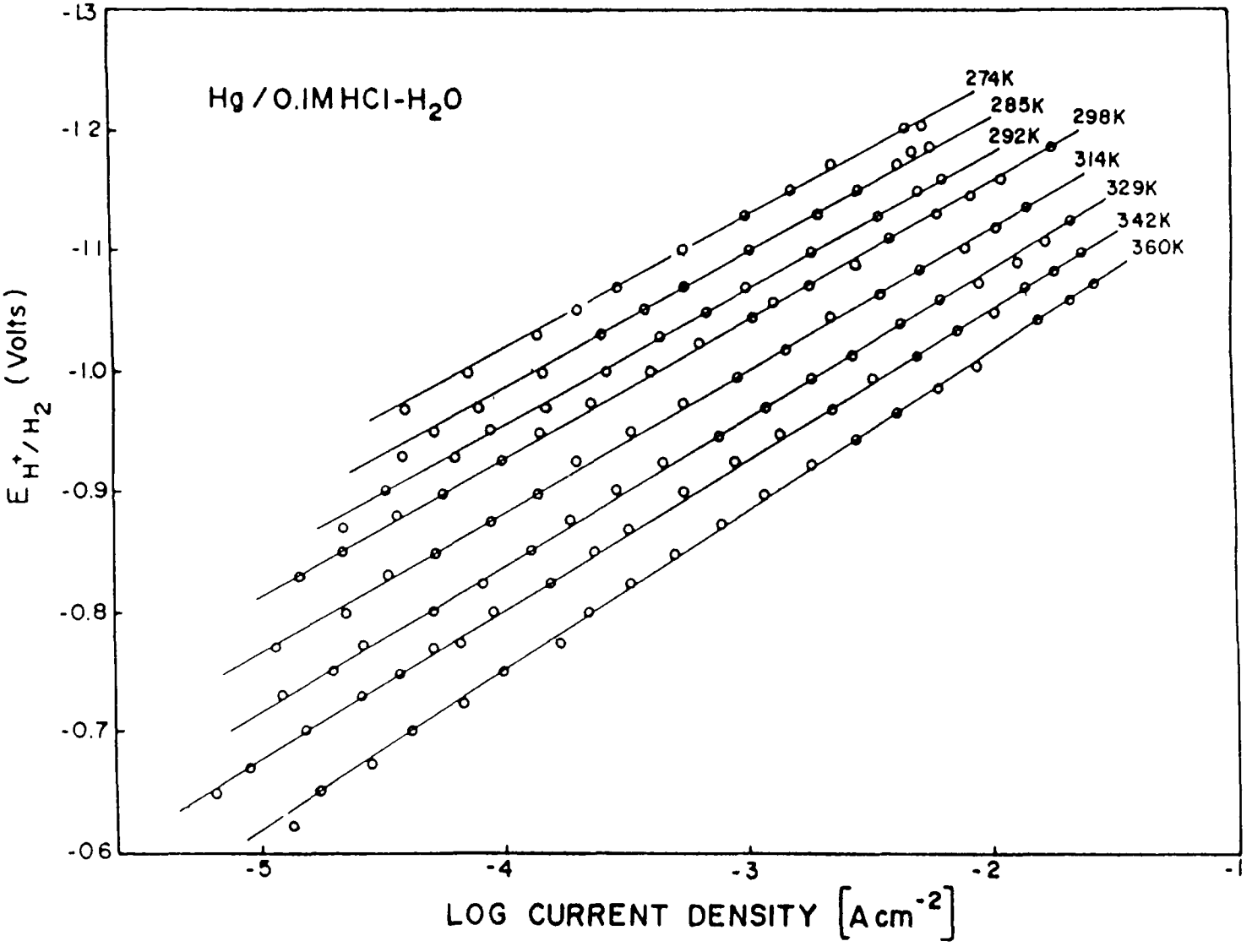

Fig. 19 Log (current)-potential relations for the h.e.r. at Hg in 0 1M aqueous HCl as a function of temperature ($H^+|H_2$ reference electrode).

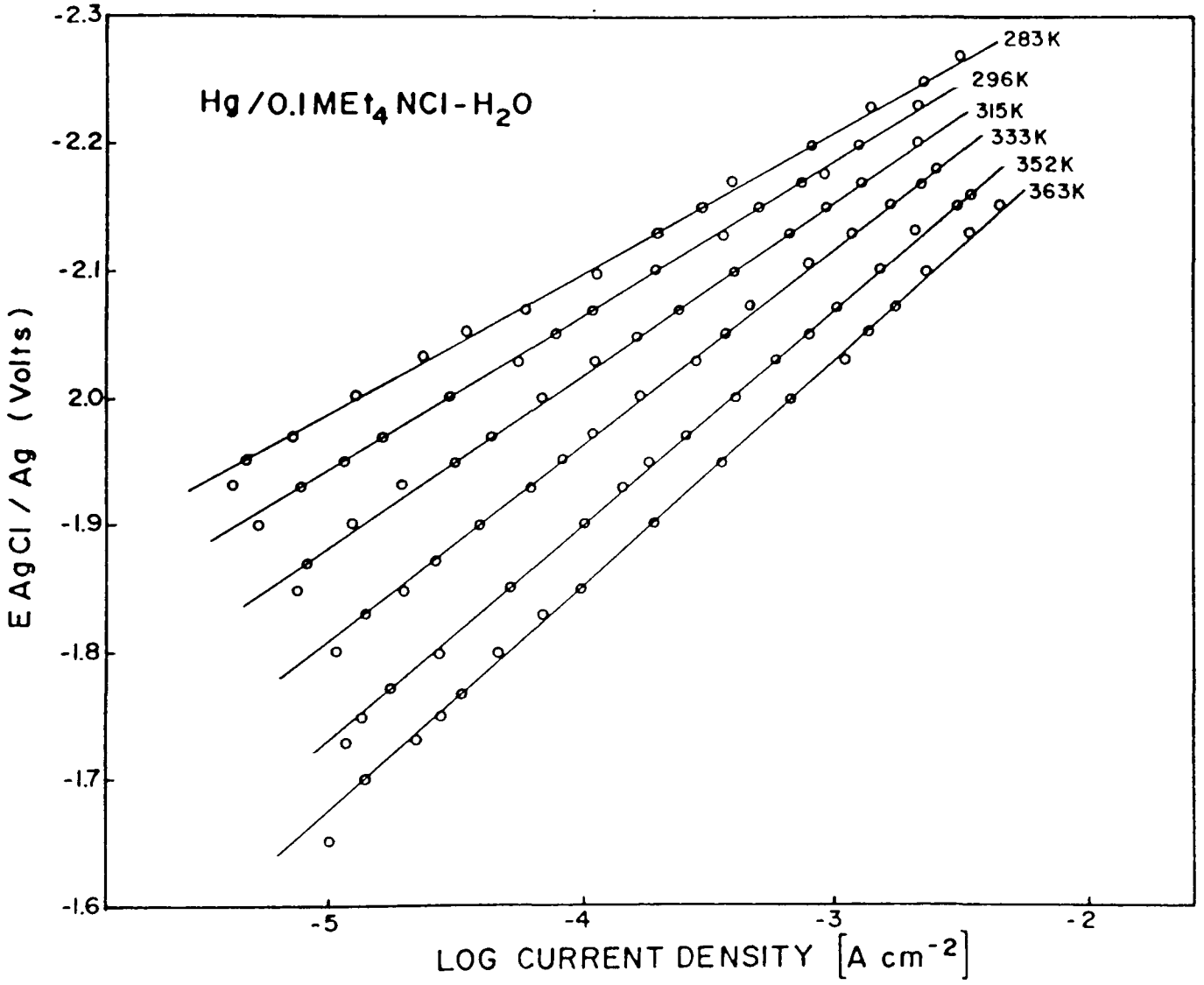

Fig. 20 Log (current)-potential relations for the h e r at Hg in 0 1M aqueous Et_4NCl as a function of temperature (AgCl|Ag reference electrode)

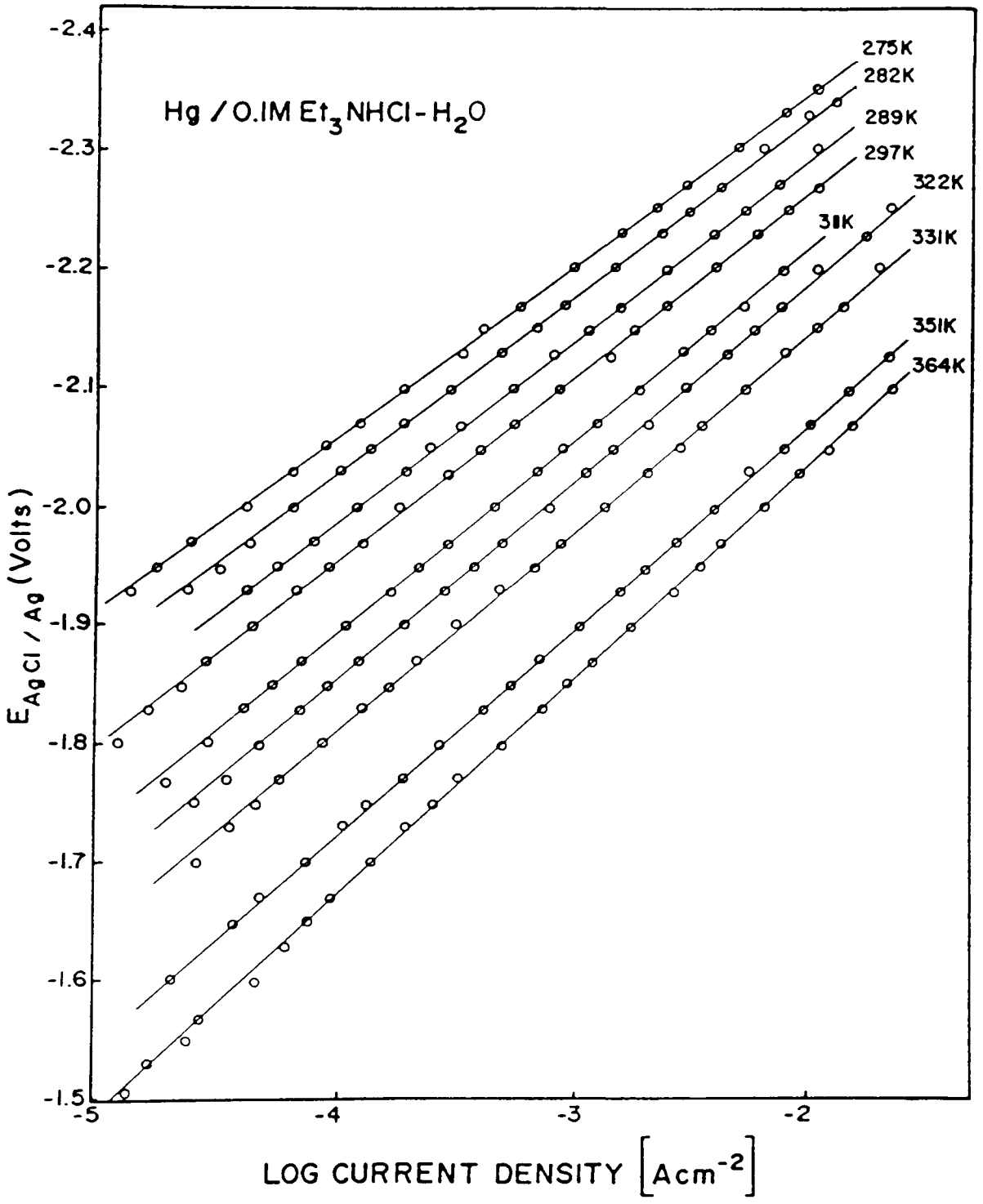

Fig. 21 Log (current)-potential relations for the h.e.r at Hg in 0 1M aqueous Et_3NHCl as a function of temperature (AgCl|Ag reference electrode)

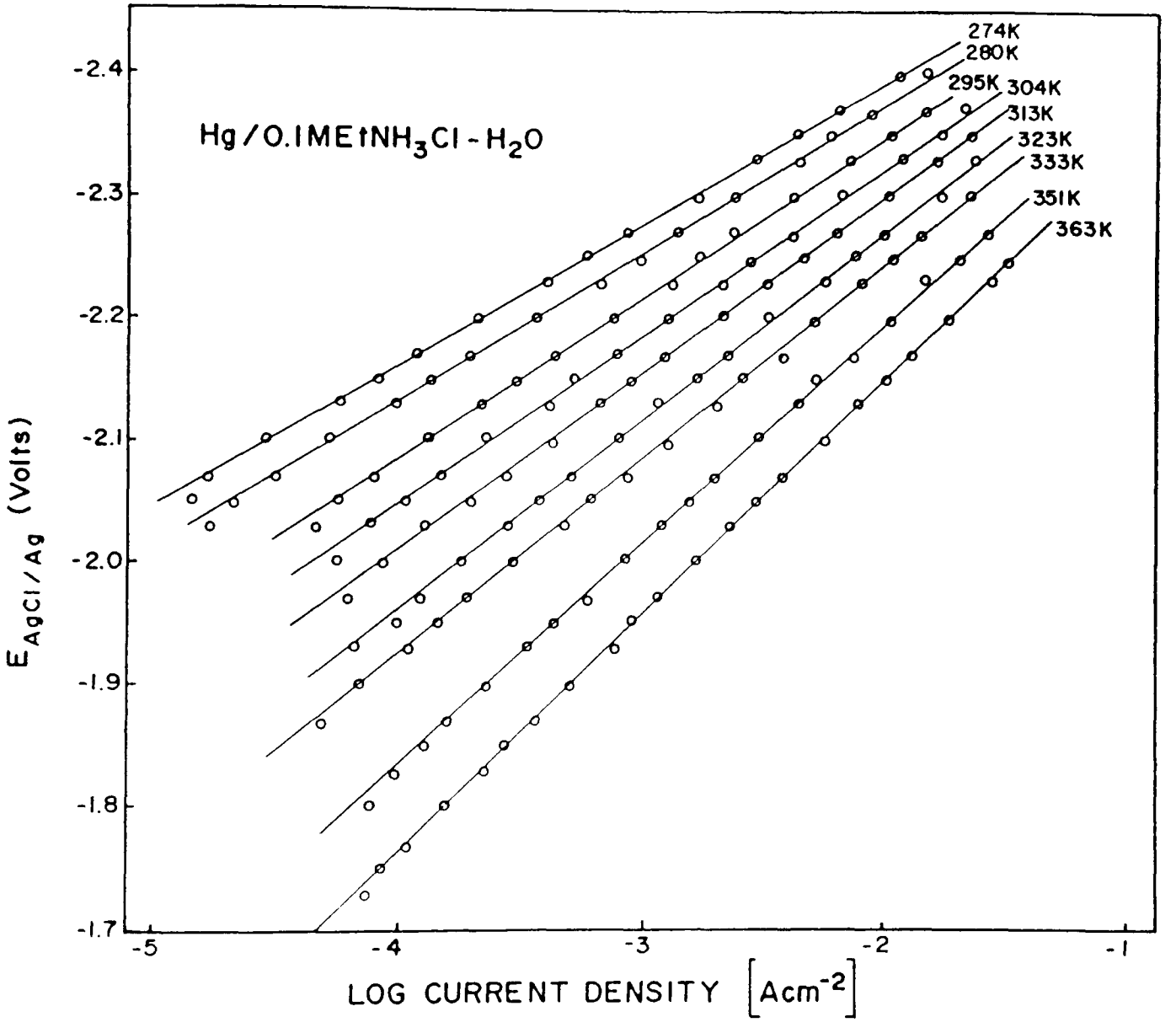

Fig. 22 Log (current)-potential relations for the h.e.r at Hg in 0 1M aqueous $EtNH_3Cl$ as a function of temperature (AgCl|Ag reference electrode)

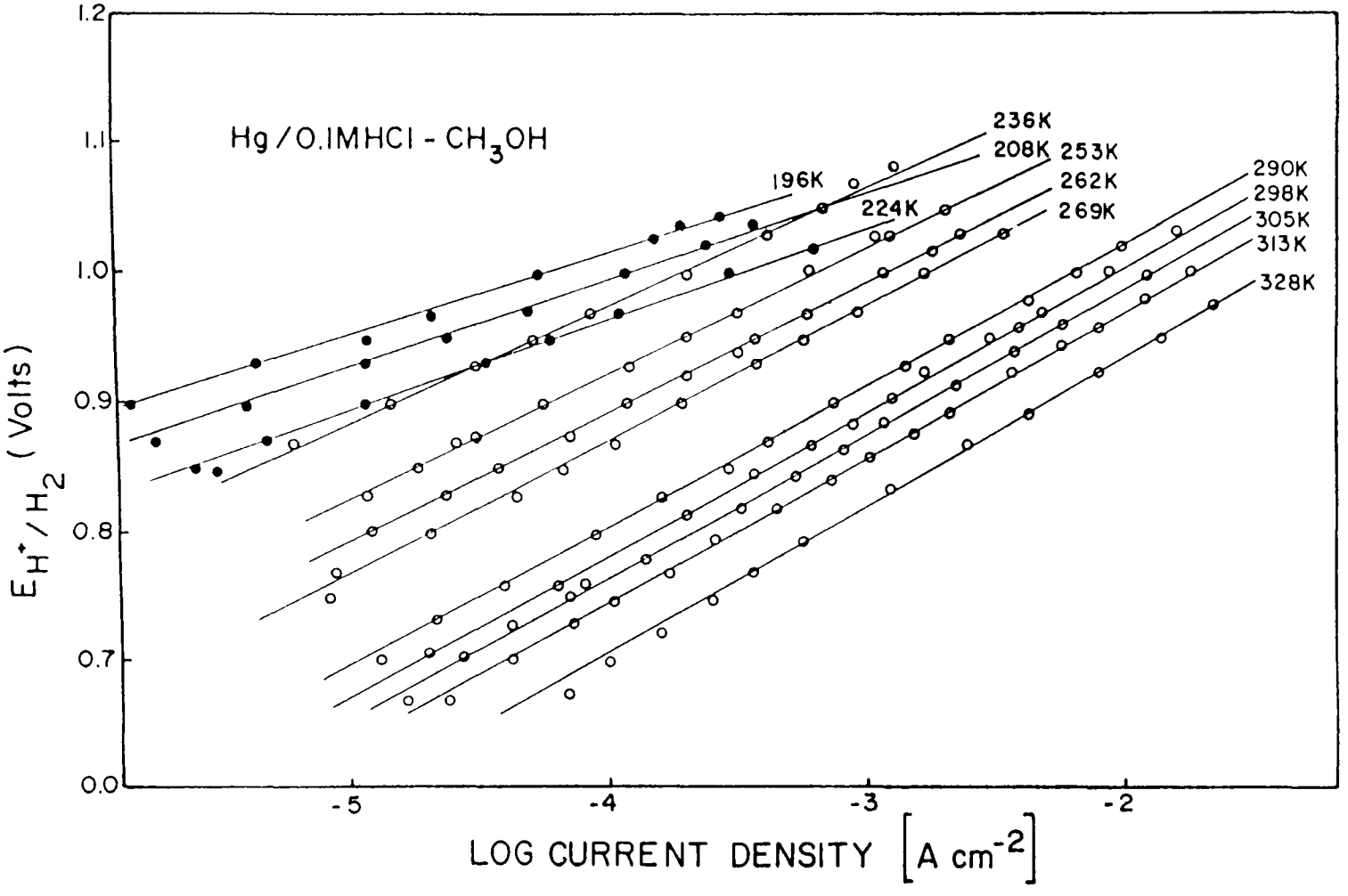

Fig 23 Log (current)-potential relations for the h.e r. at Hg from 0.1M HCl in CH_3OH as a function of temperature ($H^+|H_2$ reference electrode). •, solid Hg; o, liquid Hg

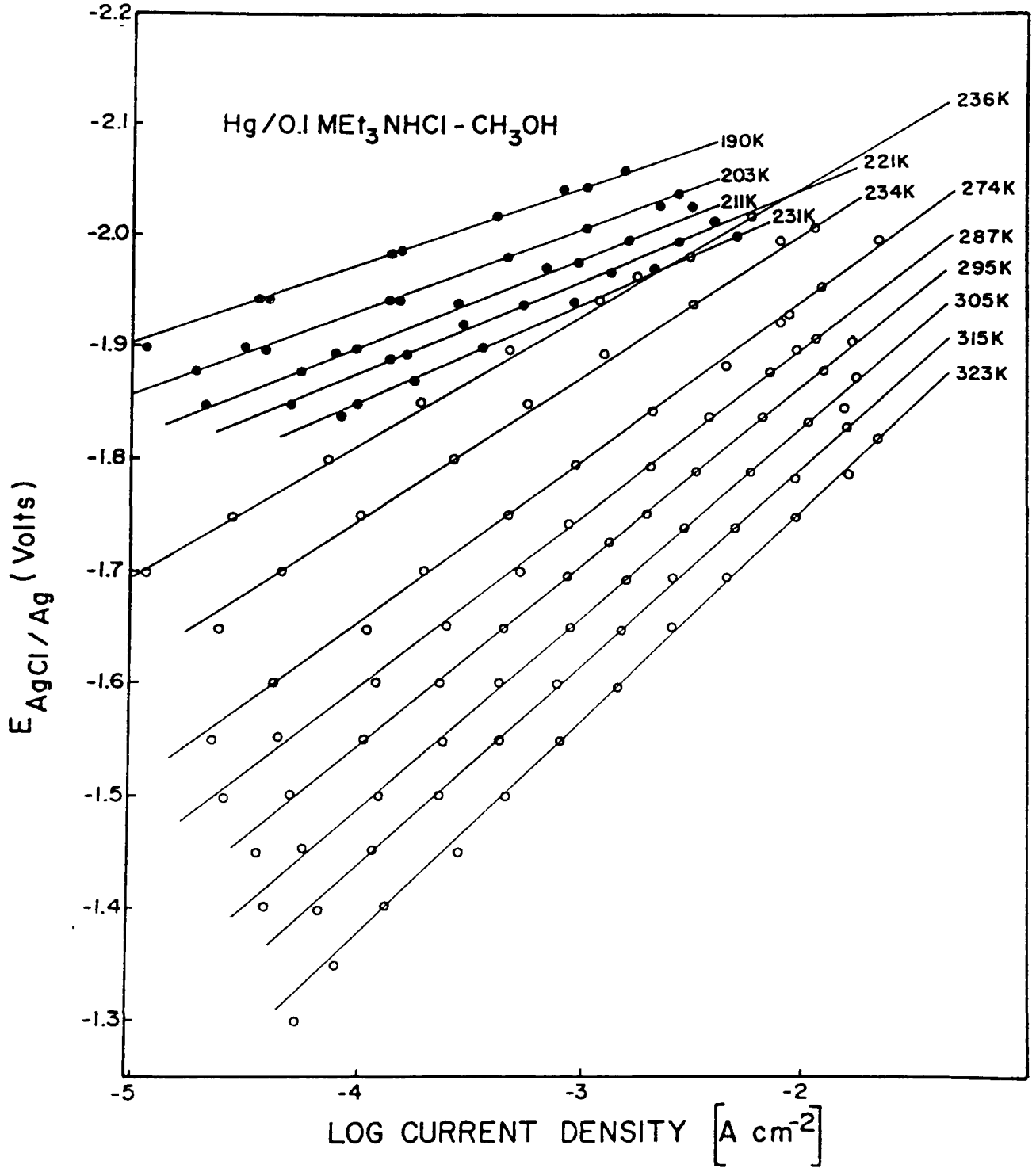

Fig. 24 Log (current)-potential relations for the h.e.r at Hg from 0.1M Et_3NHCl in CH_3OH as a function of temperature (AgCl|Ag reference electrode). •, solid Hg; o, liquid Hg.

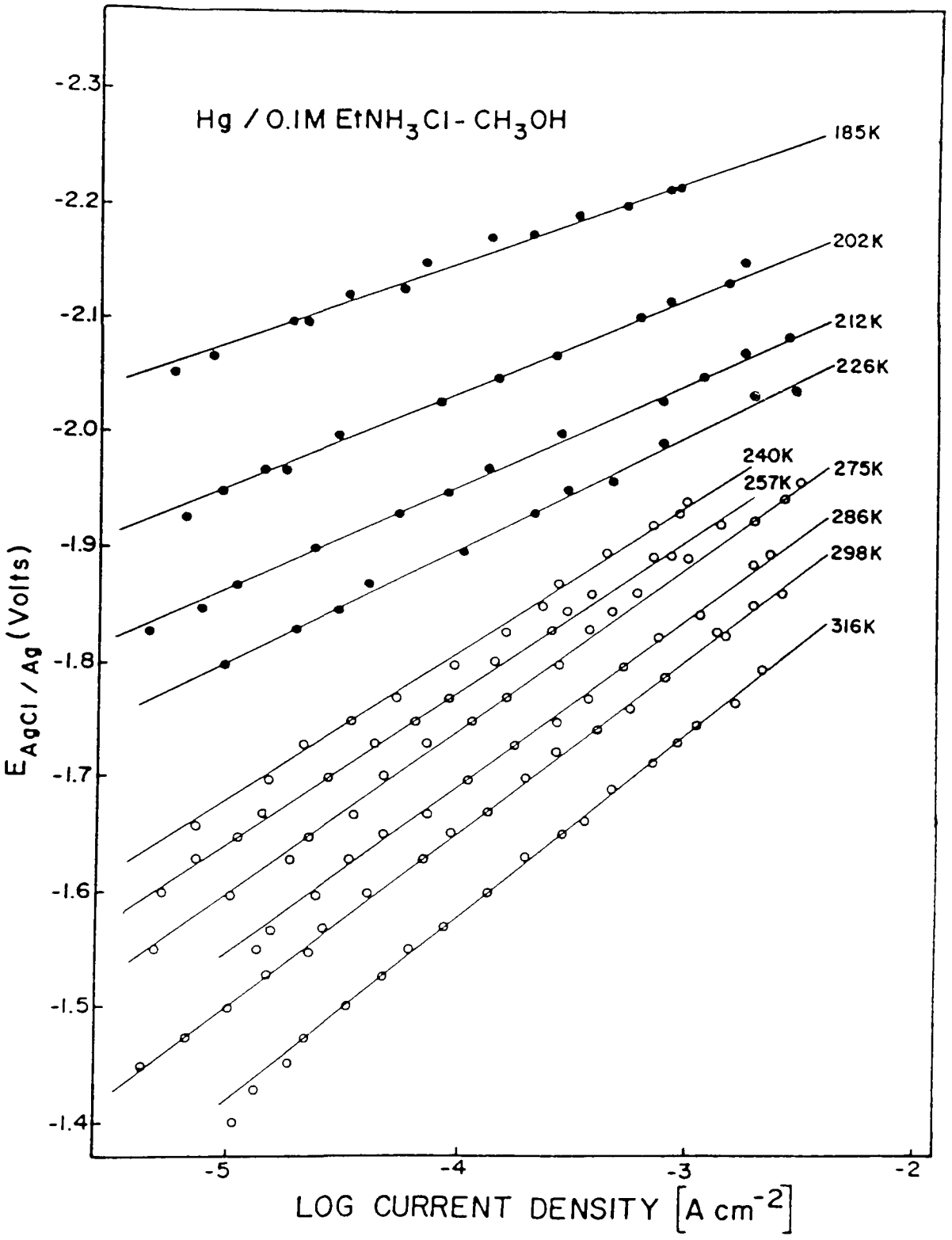

Fig 25 Log (current)-potential relations for the h e r at Hg from 0 1M $EtNH_3Cl$ in CH_3OH as a function of temperature (AgCl|Ag reference electrode). •, solid Hg; o, liquid

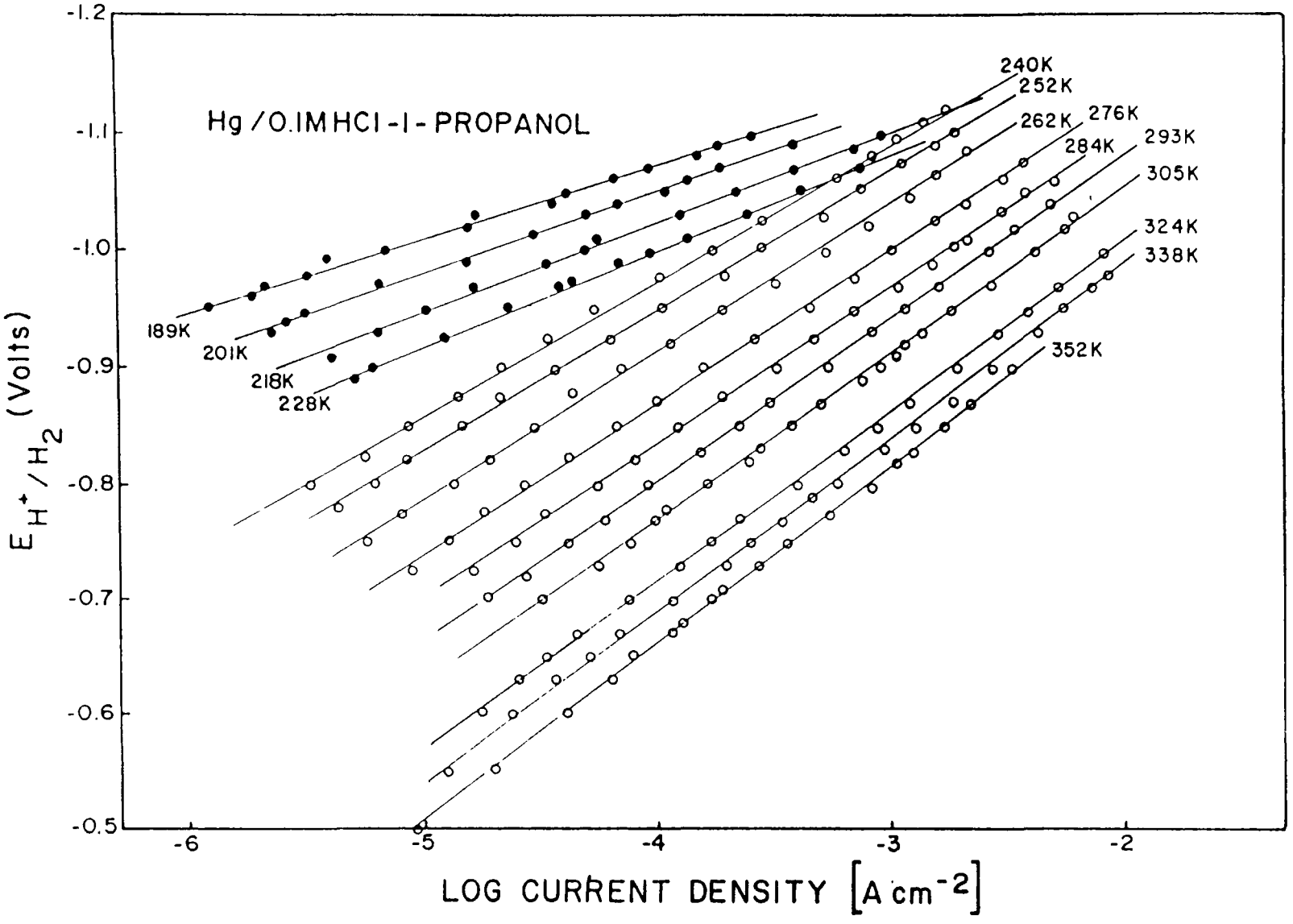

Fig 26 Log (current)-potential relations for the h.e.r. at Hg from 0 1M HCl in 1-propanol as a function of temperature ($H^+|H_2$ reference electrode). •, solid Hg; o, liquid Hg.

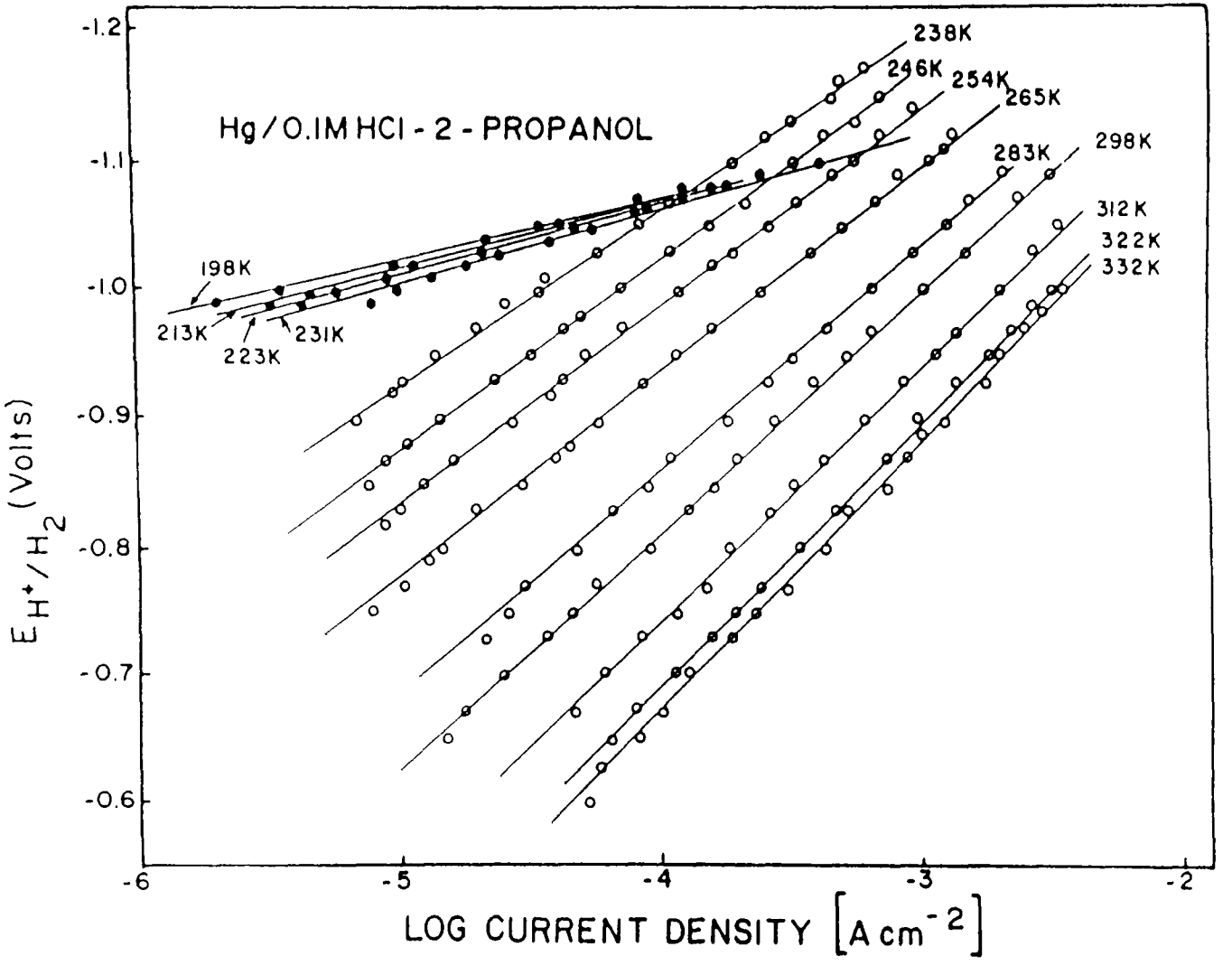

Fig 27 Log (current)-potential relations for the h.e.r. at Hg from 0 1M HCl in 2-propanol as a function of temperature ($H^+|H_2$ reference electrode). •, solid Hg; o, liquid Hg.

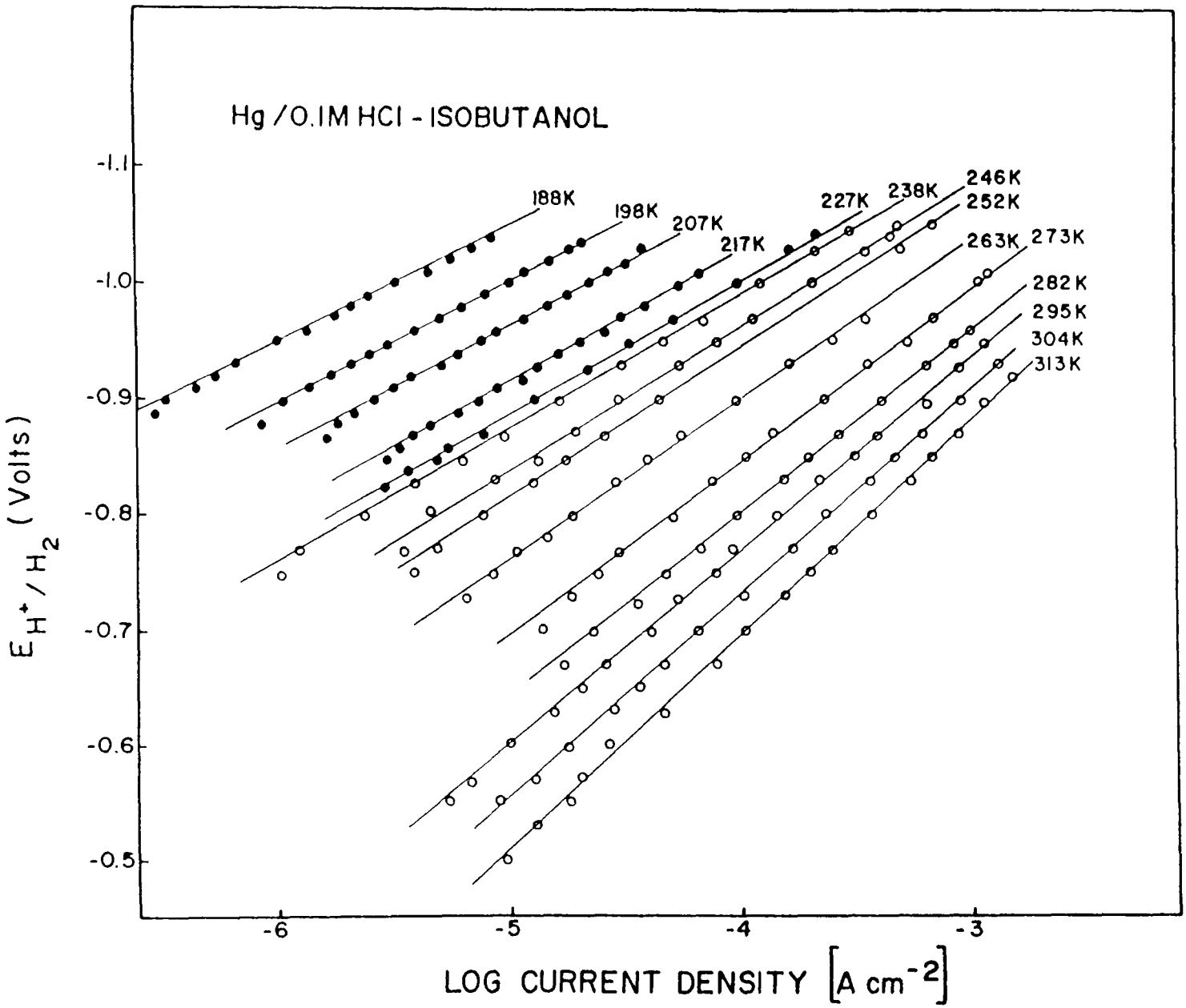

Fig 28 Log (current)-potential relations for the h.e.r. at Hg from 0 1M HCl in isobutanol as a function of temperature ($H^+|H_2$ reference electrode) •, solid Hg; o, liquid Hg.

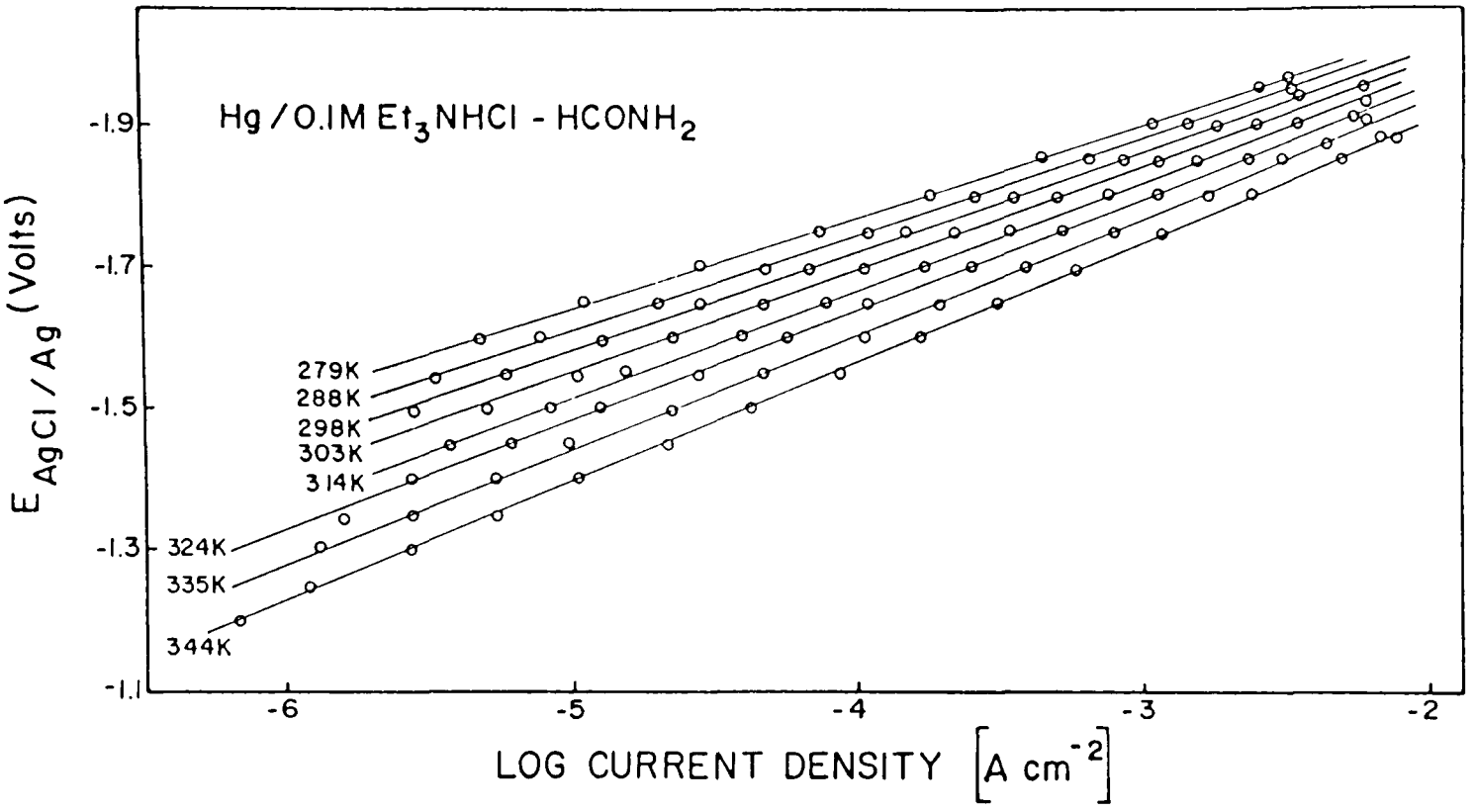

Fig. 29 Log (current)-potential relations for the h.e.r. at Hg from 0.1M Et_3NHCl in $HCONH_2$ as a function of temperature (AgCl|Ag reference electrode).

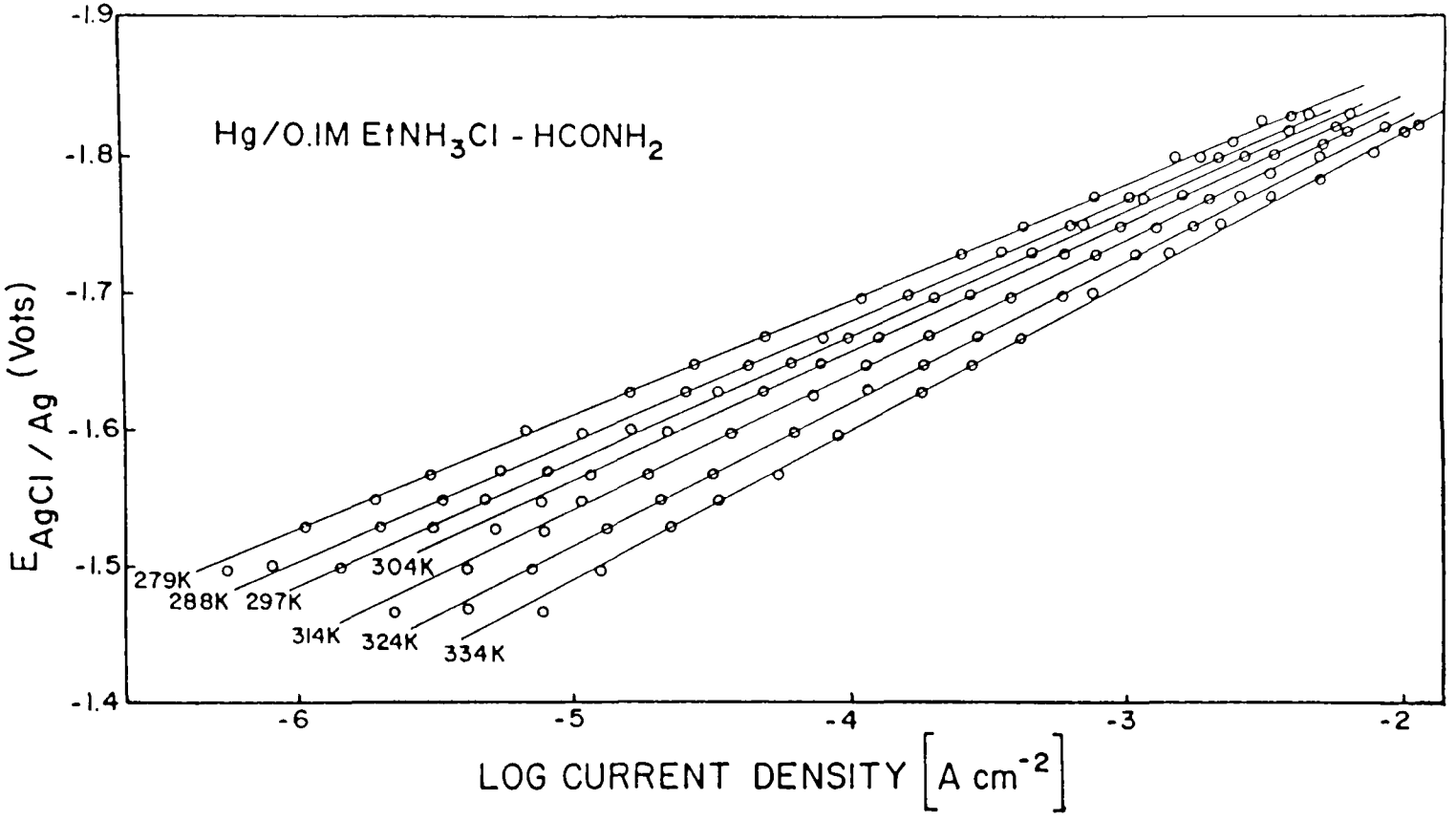

Fig 30 Log (current)-potential relations for the h.e r at Hg from 0.1M $EtNH_3Cl$ in $HCONH_2$ as a function of temperature (AgCl|Ag reference electrode).

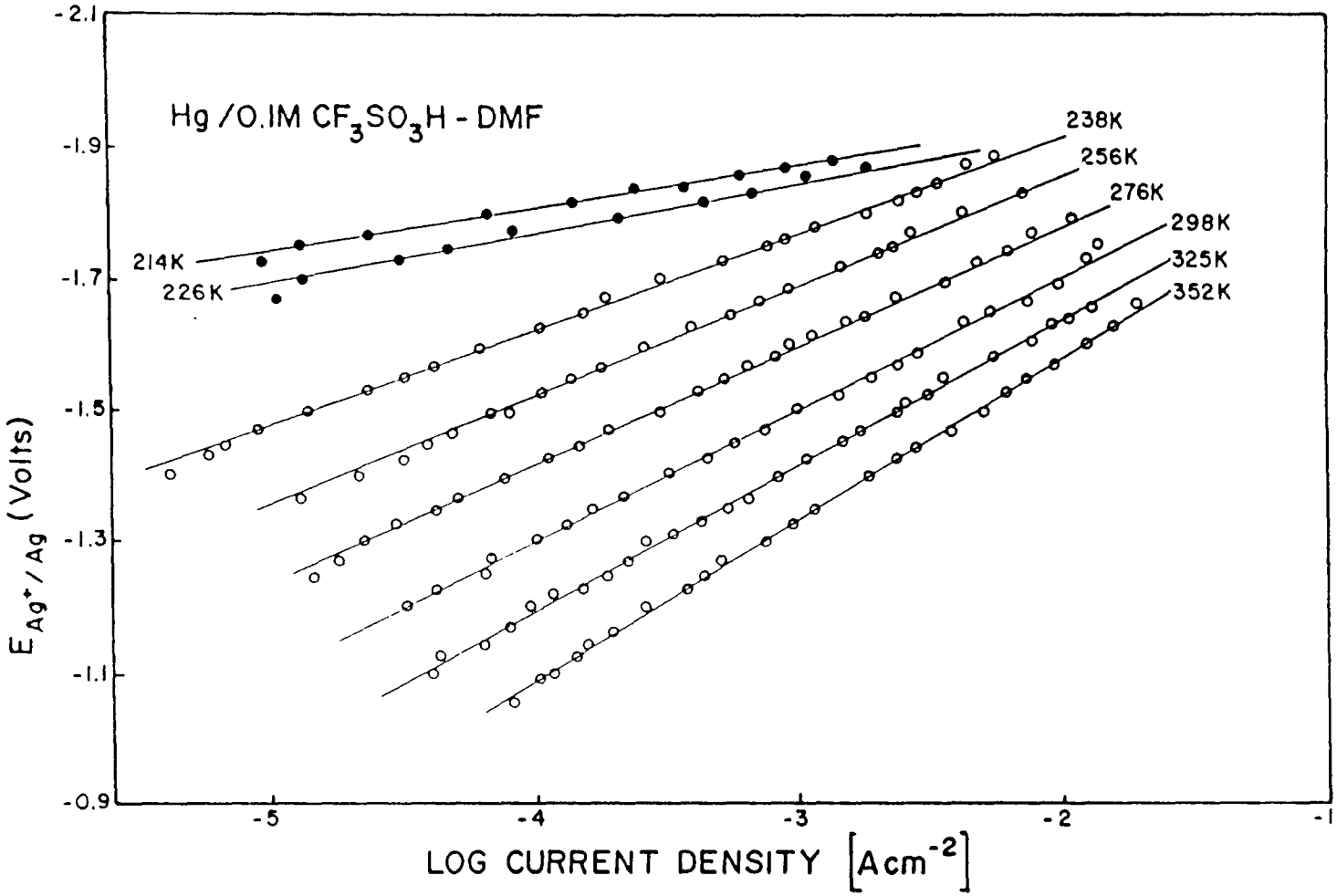

Fig. 31 Log (current)-potential relations for the h.e.r at Hg from 0.1M CF_3SO_3H in DMF as a function of temperature ($Ag^+|Ag$ reference electrode). ●, solid Hg; o, liquid Hg

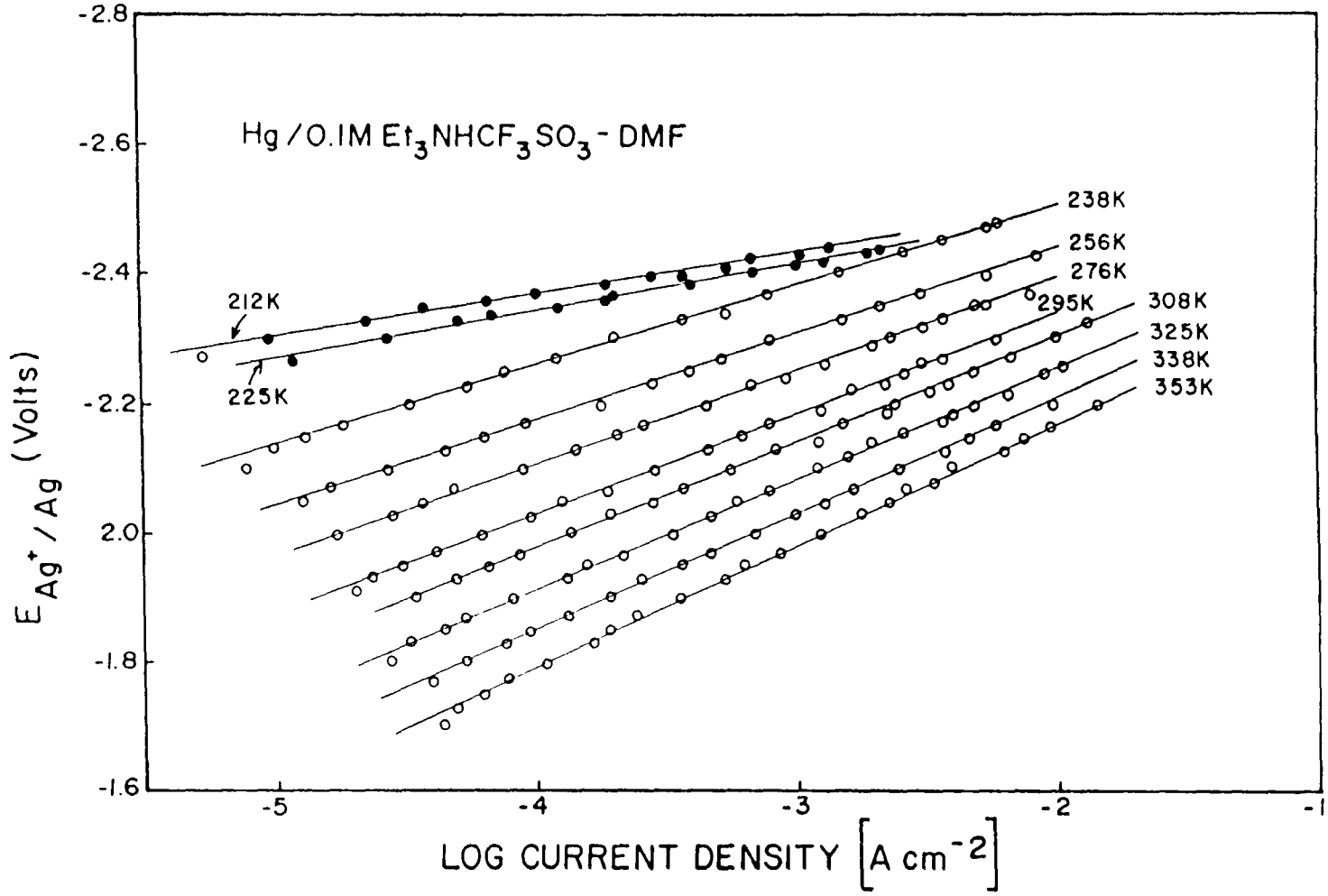

Fig 32 Log (current)-potential relations for the h.e.r. at Hg from 0 1M $Et_3NHCF_3SO_3$ in DMF as a function of temperature ($Ag^+|Ag$ reference electrode). •, solid Hg; o, liquid Hg.

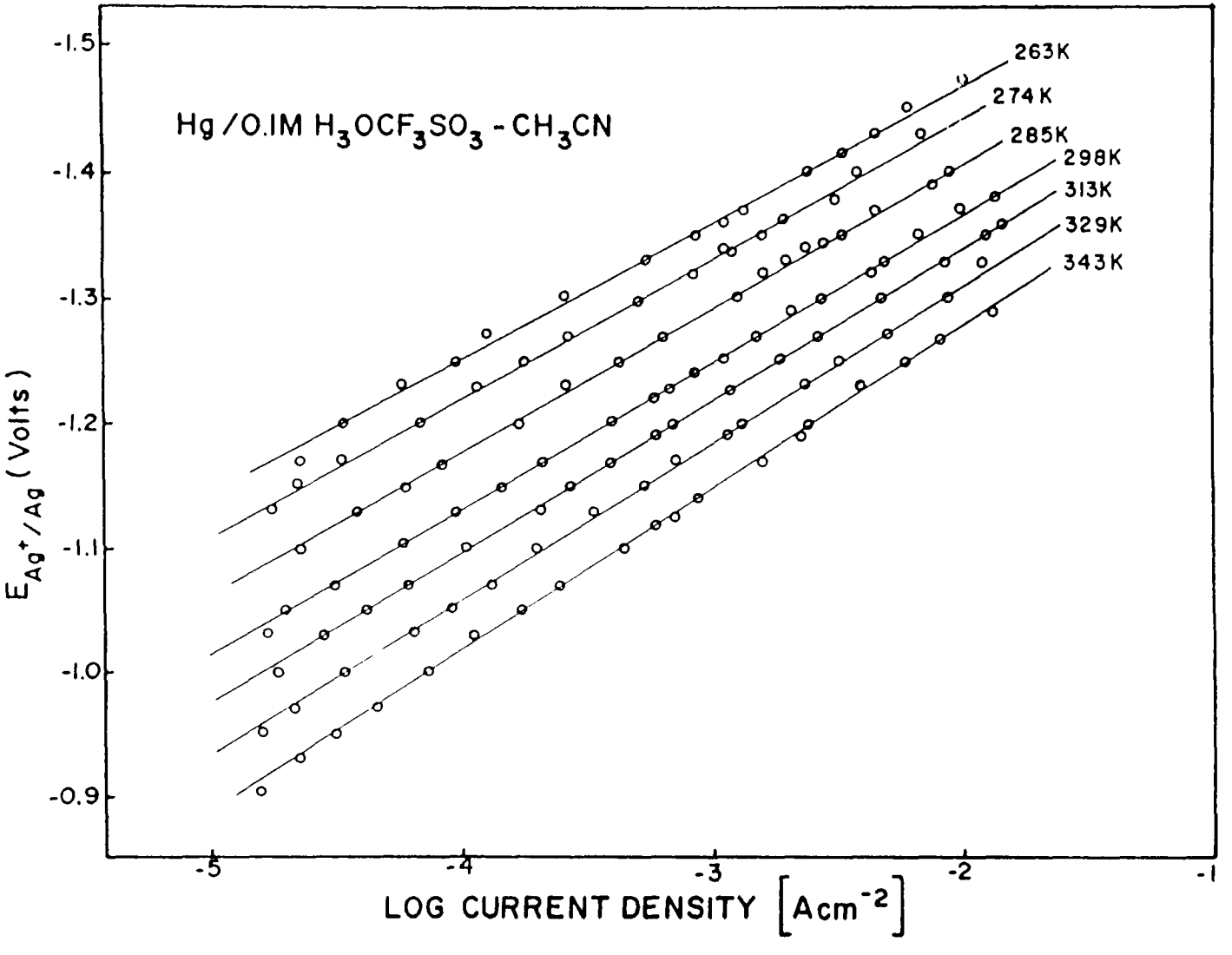

Fig. 33 Log (current)-potential relations for the h.e.r. at Hg from 0.1M $H_3OCF_3SO_3$ in CH_3CN as a function of temperature ($Ag^+|Ag$ reference electrode).

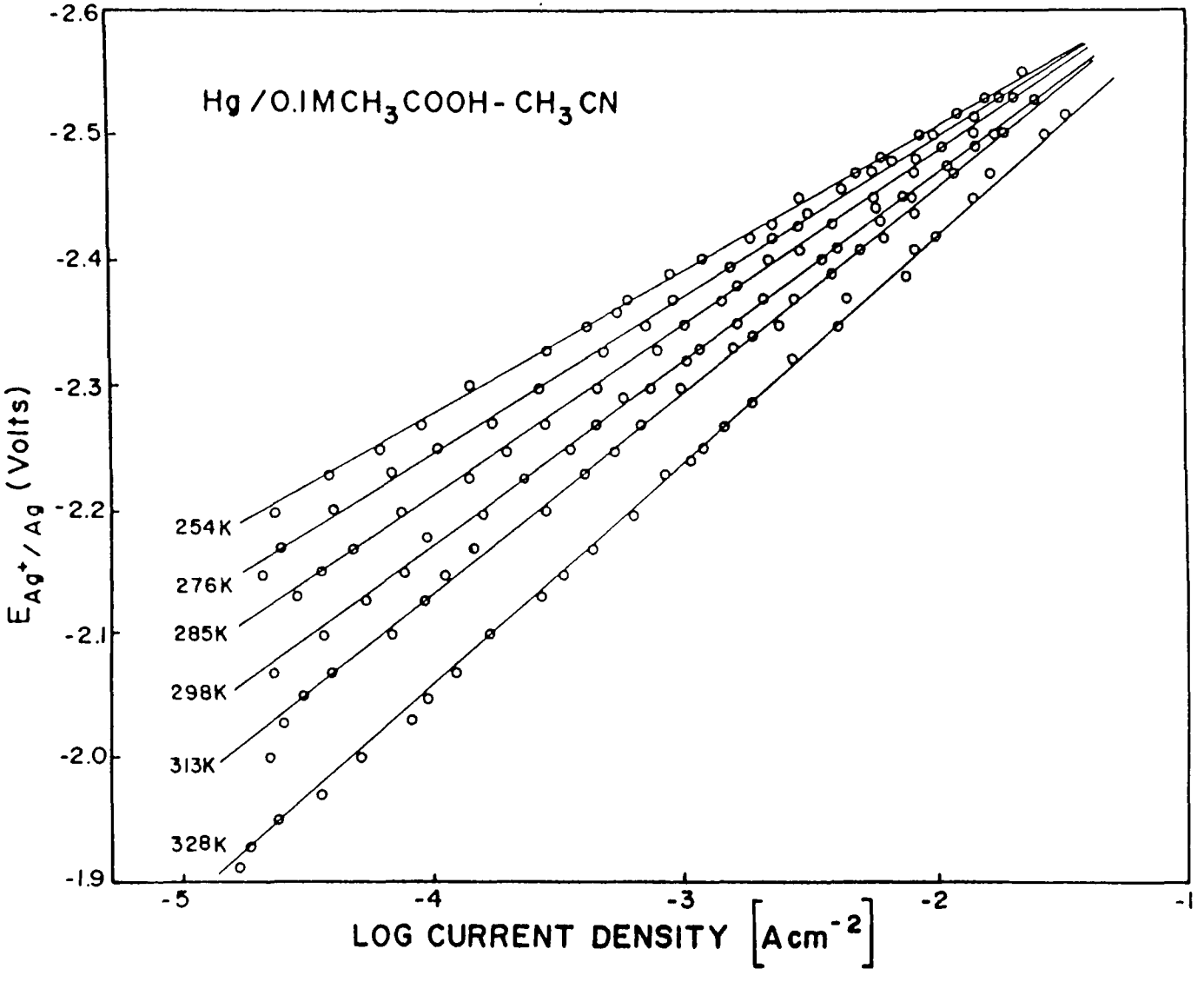

Fig. 34 Log (current)-potential relations for the h.e.r at Hg from 0.1M CH_3COOH in CH_3CN as a function of temperature ($Ag^+|Ag$ reference electrode).

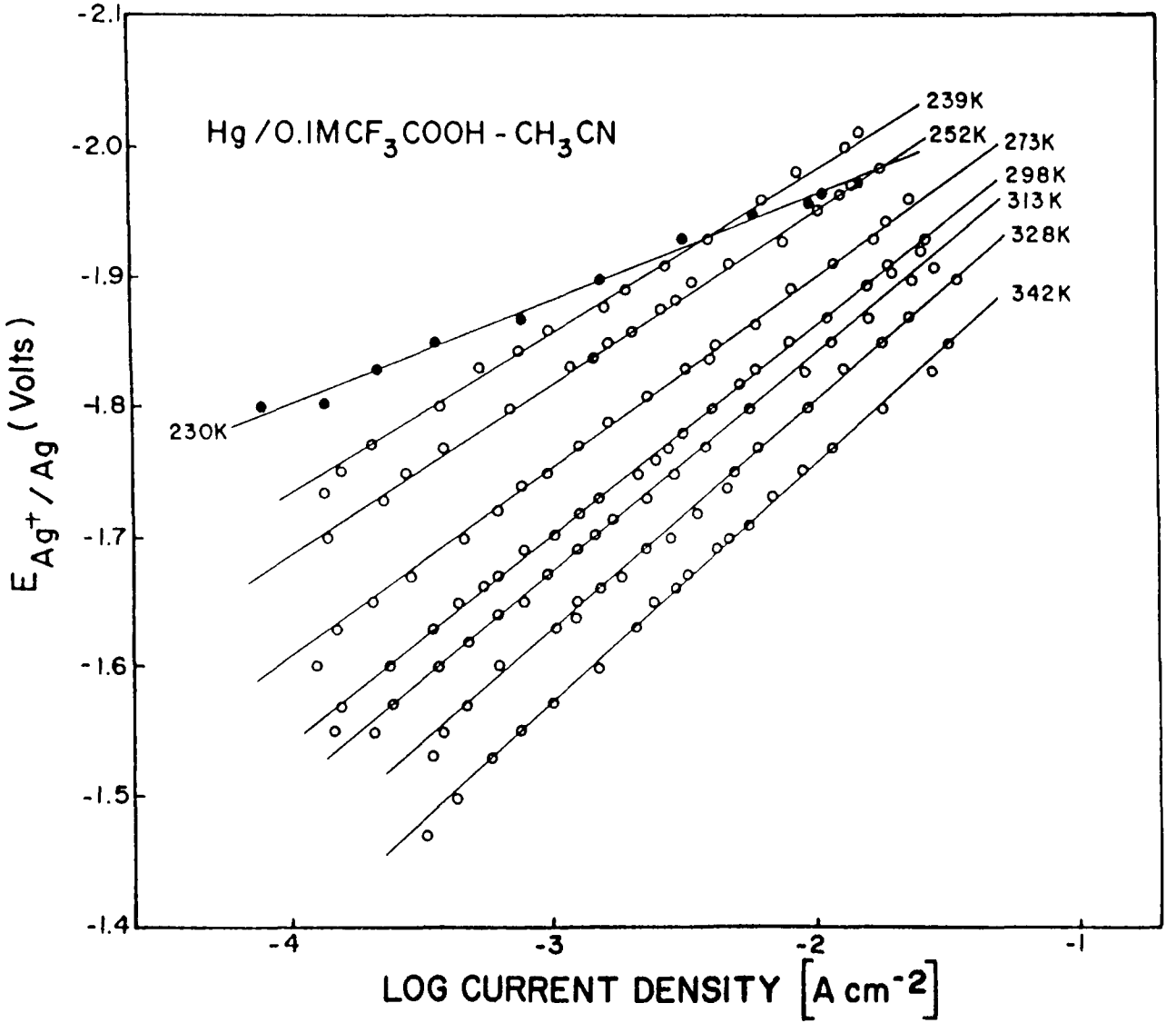

Fig 35 Log (current)-potential relations for the h.e.r. at Hg from 0 1M CF_3COOH in CH_3CN as a function of temperature ($Ag^+|Ag$ reference electrode). •, solid Hg; o, liquid Hg.

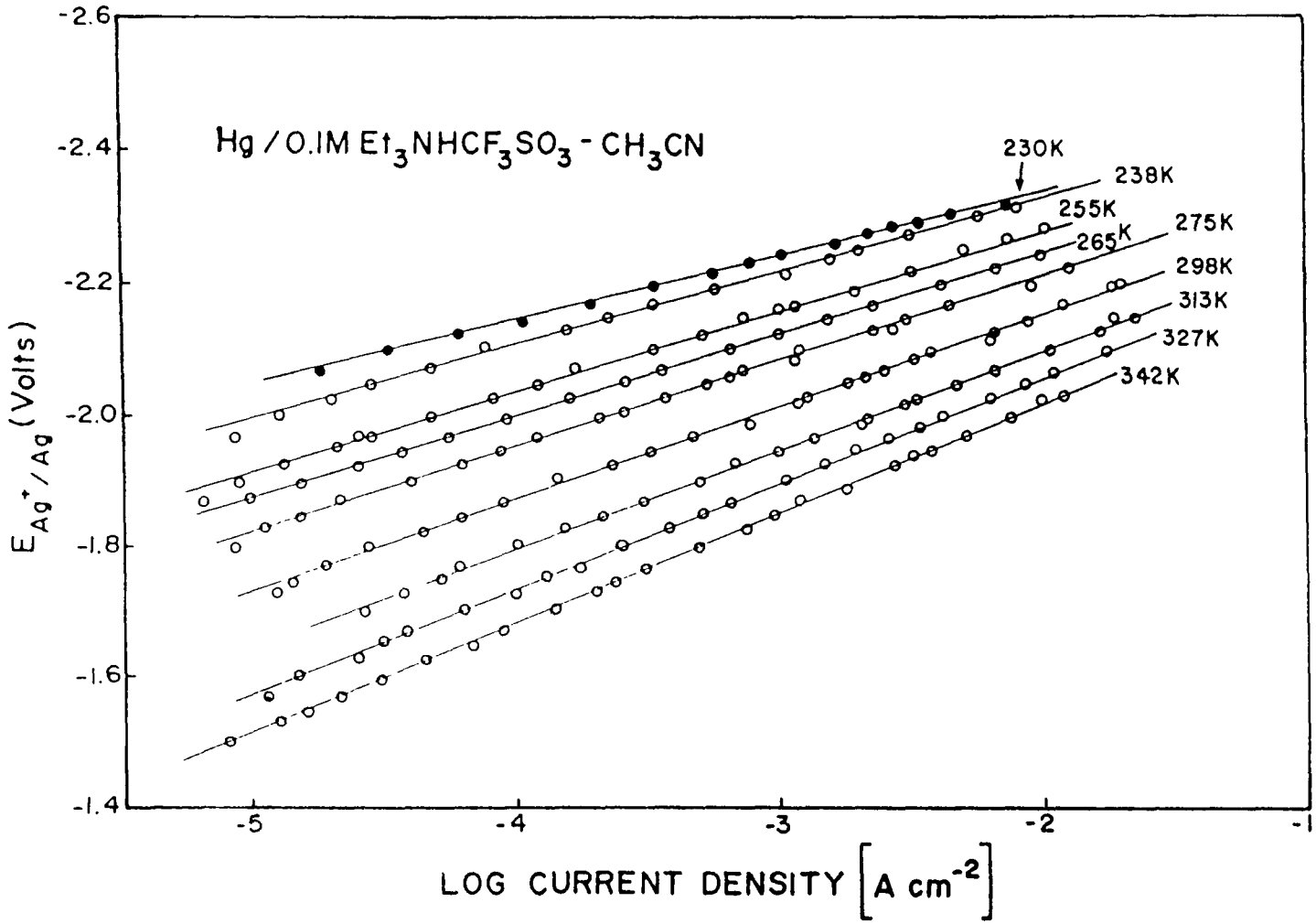

Fig. 36 Log (current)-potential relations for the h.e.r. at Hg from 0 1M $Et_3NHCF_3SO_3$ in CH_3CN as a function of temperature ($Ag^+|Ag$ reference electrode). •, solid Hg; o, liquid Hg.

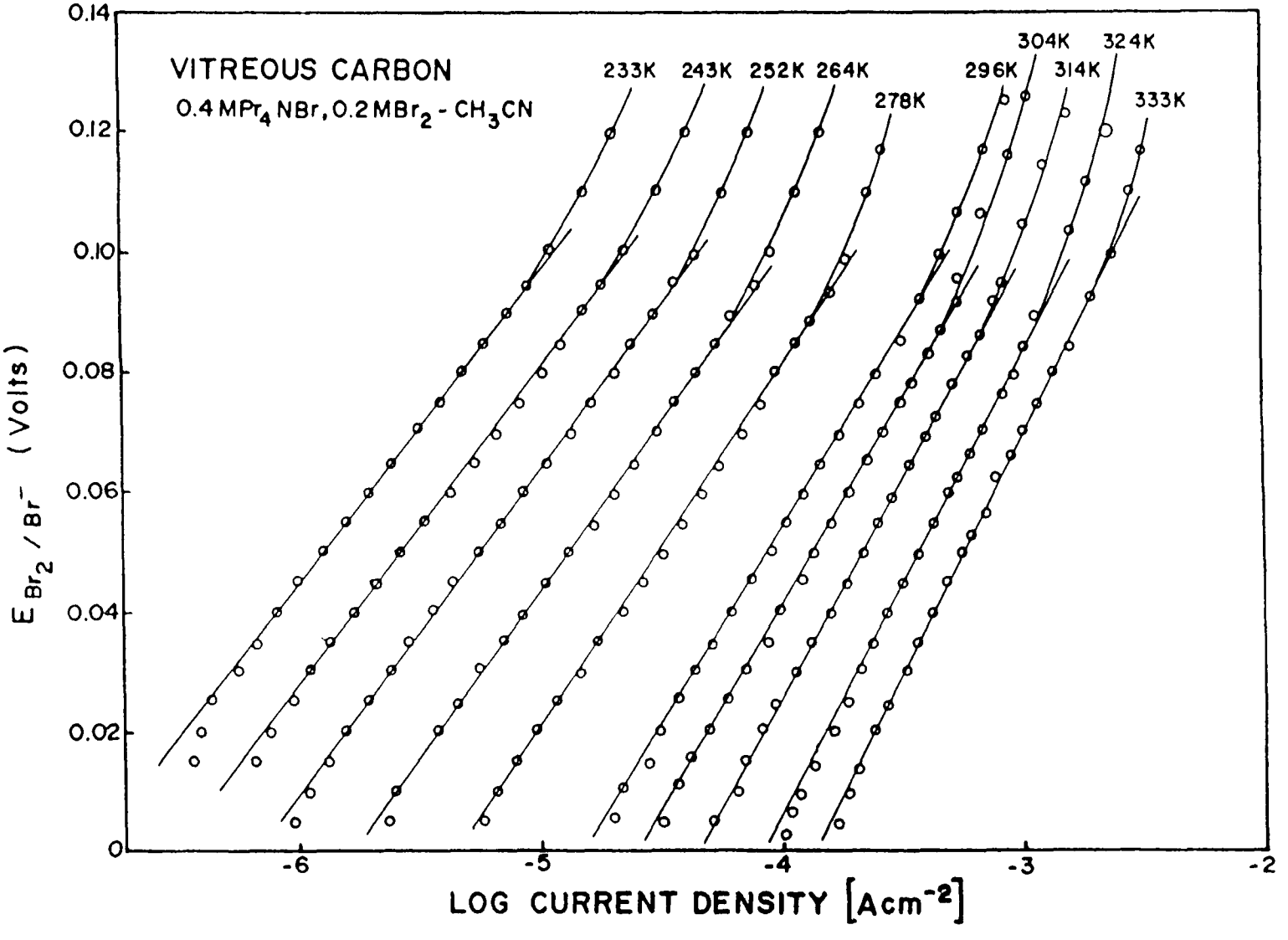

Fig 37 Log (current)-potential relations for the b.e.r. at vitreous carbon from 0.4M Pr_4NBr, 0.2M Br_2 in CH_3CN as a function of temperature ($Br_2|Br^-$ reference electrode)

2. Non-Isothermal Cell Measurements

Non-isothermal cell potentials as a function of temperature for the reference electrodes: $H^+|H_2$ in H_2O, CH_3OH, 1-propanol, 2-propanol, isobutanol; $AgCl|Ag$ in H_2O, CH_3OH, $HCONH_2$; $Ag^+|Ag$ in DMF, AN; $AgBr|Ag$ and $Br_2|Br$ in AN are shown in Fig. 38-48; these results will be discussed in Chapter 5. All non-isothermal cell measurements were made relative to a reference electrode temperature of 298 K and the reference electrode at this temperature was the negative pole of the cell.

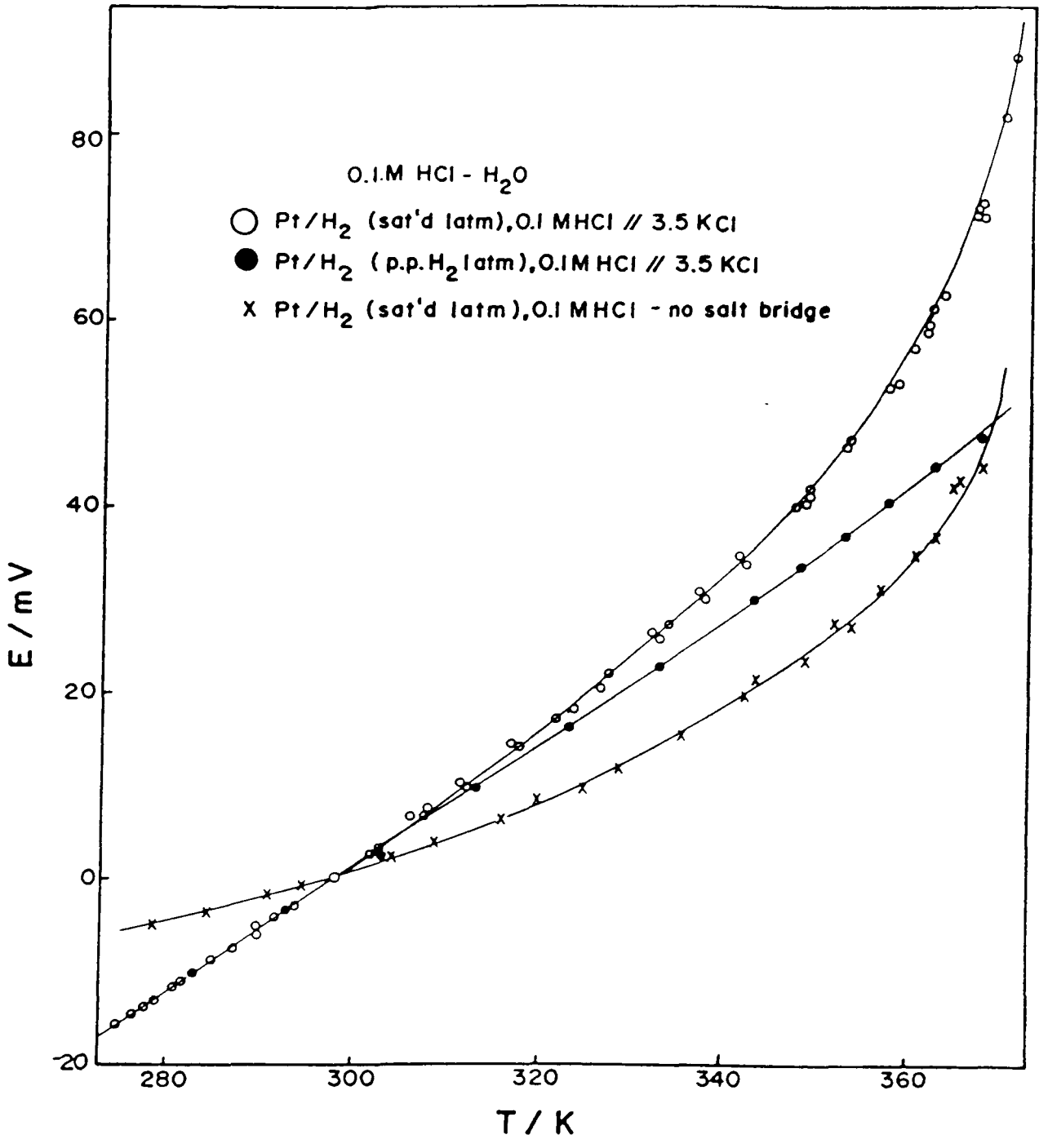

Fig 38 Non-isothermal cell potential for $H^+|H_2$ reference electrode in 0 1M aqueous HCl referred to 298 K.

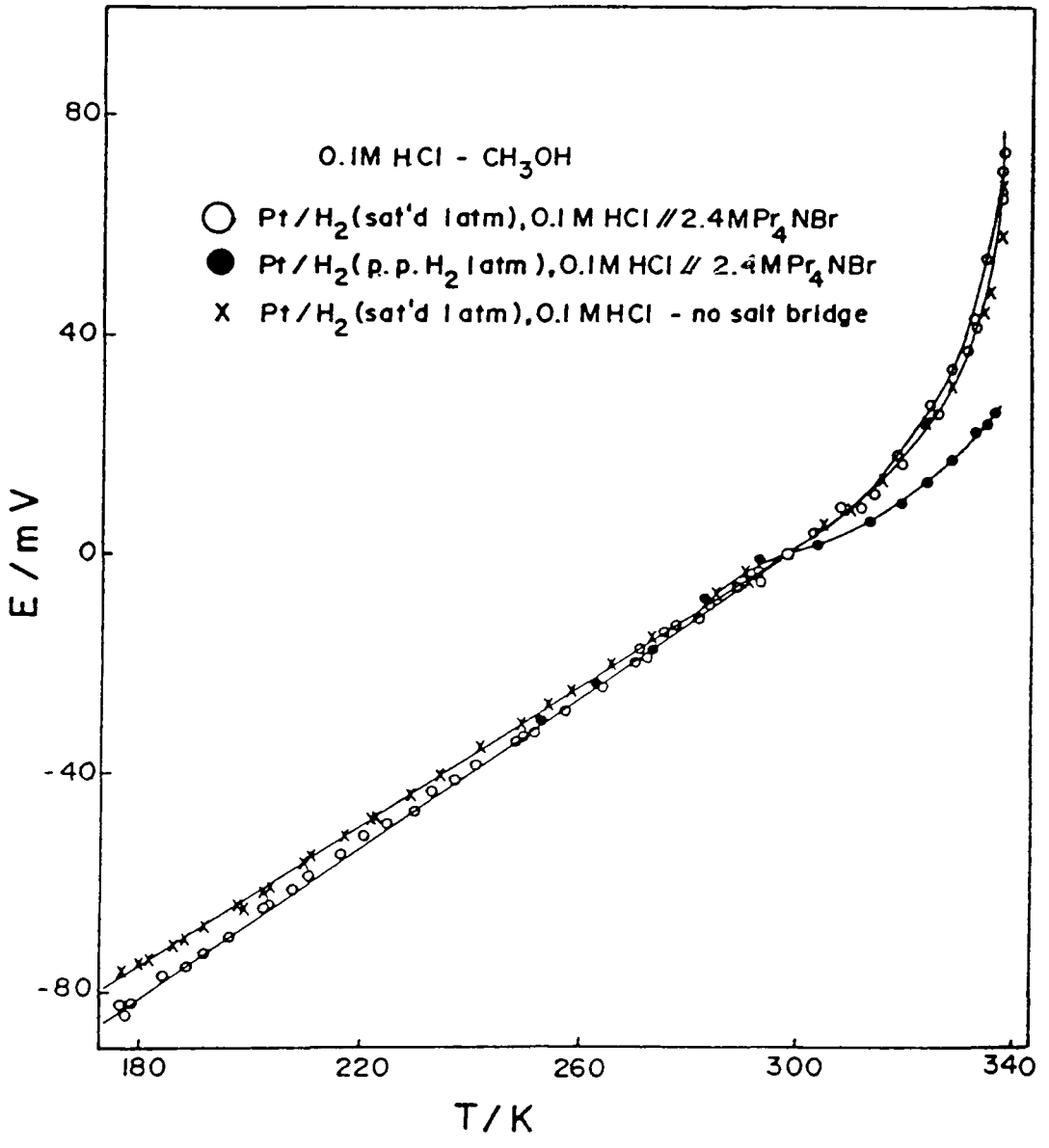

Fig. 39 Non-isothermal cell potentials for the $H^+|H_2$ reference electrode in 0 1M HCl in CH_3OH referred to 298 K

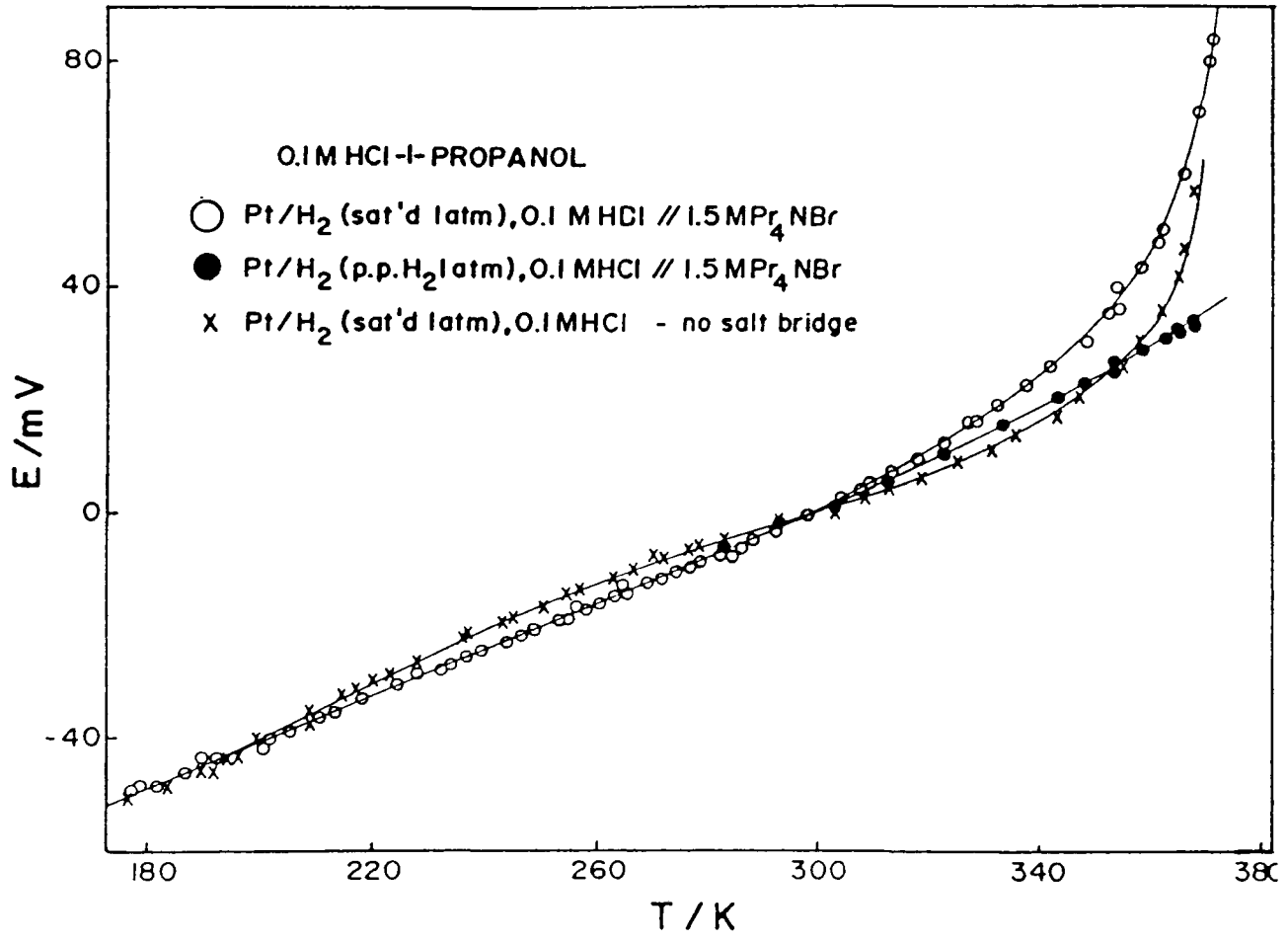

Fig. 40 Non-isothermal cell potentials for the $H^+|H_2$ reference electrode in 0 1M HCl in 1-propanol referred to 298 K.

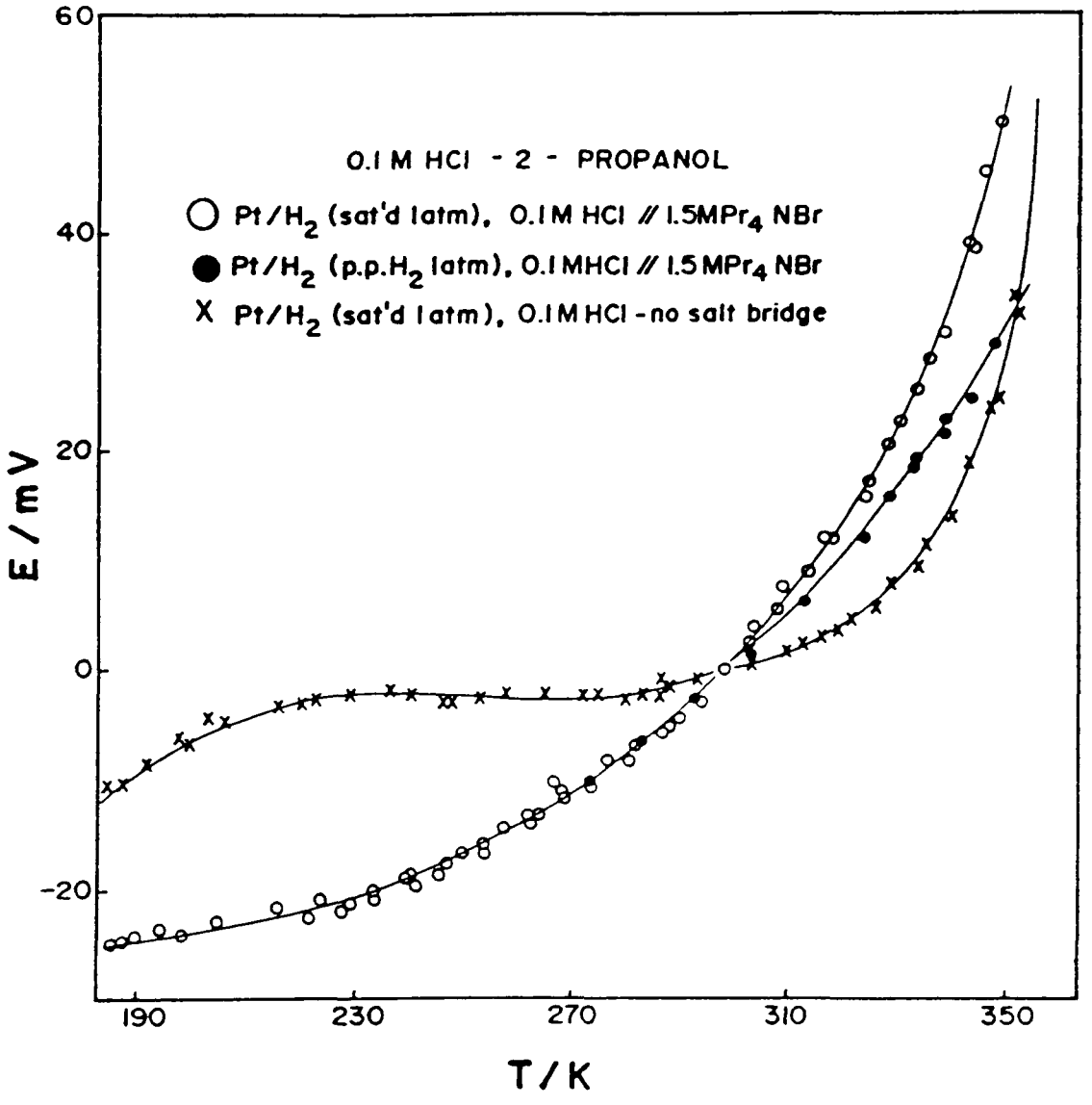

Fig 41 Non-isothermal cell potential for the $H^+|H_2$ reference electrode in 0.1M HCl in 2-propanol referred to 298 K

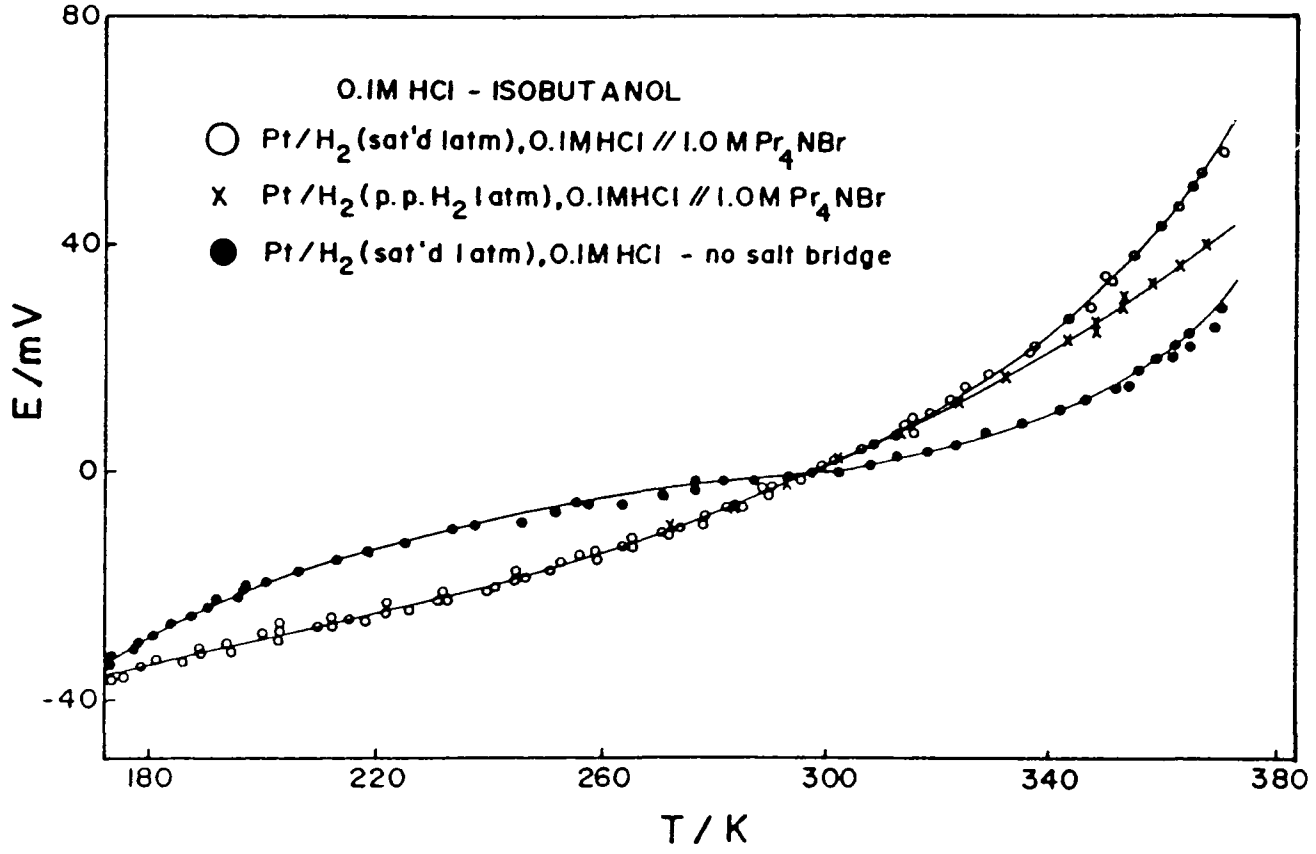

Fig 42 Non-isothermal cell potentials for the $H^+|H_2$ reference electrode in 0 1M HCl in isobutanol referred to 298 K

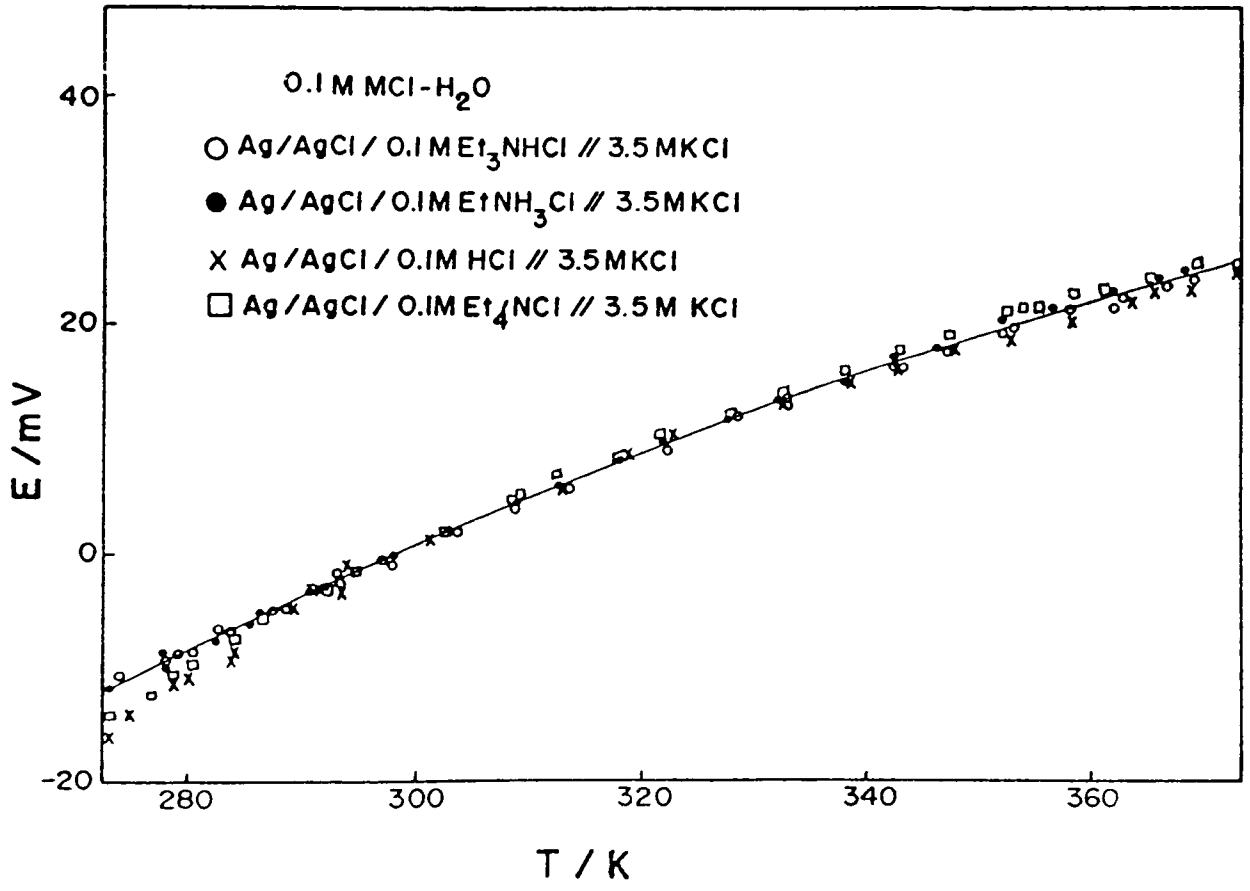

Fig 43 Non-isothermal cell potentials for the AgCl|Ag reference electrode in 0 1M aqueous Cl solutions referred to 298 K.

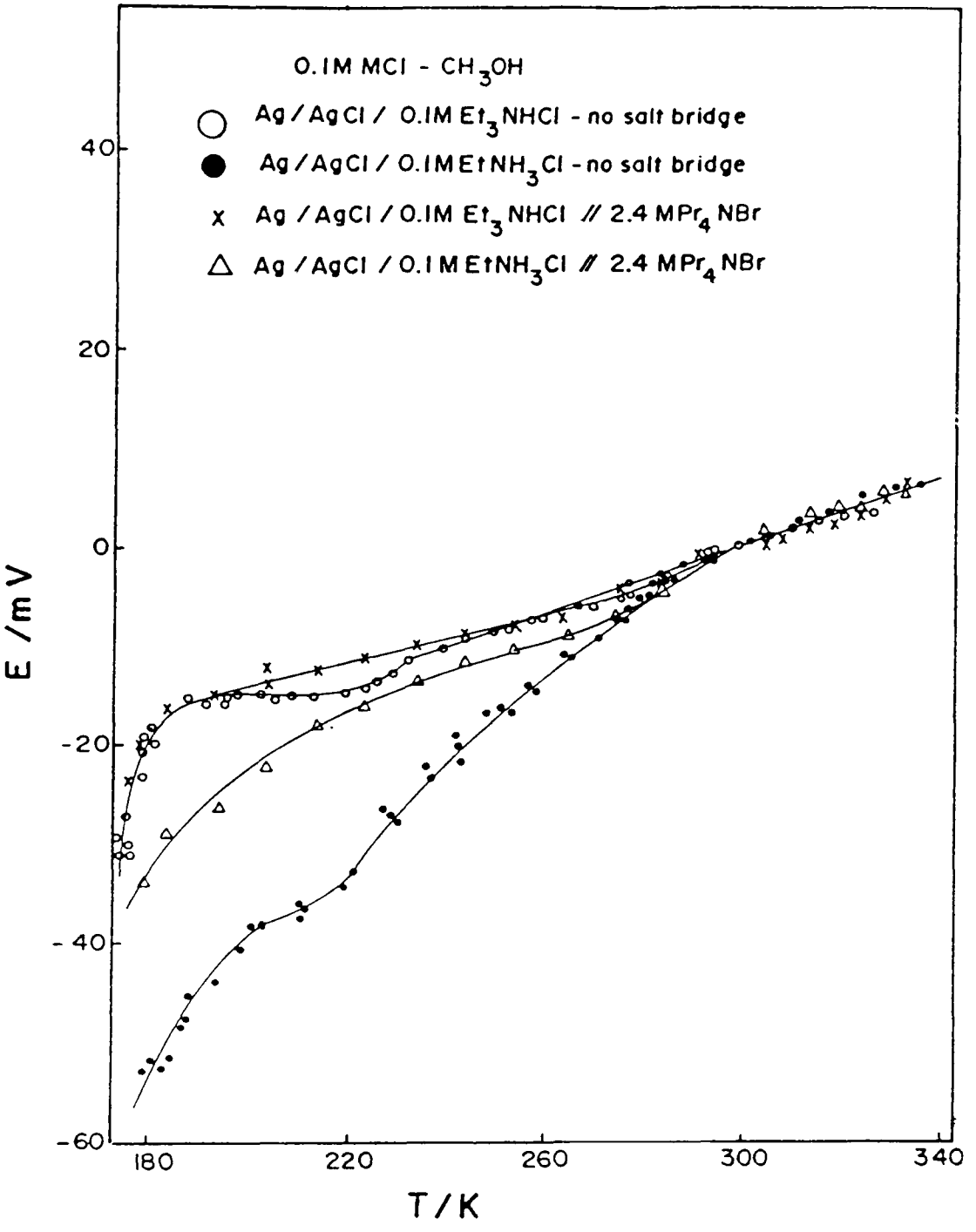

Fig 44 Non-isothermal cell potentials for the AgCl|Ag reference electrode in 0.1M Cl solutions in CH_3OH referred to 298 K.

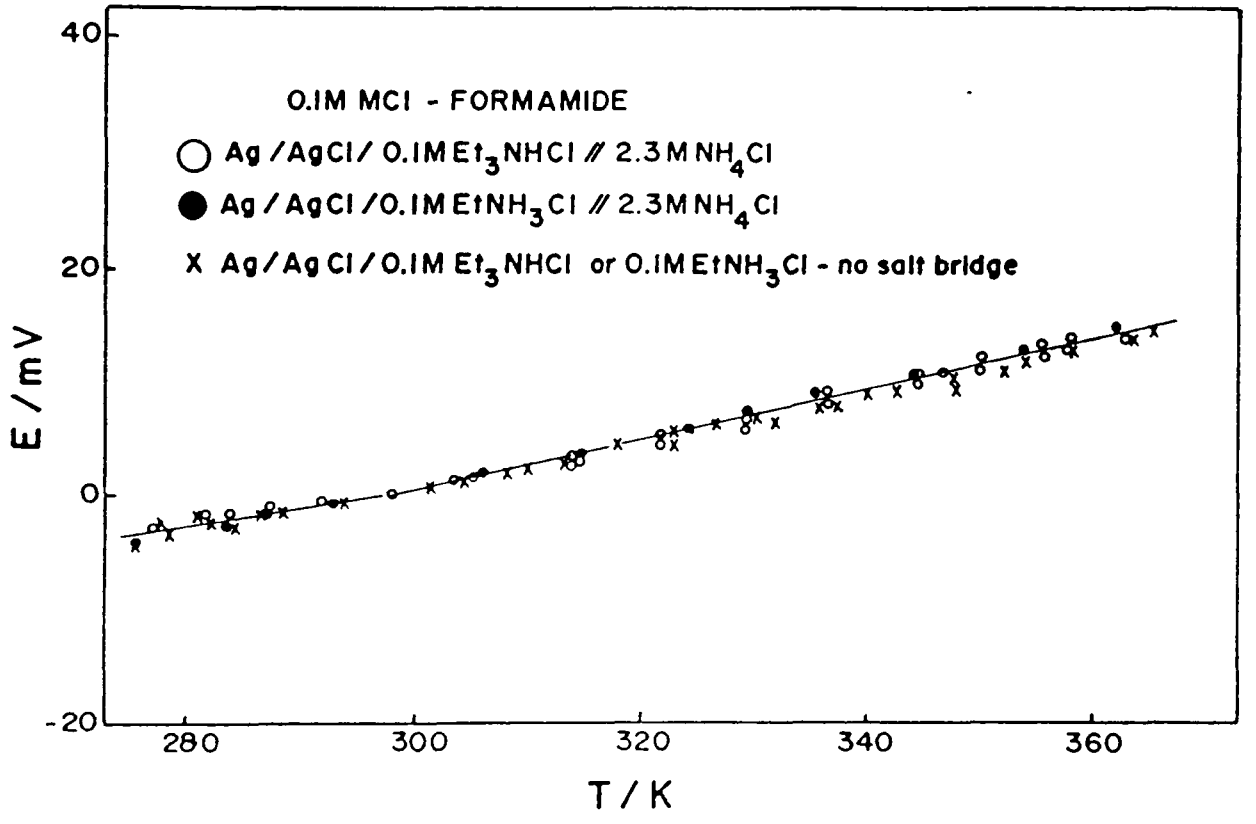

Fig 45 Non-isothermal cell potentials for the AgCl|Ag reference electrode in 0.1M Cl solutions in formamide referred to 298 K.

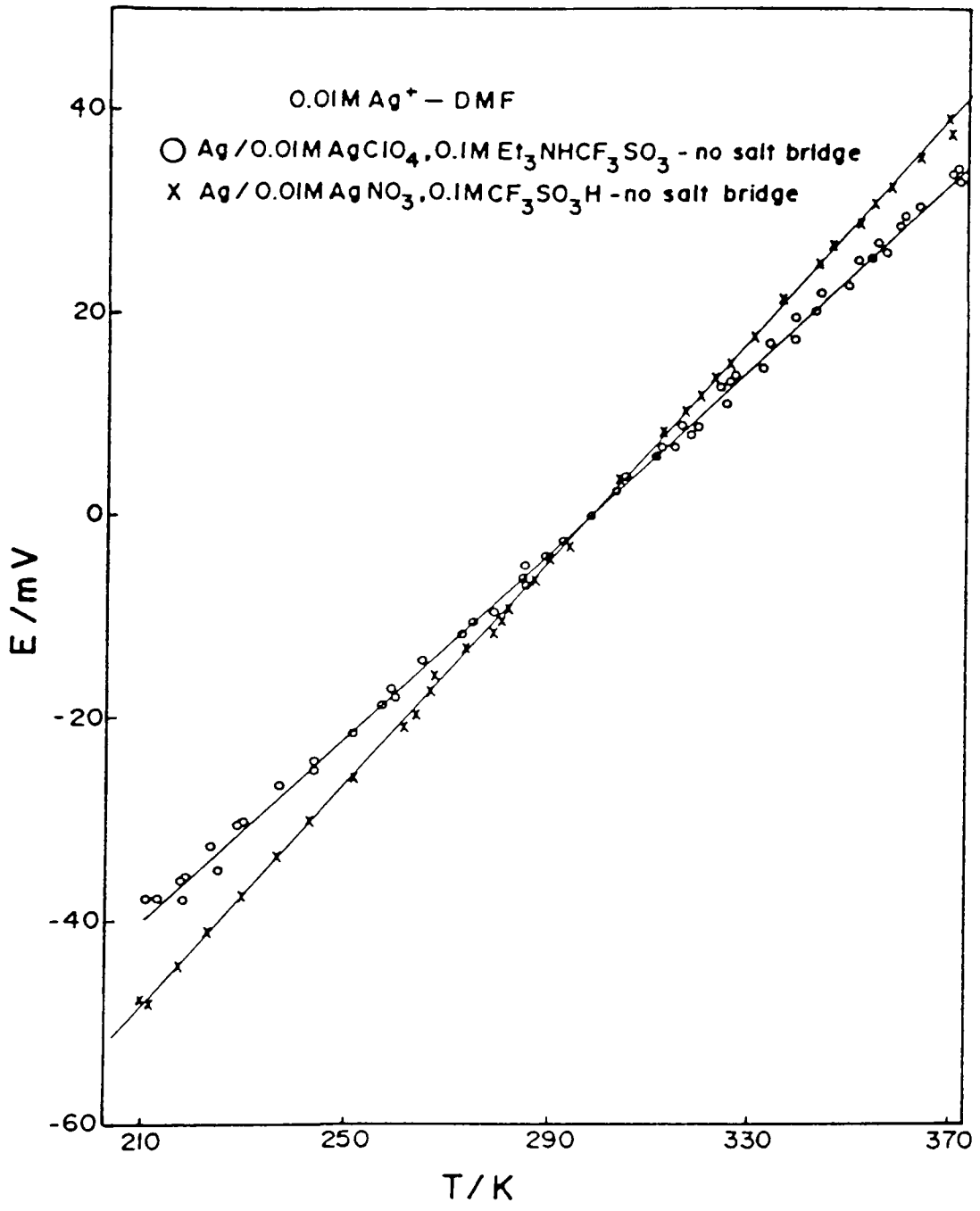

Fig 46 Non-isothermal cell potentials for the $Ag^+|Ag$ reference electrode in 0 01M Ag^+ solutions in DMF referred to 298K.

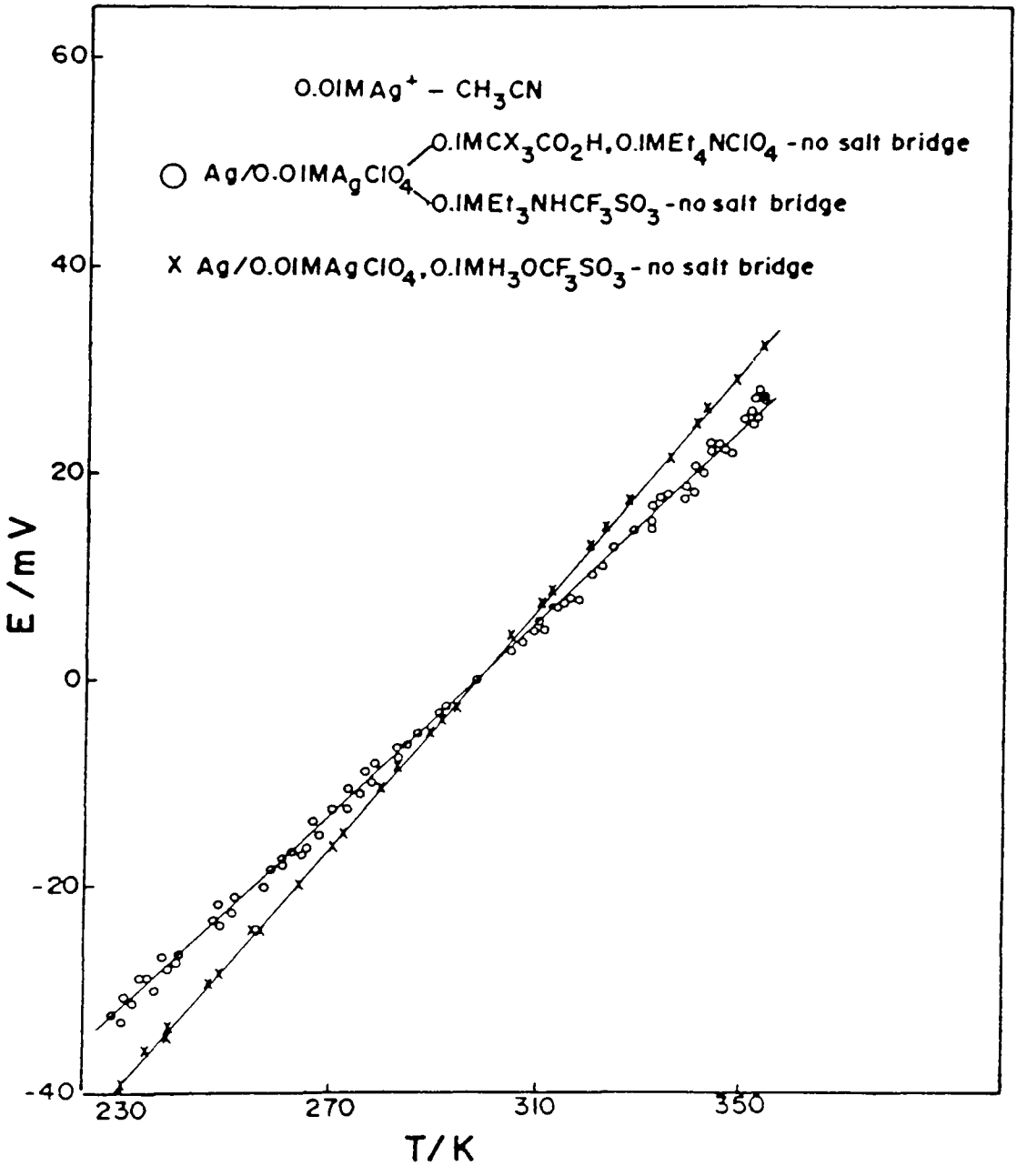

Fig. 47 Non-isothermal cell potentials for the $Ag^+|Ag$ reference electrode in 0 01M Ag^+ solutions in CH_3CN referred to 298 K

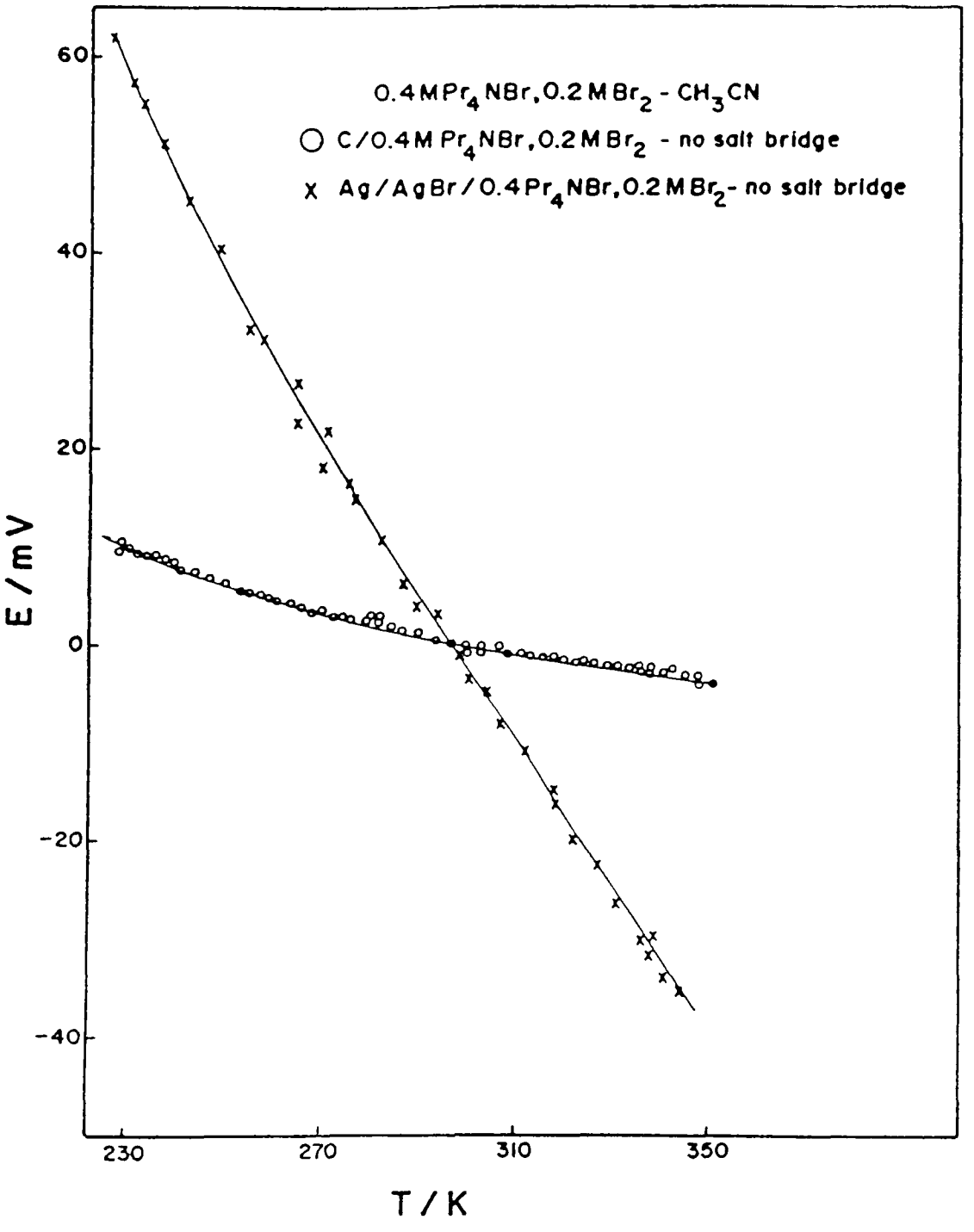

Fig 48 Non-isothermal cell potentials for the $Br_2|Br$ (at C) and $AgBr|Ag$ reference electrodes in 0 4M Pr_4NBr, 0 2M Br_2 solutions in CH_3CN referred to 298 K

CHAPTER 4

ACTIVATION PARAMETERS IN ELECTROCHEMICAL KINETIC MEASUREMENTS

1. Introduction

The Arrhenius rate equation at constant pressure is given by,

$$k = A \exp(-E^{\ddagger}_{expt.}/RT) \qquad [23]$$

where k is the chemical rate constant, A is the frequency factor and $E^{\ddagger}_{expt.}$ is the experimental energy of activation given by

$$E^{\ddagger}_{expt.} = RT + \Delta U^{\ddagger} = RT + \Delta H^{\ddagger} \quad P\Delta V^{\ddagger} \qquad [24]$$

where $\Delta U^{\ddagger}$ is the change in internal energy and $\Delta V^{\ddagger}$ is the change in volume, in going from the initial to the activated state for a process at constant pressure. For a reaction in solution or in a condensed system, $\Delta V^{\ddagger}$ is very small so that $P\Delta V^{\ddagger} \approx 0$, and eqn.[24] may therefore be written as

$$E^{\ddagger}_{expt.} = \Delta H^{\ddagger} + RT \qquad [25]$$

In transition state theory (96) the rate constant of a chemical process is given in terms of the Gibbs energy of activation by

$$k = \kappa \frac{kT}{h} \exp(-\Delta G^{\ddagger}/RT) = \kappa \frac{kT}{h} \exp(\Delta S^{\ddagger}/R)\exp(-\Delta H^{\ddagger}/RT) \qquad [26]$$

where k is Boltzmann's constant, κ is a transmission coefficient (normally taken as near 1) for passage of activated complexes over the energy barrier and $\Delta G^{\ddagger}$ is the chemical Gibbs energy of activation. The rate constant of a chemical process may also be given in terms of the experimental energy of activation by substitution of eqn.[25] into eqn.[26] to give

$$k = e\kappa \frac{\tilde{kT}}{h} \exp(\Delta S^{\ddagger}/R) \exp(E^{\ddagger}_{expt} /RT) \qquad [27]$$

Hence, for a simple homogeneous chemical reaction the experimentally measurable energy of activation and frequency factor allow the enthalpy, $\Delta H^{\ddagger}$, and entropy of activation, $\Delta S^{\ddagger}$, to be determined.

The rate constant for a simple electrode reaction, i.e , an outer-sphere reaction, has been written as (53,97)

$$\bar{k} = Z_{het.} \kappa p \exp(-\Delta \bar{G}^{\ddagger}_{\phi}/RT) \qquad [28]$$

where κ and p are constants expected to be close to unity, $\Delta \bar{G}^{\ddagger}_{\phi}$ is the electrochemical Gibbs energy of activation at electrode potential ϕ, and $Z_{het.}$ given by

$$Z_{het.} = (\tilde{k}T/2\pi m^*)^{1/2} \qquad [29]$$

is the collision number of the reacting species with unit area of the electrode interface, when it has unit concentration and when its mass is m*. For a coupled atom/electron transfer reaction, i.e., an inner-sphere reaction, such as the h.e.r use of the preexponential factor $\kappa\tilde{k}T/h$ employed in transition state theory rather than the collision frequency factor $Z_{het.}\ \kappa p$ results in a more realistic expression for the rate constant given by

$$\bar{k} = \kappa \frac{\tilde{k}T}{h} \exp(-\Delta \bar{G}^{\ddagger}_{\phi}/RT) \qquad [30]$$

The electrochemical Gibbs energy of activation which is potential-dependent can be written in terms of the chemical Gibbs energy of activation, $\Delta G^{\ddagger}_{\phi=o}$ and electrical component terms:

$$\Delta \bar{G}^{\ddagger}_{\phi} = \Delta G^{\ddagger}_{\phi=o} \mp \beta\phi nF = \Delta H^{\ddagger}_{\phi=o} - T\Delta S^{\ddagger}_{\phi=o} \mp \beta\phi nF \qquad [31]$$

where β is a barrier symmetry factor (discussed in detail in

chapter 5 B). n is the number of electronic charges transferred in the rate-determining step, usually one, and ϕ is the metal solution potential difference* Substitution of eqn.[31] into eqn.[30] gives

$$\bar{k} = \kappa \frac{\bar{k}T}{h} \exp(\Delta S^{\ddagger}_{\phi=0}/R)\exp(-\Delta H^{\ddagger}_{\phi=0}/RT)\exp(\pm\beta\phi nF/RT) \qquad [32]$$

so that the experimentally measurable energy of activation and frequency factor for an electrode process cannot simply be associated with $\Delta H^{\ddagger}_{\phi=0}$ and $\Delta S^{\ddagger}_{\phi=0}$ as in the case of a simple homogeneous chemical reaction; these quantities must be defined in relation to ϕ.

2. Relation between Apparent and True Activation Parameters

An unavoidable problem arises in electrode-kinetic studies conducted over a range of temperatures If the rates (current-densities) are measured at various temperatures, at a given constant overpotential (e.g., $\eta = 0$, so that the rates are treated in terms of the exchange-current densities, i_o, as a f(T) or of the standard rate constants at the reversible potential), then, because of the usually significant T-variation of the absolute potential difference of the reversible electrode, e g., $H^+|H_2$, only an "apparent" heat of activation results from an Arrhenius plot of ln $i(\eta)$ or ln i_o versus T^{-1} Temkin (98) referred to this as the "real" heat of activation, since this is the only $\Delta H^{\ddagger}$ quantity that can be unambiguously

---

* Here and following the upper and lower signs in the notation "$\pm$" ("$_+$") refer to anodic and cathodic processes respectively.

measured, it is also the quantity that can be related to theoretical representations of $\Delta H^{\ddagger}$ through energy profile diagrams, as he also showed.

From the point of view of thinking of comparison between electrochemical $\Delta\bar{H}^{\ddagger}_{\phi}$ and $\Delta\bar{S}^{\ddagger}_{\phi}$ quantities with those for analogous homogeneous processes (where effects due to changes in potential are absent), it is desirable to be able to consider the "true" activation quantities $\Delta H^{\ddagger}_{\phi=o}$ and $\Delta S^{\ddagger}_{\phi=o}$ for an electrode-solution potential difference $\phi = 0$. These functions Temkin referred to as "ideal" quantities but they are not directly accessible to experiment, since the condition of $\phi = 0$ is not experimentally definable (but at Hg an approximation to it can be realized see section C-12, chapter 5). However, the activation quantities $\Delta\bar{H}^{\ddagger}_{\phi}$ and $\Delta\bar{S}^{\ddagger}_{\phi}$ can be practically measured at a fixed, almost temperature-independent electrode-solution potential ϕ (see section A, chapter 5) so that a "chemically" meaningful comparison of these quantities can be made.

A direct treatment of the relation between apparent and true activation quantities has been given by Conway (99); a similar approach will be followed here, as outlined below. The electrode reaction current-density $i(\eta)$ at a given over-potential, η, can be expressed in terms of eqn.[32] for the electrochemical rate constant as,

$$i_{\eta} = zFcf(\theta)\kappa\frac{\tilde{k}T}{h}\exp(\Delta S^{\ddagger}_{\phi=o}/R)\exp(-\Delta H^{\ddagger}_{\phi=o}/RT)\exp[\pm\beta(\phi_R+\eta)nF/RT] \qquad [33]$$

where z is the total number of electrons transferred in the overall process, c is an appropriate reactant surface

concentration expression (taking into account the distribution of the reactant between solution and interface in the double layer), $f(\theta)$ is a surface coverage term which is a function of coverage, θ (or free sites, $1\ \theta$) by chemisorbed intermediates and/or specifically adsorbed anions, ϕ_R is the reversible potential when the reaction is at equilibrium ($\eta = 0$, $i = i_o$, the exchange current-density) and η is the overpotential ($\eta = \phi - \phi_R$). For a given reactant concentration, if double-layer ion distribution and surface coverage effects are temperature independent, then

$$[\partial \ln i/\partial(1/T)]_\eta = [\partial \ln \bar{k}/\partial(1/T)]_\eta \qquad [34]$$

and if the linear term in T in $\tilde{k}T/h$ is neglected and $\Delta H^{\ddagger}_{\phi=o}$ and $\Delta S^{\ddagger}_{\phi=o}$ are assumed to be independent of T, then the apparent heat of activation is given by

$$\Delta \bar{H}^{\ddagger}_{\eta} = -R[\partial \ln i/\partial(1/T)]_\eta \qquad [35]$$

$$= \Delta H^{\ddagger}_{\phi=o} \mp \beta\phi_R nF \pm \beta nFT(\partial\phi_R/\partial T) \pm \phi_R nFT(\partial\beta/\partial T) \mp \beta nF\eta \pm nFT\eta(\partial\beta/\partial T)$$

$$= \Delta H^{\ddagger}_{\phi=o} \pm \beta\Delta G_R \pm \beta T\Delta S_R \mp T\Delta G_R(\partial\beta/\partial T) \mp \beta nF\eta \pm nFT\eta(\partial\beta/\partial T)$$

where ΔH_R and ΔS_R are the Gibbs energy and entropy change for the overall reaction at equilibrium. It is obvious that the apparent heat of activation, $\Delta \bar{H}^{\ddagger}_{\eta}$ depends on the particular value of the overpotential chosen and when $\eta = 0$ eqn.[35] reduces to the less complex result,

$$\Delta \bar{H}^{\ddagger}_{\eta=o} = -R[\partial \ln i_o/\partial(1/T)]_{\eta=o} \qquad [36]$$

$$= \Delta H^{\ddagger}_{\phi=o} \pm \beta\Delta G_R \pm \beta T\Delta S_R \mp T\Delta G_R(\partial\beta/\partial T)$$

$$= (\Delta H^{\ddagger}_{\phi=o} \pm \beta\Delta H_R) \mp T\Delta G_R(\partial\beta/\partial T)$$

where ΔH_R is the enthalpy change for the overall reaction at

equilibrium. Similarly, the logarithm of the apparent frequency factor is given by

$$\ln A_\eta = \ln i_\eta + \Delta\bar{H}^{\ddagger}_{\eta}/RT \qquad [37]$$

$$= \ln[zFcf(\theta)\kappa\bar{k}T/h]+(\Delta S^{\ddagger}_{\phi=o}\pm\beta\Delta S_R)/R-(\Delta G_R/R)(\partial\beta/\partial T)\pm(nF\eta/R)(\partial\beta/\partial T)$$

and when $\eta = 0$, reduces to the less complex result,

$$\ln A_{\eta=o}=\ln[zFcf(\theta)\kappa\bar{k}T/h]+(\Delta S^{\ddagger}_{\phi=o}\pm\beta\Delta S_R)/R-(\Delta G_R/R)(\partial\beta/\partial T) \qquad [38]$$

In the conventional treatment of apparent and true activation quantities, β is assumed to be independent of temperature so that the terms containing $(\partial\beta/\partial T)$ in eqns.[36] and [38] are not included. The effect of a temperature-dependent β on the derivation of the activation quantities will, however, be examined in section B, chapter 5.

Eqns.[36] and [38] indicate that what is experimentally accessible at $\eta = 0$ is the "apparent" heat of activation $\Delta\bar{H}^{\ddagger}_{\eta=o} = \Delta H^{\ddagger}_{\phi=o} \pm \beta\Delta H_R$, where ΔH_R is the heat of the overall single electrode reaction at the reversible potential; or an "apparent" entropy of activation $\Delta\bar{S}^{\ddagger}_{\eta=o} = \Delta S^{\ddagger}_{\phi=o} \pm \beta\Delta S_R$ where ΔS_R is the single electrode entropy change at $\eta = 0$ for the overall reaction. The situation is further complicated if the terms containing $(\partial\beta/\partial T)$ are significant. However, for a given electrode reaction (e.g., the h.e.r.) proceeding under different conditions (e.g., at different metals or with different isotopes of the reactant at the same metal), the difference of the apparent heats of activation gives the difference of the true enthalpies of activation and the ratio of the apparent frequency factors is the same as the ratio of the true frequency factors.

Of course, this is only correct if i) the reference electrode potential and its temperature-dependence are not changed under the different experimental conditions and ii) if β and $\partial\beta/\partial T$ do not change significantly.

3. Extrathermodynamic Approaches in the Evaluation of True Activation Parameters

As was indicated before, it is a well known problem that only apparent heats of activation and apparent frequency factors are thermodynamically accessible from experimental electrode kinetic measurements (98) over a range of temperatures. Electrochemical activation quantities are determined from either i) measurements of current densities at constant electrode potential (referred to some reference electrode in the system) as a function of temperature or ii) the temperature coefficient of overpotential (referred to some reference electrode in the system) at constant current density. In both methods, the unknown absolute metal/solution potential differences at the reference electrode will vary with temperature because of the half-cell reaction entropy change, which is impossible to measure directly without introduction of some approximation or extrathermodynamic assumption.

In order to estimate the true enthalpies and entropies of activation from the heat of activation and the frequency factor of the experimental electrochemical Arrhenius relation, an extrathermodynamic approach is required.

a) Estimation of ΔH_R for the Reference Electrode

In order to recover the true enthalpy of activation, $\Delta H^{\ddagger}_{\phi=0}$, from the apparent heat of activation (eqn.[36]), β must be known from experiment and ΔH_R must be estimated by a non-thermodynamic calculation. For example, for the hydrogen reference electrode, calculations of ΔH_R for the half-cell reaction involves the cycle,

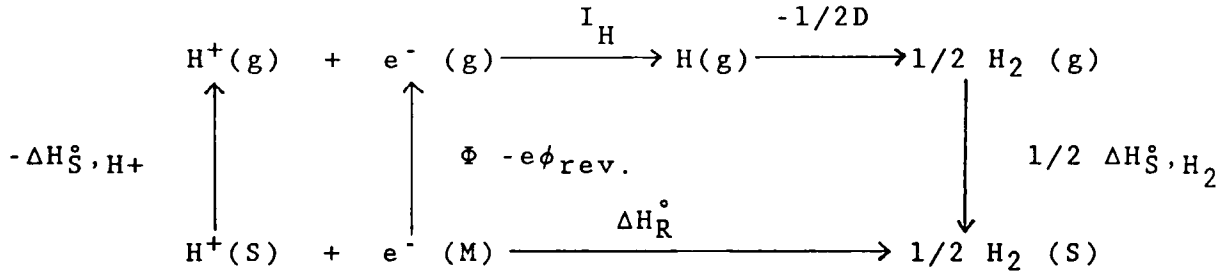

where

$$\Delta H^{\circ}_R = -\Delta H^{\circ}_{S,H+} + (\Phi - e\phi_{rev.})\, N_A - I_H \quad 1/2D + 1/2\Delta H^{\circ}_{S,H_2} \qquad [39]$$

and $\Delta H^{\circ}_{S,H^+}$ is the heat of solvation of H^+, I_H is the ionization energy of H to H^+, D is the dissociation energy of H_2 to 2H, $\Delta H^{\circ}_{S,H_2}$ is the heat of solvation of H_2 and Φ is the electron work function of the metal, i.e., when the metal/solution p.d. $\phi = 0$. Generally, values of the single ion enthalpy of solvation are known only to within 20 to 40 kJ mole ^{1} and the electron work function for clean surfaces is known only to within 10 to 20 kJ (100,101), so that the true $\Delta H^{\ddagger}_{\phi=0}$ cannot be calculated very precisely from the experimental apparent heat of activation.

b) Estimation of ΔS_R for the Reference Electrode

The true entropy of activation, $\Delta S^{\ddagger}_{\phi=0}$ (or the true frequency

factor) can be recovered analogously from the apparent frequency factor (eqn.[38]), if β is known from experiment and ΔS_R is estimated by an extrathermodynamic method. Fortunately, ΔS_R for the half-cell reaction can be estimated much more reliably than the corresponding ΔH_R, considered above. For example, for the hydrogen reference electrode,

$$\Delta S^\circ = 1/2\ S^\circ(H_2) \quad \bar{S}^\circ(H^+) \quad \bar{S}^\circ(\bar{e}) \qquad [40]$$

where $S^\circ(H_2)$ is an accurately known thermodynamic quantity, $\bar{S}^\circ(\bar{e})$ is normally assumed to be zero, and the absolute partial ionic entropy, $\bar{S}^\circ(H^+)$, can be determined by one or more relatively reliable extrathermodynamic methods (102) to within $\pm$ 4.0 J mole $^{1}K^{-1}$ (or $\pm$1.2 kJ mole ^{1} for $T\Delta S^\circ$ at 298 K). The most reliable method of evaluating single ionic entropies is the electrochemical method using thermocells, as used in the work reported here, and as discussed in detail in section A, chapter 5.

Strictly speaking, if β is temperature-dependent then the terms containing $(\partial\beta/\partial T)$ in eqns [36] and [38] should be taken into account in estimating the true $\Delta H^{\ddagger}_{\phi=0}$ and true $\Delta S^{\ddagger}_{\phi=0}$ values. The temperature coefficient of β, i.e., $\partial\beta/\partial T$, can be determined from experiment (as evaluated in the present work-see section 5-B) but ΔG_R must be estimated by a non-thermodynamic calculation and for most one-election half-cell reactions it is in the range of 0 to $\pm$ 96 kJ mole ^{1} (103).

4 Evaluation of Activation Parameters at a Fixed Metal-Solution Potential-Difference ϕ

Another approach to obtaining activation parameters is to make kinetic measurements referred to the potential of a reference electrode maintained at constant temperature while the temperature of the working electrode is varied. An experimentally more convenient but equivalent approach, is to make regular electrode kinetic measurements with the reference electrode at the same but varied temperature as that of the working electrode (isothermal measurement) and then to correct the potential scale used, at each temperature, with data derived experimentally from separately measured potentials of a non-isothermal reference cell (thermocell) under conditions, as used in the work reported here, where the thermal junction potential is minimized. The effect of non-isothermal reference cell potential corrections, $\Delta\phi(T)$, on steady-state polarization measurements is shown in terms of a working diagram in Fig. 49; these corrections lead to parallel shifts of the Tafel line so the current-density would be either increased or decreased at a fixed metal solution potential difference ϕ

The reference electrode potential can be fixed for different solution compositions by using appropriate reference electrode cells and correcting the kinetic data to a common potential scale. For a change in reference electrode potential from ϕ_2 to ϕ_1 with a change of solution composition, the effect of a potential correction $(\phi_2-\phi_1)$ on steady-state polarization

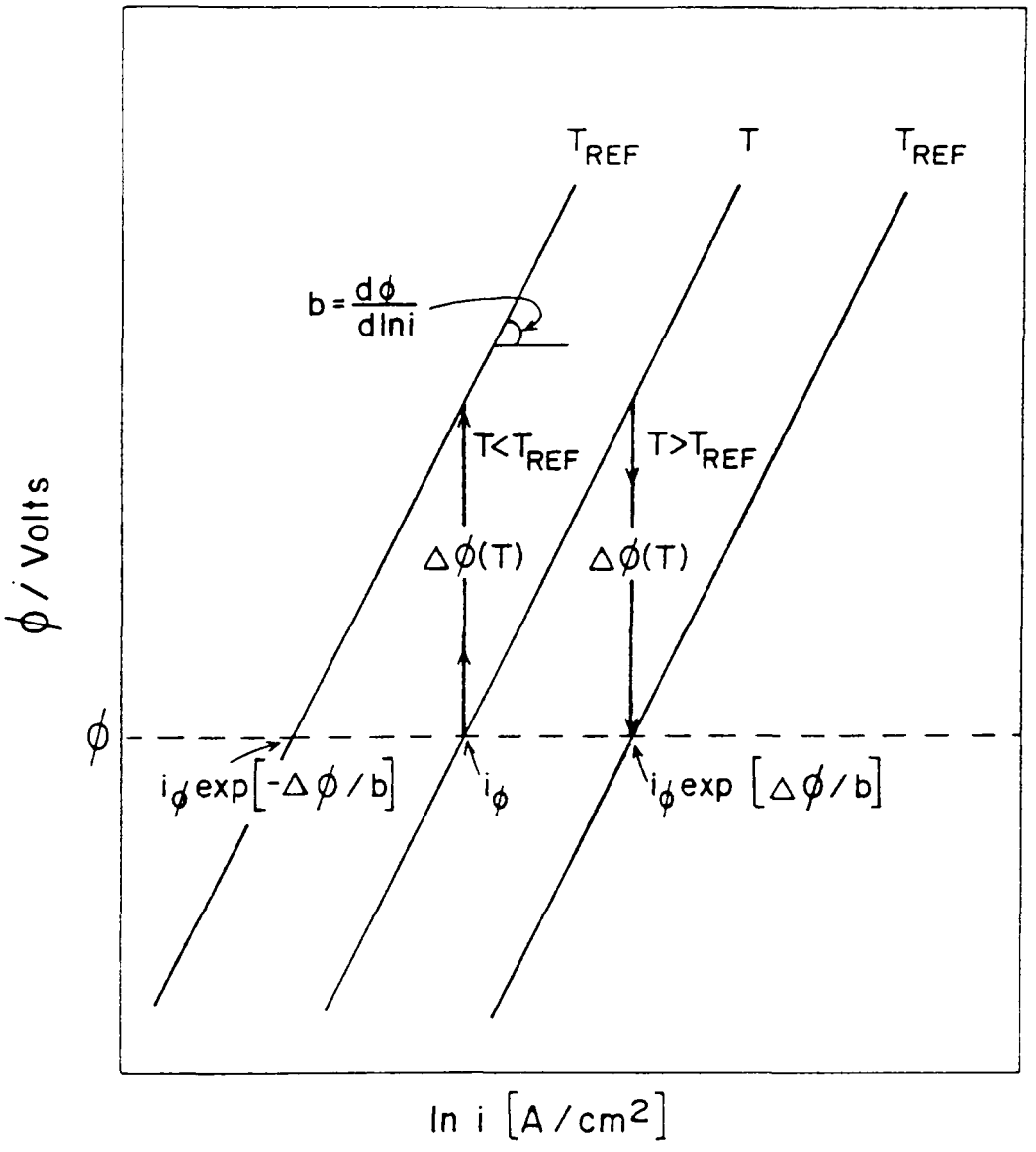

Fig. 49 Effect of non isothermal cell (thermocell) corrections on steady-state polarization measurements

measurements is shown in terms of the working diagram, Fig. 50; these corrections also result in either an increase or decrease of the current-density at a fixed metal-solution potential difference ϕ_1, but the slopes are, of course, unaffected by the correction procedure.

The slopes and intercepts of electrochemical Arrhenius plots of ln i_ϕ vs T^{-1} at a fixed metal-solution potential ϕ will give the heat of activation and the electrochemical frequency factor also at the constant metal-solution potential ϕ.

5. Relation Between True Activation Parameters and Those Determined at a Fixed Electrode Potential ϕ

For a fixed reference electrode potential, ϕ'_R, which does not change with temperature and solution composition at the working electrode and at a fixed applied potential V relative to the reference electrode, the heat of activation at a fixed metal-solution potential-difference $\phi = \phi'_R + V$ is given, for an ideal system with no junction potential by

$$\Delta\bar{H}^{\ddagger}_{\phi} = -R[\partial \ln i/\partial(1/T)]_{\phi} \qquad [41]$$

$$= \Delta H^{\ddagger}_{\phi=0} \mp \beta\phi nF \pm \phi nFT(\partial\beta/\partial T)$$

Similarly, the logarithm of the frequency factor at a fixed metal-solution potential-difference $\phi = \phi'_R + V$ is given by

$$\ln A_\phi = \ln i_\phi + \Delta\bar{H}^{\ddagger}_{\phi}/RT \qquad [42]$$

$$= \ln (zFcf(\theta)\kappa\tilde{k}T/h) + \Delta S^{\ddagger}_{\phi=0}/R \pm (nF\phi/R)(\partial\beta/\partial T)$$

However, in practice there will be some small error in the non-

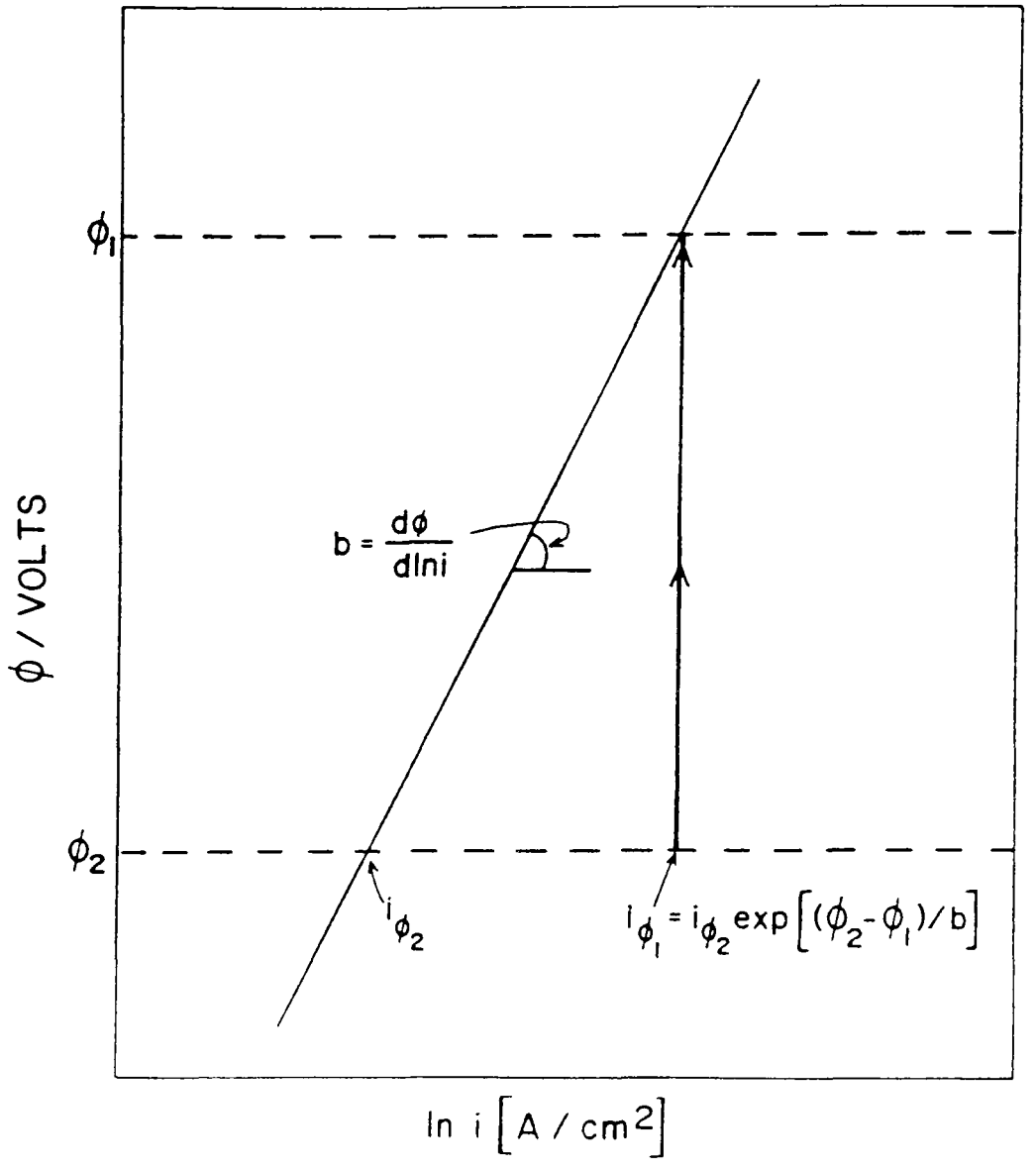

Fig 50 Effect of reference electrode cell (isothermal cell) corrections on steady-state polarization measurements

isothermal cell corrections ($\Delta\phi_{t.l.j.}$, t.l.j. = thermal liquid junction) and in the isothermal cell corrections (E_j), so that there will be an error in the experimentally estimated heat of activation at fixed ϕ of

$$\delta\Delta\bar{H}^{\ddagger}_{\phi} = \pm \beta nFT\,(\partial\phi_{t.l.j}/\partial T) \pm \beta nFE_j \pm nFTE_j(\partial\beta/\partial T) \qquad [43]$$

and an error in the logarithm of the experimental frequency factor at fixed ϕ of

$$\delta \ln A_{\phi} = \pm (\beta nF/R)(\partial\phi_{t.l.j.}/\partial T) \pm (nFE_j/R)(\partial\beta/\partial T) \qquad [44]$$

An upper limit of these errors can be estimated if the following assumptions are made: i) that $\beta = 0.5$ and is temperature independent ii) that $d\phi_{t.l.j.}/dT = 50\ \mu VK^{-1}$ say, since for most aqueous electrolytes it is found that $d\phi_{t.l\ j.}/dT \leq 50\ \mu VK^{-1}$ (78,104,105) and iii) that there is a large junction potential of $E_j = 0.1$ V (practically, E_j is usually much less than this). When this is done, reasonable errors of $\pm$ 5.5 kJ $mole^{-1}$ for $\Delta\bar{H}^{\ddagger}_{\phi}$ and 0.3 for ln A_{ϕ} (or 2.5 $JK^{-1}mole^{-1}$ for $\Delta\bar{S}^{\ddagger}_{\phi}$) are calculated, indicating that the extrathermodynamic approach used here provides a reliable procedure for evaluating activation parameters at a fixed metal solution potential-difference ϕ. Conditions under which the unavoidable irreversible liquid and thermal junction potentials can be minimized or reliably estimated are discussed in detail in section A, chapter 5.

CHAPTER 5

RESULTS AND DISCUSSION

A. Isothermal and Non-Isothermal Cell Measurements

1 Introduction

In order to obtain activation parameters at a constant metal solution potential (or field) rather than constant overpotential, i.e., as measured against a reference electrode in the same solution at changing temperature, it is practically desirable to make measurements with respect to a reference electrode potential, ϕ_R, invariant with temperature and solution composition at the working electrode

The most convenient method involves the use of isothermal and non-isothermal reference electrochemical cells to fix ϕ_R, so that the steady-state polarization data measured at various temperatures, can be corrected to a common potential scale However, physical separation of the reference electrodes which are at different temperatures and/or in different solution environments, creates an irreversible liquid junction potential difference between them. The direct measurement of a junction potential is not feasible because it is impossible to measure directly single-electrode potentials and corresponding single ion properties. However, it is possible to estimate junction potentials indirectly or to make calculations based on assumptions about the single ion properties and the geometry and distribution of ions in the region of the junction.

Many methods have been proposed for the estimation of single ion effects and have been summarized in several publications (102, 106) For all reference cell corrections in the present work, procedures have been adopted that enable the assumption to be made that the unknown irreversible liquid junction potential can be made negligible compared to the difference of the Galvani metal-solution potential drops at the two single electrode interfaces, or can be corrected for in a reliable way.

2. Isothermal Reference Electrode Cell Measurements

The potentials of each of the reference electrodes used are referred to that of the hydrogen reference electrode in 0.1M $HCl(H_2O)$ at 298 K using the following isothermal reference cell:

$$Pt|H_2,\ 0\ 1M\ HCl(H_2O)||KCl_{sat}(H_2O)||Electrolyte(S)|\begin{matrix}Reference\\Electrode\end{matrix}$$

The saturated aqueous KCl salt bridge, as in the above cell, has been widely used with nonaqueous solutions for potentiometric titrations, polarographic and kinetic studies, and to relate potentials from one reference electrode scale to another (87, 107). Most of the experimental difficulties that arise with this aqueous-nonaqueous liquid junction are a result of precipitation of KCl in the junction due to its low solubility in many solvents, e g., pK_{sp} of KCl in CH_3CN is 7.2 However, when measurements are completed within a short period of time, the liquid junction potential drift is negligible and the cell potential is reproducible to within a few millivolts

(87). The reference cell potentials for the different reference electrodes used in this study are shown in Table 2 and were found to be quite stable (variation < 3 mV) over a 60 minute period. However, larger variations in cell potential were found between measurements in separate experiments and could be as high as 15 mV, as in the case of DMF as the solvent.

a) Ionic Junction Potential ($E_{j,ion}$)

The emf of the isothermal reference cell can be written as

$$E_{cell} = \phi_{R1} - \phi_{R2} + E_{j,ion} + E_{j,solvent} \qquad [45]$$

where ϕ_{R1} and ϕ_{R2} are the Galvani metal-solution potential differences at each electrode, and $E_{j,ion}$ and $E_{j,solvent}$ are the contributions to the liquid junction potential due to transport of the ions and solvent molecules (cf. ref 108) across the boundary, respectively. If the ionic strength of the bridge solution is at least ten times that of the solutions at the electrodes, then the bridge solution mainly determines the junction potential. This condition was satisfied for all the electrolyte solutions used in the present work ($I \leq 0$ 1M, cf 3 5M KCl) and therefore $E_{j,ion}$ can be given by the expression derived by Guggenheim (109),

$$E_{j,ion} = -1/F \int_{H_2O}^{S} \Sigma t_{K+} d\mu_{K+} + 1/F \int_{H_2O}^{S} \Sigma t_{Cl-} d\mu_{Cl} \qquad [46]$$

where t_{K+} and t_{Cl} are the transport numbers, $d\mu_{K+}$ and $d\mu_{Cl}$ are the chemical potential changes for the indicated ions crossing the junction.

TABLE 2

E.m.f.'s of the Cell

Pt/H_2.0.1M HCl(H_2O)||KCl_{sat}(H_2O)||Electrolyte(S)|R

for Different Reference Electrodes(R) and Solvents(S), at 298 K

Solvent	Electrolyte*	R	E_{cell}/V
CH_3OH	0.1M HCl	$H^+\|H_2$	0.104 ± 0.003
1 Propanol	0.1M HCl	$H^+\|H_2$	0.118 ± 0.003
2-Propanol	0.1M HCl	$H^+\|H_2$	0.099 ± 0.003
Isobutanol	0.1M HCl	$H^+\|H_2$	0.112 ± 0.005
H_2O	0.1M MCl**	AgCl|Ag	0.353 ± 0 003
CH_3OH	0.1M MCl***	AgCl|Ag	0.161 ± 0.004
$HCONH_2$	0.1M MCl***	AgCl|Ag	0.292 ± 0.002
DMF	0.01M $AgClO_4$	$Ag^+\|Ag$	0.734 ± 0.015
AN	0.01M $AgClO_4$	$Ag^+\|Ag$	0.584 ± 0.008

* Nominal molar concentration not corrected for ionic association.

** M = H^+; $EtNH_3^+$, Et_3NH^+

*** M = $EtNH_3^+$, Et_3NH^+

Table 3 shows that the limiting ionic transference numbers of K^+ and Cl^-, based on limiting ionic conductances ($t^{\circ}_{\pm} = \Lambda^{\circ}_{\pm}/\Lambda^{\circ}$), are approximately equal in the solvents studied here. The transference numbers in the electrolyte solutions ($t_{\pm} = \Lambda_{\pm}/\Lambda$) should be approximately the same as the limiting ionic transfer numbers at infinitesimal ionic strength because they are conductance ratios and therefore less sensitive to changes in solution ionic strength than conductances themselves.

Typical examples are provided by 0.01M NaCl in CH_3OH at 298 K which has a cation transference number 1.1% less than the limiting value but has a conductance which is 21% lower (110) and 0.1M KCl in formamide at 298 K which has a cation transference number 1.6% less than the limiting value but has a conductance which is 16% lower (110). It seems reasonable, therefore, to take the transport numbers for K^+ and Cl^- as 0.5 throughout the cell and therefore the junction potential due to the ions is then given by

$$E_{j,ion} = -\frac{0.5}{F} {}^{H_2O}\Delta S_{\mu_{K+}} + \frac{0.5}{F} {}^{H_2O}\Delta S_{\mu_{Cl}} \qquad [47]$$

where ${}^{H_2O}\Delta S_{\mu_{K+}}$ and ${}^{H_2O}\Delta S_{\mu_{Cl}}$ represent the change in chemical potential (Gibbs energy of transfer, ΔG_t) of K^+ and Cl^- on crossing from water to solvent S. Table 3 shows the standard Gibbs energies of transfer of K^+ and Cl from water at infinite dilution to the solvent of interest, also at infinite dilution, and the resultant calculated junction potentials.

These free energy values (111) have been obtained as a

TABLE 3

Limiting Ionic Transference Numbers, Free Energies of Transfer, and Ionic Junction Potentials for KCl in Different Solvents at 298 K.

Solvent	$t^{\circ *}_{K^+}$	$t^{\circ *}_{Cl^-}$	$^{a}\Delta G^{\circ}_{t}$/kJmole^{-1} (K^+, $H_2O \rightarrow S$)	$^{a}\Delta G^{\circ}_{t}$/kJmole^{-1} (Cl^-, $H_2O \rightarrow S$)	$E^{**}_{j,ion}$/V
H_2O	0.490	0.510	0	0	≈0
CH_3OH	0.501	0.499	9.6	13.2	0 019
1 Propanol	0.520	0.488	18.0	26.0	0.042
2-Propanol	0.433	0.567	22.8	28.5	0.030
Isobutanol***	---	---	--	--	
$HCONH_2$	0.427	0.573	-4.3	13.7	0.093
DMF	0.359	0.641	10.3	48.3	0.304
AN	0.459	0.541	8.1	42.1	0 176

* Values from limiting ionic conductivities ($t^{\circ}_{\pm} = \Lambda^{\circ}_{\pm}/\Lambda^{\circ}$); ref. 82.

** $E_{j,ion} \approx (0.5/F)\{\Delta G^{\circ}_{t}(Cl^-, H_2O \rightarrow S) - \Delta G^{\circ}_{t}(K^+, H_2O \rightarrow S)\}$.

*** No literature data found.

a. ref. 111.

weighted average of the reported values based on the reliability of the experimental data and the acceptability of the extrathermodynamic assumption. However, an indication of the uncertainty in these single ion values is given by the wide range of data from 42 references for the standard Gibbs energy

of transfer of K^+ from H_2O to CH_3OH (-24 kJ mole ^{1} to +19.4 kJ mole ^{1}) and Cl^- from H_2O to CH_3OH (26.1 kJ mole ^{1} to +46 kJ $mole^{-1}$). Although the solutions in the reference cell are not at infinite dilution ($I \leq 0.1M$) it seems reasonable to assume that the difference of the Gibbs energies of transfer of K^+ and Cl^- will help to cancel any concentration effects and therefore the values for infinite dilution can be used in eqn.[47].

For electrolytes such as TEAPic, Bu_4NBPh_4 and Ph_4AsBPh_4, where the ions are large, of similar size, and have a single charge buried at the centre of inert ligands, the medium effects are usually assumed to be equal for the cation and anion, e.g., $\Delta G_t(Ph_4As^+) = \Delta G_t(BPh_4^-)$. This "reference electrolyte" assumption is the basis of most of the extrathermodynamic assumptions which are used to separate thermodynamic properties of electrolytes into those of individual ions (93). Ideally, electrolytes such as Ph_4AsBPh_4 would be preferred to KCl for use as bridge electrolytes but unfortunately they are not soluble enough to give concentrations in excess of the reference electrode solutions, e.g., pK_{sp} of Ph_4AsBPh in CH_3OH, AN and DMF are 8.5, 5.2 and 3.7, respectively. Also, even the suitability of these electrolytes to obtain thermodynamic properties of individual ions and to give negligible liquid junctions has been questioned recently because of the possibility that ions such as Ph_4As^+ and BPh_4^- experience specific interactions with water and other solvents (93), contrary to earlier assumptions.

b) Solvent Junction Potential ($E_{j,solvent}$)

It has been pointed out (112) that when two different solvents form a boundary, then there may also be a significant contribution to the liquid junction potential ($E_{j,solvent}$) from the transport of solvent molecules across the interface, especially if they interact strongly. Following the procedure of Cox, Parker and Waghorne (108), the liquid junction potential due to solvent transport is then given, by analogy with $E_{j,ion}$, as

$$E_{j,solvent} = \frac{1}{F}\int_{H_2O}^{S}\Sigma t_s' d\mu_s \qquad [48]$$

where $d\mu_s$ is the change in chemical potential of each solvent on crossing its junction with the other solvent and the coefficient, t_s', represents the total number of moles of solvent carried across that junction per Faraday of charge passed.

If both the transport numbers and the solvation numbers of K^+ and Cl through the junctions are approximately constant for the solvents used here, then the junction potential is given by

$$E_{j,solvent} = (t'_{H_2O}/F)\ {}^{H_2O}\Delta^{S}\mu_s(H_2O) + (t_s'/F)\,{}^{S}\Delta^{H_2O}\mu_s(S) \qquad [49]$$

where ${}^{H_2O}\Delta^{S}\mu_s(H_2O)$ represents the Gibbs energy per mole of solution of H_2O in solvent, S, and ${}^{S}\Delta^{H_2O}\mu_s(S)$ represents the Gibbs energy per mole of solution of S in H_2O and $t_s' = (t_{K+} \times n_{K+}) + (t_{Cl} \times n_{Cl})$.

Table 4 shows the Gibbs energies of solution of some solvents in other solvents and the calculated solvent junction potentials, $E_{j,solvent}$, assuming equal ionic transport numbers

TABLE 4

Solvent Junction Potentials Calculated from Free Energies of Solution of some Solvents in Other Solvents at 298 K.

Solvent	$^{a}\Delta G_s$/kJmole^{-1} ($H_2O \rightarrow S$)	$^{a}\Delta G_s$/kJmole^{-1} ($S \rightarrow H_2O$)	$E^{*}_{j,solvent}$/V
CH_3OH	-2.09	1.26	-0.009
$HCONH_2$	-0.80	7.95	0.074
DMF	-0.84	-2.09	-0.030
AN	4.81	6.28	0.115

* $E_{j,solvent} = (t'_{H_2O}/F)\Delta G_s(H_2O \rightarrow S) + (t'_s/F)\Delta G_s(S \rightarrow H_2O)$; $t'_{H_2O} \approx t'_s \approx 1$.

a ref. 108

($t_{K+} = t_{Cl} = 0.5$) and equal solvation numbers (taken here as $n_{K+} = n_{Cl} = 1$) for K^+ and Cl^-.

Appreciable liquid junction potentials are found which are consistent with experimental observations (108) that variations up to 100 mV in some cell potentials can occur from one solvent to another when the bridge solvent is changed.

c) Potential Difference of the Electrodes

Values of E_{cell}, $E_{j,ion}$, $E_{j,solvent}$ and E_e (potential difference at the electrodes), shown in Table 5, indicate that $E_{j,solvent}$ can be as large as $E_{j,ion}$ but is generally smaller

and in some cases can provide compensation, i.e., it is opposite in sign to $E_{j,ion}$. The total junction potential in the aqueous-nonaqueous reference cell, using a concentrated aqueous KCl bridge can be appreciable and may account for as much as 57% of the observed cell potential in formamide and acetonitrile.

Standard potentials of electrodes in nonaqueous solvents against the aqueous standard hydrogen electrode can be estimated using the standard molar "chemical" Gibbs energy of transfer (111) of the ions according to:

$$E°(\text{nonaqueous}) = E°(\text{aqueous}) + \Delta G_t^\circ/nF \qquad [50]$$

where F is the Faraday constant and n the number of electrons involved in the electrode reaction. When this is done, and the activities of the ions are taken into account (Table 7), values of the potential difference of the electrodes can be derived and are as shown in Table 5, for comparison. For the aqueous AgCl|Ag electrode, the calculated value is in almost perfect agreement with the experimentally determined value but, for the aqueous/nonaqueous potentials, there are large differences. Strictly speaking, the standard "real" Gibbs energy of transfer should be used in eqn.[50], and so should include a surface potential term, i.e., $\Delta\alpha_t^\circ = \Delta G_t^\circ + (\chi_S \quad \chi_W)$, where χ_S and χ_W are the surface potentials of the nonaqueous solvent and water, respectively. Estimates of surface potentials vary considerably but the results of several authors (113, 114, 115) indicate they can be large, viz. $\chi(CH_3OH) \quad \chi(H_2O) \approx -0.14$ V to -0 3 V, $\chi(AN) \quad \chi(H_2O) \approx -0.03$ to -0.30 V, and therefore may

TABLE 5

E.m.f's of the Cell Pt|H_2, 0.1M HCl(H_2O)||KCl_{sat}(H_2O)|| Electrolytes (S)|R at 298 K, corrected for Ionic and Solvent Junction Potentials

Solvent	* E_{cell}/V	** $E_{j,ion}$/V	*** $E_{j,solvent}$/V	**** E_e/V	(iii) E_{calc}/V
			R = H^+| H_2		
CH_3OH	0.104	0.019	-0.009	0.094	0.088
1-Propanol	0.118	0.042	--	(i) (0.085)	0.048
2-Propanol	0.099	0.030		(i) (0.078)	-0.020
Isobutanol	0.112			(ii) (0.086)	0.098
			R = AgCl|Ag		
H_2O	0.353	0	0	0.353	0.354
CH_3OH	0.265	0.019	-0.009	0.255	0.506
$HCONH_2$	0.292	0.093	0.074	0.125	0.493
			R = Ag^+|Ag		
DMF	0.734	0.304	-0.030	0.460	0.514
AN	0.584	0.176	0.155	0.253	0.489

* From Table 2.
** From Table 3.
*** From Table 4.
**** $E_e = \phi_{R1} \quad \phi_{R2} = E_{cell} \quad E_{j,ion} - E_{j,solvent}$.
(i) Assumption; $E_{j,solvent} \approx -0.009$V.
(ii) Assumptions; $E_{j,ion} \approx 0.035$ V; $E_{j,solvent} \approx -0.009$V.
(iii) Based on E°(nonaqueous) = E°(aqueous) + $\Delta G_t^\circ/nF$, and the activities of the ions (Table 6); the surface potential term χ(nonaqueous) - χ(aqueous), is neglected.

account for some of the difference between the calculated cell potentials and the experimental cell potentials. The dilemma of which cell potentials to use from Table 5 to correct the polarization data, is a result of the unavoidable uncertainty in the extrathermodynamic assumptions and single ion values used in the experimental and calculated evaluations of the cell potential. The experimental cell potentials using a saturated aqueous KCl salt bridge, i.e., E_{cell}, were used in the present work, and these values should result in an error of less than 100 mV for the alcohols and $HCONH_2$, but may result in larger errors of up to ca. 200 mV for AN and DMF, where the ionic and solvent junction potentials tend to be larger

3. Non-Isothermal Reference Electrode Cell Measurements

Non-isothermal reference electrode cells have been used in studies of half-cell reaction entropies (104, 105, 78) and more recently by Weaver et al. (77) in the study of temperature effects on the rates of redox processes at electrode surfaces In the present work, a non-isothermal cell arrangement was used mainly to correct polarization measurements taken with the reference electrode at the same, but varied, temperature of the working electrode to a fixed reference electrode potential, ϕ_R, invariant with temperature.

The cell shown below is for the aqueous hydrogen reference half-cell, but the reference electrode half-cell and salt bridge solution will be different for different systems:

$Cu|Pt|H^+,H_2||KCl(3\ 5M)|KCl(3.5M)||H^+,H_2|Pt|Pt|Cu$

←T=298 K (fixed) ✕--T(varied) ✕--T=298 K→

The cell was constructed so that the temperature gradient arose over a short distance (< 1 cm) within the salt bridge. The junctions were established at two closed but wetted ground-glass plugs (see Fig. 15). This cell geometry is unfavorable to the development of concentration polarization due to thermal diffusion (Soret effect) Thermal diffusion of the electrolyte tends to concentrate electrolytes in the cold region and the resultant concentration gradient changes the cell potential until the thermal diffusion process is fully developed. The absence of any significant Soret effect was indicated by stable cell potentials (< 1 mV) for up to 24 h under non-isothermal conditions.

a) Temperature Dependence of the Reversible Potential and the Cell Potential

If the isothermal liquid junction potential, $E_{j,ion}$, is reduced to negligibly small values by the use of a suitable concentrated salt bridge with ions of approximately equal mobility, then the non-isothermal cell potential is given by,

$$E_{cell} = \Delta\phi_{t.l\ j} + \Delta\phi_{tc} + \Delta\phi_m \qquad [51]$$

and the overall temperature coefficient of the cell potential by;

$$dE_{cell}/dT = d\phi_{t.l\ j}/dT + d\phi_{tc}/dT + d\phi_m/dT \qquad [52]$$

where $\phi_{t.l\ j}$ is the thermal liquid junction potential difference in the salt bridge, ϕ_{tc} is the thermoelectric

potential difference between the hot and cold regions of the metal conductors, and ϕ_m is the Galvani metal-solution potential drop at the electrode surface.

The potential gradient which accompanies a temperature gradient along a conductor ($\Delta\phi_{tc}$) is the Thomson thermoelectric effect and absolute values of its temperature coefficient ($d\phi_{tc}/dT$) are known for a number of metals and found to be only a few microvolts per degree (104). For Pt used in this work, $d\phi_{tc}/dT$ is about 6 μVK^{-1} (78) in the temperature range 273-373 K. This value is negligible when compared with measured values of dE_{cell}/dT, and for maximum variations in temperature of about 100 K, $\Delta\phi_{tc}$ will also be negligible compared to the non-isothermal cell potential. Any effects due to metal-metal (e g., Cu-Pt) junctions were virtually eliminated by keeping all such junctions near 298 K.

Absolute values of the thermal liquid junction potential ($\Delta\phi_{t\ l.j}$) are thermodynamically inaccessible but estimates of this potential indicate that for most aqueous electrolytes $d\phi_{t.l.j.}/dT \leq 50\ \mu VK^{-1}$(104, 105, 78) For protonic solutions, where the proton has relatively a very high mobility, the thermal liquid junction potential can be appreciably higher, i.e., $d\phi_{t.l\ j}/dT$ can be up to <u>ca</u>. 0.4 mVK^{-1}.

The use of a non-isothermal saturated KCl salt bridge, similar to the arrangement described above, has been assumed by deBethune et al. (105) to have virtually zero thermal liquid junction potential and will introduce an error by no more than

ca. 0.03 mVK^{-1} and probably a lot less. Based on these observations, it seems reasonable to assume a zero thermal liquid junction potential for nonaqueous reference electrode systems employing a concentrated salt bridge consisting of ions of nearly equal mobility in the same nonaqueous solvent.

Considering experimental errors and the validity of the assumptions, it seems best to assign an error of not less than ± 0.03 mVK^{-1} to $d\phi_m/dT$ determined from the temperature coefficient of the non-isothermal cell, i.e., $dE/dT = d\phi_m/dT \pm 0.03\ mVK^{-1}$ which, although not negligible compared to $\Delta\phi_m$, will only result in a small error when E_{cell} is used to correct the kinetic polarization data. For example, if a Tafel slope of 120 mV per decade of current is assumed, then in the worst case the error will be 3/120 x 100 = 2.5% of a decade in current.

b) Results of Non-Isothermal Cell Measurements

All non-isothermal cell measurements were made relative to a reference electrode temperature at 298 K and the reference electrode at this temperature was the negative pole of the cell. Temperature cycling did not produce hysteresis effects, and measurements were reproducible to within ± 0.5 mV.

The non-isothermal cell potentials for the $H^+|H_2$, AgCl|Ag, $Ag^+|Ag$, AgBr|Ag and $Br_2|Br$ reference electrodes in different systems are shown in chapter 3 in Figs. 38-42, Figs. 43-45, Figs. 46-47 and Fig. 48, respectively. Table 6, lists the temperature coefficients of the non-isothermal cell potentials at 298 K and the particular salt bridge used. The salt-bridge

concentration was below the solubility limit even at the lowest temperatures that were employed.

Appreciable thermal liquid junction potentials were found for the aqueous and alcoholic HCl solutions (see Table 6) when no salt-bridge was used. For the partially substituted alkyl ammonium salts in H_2O, $HCONH_2$ and CH_3OH (in the temperature range 273 to 335 K), only negligible changes in the cell potential (< 0.5 mV) were found when the salt-bridge was replaced by the electrolyte, i.e., $\Delta\phi_{t.l.j.} \approx 0$. For the aprotic solvents AN and DMF, no salt-bridge was used as the thermal liquid junction potentials should be negligibly small for neutral electrolytes and probably for protonic solutions as well, since all the ions including the proton have nearly equal ionic mobility in these solvents

It can be seen from Fig. 44, that there is an appreciable difference in the non-isothermal cell potentials for 0.1M $EtNH_3Cl$ in CH_3OH for measurements with and without a salt bridge below 273 K. This is probably due to increased association of $EtNH_3Cl$ at lower temperatures which tends to reduce the free electrolyte concentration in the cold region of the thermal gradient and changes the cell potential due to the resultant concentration gradient.

In most cases where the solution composition was changed in the same solvent, only negligible changes in the non-isothermal cell potentials were found for the Ag|AgCl and $Ag^+|Ag$ reference electrodes, indicating that the activities of the Cl and Ag^+

TABLE 6

Temperature Coefficients of Non-Isothermal Cell Potentials for Different Reference Electrodes and Solvents at 298 K

Solvent	Electrolyte	R	Salt Bridge	dE/dT (Salt Bridge) mVK^{-1}	dE/dT (No Bridge) mVK^{-1}	t.l.j.p.* mVK^{-1}
H_2O	0.1M HCl	$H^+\|H_2$	3.5M KCl (t_+° - 0.49)	0.673	0.297	-0.376
CH_3OH	0.1M HCl	$H^+\|H_2$	2.4M Pr_4NBr (t_+° - 0.45)	0.684	0.640	-0.044
1-Pr[1]	0.1M HCl	$H^+\|H_2$	1.5M Pr_4NBr (t_+° - 0.50)	0.413	0.312	-0.101
2-Pr[1]	0.1M HCl	$H^+\|H_2$	1.5M Pr_4NBr (t_+° - 0.50)	0.505	0.155	-0.350
Isobut[2]	0.1M HCl	$H^+\|H_2$	1.0M Pr_4NBr (t_+° - 0.51)	0.397	0.147	-0.250
H_2O	0.1M MCl**	AgCl|Ag	3.5M KCl (t_+° - 0.49)	0.436	0.436	≈ 0
CH_3OH	0.1M MCl***	AgCl|Ag	2.4M Pr_4NBr (t_+° - 0.45)	0.171	0.171	≈ 0
$HCONH_2$	0.1M MCl***	AgCl|Ag	2.3M NH_4Cl (t_+° - 0.47)	0.193	0.193	≈ 0
DMF	0.01M $AgClO_4$ (0.1M $Et_3NHCF_3SO_3$)	$Ag^+\|Ag$	None	--	0.455	--
DMF	0.01M $AgNO_3$ (0.1M CF_3SO_3H)	$Ag^+\|Ag$	None	--	0.543	--
AN	0.01M $AgClO_4$ (0.1M Et_4ClO_4)	$Ag^+\|Ag$	None	--	0.465	--
AN	0.01M $AgClO_4$ (0.1M $H_3OCF_3SO_3$)	$Ag^+\|Ag$	None	--	0.576	--
AN	0.4M Pr_4NBr| 0.2M Br_2	$Br_2\|Br^-$	None	--	-0.073	--
AN	0.4M Pr_4NBr| 0.2M Br_2	AgBr|Br	None	--	-0.758	--

* t.l.j.p. =thermal liquid junction potential = $(dE/dT)_{no\ bridge} - (dE/dT)_{salt\ bridge}$

** M - H^+, $EtNH_3^+$, Et_3NH^+

*** M - $EtNH_3^+$, Et_3NH^+

[1] Propanol

[2] Isobutanol

ions were not affected significantly. However, even with the same salt bridge, there were appreciable differences in the non isothermal measurements below 283 K between 0 1M Et_3NHCl and 0.1M $EtNH_3Cl$ in methanol (See Fig. 44), probably as a result of increased association of $EtNH_3Cl$ at lower temperatures which would change the Ag|AgCl reference electrode potential.

Non-isothermal cell measurements of the $Ag^+|Ag$ reference electrode in DMF shown in Fig. 46, show a difference between 0.01M $AgClO_4$ and 0.01M $AgNO_3$, most likely because of appreciable association of $AgNO_3$ in DMF, for which K_A=401 mole $^{-1}$l at 298 K (87). Non-isothermal cell measurements of the $Ag^+|Ag$ reference electrode for 0.01M $AgClO_4$ in different AN solutions (Fig. 47) only show a difference in potential as a f(T) when $H_3OCF_3SO_3$ is present at 0.1M concentration. This is most likely a result of i) H_3O^+ significantly affecting the Ag^+ ion activity and/or ii) a thermal liquid junction potential due to the significantly different ionic mobilities of H_3O^+ and CF_3SO_3 (no literature values for the conductivity of $H_3OCF_3SO_3$ in AN were found).

c) Entropies of Half-Cell Reactions in Relation to Single Ion Entropies

Based on reasonable assumptions and the use of concentrated salt bridges, the temperature coefficient of the non-isothermal cell potential can be identified with the temperature coefficient of the particular reference electrode used This allows half-cell reaction entropies and absolute values of

single ion entropies to be determined (78):

$$F(dE_{cell}/dT) \approx F(d\phi_m/dT) = \Delta S_R \quad [53]$$

In order to obtain the "standard" half-cell reaction and single ion entropies, the activity coefficients and their temperature coefficients should be known at 298 K. Since such data are scarce for nonaqueous solvents, the Debye-Hückel expression shown below was used in most cases:

$$\log \gamma_{\pm} = |z_1 z_2| A_v I^{1/2}/(1 + aB_v I^{1/2}) \quad [54]$$

where A_v and B_v are functions of solvent and temperature,

$$A_v = 1.8246 \times 10^6 \, d_o^{1/2} \, (\epsilon T)^{-3/2} \quad [55]$$

$$B_v = 50.29 \times 10^8 \, d_o^{1/2} \, (\epsilon T)^{-1/2} \quad [56]$$

and, I, the ionic strength is the usual function of concentration:

$$I = 1/2 \, \Sigma \, m_i \, z_i^2 \quad [57]$$

Values of the dielectric constant (ϵ) and the density (d_o) have been determined for a number of nonaqueous solvents at different temperatures (82, 66), as have values of the distance of closest approach of ions (a) for a number of electrolytes in different solvents (66). The activity coefficient expression above, is only for free ions and therefore ion association must be taken into account especially for solvents having $\epsilon \leq 35$.

Values of $\gamma_{\pm}$ which are on a molal basis were converted to values on a concentration basis, $y_{\pm}$, through the relation (116).

$$y_{\pm} = \frac{m d_o}{c} \gamma_{\pm} \quad [58]$$

Values of the activity coefficients ($y_{\pm}$) and their temperature coefficients $d\ln y_{\pm}/dT$ at 298 K thus derived are shown in Table 7.

TABLE 7

Activity Coefficients of Electrolytes in Different Solvents from the Debye-Hückel Expression* at 298 K

Solvent	Electrolyte	αC** Mole l^{-1}	A_v*	$10^{-8} B_v$*	a Å	$y_\pm$	$10^4 \frac{d\ln y_\pm}{dT}$*** K^{-1}
H_2O	HCl	0.1	0.510	0.3285	4.5	0.780 (0.797)[b]	-5.023[b]
CH_3OH	HCl	0.079	1.686	0.4522	3.4	0.436 (0.437)[c]	5.758
	MCl(i)	0.1	1.686	0.4522	≈3.8	0.424	5.757
1-Propanol	HCl	0.048	3.529	0.5826	3.9	0.279	6.648
2-Propanol	HCl	0.045	4.017	0.6038	≈3.9	0.243	--
Isobutanol	HCl	0.029	5.070	0.6580	4.4	0.239	--
$HCONH_2$	MCl(i)	0.10	0.328	0.2958	7.5	0.873	-0.461
DMF	$AgClO_4$ ($Et_3NHCF_3SO_3$)	0.01 (0.1)	1.548	0.4671	4.9	0.505	-40.533
AN	$AgClO_4$ (A)(ii)	0.01 (0.1)	1.405	0.4237	4.0	0.476	-14.328

* $\log\gamma_\pm = -|z_1 z_2| A_v I^{1/2}/(1 + aB_v I^{1/2})$
$A_v = 1.8246 \times 10^6 \, d_o^{1/2} (\epsilon T)^{-3/2}$
$B_v = 50.29 \times 10^8 \, d_o^{1/2} (\epsilon T)^{-1/2}$

** αC = free ion concentration; Values of α determined from Table 1.

*** Determined using the D-H expression, and values of d_o and ϵ at different T from ref. 82.

(i) M = $EtNH_3^+$, Et_3NH^+

(ii) A = $Et_3NHCF_3SO_3$, Et_4NClO_4

a. ref. 66.
b. ref. 105.
c. ref. 122.

Note: All values of the activity coefficients on a molal scale ($\gamma_\pm$) were converted to values on the molar scale ($y_\pm$).

i) Hydrogen Reference Electrode

The hydrogen electrode used in the 0.1M alcoholic hydrochloride solutions were saturated with hydrogen gas under a total pressure of about 760 mm Hg (± 10mm). The hydrogen electrode potential in the cell is given by the Nernst equation

$$E = E^\circ + \frac{RT}{2F} \ln (a_{H+})^2 \quad \frac{RT}{2F} \ln[p(H_2,mm)/760] \quad [59]$$

and in order to correct to the standard state of hydrogen gas the term $(RT/2F)\ln [p(H_2,mm)/760]$ must be added to the hydrogen electrode potential measured in the cell. The partial pressure of hydrogen can be determined from

$$p(H_2,mm) \approx 760 \quad p(S,mm) \quad [60]$$

where p(S,mm) is the solvent vapour pressure, which should be nearly the same as that for 0.1M HCl solutions.

Values of the vapour pressure at various temperatures were obtained using the Antoine vapour-pressure relation, which usually gives very reliable values in the range of 10 to 1500 mm Hg:

$$\ln p(S,mm) = A \quad \frac{B}{T+C} \text{ or } p(S,mm) = \exp[A-B/T+C] \quad [61]$$

The Antoine vapour-pressure coefficients (117) are given in Table 8 for the solvents used with the hydrogen reference electrode.

In Figs. 38-42 (chapter 3) are shown some of the non-isothermal measurements corrected to the standard state of H_2 gas. At temperatures below 298 K the correction becomes negligible but can be appreciable at higher temperatures

TABLE 8

Antoine Vapour-Pressure Coefficients [a] for the Antoine Vapour-Pressure Relation: $\ln p(S,mm\ Hg) = A - B/(T+C)$: and Term, $d\Delta E'/dT$, for Correction to the Standard State of Hydrogen Gas

Solvent	A	B	C	$d\Delta E'/dT$* mVK^{-1}
H_2O	18.3036	3816.44	-46.13	-0.026
CH_3OH	18.5875	3626.55	-34.29	-0.141
1-Propanol	17.5439	3166.38	-80.15	-0.025
2 Propanol	18.6929	3640.20	-53.54	-0.052
Isobutanol	16.8712	2874.73	100.3	-0.014

* $\frac{d\Delta E'}{dT} = (R/2F)\, dT\ln\{[760 - p(S,mm\ Hg)]/760\}/dT$
with $\ln p(S,mm\ Hg) = A - \frac{B}{T+C}$

a Ref. 117.

The temperature derivative of the Nernst equation for the $H_2|H^+$ electrode is given by

$$\frac{dE}{dT} = \frac{dE^\circ}{dT} + (R/F)\ln a_{H^+} + (RT/F)\frac{d\ln a_{H^+}}{dT} - (R/2F)\frac{dT\ln\{p(H_2,mmHg)/760\}}{dT} \quad [62]$$

where the last term on the right hand side can be evaluated by substitution of the Antoine equation for the vapour pressure of

the solvent (Table 8), i.e.

$$\frac{d\Delta E'}{dT} = (R/2F)\ \frac{dT\ln\{[(760-p(S,mm\ Hg)]/760\}}{dT} \qquad [63]$$

with $\ln p(S,mm\ Hg) = A - \frac{B}{T+C}$

If $y_+ = y_\pm$ is taken, since individual ionic activity coefficients cannot be directly measured, then $a_{H^+} = y_\pm C'$ and $d \ln a_{H^+}/dT = d \ln y_\pm/dT$ if the free ion concentration, C', is constant. Values of the various terms of equation [62], and the resultant temperature coefficients of the standard hydrogen electrode in a series of solvents are listed in Table 9.

Values of $\frac{RT}{F} d \ln y_\pm/dT$ could not be determined for 2-propanol and isobutanol because of insufficient density and dielectric data to determine $y_\pm$ at different temperatures. However, this term is only of the order of 2% of dE/dT, so that its neglect should not introduce significant error.

The standard half-cell reaction entropy and the standard ionic entropy of the H^+ ion are determined from the temperature coefficient of the standard hydrogen electrode potential,

$$F(dE°/dT) = \Delta S°_R = 1/2\ S°(H_2) - \bar{S}°(H^+) \qquad [64]$$

where the absolute entropy of H_2 gas, $S°(H_2)$, is 130.59 J mole ^{1} K^{-1} at 298 K (105). The reaction entropies and H^+ ion entropies are shown in Table 9 for the various solvents used. From the present results, the standard ionic entropy of H^+ in water is calculated to be -19.4 J mole-$^{1}K^{-1}\pm$3.0 J mole $^{1}K^{-1}$ and compares well with the majority of literature values which are close to 20.9 J mole $^{1}K^{-1}$ (106). The standard ionic entropy of H^+ in

TABLE 9

dE_{cell}/dT, $dE°/dT$, ΔS_R° and $\bar{S}°(H^+)$ for the Hydrogen Reference Electrode in Different Solvents at 298 K

Solvent	$\frac{dE_{cell}}{dT}$ mVK^{-1} *	$\frac{R\ln a_{H^+}}{F}$ mVK^{-1}	$\frac{RT}{F}\frac{d\ln a_{H+}}{dT}$ mVK^{-1} **	$\frac{d\Delta E'}{dT}$ mVK^{-1} ***	$\frac{dE°}{dT}$ mVK^{-1} (i)	$\Delta S_R^{\circ}\pm 3.0$ $Jmole^{-1}K^{-1}$ (ii)	$\bar{S}°(H^+)\pm 3.0$ $Jmole^{-1}K^{-1}$ (ii)
H_2O	0.673	-0.218	-0.013	-0.026	0.878	84.7	-19.4
CH_3OH	0.684	-0.293	0.015	-0.141	0.821	79.3	-14.0
1-Propanol	0.413	-0.372	0.017	-0.025	0.743	71.7	6.4
2-Propanol	0.505	-0.378	--	-0.052	0.831	80.2	-14.9
Isobutanol	0.397	-0.428	--	-0.014	0.811	78.3	-13.0

* From Table 6

** $a_{H^+} = \alpha C y_{\pm}$, $(RT/F)(d\ln a_{H^+}/dT) = (RT/F)(d\ln y_{\pm}/dT)$, From Table 7

*** From Table 8

(i) $dE°/dT = dE_{cell}/dT + d\Delta E/dT \quad (R/F)\ln a_{H^+} \quad (RT/F)d\ln a_{H^+}/dT$

(ii) $\Delta S_R^{\circ} = F(dE°/dT) - 1/2\ S°(H_2) \quad \bar{S}°(H^+)$

CH_3OH is calculated to be -14.0 J mole $^{1}K^{-1}$ $\pm$ 3.0 J $mole^{-1}K^{-1}$ and does not compare well with values of -63.2 J mole $^{1}K^{-1}$ in CH_3OH and -83.3 J $mole^{-1}K^{-1}$ in EtOH determined by Criss, Held and Luksha (118) using the so-called correspondence principle.

The correspondence method (106,118) has been used almost exclusively to divide experimental partial molal entropies of electrolytes in nonaqueous solvents into their ionic components.

The method involves assigning an arbitrary entropy value to a reference ion (usually H^+) in the nonaqueous solvent which will then fix the (relative) entropy values of the other ions in the same solvent. Values of $\bar{S}^{\circ}_{ion}$ for ions in aqueous solution are then plotted against the "corresponding" $\bar{S}^{\circ}_{ion}$ values in the nonaqueous solvent and a proper choice of the ionic entropy of the reference ion will result in a linear relationship, with both cations and anions falling on the same straight line.

ii) Silver-Silver Chloride Reference Electrode

The temperature derivative of the Nernst equation for the silver chloride electrode is given by

$$\frac{dE}{dT} = \frac{dE^{\circ}}{dT} \quad (R/F)\ln a_{Cl} \quad (RT/F)\frac{d \ln a_{Cl}}{dT} \qquad [65]$$

and values of the different terms in the equation and the resultant temperature coefficients of the standard Ag|AgCl electrode potential in H_2O, CH_3OH and $HCONH_2$ are listed in Table 10.

The standard half-cell reaction entropy and the standard ionic entropy of the chloride ion are determined from the temperature coefficient of the standard Ag|AgCl electrode:

$$F\ (dE^{\circ}/dT) = S^{\circ}(Ag) + \bar{S}^{\circ}(Cl^-) \quad S^{\circ}(AgCl) \qquad [66]$$

where the absolute entropies of silver, $S^{\circ}(Ag)$, and silver chloride, $S^{\circ}(AgCl)$, are 42.8 J mole $^{1}K^{-1}$ and 96.1 J mole $^{1}K^{-1}$, respectively at 298 K (119). The reaction entropies and Cl^- ion entropies are shown in Table 10, for the solvents used. The standard ionic entropy of Cl^- in water is calculated to be 76 0

TABLE 10

dE_{cell}/dT, $dE°/dT$, ΔS°_{R}, and $\bar{S}°(Cl^{-})$ for the Silver-Silver Chloride Reference Electrode in Different Solvents at 298 K

Solvent	$\frac{dE_{cell}}{dT}$ mVK^{-1} *	$\frac{R\ln a_{Cl^-}}{F}$ mVK^{-1}	$\frac{RT}{F}\frac{d\ln a_{Cl}}{dT}$ **	$\frac{dE°}{dT}$ mVK^{-1} (i)	$\Delta S^{\circ}_{R} \pm 3.0$ $Jmole^{-1}K^{-1}$ (ii)	$\bar{S}°(Cl^{-}) \pm 3.0$ $Jmole^{-1}K^{-1}$ (ii)
H_2O	0.467	-0.220	-0.013	0.234	22.6	76.0
CH_3OH	0.171	-0.272	0.015	-0.086	-8.3	45.1
$HCONH_2$	0.193	-0.210	-0.001	-0.018	1.8	51.7

* From Table 6

** $a_{Cl^-} = \alpha C y_{\pm}$; $(RT/F)(d\ln a_{Cl^-}/dT) - (RT/F)(d\ln y_{\pm}/dT)$; From Table 7

(i) $dE°/dT = dE_{cell}/dT + (R/F)\ln a_{Cl^-} + (RT/F)(d\ln a_{Cl^-}/dT)$

(ii) $\Delta S^{\circ}_{R} = F(dE°/dT) = S°(Ag) + \bar{S}°(Cl^{-}) \quad S°(AgCl)$

J mole $^{1}K^{-1} \pm 3.0$ J mole $^{1}K^{-1}$ and compares well with the majority of literature values which are in the range from 75.3 to 79.5 J mole $^{1}K^{-1}$ (106,120). The standard ionic entropy of Cl is calculated to be 45.1 J mole $^{1}K^{-1} \pm 3.0$ J mole $^{1}K^{-1}$ in CH_3OH and 51.7 J mole$^{-1}K^{-1} \pm 3.0$ J mole $^{1}K^{-1}$ in $HCONH_2$, compared to values of 18.4 J mole $^{1}K^{-1}$ for CH_3OH and 42.3 J mole $^{1}K^{-1}$ for $HCONH_2$ determined by Criss, Held and Luksha (118) again using the correspondence principle.

iii) Silver-Silver Ion Reference Electrode

The temperature derivative of the Nernst equation for the $Ag|Ag^+$ electrode potential can be given by

$$\frac{dE}{dT} = \frac{dE^\circ}{dT} + (R/F)\ln a_{Ag+} + (RT/F)\frac{d\ln a_{Ag+}}{dT} \qquad [67]$$

Values of the different terms in the equation and the resultant temperature coefficients of the standard electrode potential in DMF and AN are given in Table 11.

The temperature coefficients of the non-isothermal cell potential (dE_{cell}/dT) and the standard electrode (dE°/dT) for 0.01M $AgClO_4$ in AN are 0.46 mVK^{-1} ± 0.02 mVK^{-1}, and 0.96 mVK^{-1} ± 0.03 mVK^{-1}, respectively. These values are in reasonable agreement with values of dE_{cell}/dT = 0.43 mVK^{-1} and dE°/dT = 0.9 mVK^{-1}, determined by Kratochvil et al. (121) for 0.01 M $AgNO_3$ in AN, using a 0.1M Et_4NClO_4 salt bridge.

The standard half-cell reaction entropies and the standard ionic entropies of the silver ion are determined from the temperature coefficient of the standard $Ag|Ag^+$ electrode.

$$F\frac{dE^\circ}{dT} = S^\circ(Ag) \quad \bar{S}^\circ(Ag^+) \qquad [68]$$

and are also shown in Table 11, for DMF and AN. The standard ionic entropy determined for Ag^+ in AN is 50.2 J mole $^1K^{-1}$ ± 3.0 J mole $^1K^{-1}$ and in DMF is -55.2 J mole $^1K^{-1}$ ± 3.0 J mole^{-1} K^{-1} and does not compare well with the value of -6.5 J mole $^1K^{-1}$ calculated from the empirical relation of Criss and Salomon for DMF (106), viz.

$$\bar{S}^\circ_{ion}(X) = -9.0 + 0.44\ \bar{S}^\circ_{ion}(aq) \qquad [69]$$

TABLE 11

dE_{cell}/dT, $dE°/dT$, $\Delta S_R^{\circ}(Ag^+)$ and $\bar{S}°(Ag^+)$ for the Silver-Silver Ion Reference Electrode in AN and DMF at 298 K

Solvent	$\frac{dE_{cell}}{dT}$ mVK^{-1} *	$\frac{R\ln a_{Ag^+}}{F}$ mVK^{-1}	$\frac{RT}{F}\frac{d\ln a_{Ag^+}}{dT}$ mVK^{-1} **	$\frac{dE°}{dT}$ mVK^{-1} (i)	$\Delta S_R^{\circ}\pm3.0$ $Jmole^{-1}K^{-1}$ (ii)	$\bar{S}°(Ag^+)\pm3.0$ $Jmole^{-1}K^{-1}$ (ii)
DMF	0.455	-0.456	-0.104	1.015	97.9	55.2
AN	0.464	-0.461	-0.037	0.963	92.9	-50.2

* From Table 6.

** $a_{Ag+} = \alpha C y_{\pm}$; $(RT/F)(d\ln a_{Ag^+}/dT) = (RT/F)(d\ln y_{\pm}/dT)$; From Table 7

(i) $dE°/dT = dE_{cell}/dT - (R/F)\ln a_{Ag^+} - (RT/F)(d\ln a_{Ag^+}/dT)$.

(ii) $\Delta S_R^{\circ} = F(dE°/dT) = S°(Ag) \quad \bar{S}°(Ag^+)$.

using a value of $\bar{S}°(Ag^+) = 70.7$ J $mole^{-1}K^{-1}$ for H_2O (120).

d) Choice of Method for Determination of Single Ion Entropies in Nonaqueous Solutions

It is doubtful if errors in the non-isothermal electrode potential method could account for the large differences in the single ion entropies of H^+, determined by the "correspondence" and the "electrochemical" methods. For example, if a large thermal liquid junction potential of -0.4 mVK^{-1} is assumed (cf. -0.044 mVK^{-1} estimated from measurements with and without a salt bridge) for non-isothermal cell measurements without a salt bridge in hydrochloric solutions in CH_3OH, then the resultant ionic entropy of H^+ in CH_3OH is found to be -48.1 J $mole^{-1}K^{-1}$,

still appreciably different from the value of -63 2 J $mole^{-1}K^{-1}$ found using the correspondence method. The "electrochemical non-isothermal approach" seems to be more reliable because it is a direct measure of ionic entropy, whereas the "correspondence method" is based entirely on some assumptions and data on the entropies of ions in aqueous solutions. This method may not account for specificity of the ion-solvent interactions in non-aqueous solvents, where especially the structural component of the ionic solvation entropy may be quite different from that in water especially for solvents less associated than water

B. Temperature Dependence of the Tafel Slope and Symmetry Factor for the H_2 Evolution and Br_2 Evolution Reactions

1. Introduction

The exponential dependence of the rate of heterogeneous electron transfer reactions on electrode potential is usually treated in terms of the applied potential reducing the Gibbs energy of activation for the process (20, 96) In particular, some fraction, β, of the applied potential has been assumed to modify the energy of activation for the process through a change of the Fermi level of the electrons relative to "vacuum". For an electrode process the electrochemical Gibbs energy of activation, $\Delta\bar{G}^{\ddagger}_{\phi}$, is potential-dependent and can be written in terms of a chemical Gibbs energy of activation $\Delta G^{\ddagger}_{\phi=o}$, modified by an electrical energy component $\mp\beta\phi nF$:

$$\Delta\bar{G}^{\ddagger}_{\phi} = \Delta G^{\ddagger}_{\phi=o} \mp \beta\phi nF = \Delta H^{\ddagger}_{\phi=o} - T\Delta S^{\ddagger}_{\phi=o} \mp \beta\phi nF \qquad [70]$$

where β is the symmetry factor analogous to the Brϕnsted coefficient (123,124) in acid-base reactions, n is the number of electronic charges transferred in the rate-determining step, usually one, and ϕ is the metal-solution potential difference.

In eqn.[70], it has been the conventional assumption in almost all electrode-kinetic work that the applied potential modifies only the enthalpy or energy of activation, i.e., the entropy of activation has been assumed implicitly to be independent of electrode potential.

The electrode reaction current density, i, may be written formally as

$$i = Kc\exp\left[-\Delta\bar{G}^{\ddagger}_{\phi}/RT\right] \times f(\theta) \qquad [71]$$

where c is an appropriate reactant surface concentration expression, (taking into account the distribution of the reactant between solution and interface), K is a combination of constants, and $f(\theta)$ is a surface coverage term which is a function of coverage, θ (or free sites, $1-\theta$) by chemisorbed intermediates and/or specifically adsorbed anions. Eqn.[70] in eqn.[71] leads to the well known Tafel equation expressing a linear relationship between applied potential, ϕ (or ΔV), and the logarithm of the electrochemical rate constant corresponding to the electrode reaction rate measured by the current-density.

This logarithmic relationship is an example of a "linear free-energy relation" of the type characterized by the Brønsted relationship for proton transfer rate constants in relation to acid/base pK's. Electrode reactions provide in fact one of the best examples of the "linear free energy relation" in physical chemistry since the linear relations are maintained over a wide energy range, viz. ca. 1.0 eV at Hg.

The significance of β in eqn.[70] is clearly similar to that of α in Brønsted's relation except that in the electrochemical case, the change of reactant Gibbs energy has usually been assumed to arise entirely from an electrical energy change of electrons at the Fermi level of the metal. It will be shown later, as a result in part of the present work, that this is an inadequate assumption since other important effects of electrode potential or interfacial field on the reactant system, other

than electrons, can also arise.

With respect to coverage effects, it is convenient to differentiate eqn.[71] for the reaction rate with respect to potential; which then gives

$$d \ln i/d\phi = \pm \beta nF/RT \pm d[\ln f(\theta)]/d\phi = \pm \alpha nF/RT \quad [72]$$

where the experimentally observed charge transfer coefficient, α, will be different from the symmetry factor if adsorption effects, arising from the term $d[\ln f(\theta)]/d\phi$, are important. It is well established that the hydrogen evolution reaction (h.e.r.) at Hg in acid solutions proceeds with a rate-controlling proton discharge step and consequently low coverage by adsorbed H arises in the steady-state. Thus, for this simple proton and electron transfer reaction, the empirically derived transfer coefficient and symmetry factor are identical ($\alpha \equiv \beta$), since for $\theta \rightarrow 0$, $d\ln (1-\theta)/d\phi \rightarrow 0$ with $f(\theta) \equiv 1-\theta$.

The Tafel slope, b, which characterizes the logarithmic dependence of current density on electrode potential can be written generally as,

$$b = d\phi/d\log i = \pm 2.3RT/\alpha nF \quad [73]$$

or for a simple one-electron reaction proceeding without an intermediate or without significant coverage by one,

$$b = \pm 2.3RT/\beta F \quad [74]$$

where β has usually been taken as a temperature-independent constant and to have a value of about 0.5.

Experimentally, however, it is found for a number of electrode reactions that b is rarely represented with respect to

its temperature dependence by the commonly assumed relations in [73] and [74]. In particular, b is often found to be independent of temperature or to contain a temperature-independent component, implying temperature dependence of the symmetry factor itself.

It is of interest that for a number of outer-sphere ionic redox reactions, with the exception of the $Cr(II).6H_2O|Cr(III)6H_2O$ case (6,8), studied in recent years by Weaver et al. (77,125,126,127), the transfer coefficient is found to be independent of temperature, i.e., conventional behaviour is observed. This suggests that unusual effects arise when an atom-transfer step is involved (as in the h.e.r.) and consequently complete extinction of charge of the reactant ion is involved.

A discussion and examination of the temperature-dependence of the Tafel slope, including some recently evaluated examples, has recently been given by Conway (128). A number of systems that display a temperature-dependent transfer coefficient are complex processes which involve other rate-controlling steps (e.g., electrochemical desorption of H) with adsorbed intermediates. If $d[\ln f(\theta)]/d\phi$ in eqn.[72] involves a temperature-dependent term then α can contain a temperature-dependent component. The results of greatest fundamental importance are therefore those which arise in the case of one electron discharge processes where $\alpha \equiv \beta$, and coverage by a chemisorbed intermediate is either small (<5% say) or does not

arise at all. Although the h.e.r. at Hg does not involve a potential and temperature-dependent H adsorption, specific ion adsorption (see section C-5, this chapter) can result in a temperature-dependent contribution to the symmetry factor, so that conditions must be chosen where such effects are absent or minimized.

The problem of the proper form of the temperature-dependence of the Tafel slope (and β) is essential to the fuller understanding of the activation process in electrode reactions. It is surprising that rather little attention has been given to this matter over many years.

2. Previous Work on the Potential Dependence of $\Delta\bar{S}^{\ddagger}_{\phi}$

The assumption that the entropy of activation is independent of potential, leads to the classical linear variation of b with T, through the Boltzmann factor, exp $[\pm\beta\phi F/RT]$. The Brønsted principle (4,129) is considered to apply to the shift of energy curves representing the course of the electrochemical particle and/or electron transfer process, through the change of Fermi level with potential which affects the energy of the initial state and hence $\Delta\bar{H}^{\ddagger}_{\phi}$ of the reaction.

Agar first pointed out that, formally, a temperature dependence of the symmetry factor would imply that the entropy of activation was potential dependent (130). This effect was recognized in the work of Parsons and Bockris (131) on the h.e.r. at Hg, but this point was not pursued further until more recently by Conway, MacKinnon, and Tilak (132). These authors

provided a number of new examples of the unconventional dependence of b on T and examined in some detail how the electrode field might substantially influence the entropy of activation through potential dependent solvent orientation, as well as the energy of activation as is usually assumed.

Recently, in a comparison of the rates of heterogeneous electron transfer reaction involving a number of redox couples, Weaver (77) has discussed the temperature-dependence of the apparent transfer coefficients in terms of both enthalpic and entropic contributions to the Gibbs energy of activation. For a number of outer-sphere redox reactions at Hg, Weaver's results show that values of the entropy of activation, $\Delta\bar{S}_{\phi}^{\ddagger}$, corrected for coulombic double layer-effects, are independent of potential, but dependent on the ligand structure around the metal ion.

We have recently reported an appreciable potential dependence of $\Delta\bar{S}_{\phi}^{\ddagger}$ for the h.e.r. at Hg and the bromine evolution reaction (b.e.r.) at vitreous carbon (133). In these atom and electron transfer reactions the ionic charge and associated solvation are eliminated in the course of the electrode reaction, whereas in the case of an ionic redox reaction at an electrode the solvation state or ligand shell arrangement is more or less preserved, and only outer-shell reorganization is involved in the activation process in certain cases. The direct experimental examination of the potential-dependence of $\Delta\bar{S}_{\phi}^{\ddagger}$ for an atom and electron transfer reaction such as the h.e.r., has not yet been reported by other investigators but is implicit in

the form of the observed temperature-dependence of the Tafel slope (b not simply proportional to T). These results, as well as the systematic study of the potential-dependence of the individual enthalpic and entropic components of the Gibbs energy of activation for the h.e.r. at Hg in a number of different systems are reported here. The relevance of these results to the question of the temperature-dependence of the symmetry factor and Tafel slope will be examined in the material which follows.

3. Potential Dependence of $\Delta\bar{H}_{\phi}^{\ddagger}$ and $\Delta\bar{S}_{\phi}^{\ddagger}$ in relation to the Temperature-Dependence of β and the Tafel Slope

The overall symmetry factor (or Tafel slope) should be regarded as originating from the total derivative of eqn.[70], i.e., $\Delta\bar{G}_{\phi}^{\ddagger}$, with respect to potential,

$$d(\Delta\bar{G}_{\phi}^{\ddagger})/Fd\phi = \mp d(\Delta\bar{H}_{\phi}^{\ddagger})/Fd\phi \pm T\, d(\Delta\bar{S}_{\phi}^{\ddagger})/Fd\phi = \beta \qquad [75]$$

and not just $d(\Delta\bar{H}_{\phi}^{\ddagger})/Fd\phi$ as usually assumed. The two derivatives of eqn.[75] can be experimentally determined from the slopes of Arrhenius plots of ln i_{ϕ} versus T^{-1} at various electrode potential which gives $\Delta\bar{H}_{\phi}^{\ddagger}$ values at the respective electrode potentials, ϕ, and the intercepts of such plots as $T^{-1} \rightarrow 0$ which gives the logarithm of the electrochemical frequency factor A_{ϕ} (proportional to $\Delta\bar{S}_{\phi}^{\ddagger}$) at the respective electrode potentials (see chapter 4). If the metal-solution potential difference, ϕ, at the reference electrode is fixed using non-isothermal cell measurements, then values of $\Delta\bar{H}_{\phi}^{\ddagger}$ and ln A_{ϕ} are obtained which are not influenced by the temperature-dependence of the

reference potential Of course, the potential dependence of both $\Delta\bar{H}^{\ddagger}_{\phi}$ and ln A_{ϕ} (or $\Delta\bar{S}^{\ddagger}_{\phi}$) will be independent of whether the measurements are actually made by means of an isothermal or a non-isothermal cell arrangement.

a) Relation of β_H to $\Delta\bar{H}^{\ddagger}_{\phi}$

The enthalpy of activation as a function of potential for the h.e.r. at Hg from 0.1M CF_3SO_3H in DMF and 0.1M aqueous HCl is shown in Fig. 51, and for the b.e.r at vitreous carbon from 0 4M $Pr_4NBr|0.2M\ Br_2$ in AN in Fig. 52. In all cases, $\Delta\bar{H}^{\ddagger}_{\phi}$ decreases linearly with applied potential as expected and the effectiveness of the applied potential in reducing $\Delta\bar{H}^{\ddagger}_{\phi}$ is characterized by the slopes of the lines, i e.

$$\beta_H = \mp\, d(\Delta\bar{H}^{\ddagger}_{\phi})/Fd\phi = \mp\, (\text{slope})/F \qquad [76]$$

In all the cases considered here, the potential dependence of $\Delta\bar{H}^{\ddagger}_{\phi}$ can be represented by

$$\Delta\bar{H}^{\ddagger}_{\phi} = \Delta H^{\ddagger}_{\phi=o} \mp \beta_H \phi F \qquad [77]$$

which is of the form used in eqn.[70]. When the values of β_H, thus evaluated, are compared with the overall symmetry factors, β, derived directly from the Tafel slope they are found to be quite different (Table 12). It is clear that the determined effect of potential on $\Delta\bar{H}^{\ddagger}_{\phi}$ does not account completely for the observed net activation effectiveness (β) and so some other factor(s) must operate.

b) Relation of β_S to $\Delta\bar{S}^{\ddagger}_{\phi}$

The log A_{ϕ} (proportional to $\Delta\bar{S}^{\ddagger}_{\phi}$) as a function of potential is shown in Figs 53 and 54, and in all cases there is a linear

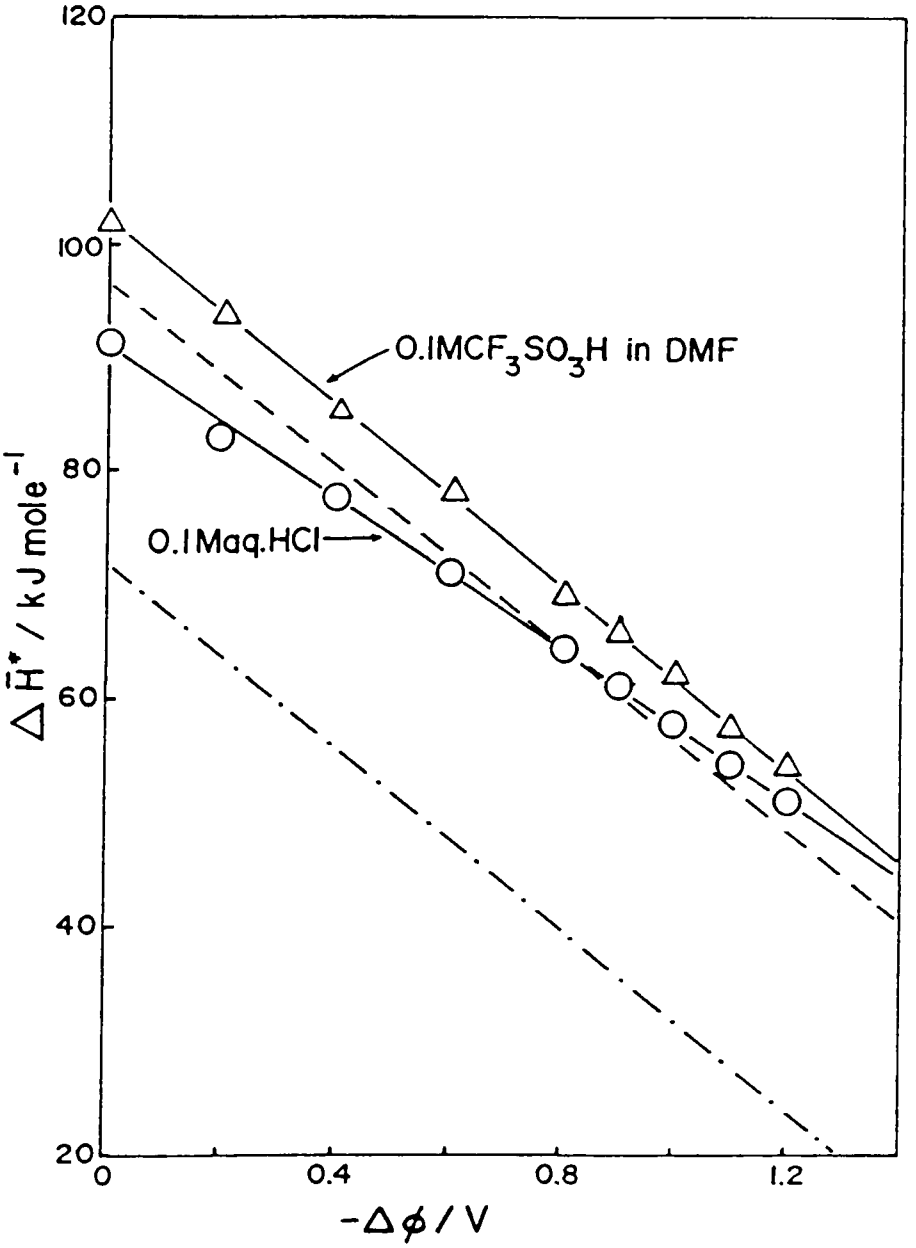

Fig. 51 Potential-dependence of the enthalpy of activation for the h.e.r. at Hg from 0.1M aqueous HCl and 0.1M CF_3SO_3H in DMF: (——) non-isothermal cell potential corrections. Broken lines for 0.1M CF_3SO_3H in DMF: (-----) apparent values derived without any reference electrode potential corrections; (-•-•-) non-isothermal cell and isothermal reference cell potential corrections, i.e., referred to $H^+|H_2$ in 0.1M aqueous HCl at 298 K.

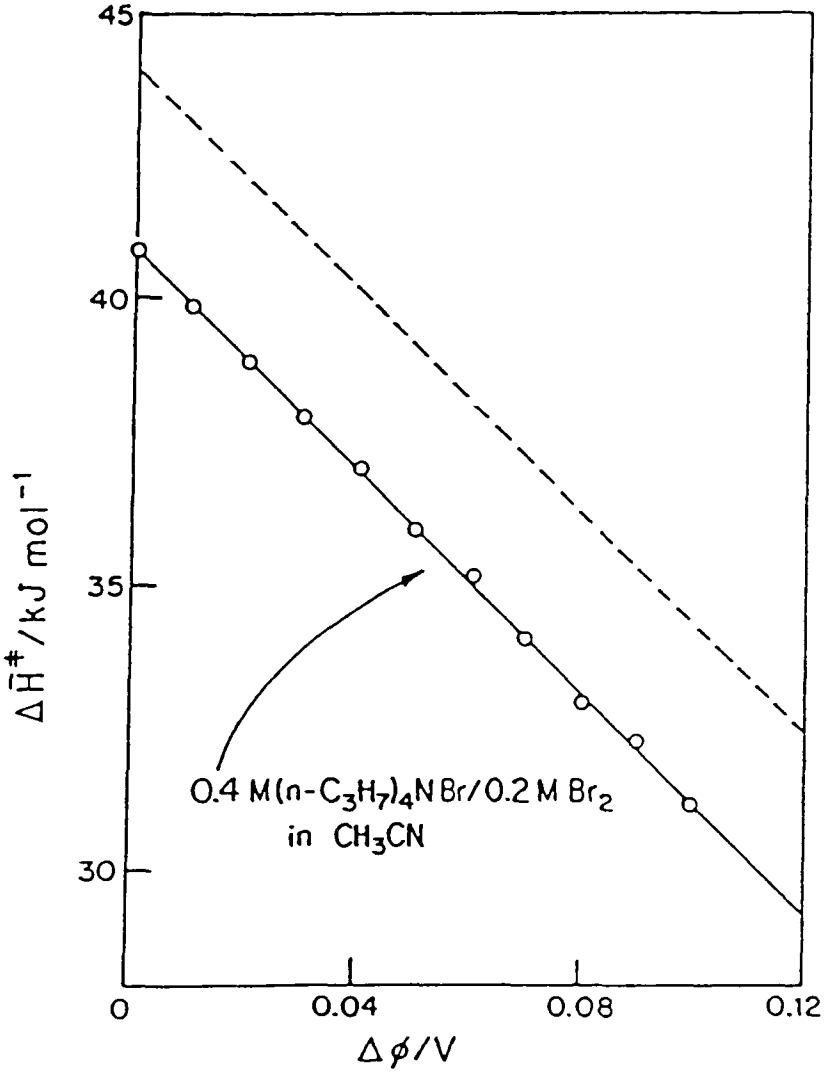

Fig. 52 Potential-dependence of the enthalpy of activation for the b.e.r. at vitreous carbon from 0 4M $Pr_4NBr|0.2M\ Br_2$ in AN: (----) apparent values derived without any reference electrode potential corrections (——) non-isothermal cell potential corrections

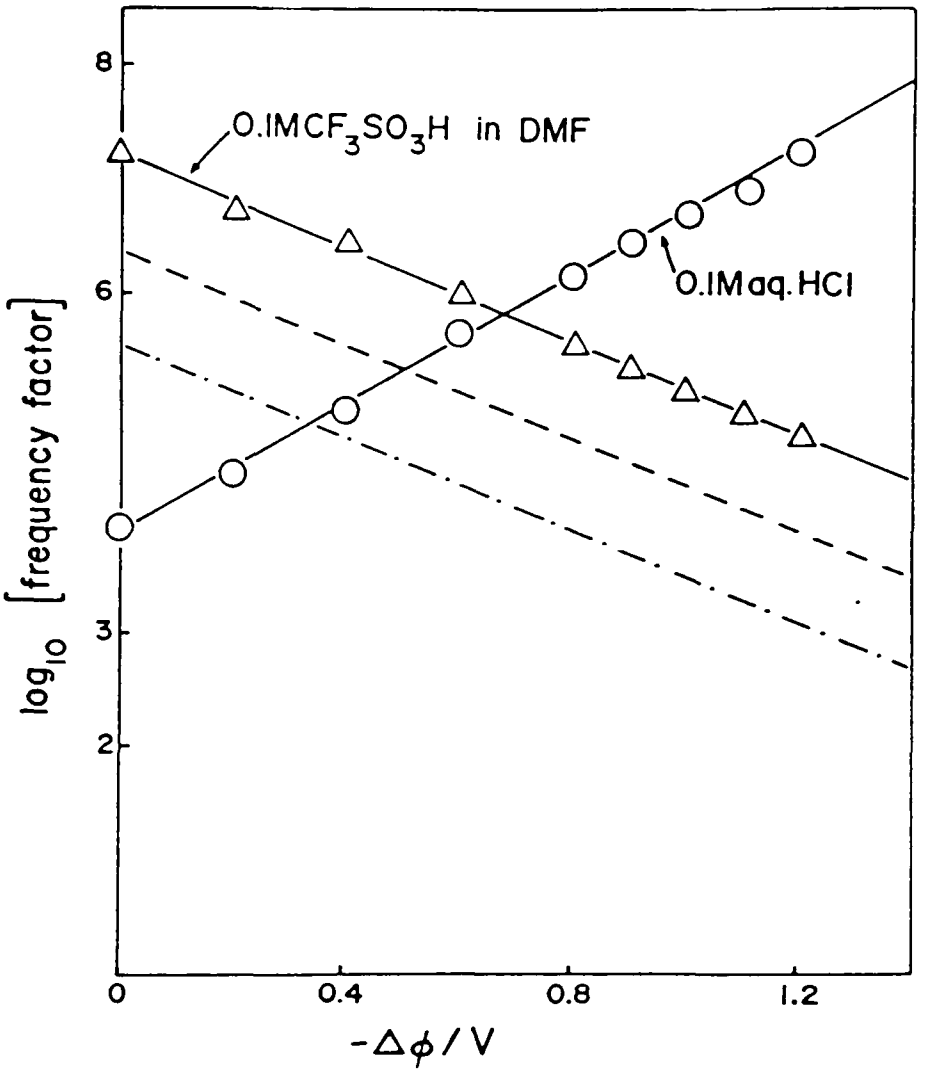

Fig. 53 Potential-dependence of log [frequency factor] (proportional to $\Delta\bar{S}^{\ddagger}_{\phi}$) for the h.e.r. at Hg from 0.1M aqueous HCl and 0.1M CF_3SO_3H in DMF: (——) non-isothermal cell potential corrections. Broken lines for 0.1M CF_3SO_3H in DMF: (- - - - -) apparent values derived without any reference electrode potential corrections; (-•-•-) non-isothermal cell and isothermal reference cell potential corrections, i.e., referred to $H^+|H_2$ in 0.1M aqueous HCl at 298 K.

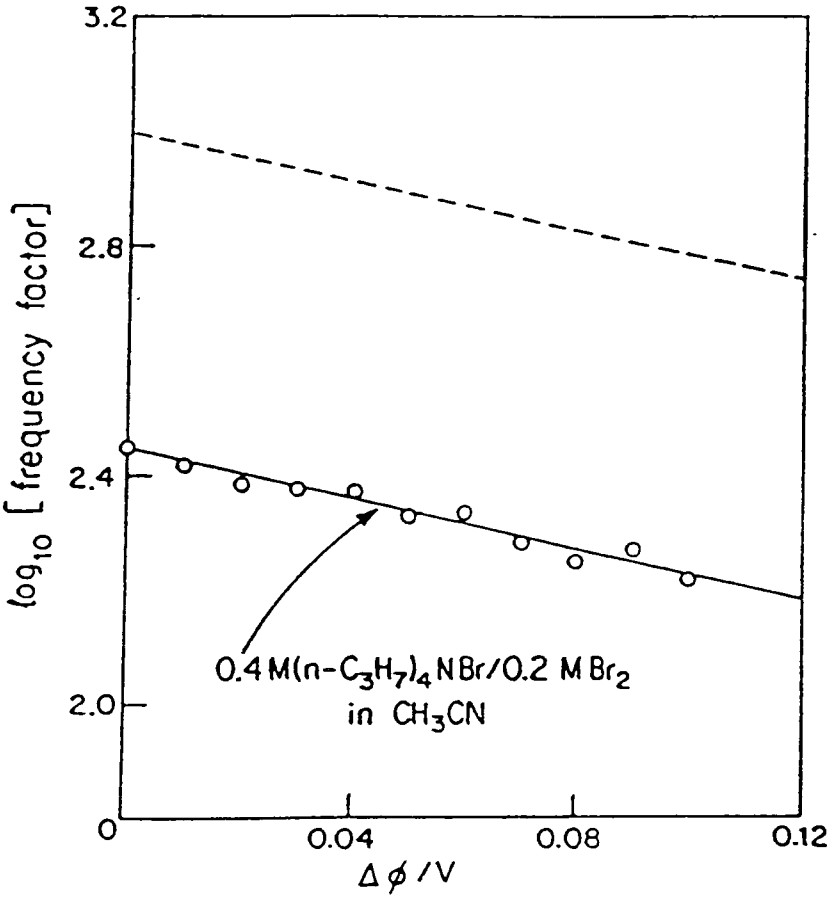

Fig 54 Potential-dependence of log [frequency factor] (proportional to $\Delta\bar{S}^{\ddagger}$) for the b e.r at vitreous carbon from 0.4M $Pr_4NBr|0.2M\ Br_2$ in AN: ( ) apparent values derived without any reference electrode potential corrections; (——) non-isothermal cell potential corrections.

TABLE 12

β_H, β_S and β Determined from the Potential Dependence of $\Delta\bar{H}^{\ddagger}_{\phi}$ and $\Delta\bar{S}^{\ddagger}_{\phi}$ for Several Systems

System	β_H *	$10^4\beta_S/K^{-1}$ **	$\beta^{calc.}$ (298 K) ***	$\beta^{obs.}$ (298 K) ****
0.1M HClaq.(h.e.r.)	0.34±0.01	5.9±0.2	0.52±0.02	0.51±0.02
0.1M CF_3SO_3H in DMF (h.e.r.)	0.42±0.02	-4 1±0.2	0.30±0.03	0.29±0.01
0.4M Pr_4NBr|0.2M Br_2 (b.e.r. at vitreous carbon)	1.07±0.05	-6 8±0 5	0.89±0.07	0.88±0 06

* $\beta_H = \mp d(\Delta\bar{H}^{\ddagger}_{\phi})/Fd\phi$

** $\beta_S = \pm d(\Delta\bar{S}^{\ddagger}_{\phi})/Fd\phi$

*** $\beta^{calc} = \beta_H + \beta_S T$

**** $\beta_{obs} = \pm 2.303RT/b^{obs}.F.$

dependence of the entropy of activation on applied potential For the h.e.r. from 0.1M CF_3SO_3H in DMF and the b e r from 0.4M Pr_4N Br|0.2M Br_2 in AN, $\Delta\bar{S}^{\ddagger}_{\phi}$ evidently decreases with potential while for the h.e.r from 0 1M aqueous HCl, $\Delta\bar{S}^{\ddagger}_{\phi}$ increases linearly with potential. In all the cases considered here, the potential dependence of $\Delta\bar{S}^{\ddagger}_{\phi}$ can be represented by

$$\Delta\bar{S}^{\ddagger}_{\phi} = \Delta S^{\ddagger}_{\phi=o} \pm \beta_S\phi F \qquad [78]$$

where

$$\beta_S = \pm d(\Delta\bar{S}^{\ddagger}_{\phi})/Fd\phi = \pm 2.3R(slope)/F \qquad [79]$$

and the values of β_S are shown in Table 12

c) Relation of β to β_H and β_S

The two derivatives of eqn.[75] can be replaced by eqns.[76] and [79] which are the experimentally determined linear dependence of $\Delta\bar{H}^{\ddagger}_{\phi}$ and $\Delta\bar{S}^{\ddagger}_{\phi}$ on potential, respectively. Thus

$$\beta = \beta_H + \beta_S T \qquad [80]$$

and the overall symmetry factor, β, is seen to have a temperature independent component, β_H, corresponding to conventional behaviour and a temperature dependent component, $\beta_S T$, which arises from the potential dependence of the entropy of activation.

Values of β calculated for eqn.[80] are of course consistent with the values of β derived from the observed Tafel slope, $b = \pm 2.3\ RT/\beta F$ (Table 12), as is to be expected. Clearly, the Tafel slope is given by

$$b = \pm 2.3RT/(\beta_H + \beta_S T)F \qquad [81]$$

and a plot of b^{-1} versus T^{-1},

$$b^{-1} = \pm (\beta_H F/2.3R)T^{-1} \pm \beta_S F/2.3R \qquad [82]$$

allows β_H and β_S to be determined, provided $\Delta\bar{H}^{\ddagger}_{\phi}$, and $\Delta\bar{S}^{\ddagger}_{\phi}$ have the linear forms given in eqns.[76] and [79], respectively.

The dashed lines ( ) in Figs. 51 and 53 for the h.e.r. from 0.1M CF_3SO_3H in DMF and in Figs. 52 and 54 for the b.e.r. from 0.4M $Pr_4NBr|0.2M\ Br_2$, refer to the "apparent" $\Delta\bar{H}^{\ddagger}_{\phi}$ and $\log A_{\phi}$ values, which were derived directly without any reference electrode potential corrections. The other broken line (-•-•) in Figs. 51 and 53 for the h.e.r. from 0.1M CF_3SO_3H in DMF shows the effect of both non-isothermal cell and isothermal reference

cell potential corrections (i e , referred to the $H^+|H_2$ reference electrode in 0 1M aqueous HCl at 298 K) on the $\Delta\bar{H}^{\ddagger}_{\phi}$ and log A_{ϕ} values. Clearly, the slopes of these lines, and hence the associated β_H and β_S values, are independent, as expected, of potential corrections Like the overall symmetry factor itself (β) its enthalpic and entropic components are not dependent on the reference electrode used or its variation with temperature. This allows a comparison of these components in different media without the requirement of fixing the metal solution potential-difference at the reference electrode.

4. Relation of β to Brønsted Behaviour for Homogeneous Proton Transfer

It would be of interest to examine the temperature dependence of the Brønsted coefficient α (123,124) for homogeneous proton transfer reactions but, unfortunately, the required values of α at several temperatures for a "well behaved" system are not available. However, the dependence of $\Delta S^{\ddagger}$ on ln K_a or on ΔG_R ($\Delta G_R = -RT \ln K_a$) for a series of homogeneous reactions of a similar kind provides a basis for comparison with the potential dependence of $\Delta\bar{S}^{\ddagger}_{\phi}$ for the h e r and b.e r in the electrochemical case In a kinetic study of the second deprotonation step of a series of intramolecularly H-bonded substituted malonic acids, Eyring et al (134, 135) have found a linear Brønsted relation and also a linear relationship between $\Delta H^{\ddagger}$ and $\Delta S^{\ddagger}$ for reactions of the type

$$AH^- + OH^- \rightleftarrows A^{2-} + H_2O \qquad [83]$$

Hence, for such a series of homogeneous proton transfer reactions, $\Delta S^{\ddagger}$ varies linearly with changes in ΔG_R (analogous to changes in electrode potential in the electrochemical case) and could be expected to result in a temperature dependence of α analogous to that found here for the electrochemical symmetry factor, β. Extension of Brønsted behaviour for homogeneous proton transfer to heterogeneous proton|electron transfer would seem to lead naturally to the possibility of a potential dependent entropy of activation of the kind that is observed (see below) in the present work.

5. Experimental Temperature Dependence of b in relation to β, β_H and β_S

Plots of b versus T and b^{-1} versus T^{-1} for the h.e.r. at Hg from various proton donors in H_2O, methanol, other alcohols (1 propanol, 2-propanol and isobutanol), formamide, DMF, and AN, are shown in Figs. 55a,b 60a,b, respectively. The behaviour of the b.e.r. from 0.4M Pr_4NBr|0 2M Br_2 in AN at vitreous carbon is included in Figs 60a-b in order to provide comparative information on the behaviour of an anodic reaction from a relatively unstructured solvent.

a) Anodic Bromine Evolution Reaction

Conway, MacKinnon and Tilak (132) reported a temperature-independent Tafel slope for the anodic b e.r at pyrolytic graphite from 0.4M Pr_4NBr in AN. Reanalysis of their data with a b^{-1} versus T^{-1} plot, gives the β_H and β_S components shown in

Table 13, and $\beta_S T >> \beta_H$ is found for the temperature range studied, i.e., the activation process is mainly entropy controlled as far as the effect of potential is concerned. For the anodic b.e.r. at vitreous carbon from 0.4M $Pr_4NBr|0.2M\ Br_2$ in AN studied here, the behaviour is, however, quite different and $\beta_H > \beta_S T$ in the same temperature range, i.e., the process is more enthalpy controlled. The difference in behaviour of the symmetry factor and Tafel slope with temperature is probably due to the different electrocatalytic surfaces that pyrolytic graphite and vitreous carbon present for the reaction.

TABLE 13

β_H, β_S and β and the Observed Tafel Slope for the B.E.R. in AN at Different Substrates

System	β_H*	$10^4 \beta_S^*/K^{-1}$	$\beta^{calc.}$** (298 K)	$b^{obs.}/V$ (298 K)
0.4M $Pr_4NBr|0.2M\ Br_2$ (b.e.r. at vitreous carbon)	1.07±0.05	6.8±0.5	0.89±0.07	0.068±0.005
0.4M Pr_4NBr (b.e.r. at pyrolytic graphite)$^{\alpha}$	0.1±0.1	25 ± 3	0.84±0.09	0.070±0.007

* From b^{-1} vs T^{-1} plots

** $\beta^{calc.} = \beta_H + \beta_S T$

$^{\alpha}$ From results of ref. 132

Impedance measurements at vitreous carbon indicated little or no adsorption pseudocapacitance in the potential range of 0.01 V to ca. 0.1 V, studied (see section 2, chapter 2). However, at pyrolytic graphite, a measurable adsorption pseudocapacitance was found in the same potential range, which was dependent on edge or basal-plane exposure. Since the Tafel slope is unusually low at both substrates (Table 13), it is unlikely that the kinetics are controlled only by a simple Br^- ion discharge step. Temperature-dependent adsorption effects, involving the Br^- ion, $Br\cdot$ and the solvent are probably significant at both surfaces, but are less important at vitreous carbon than at the pyrolytic graphite.

b) H.E.R. at Liquid Hg

Values of β_H and β_S determined from the b^{-1} versus T^{-1} plots, the derived β values, and the observed Tafel slopes are shown in Table 14 for the h.e.r. at liquid Hg from various proton sources in several solvents.

The activation parameters β_H, β_S and β for the h.e.r. at Hg from 0.1M aqueous HCl and 0 1M $H_3OCF_3SO_3$ in AN are almost identical. Water is an unavoidable product of H_3O^+ discharge in AN and, under the conditions of the experiment here, the maximum calculated concentration of H_2O is < 1% of the H_3O^+ concentration, so that H_3O^+ is mainly surrounded by AN molecules in solution. However, the situation at the Hg electrode surface where H_2O is produced may be significantly different, with the double layer composition more like that in aqueous solution,

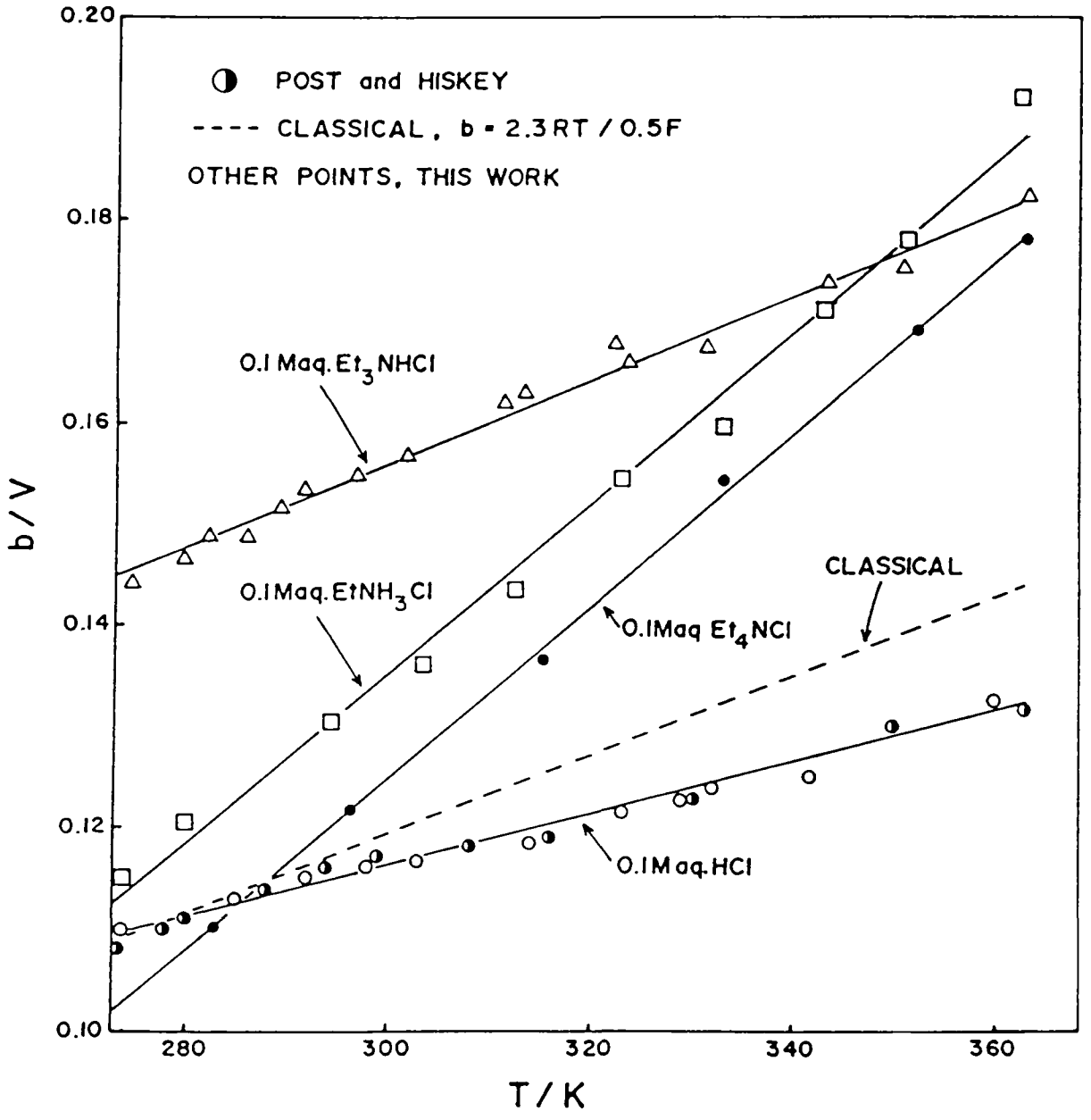

Fig. 55a Temperature-dependence of b for the h.e r at Hg from different aqueous proton sources

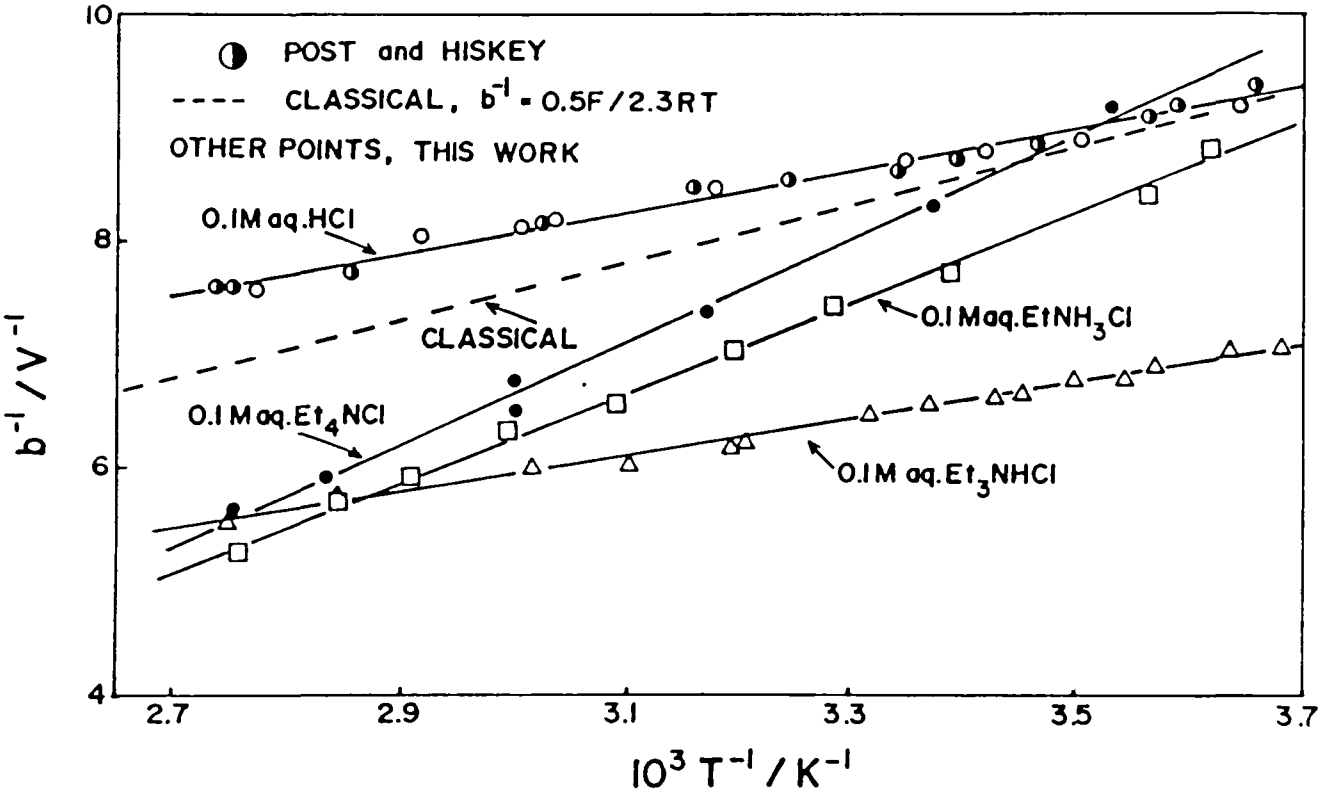

Fig 55b Dependence of b^{-1} on T^{-1} for the h.e r at Hg from different aqueous proton sources

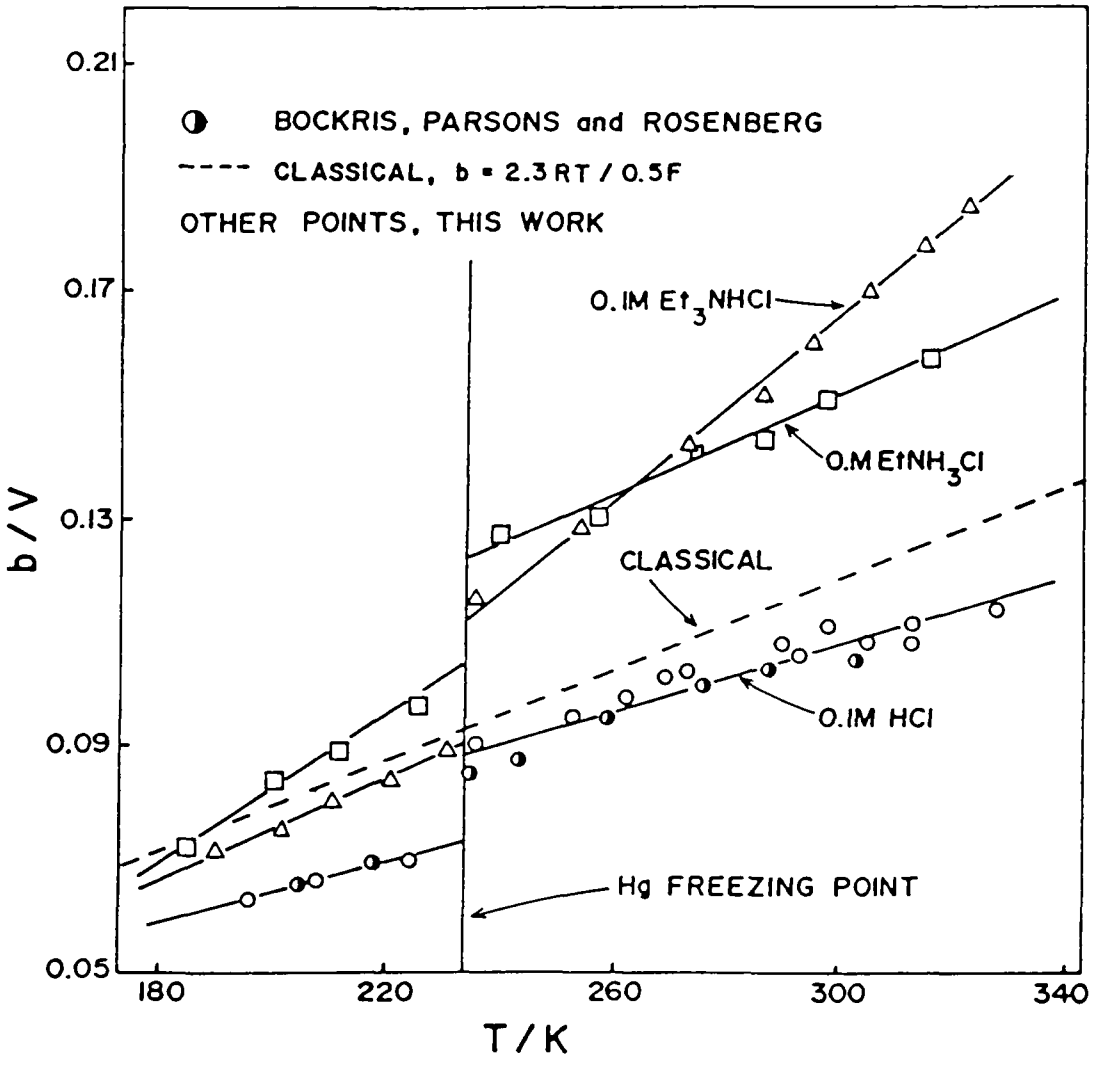

Fig 56a Temperature-dependence of b for the h e r at Hg from different proton sources in CH_3OH.

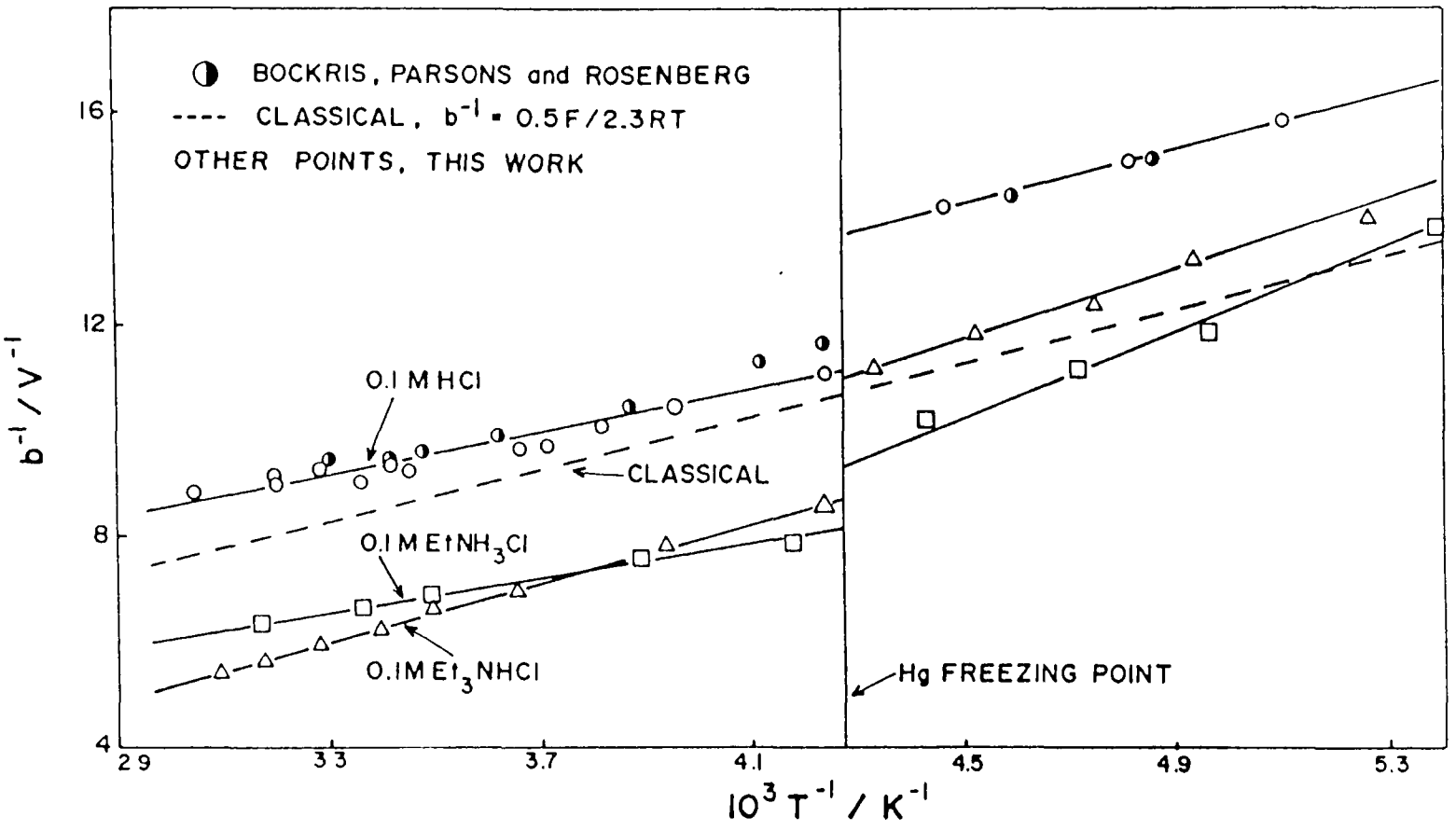

Fig 56b Dependence of b^{-1} on T^{-1} for the h.e r at Hg from different proton sources in CH_3OH.

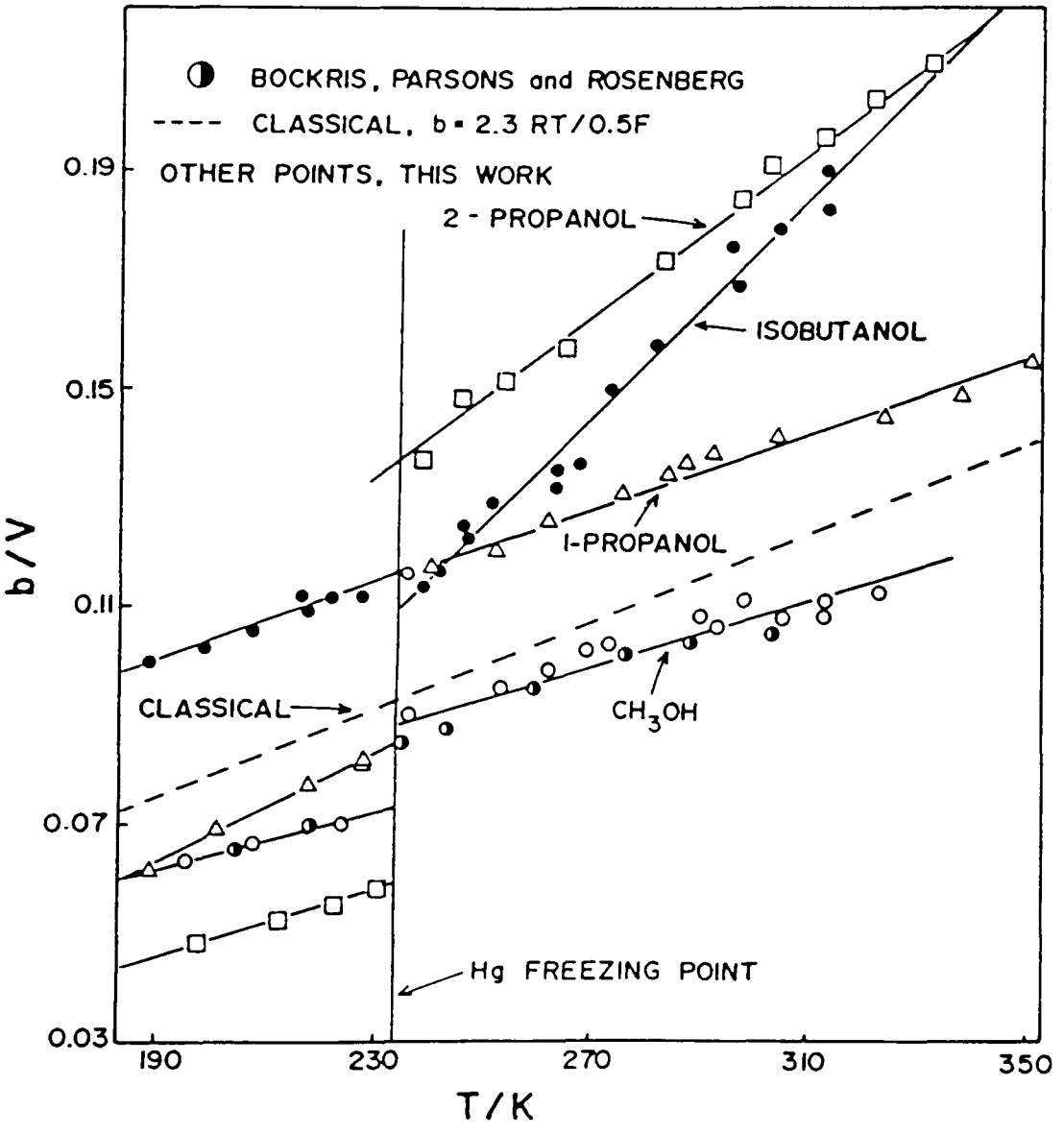

Fig. 57a Temperature-dependence of b for the h e r. at Hg from 0.1M HCl in different alcohols.

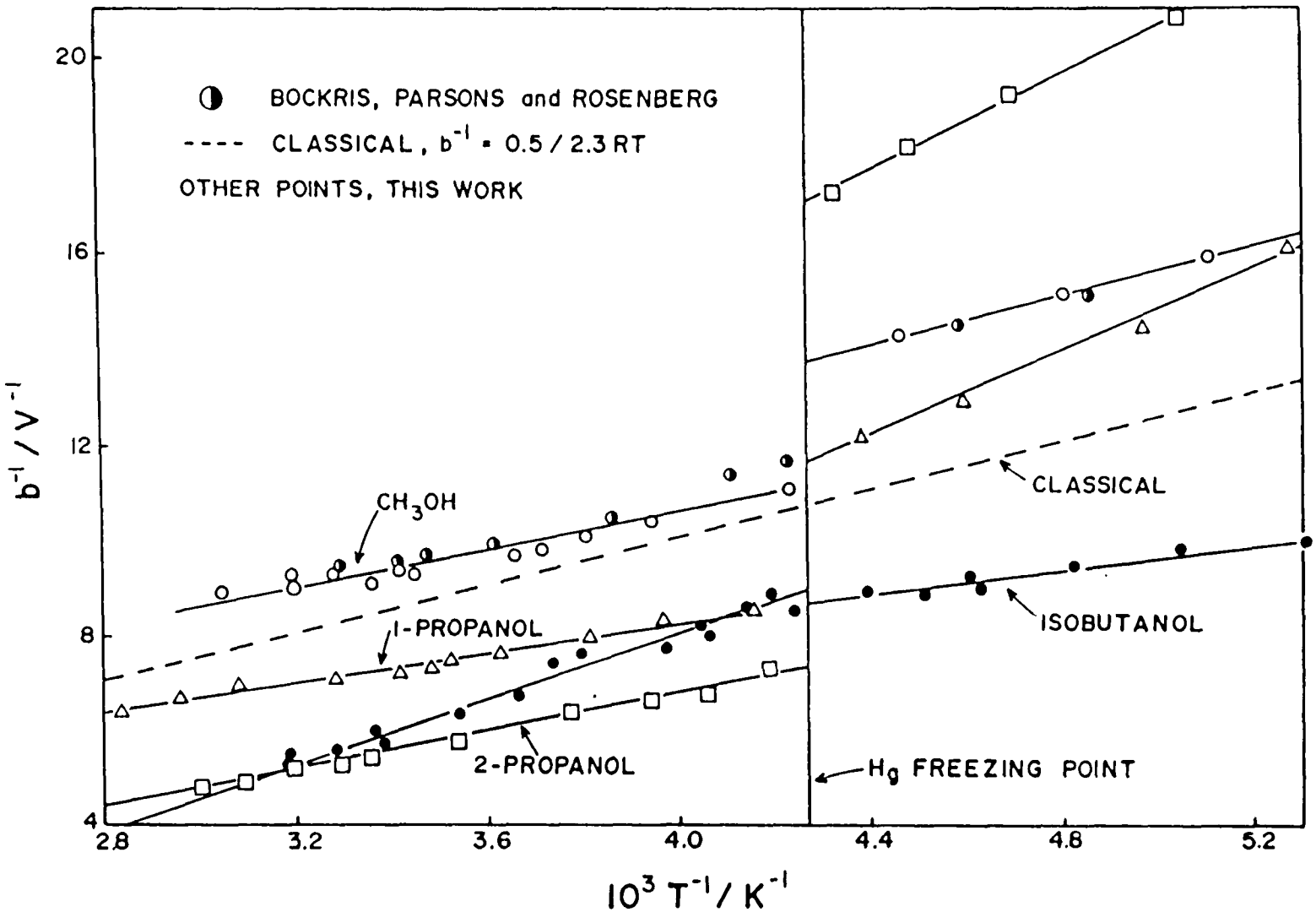

Fig 57b Dependence of b^{-1} on T^{-1} for the h.e r. at Hg from 0.1M HCl in different alcohols

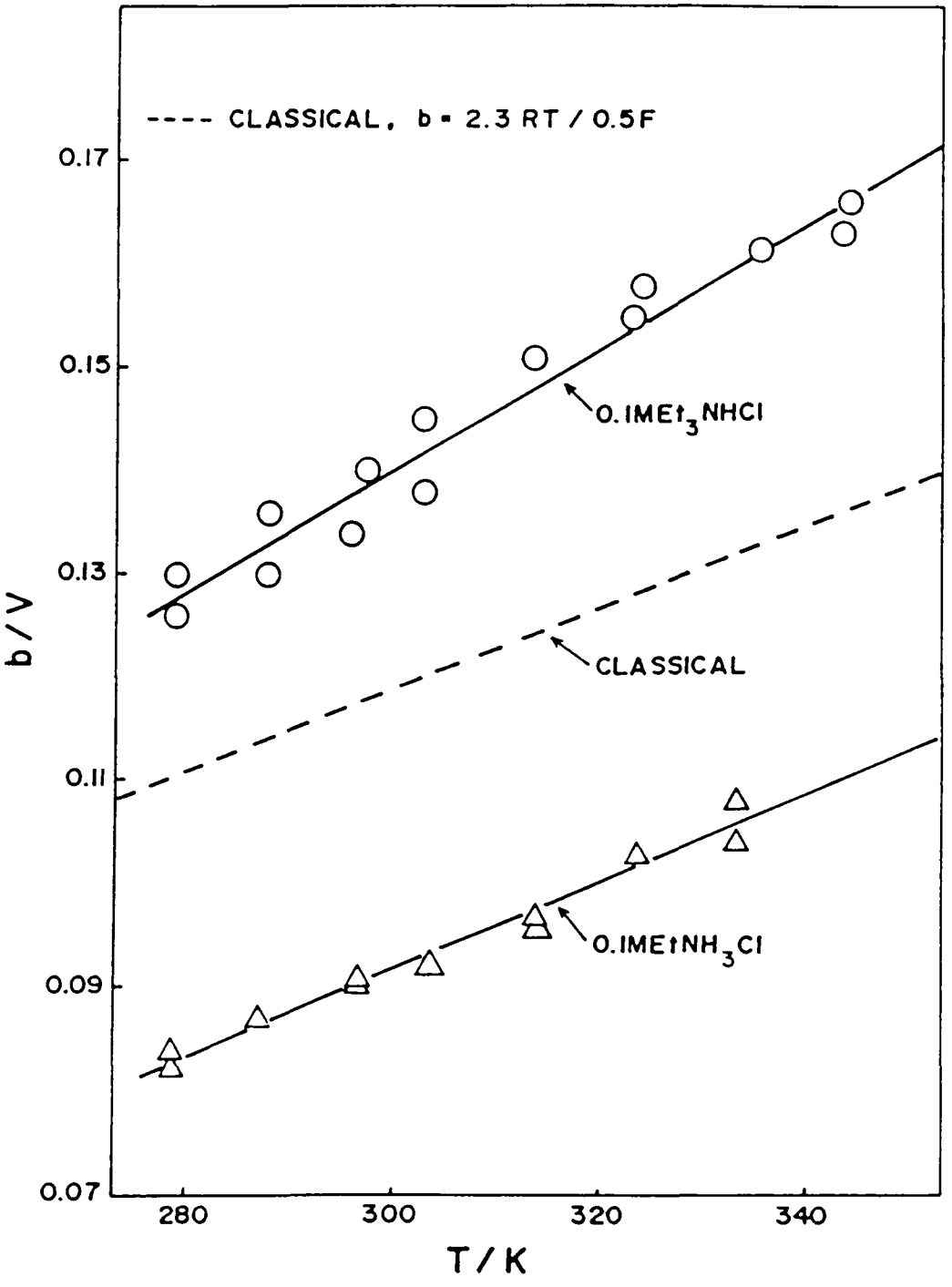

Fig 58a Temperature-dependence of b for the her at Hg from different proton sources in $HCONH_2$.

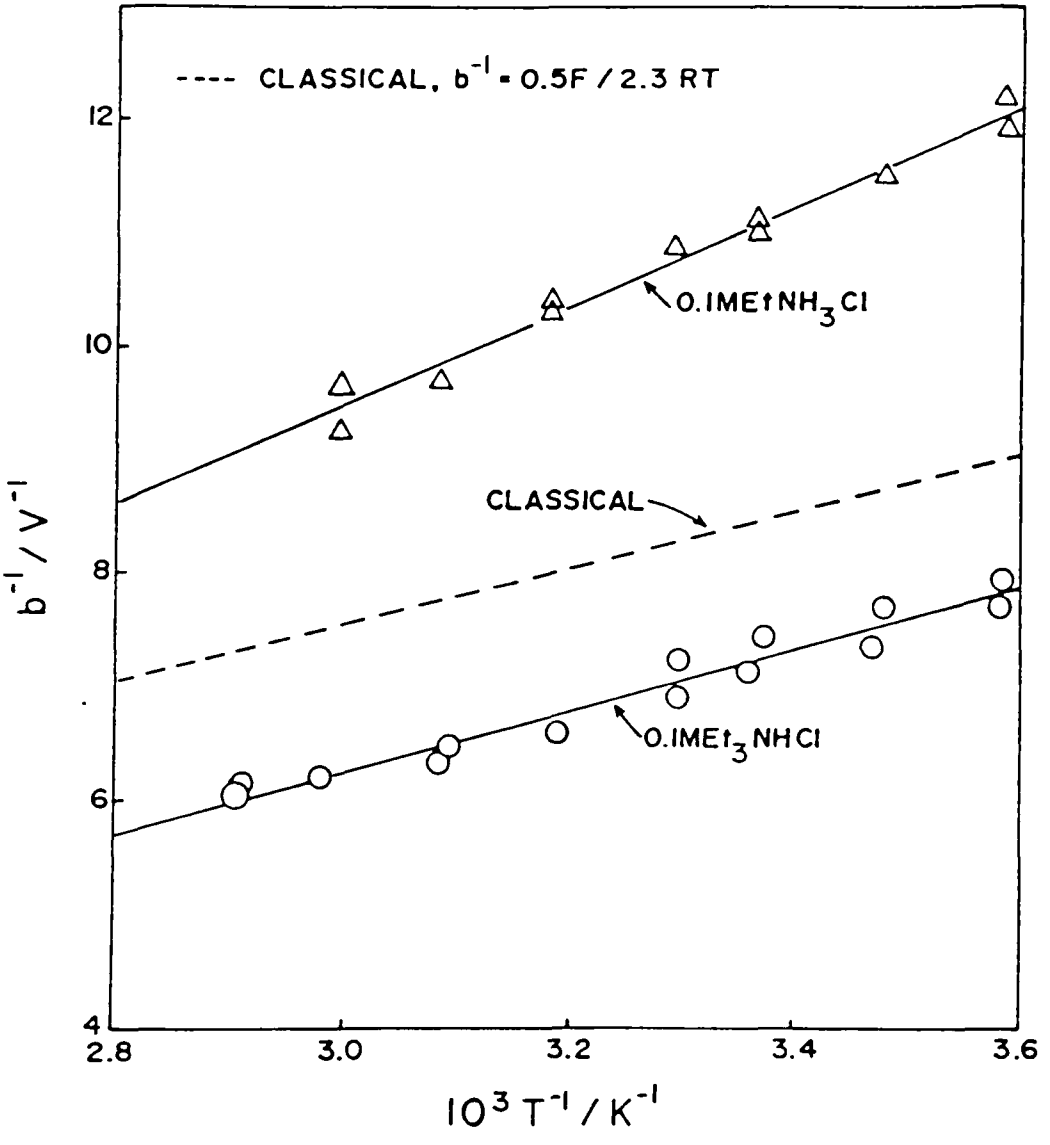

Fig 58b Dependence of b^{-1} on T^{-1} for the h.e r. at Hg from different proton sources in $HCONH_2$

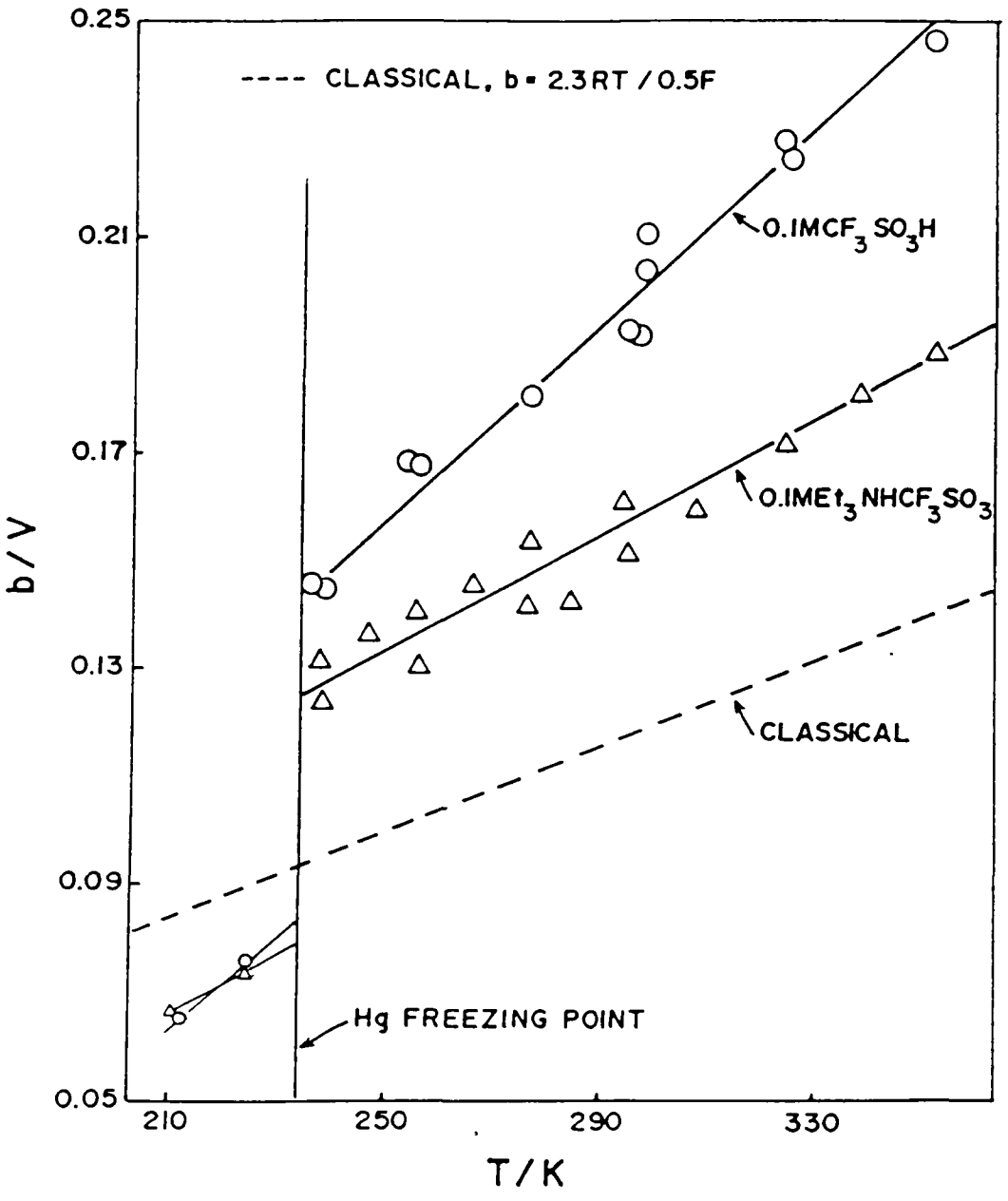

Fig. 59a Temperature-dependence of b for the her at Hg from different proton sources in DMF

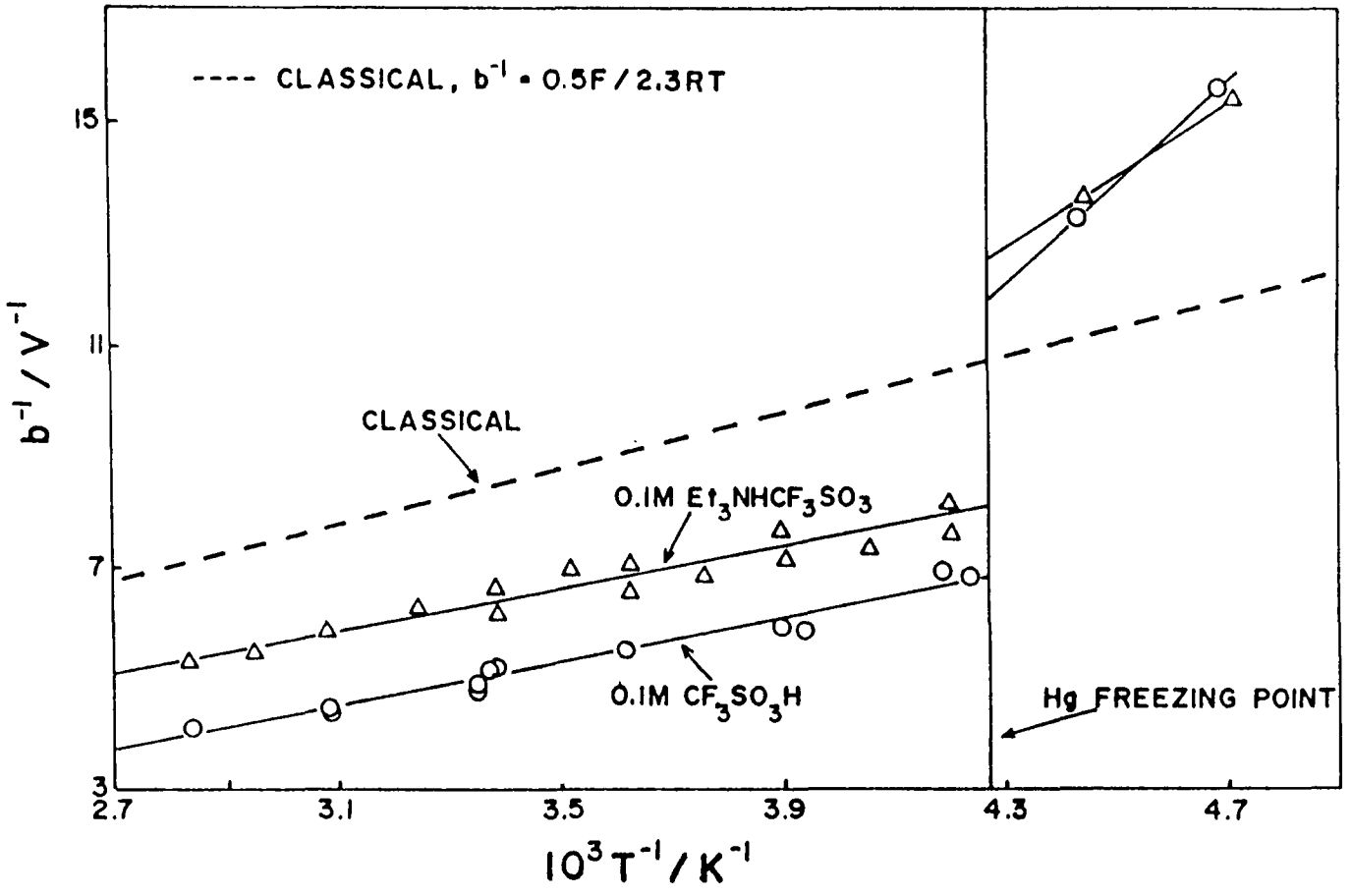

Fig 59b Dependence of b^{-1} on T^{-1} for the h.e r at Hg from different proton sources in DMF

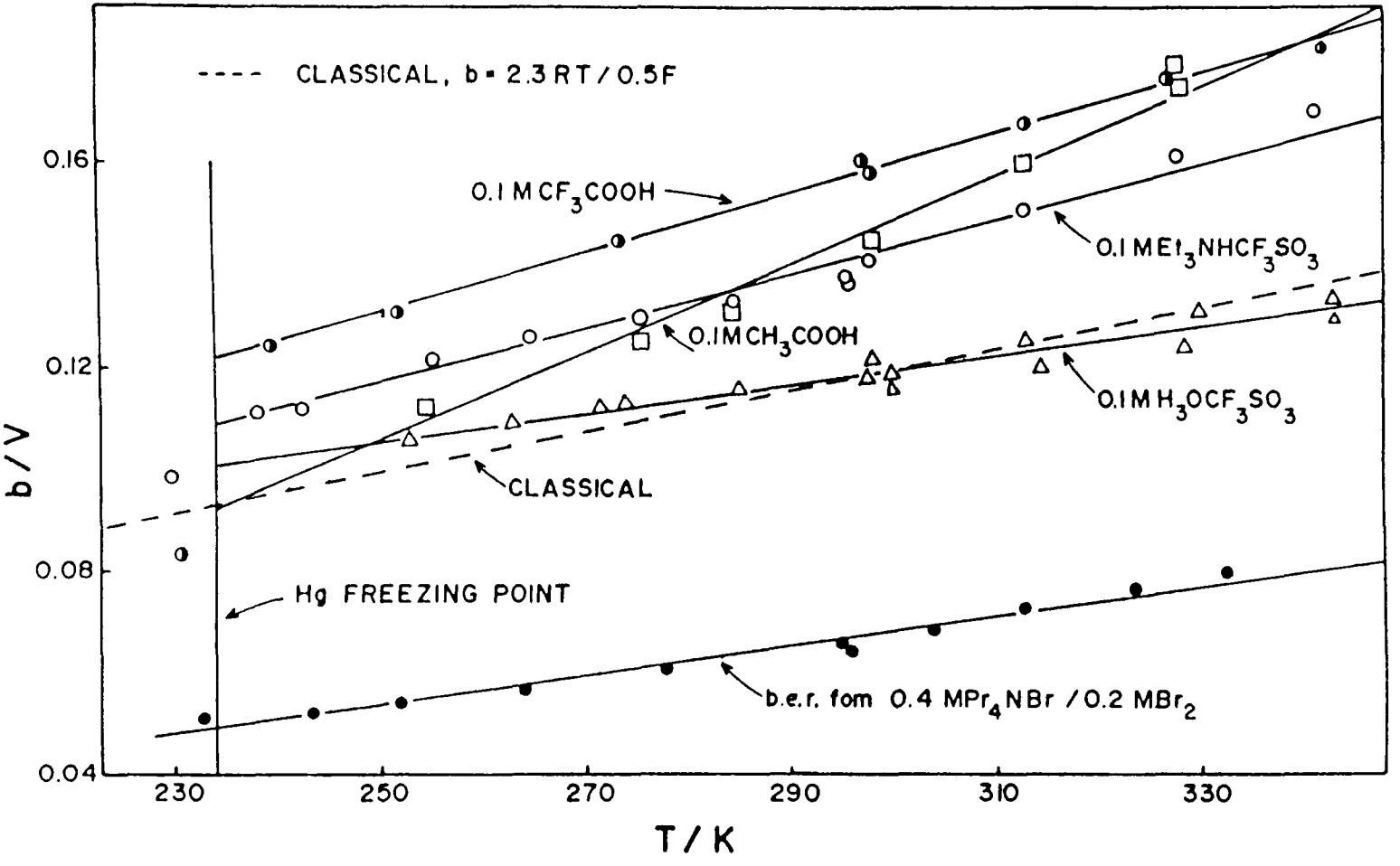

Fig 60a Temperature-dependence of b for i) the h e.r. at Hg from different proton sources in AN and ii) the b.e r. at vitreous carbon in AN

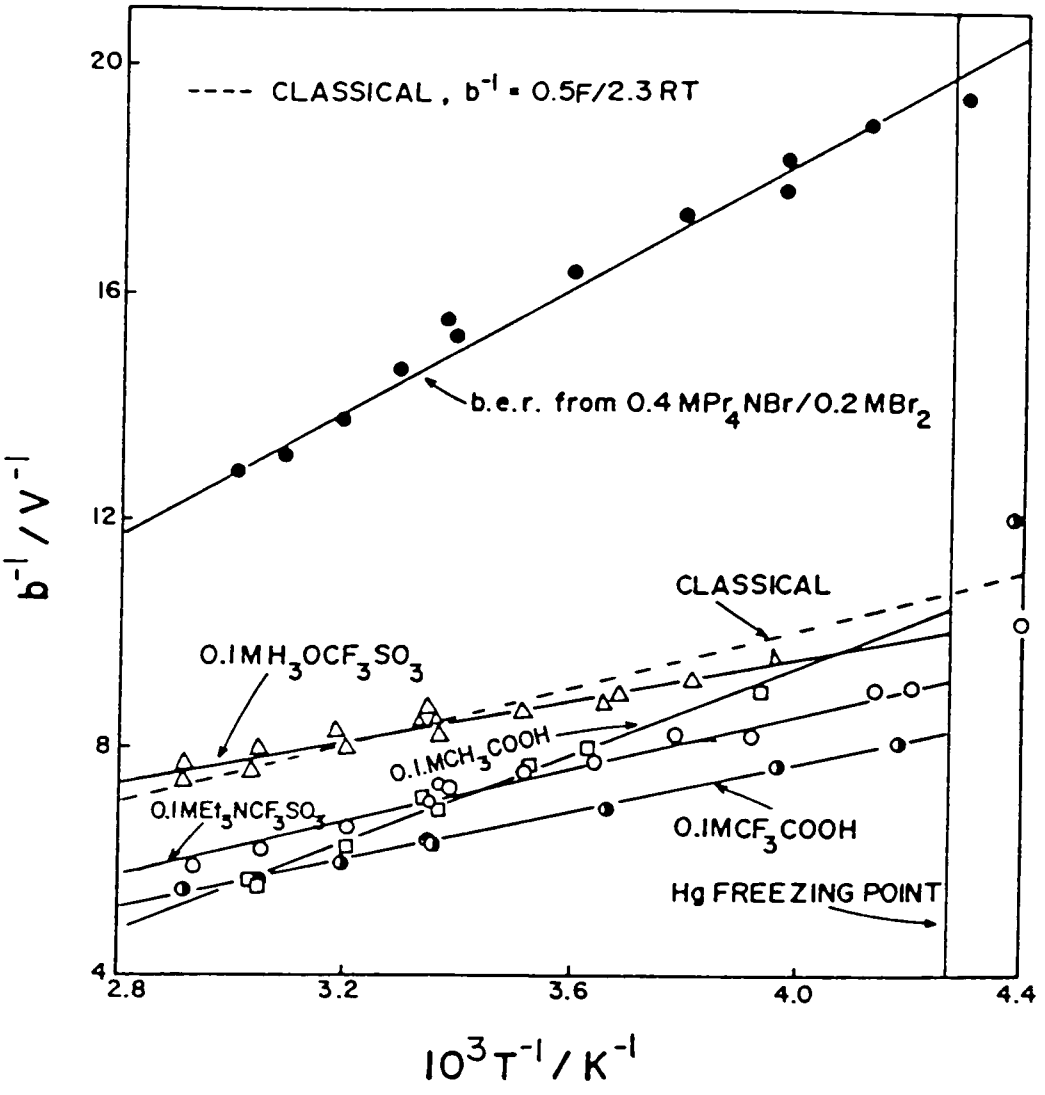

Fig 60b Dependence of b^{-1} on T^{-1} for i) the h e r. at Hg from different proton sources in AN and ii) the b e r at vitreous carbon in AN.

especially because water is somewhat more strongly adsorbed at Hg than AN (136) based on the work of adhesion, i.e., the work of adhesion at Hg for AN is 12.0 μJ cm^{-2} and for H_2O it is 13.1 μJ cm^{-2}.

The similarity of the activation parameters for the same proton donor, H_3O^+, in the above two substantially different solvent media indicates that the solvent medium has only a small effect on the potential-dependence of $\Delta\bar{H}^{\ddagger}_{\phi}$ and $\Delta\bar{S}^{\ddagger}_{\phi}$, and hence the associated β_H, β_S, and β values. Similar, but different proton donors such as Et_3NH^+ and $EtNH_3^+$, where the reactive bond centre is the same (i.e., N-H^+) should have similar, although not identical, electrostatic interactions with the same solvent medium, because of their different dimensions.

The appreciable differences in β_H. β_S, and β found for these proton donors in a particular solvent (Table 14) would also seem to indicate that the macroscopic properties of the solvent medium has <u>only a small effect</u> on the activation process determining β for proton discharge from H_3O^+ or $R_nNH^+_{4-n}$ proton sources. It is evident from the appreciable differences that are found in β_H, β_S and β for the <u>same</u> proton donor in <u>different</u> solvents (Table 14), that the solvent is important in the activation process but apparently mainly through short-range specific effects in or near the electrode double-layer and not significantly through long-range solvent effects such as those involved in outer solvation-shell reorganization.

In the recent quantum-mechanical treatments of proton

discharge, e.g., of Dogonadze, Kuznetzov and Levich (48), simplifications involved neglect of specific solvational and solvent structure aspects of the activation process (see section 5, chapter 1). From the results obtained here, it is found that

TABLE 14

β_H, β_S, β and the Observed Tafel Slope for the H.E.R. at Liquid Hg, from Different Proton Sources in Several Solvents

Electrolyte (0.1M)	Solvent	β_H^*	$10^4\beta_S/K^{-1}$*	β^{calc}** (298 K) ±0.02	$b^{obs.}/V$ (298 K) ±0.005V
HCl	H_2O	0.34	5.9	0.52	0.116
$EtNH_3Cl$	H_2O	0.75	10.1	0.45	0.133
Et_3NHCl	H_2O	0.30	2.7	0.38	0.155
Et_4NCl	H_2O	0.89	13.6	0.49	0.123
$EtNH_3Cl$	$HCONH_2$	0.87	7.3	0.65	0.091
Et_3NHCl	$HCONH_2$	0.56	4.2	0.43	0.139
$EtNH_3Cl$	CH_3OH	0.24	5.3	0.39	0.150
Et_3NHCl	CH_3OH	0.56	6.7	0.36	0.170
HCl	CH_3OH	0.40	4.9	0.55	0.107
HCl(1.0M)[a]	CH_3OH	0.21	9.7	0.50	0.118
HCl	1 Propanol	0.31	4.0	0.43	0.138
HCl	2-Propanol	0.39	- 2.3	0.33	0.185
HCl	Isobutanol	0.70	11.9	0.34	0.173
CF_3SO_3H	DMF	0.42	4.1	0.30	0.201
$Et_3NHCF_3SO_3$	DMF	0.39	0.4	0.38	0.159
$Et_3NHCF_3SO_3$	AN	0.47	1.6	0.42	0.142
$H_3OCF_3SO_3$	AN	0.36	4.5	0.50	0.119
CH_3COOH (0.1M Et_4ClO_4)	AN	0.77	12.1	0.41	0 147
CF_3COOH (0.1M Et_4ClO_4)	AN	0.42	1.5	0.38	0 159

* From b^{-1} vs T^{-1} plots.

** $\beta^{calc.} = \beta_H + \beta_S T$

[a] From results of refs. 37 and 38.

specific as well as general medium effects have to be included in any interpretation of the electrochemical kinetic behaviour of the h.e.r. and probably also in other electrode processes For a further discussion of these results in relation to the work of Krishtalik and coworkers (137,138,139,140) on the question of medium and bond-nature effects in proton discharge, see section C-13, this chapter.

c) H.E.R. at Solid Hg

Values of β_H and β_S determined from the b^{-1} versus T^{-1} plots, the overall β values, and the observed Tafel slopes, are shown in Table 15 for the h.e.r at solid Hg from different proton sources in several solvents.

Appreciable differences in β_H, β_S and β are found for the h.e.r. on liquid and solid Hg in the same solution as shown in Table 16. Although specific adsorption of anions increases with decreasing temperature, the Tafel behaviour at solid Hg ($T \leq 234$ K) is not unusually different from that at higher temperatures. Only for 0.1M HCl in 2-propanol is β unusually high (β = 0 80 at 233 K) which may indicate the role of an anion adsorption effect. Clearly, the substrate affects the potential dependence of $\Delta\bar{H}_{\phi}^{\ddagger}$ and $\Delta\bar{S}_{\phi}^{\ddagger}$, and hence the associated β_H, β_S and β values The Tafel slope decreases and the symmetry factor increases discontinuously at the melting point of Hg. Bockris et al (141) also observed this effect for 0.1N HCl in methanol and ascribed it to a distortion of the energy barrier which results from restriction of translational motion of the activated state

TABLE 15

β_H, β_S, β and the Observed Tafel Slope for the H.E.R. at Solid Hg(i) from Different Proton Sources in Several Solvents

Electrolyte (0.1M)	Solvent	β_H*	$10^4\beta_S/K^{-1}$*	β (233 K) ±0.03	$b^{obs.}/V$ (233 K) ±0.003V
$EtNH_3Cl$	CH_3OH	0.82	16.3	0.44**	0.104
Et_3NHCl	CH_3OH	0.64	5.5	0.51**	0.090
HCl	CH_3OH	0.49	6.3	0.64**	0.073
HCl	1 Propanol	0.85	13.1	0.54**	0.084
HCl	2-Propanol	0.97	7.3	0.80**	0.058
HCl	Isobutanol	0.25	6.6	0.40**	0.115
CF_3SO_3H	DMF			0.56***	0.082
$Et_3NHCF_3SO_3$	DMF	--		0.59***	0.078
$Et_3NHCF_3SO_3$	AN			≈ 0.47***	≈0 098

* From b^{-1} vs T^{-1} plots

** $\beta = \beta^{calc.} = \beta_H + \beta_S T$

*** $\beta = \beta^{obs.} = \pm 2\ 303RT/b^{obs}\ F$

(i) F P. (Hg) = 234.16 K.

TABLE 16

Change in b and β at the Freezing Point of Hg (234.16 K) for the H.E.R. from Different Proton Sources in Several Solvents

Electrolyte (0.1M)	Solvent	$\Delta b/V^*$ (234K) ±0.008 V	$\Delta\beta^{**}$ (234 K) ± 0.05
$EtNH_3Cl$	CH_3OH	-0.019	0.08
Et_3NHCl	CH_3OH	-0.022	0.11
HCl	CH_3OH	-0.015	0.13
HCl	1-Propanol	-0.032	0.14
HCl	2 Propanol	-0.078	0.46
HCl	Isobutanol	+0.005	-0.02
CF_3SO_3H	DMF	-0.061	0.24
$Et_3NHCF_3SO_3$	DMF	-0.045	0.21
$Et_3NHCF_3SO_3$	AN	-0.011	0 04

* Δb = b (solid Hg) b (liq. Hg); b values from Tables 14 and 15.

** $\Delta\beta = \beta$ (solid Hg) β (liq Hg); β values from Tables 14 and 15.

upon freezing of the electrode. Only the activated state and final state should be affected on solidification, as the initial state of the solvated proton donor in the Helmholtz layer remains the same However, the adsorption and freedom of

orientation of O-containing solvent molecules may depend on the state of the Hg surface, solid or liquid.

The value of β for a discharge reaction has been defined as

$$\beta = \frac{\text{Distance along reaction coordinate between initial and activated state}}{\text{Distance along reaction coordinate between initial and final state}} \quad [84]^*$$

where the initial state consists of a solvated proton donor in the outer Helmholtz plane of the electrode, the final state consists of an adsorbed hydrogen atom on the metal surface and the activated state corresponds to the peak of the energy barrier between the initial and final states (142).

Qualitatively, a decrease in the entropy of the activated state will increase the free energies of the final and activated states with respect to that of the initial state. The resultant distortion of the energy barrier brings the activated state slightly closer to the final state, while the distance between the initial and final states remains approximately the same and hence from equation [84], β is increased.

d) Comparison with Previous Work on the Temperature-Dependence of the Tafel Slope

Although the h.e.r. has been studied extensively at Hg, relatively few investigations of the temperature-dependence of

---

* This representation of β is an alternative one to that based on the effect of shifting energy profile curves. It only gives the same result as the latter if the energy curves approximate to straight-lines in the region of the crossing points over an appreciable range of potentials.

the Tafel slope have been made at Hg. The data of Post and Hiskey (143) for aqueous 0.1M HCl have been plotted with the data of the present work in Figs. 55a-b. and are in excellent agreement. Also, the data of Bockris, Parsons and Rosenberg (141) for 0.1N HCl in methanol have been plotted with the data of the present work in Figs. 56a,b 57a,b, and are in reasonable agreement. However, treatment of the data for this system did not give b independent of temperature between 276 and 303 K but conventional behaviour (b linear in T) was found below 276 K, as indicated by the plot shown in the paper of Bockris et al. The work of Conway et al. (132, 37, 38) for 1.0N HCl in methanol, was not included for comparison because of the tenfold difference in acid concentration. Reanalysis of their data, by means of a b^{-1} versus T^{-1} plot, gives the β_H and β_S components shown in Table 14, which are rather different from those found in the present work for 0.1M HCl in methanol, although the overall symmetry factor is about the same. This would indicate the HCl concentration significantly affects the potential dependence of $\Delta\bar{H}^{\ddagger}_{\phi}$ and $\Delta\bar{S}^{\ddagger}_{\phi}$, i.e , Cl adsorption may be a factor, especially in the more concentrated solution (see section C-5, this chapter).

6. Various Types of Tafel Slope Behaviour Observed

The expected temperature-dependence of the Tafel slope over the temperature range of 0 to 350 K, based on some of the experimentally determined β_H and β_S values (Tables 13 and 14) and eqn.[12] is shown in Fig. 61 for various systems which

illustrate that several different types of temperature behaviour are possible:

i) For 0.1M CF_3SO_3H in DMF and 0.1M $EtNH_3Cl$ in formamide, β_S and β_H are of opposite sign so that a singularity in b *vs* T will arise when $\beta_H = T\beta_S$, i.e. where, $\beta \rightarrow 0$. This situation, which is not experimentally accessible here, may correspond to the limiting kinetic behaviour that has been called "activationless" (144). The limiting kinetic behaviour that has been called "barrierless", i.e., when $\beta = 1$ (144), is approached at low temperatures by systems such as 0.1M $EtNH_3Cl$ in formamide ($\beta = 0.87 \quad 7.3 \times 10^{-4}T$) which have large enthalpic components of β. For a discussion of activationless and barrierless discharge, see section 5, chapter 1 and ref. 144.

ii) For the h.e.r. from 0.1M $Et_3NHCF_3SO_3$ in DMF, the entropic component is very small, and $\beta_H >> \beta_S T$ over the experimental temperature range (235 353 K) so that β is almost completely "enthalpy-controlled". This case corresponds to conventional Tafel behaviour with $\beta \approx 0.39$.

iii) For 0.1M aqueous HCl, both β_H and β_S are positive so that at sufficiently high temperatures. with $\beta_S T >> \beta_H$, a limiting form of equation [81] is reached,

$$b \approx \pm 2.3RT/\beta_S TF = \text{constant} \qquad [85]$$

hence the Tafel slope is virtually independent of temperature and is then almost completely "entropy-controlled."

Appleby (145) and Yeager et al. (146) have reported this type of temperature dependence of b for the oxygen evolution and oxygen reduction reactions, respectively. Also, this behaviour was found by Conway et al (132) for the b e r. at pyrolytic graphite from 0.4M Pr_4NBr in AN and is shown in Fig. 61. Similar behaviour arises in Stout's results (147) for azide discharge at Pt which gave rise to Agar's comment (130) on this type of result. In the experimental temperature range for these reactions β is almost completely "entropy-controlled" and an increase of electrode potential must apparently have its main effect on $\Delta\bar{S}_{\phi}^{\ddagger}$ rather than on $\Delta\bar{H}_{\phi}^{\ddagger}$. In relation to this conclusion, it is of interest that many thermodynamic and kinetic properties of aqueous systems are controlled as much by entropy as enthalpy, a fact first noted by Butler (148).

Conway et al. (132) proposed empirically a different kind of relation between b and T, viz.

$$b = \pm 2\ 3RT/\beta' F + c \qquad [86]$$

to fit the observed temperature-dependence of b for the h.e.r at Hg, where β' is a constant symmetry factor and c is a constant. It can be seen from Fig. 61 that over an appreciable temperature range of about 150 K which includes room temperature, the empirical eqn [86] fits the temperature dependence of the Tafel slope almost as well as a plot based on eqn.[81], if a reasonable experimental error of ± 0 005 V is assumed for the Tafel slopes. Thus, plots of b^{-1} *vs* T^{-1} and b *vs* T shown in Figs 55a,b 60a,b, are linear within

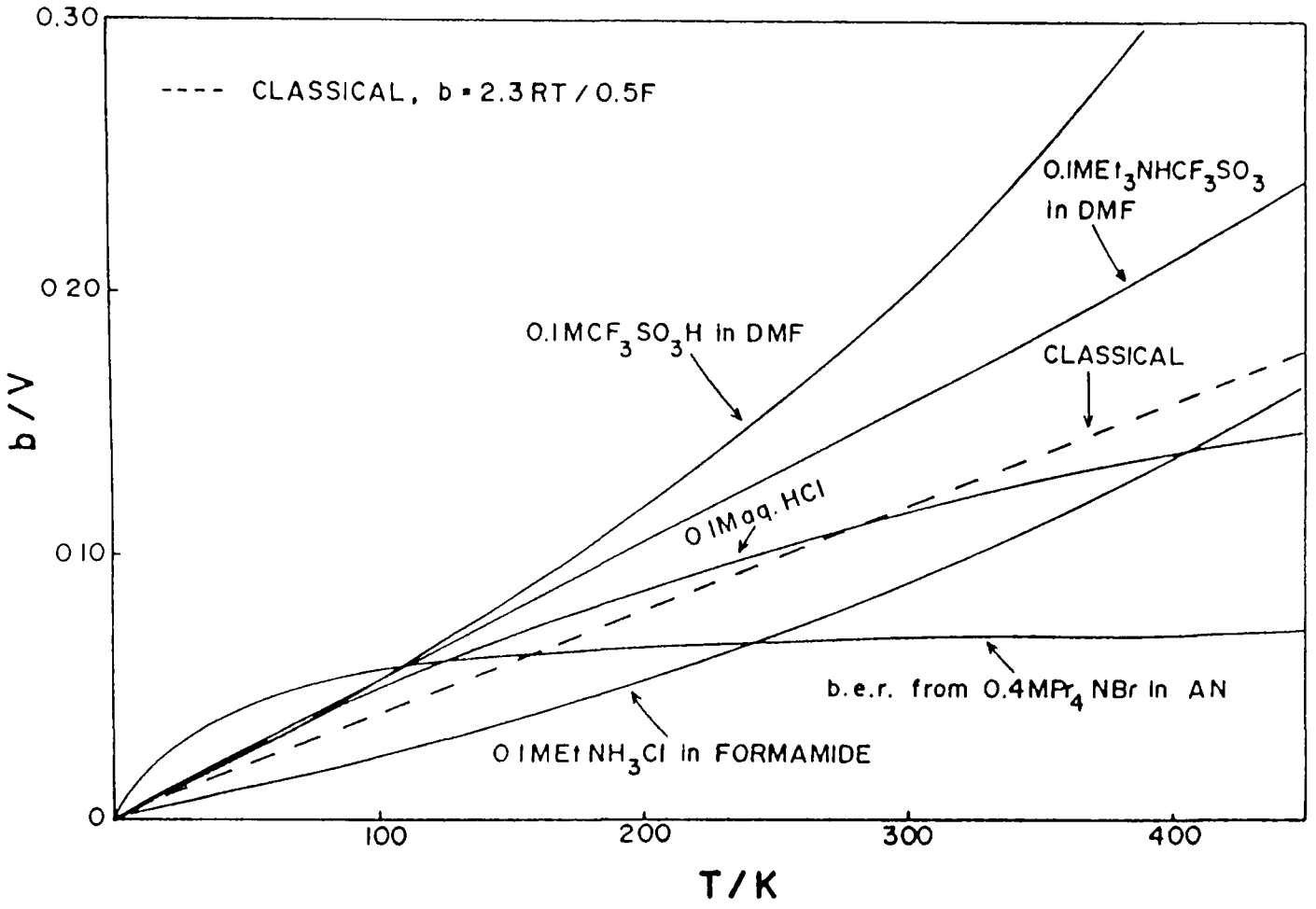

Fig 61 Temperature-dependence of the Tafel slope $b = \pm 2.3RT/(\beta_H + \beta_S\Gamma)F$ based on the activation parameters β_H and β_S for i) the h e r at Hg in the media indicated and ii) the b e r at pyrolytic graphite in AN (ref 132)

experimental error and represent the observed b(T) behaviour of the systems studied here, equally well.

In order to make a choice between representation of the b data by eqns.[81] and [86] Tafel behaviour should be investigated over a very large temperature range (e.g. >200 K) and/or a system has to be found which shows appreciable curvature in the b vs T plot in the experimentally accessible temperature range, i.e., $T\beta_S$ becomes equal to β_H below the boiling point of the solvent, when β_S is negative.

From a fundamental point of view, it is significant that eqn.[81] arises from a consideration of the experimental potential-dependence of the enthalpy and entropy of activation and is not just an empirical relation like eqn.[86]. Thus eqn.[81] is to be preferred.

The change in energy of the Fermi level relative to "vacuum" with applied potential must always have some effect on an electrode reaction, and therefore the enthalpic component, β_H, should it seems, always have a nonzero value, i.e., $\beta_H > 0$. In cases where b is almost independent of temperature, so that β_H is apparently zero, a nonzero value of β_H could always be found within the experimental error of the system but it would be small. A nonzero value of β_H is important in that the Tafel slope of eqn.[81] will always then be zero at T = 0 K, if $\beta_H \neq 0$. However, the empirical eqn [86] leads to a finite nonzero intercept, c, at T = 0 K which can be negative or positive.

This raises a number of fundamental problems concerning the

significance of a nonzero intercept and clearly leads to impossible behaviour in two cases: i) when the intercept is negative, a decrease in current with increased overpotential is implied and ii) when b is approximately independent of temperature (i.e., $b(T) \approx c$), $\beta' >> 1$ is implied. For the h.e.r. at Hg, a positive intercept has been qualitatively associated with proton tunneling (128,132) but for electrode reactions such as the b.e.r. involving heavier particles, quantum effects would be negligible.

7. Relation of β, β_H and β_S to Solvent Dielectric Constant

Further evidence for the importance of specific effects in the h.e.r. is provided from the data of Figs. 62-64, where plots of the activation parameters β_H, β_S and β against the reciprocal of the solvent dielectric constant, ϵ, (a macroscopic solvent property) do not show any systematic relation. However, there appear to be two specific correlations:

i) for proton donors with an $O\text{-}H^+$ reactive bond-centre (e.g., H_3O^+, ROH_2^+), there is a decrease in β_S with decreasing solvent dielectric constant (Fig. 63).

ii) for a given proton donor, there is a trend of decreasing β with decreasing solvent dielectric constant (Fig. 64).

No correlation is found between the activation parameters and solvent donicity.

The tendency of β to decrease with decreasing solvent dielectric constant can be explained qualitatively in terms of distance along the reaction coordinate of a Gibbs energy

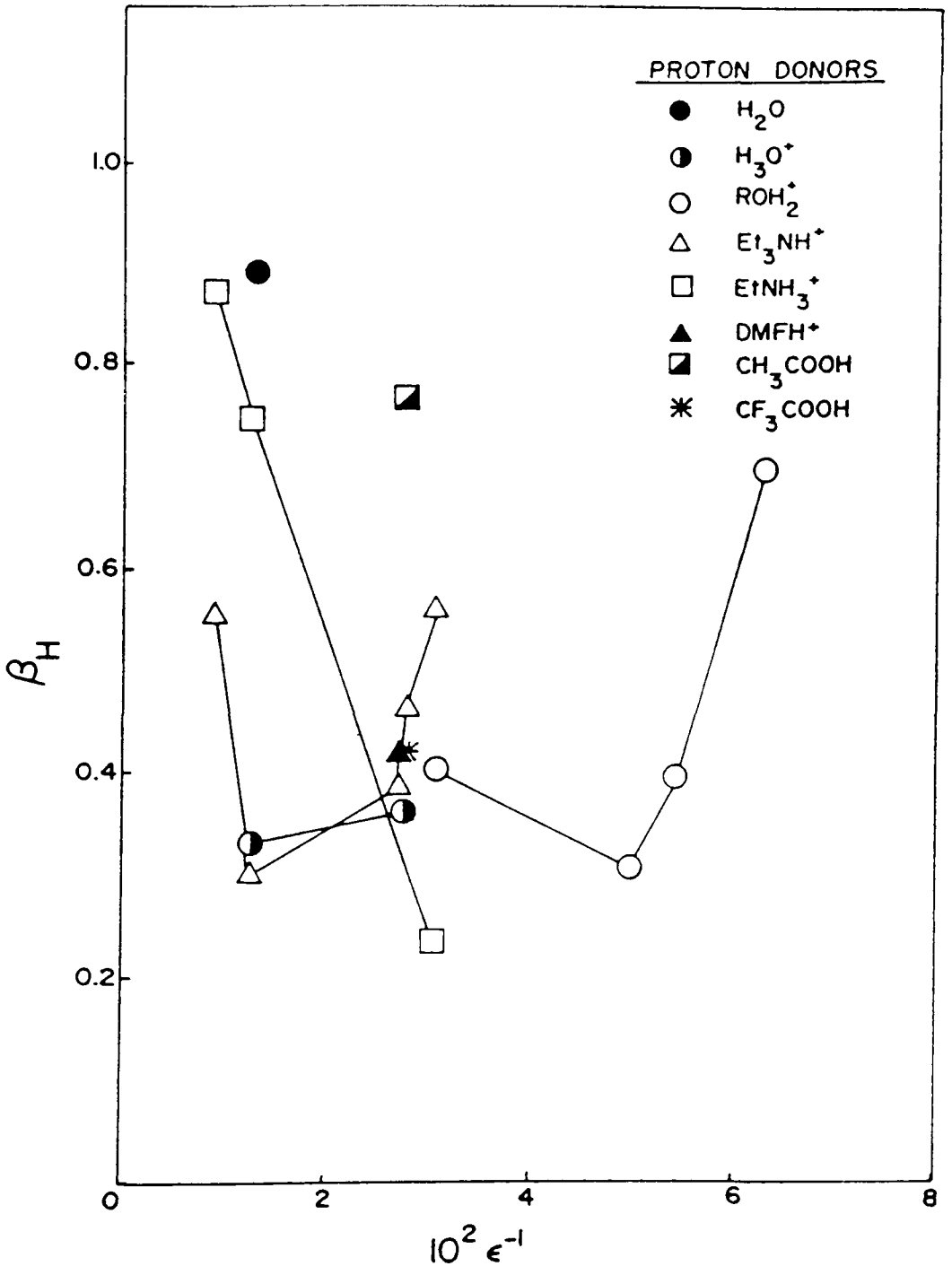

Fig. 62 β_H as a function of the reciprocal of the solvent dielectric constant (ϵ^{-1}) for the h.e.r at Hg from different proton donors

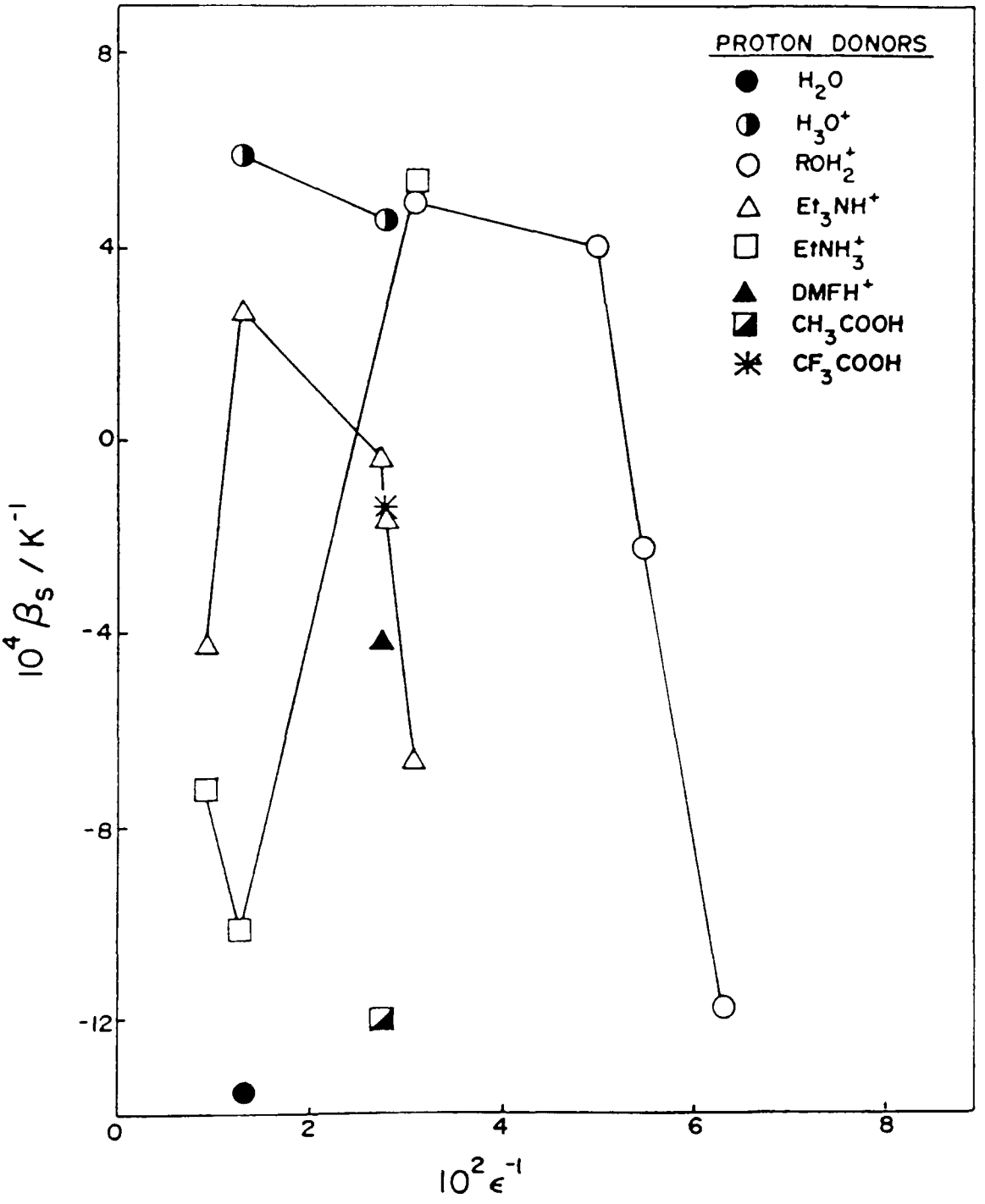

Fig. 63 β_S as a function of the reciprocal of the solvent dielectric constant (ϵ^{-1}) for the h.e r at Hg from different proton donors

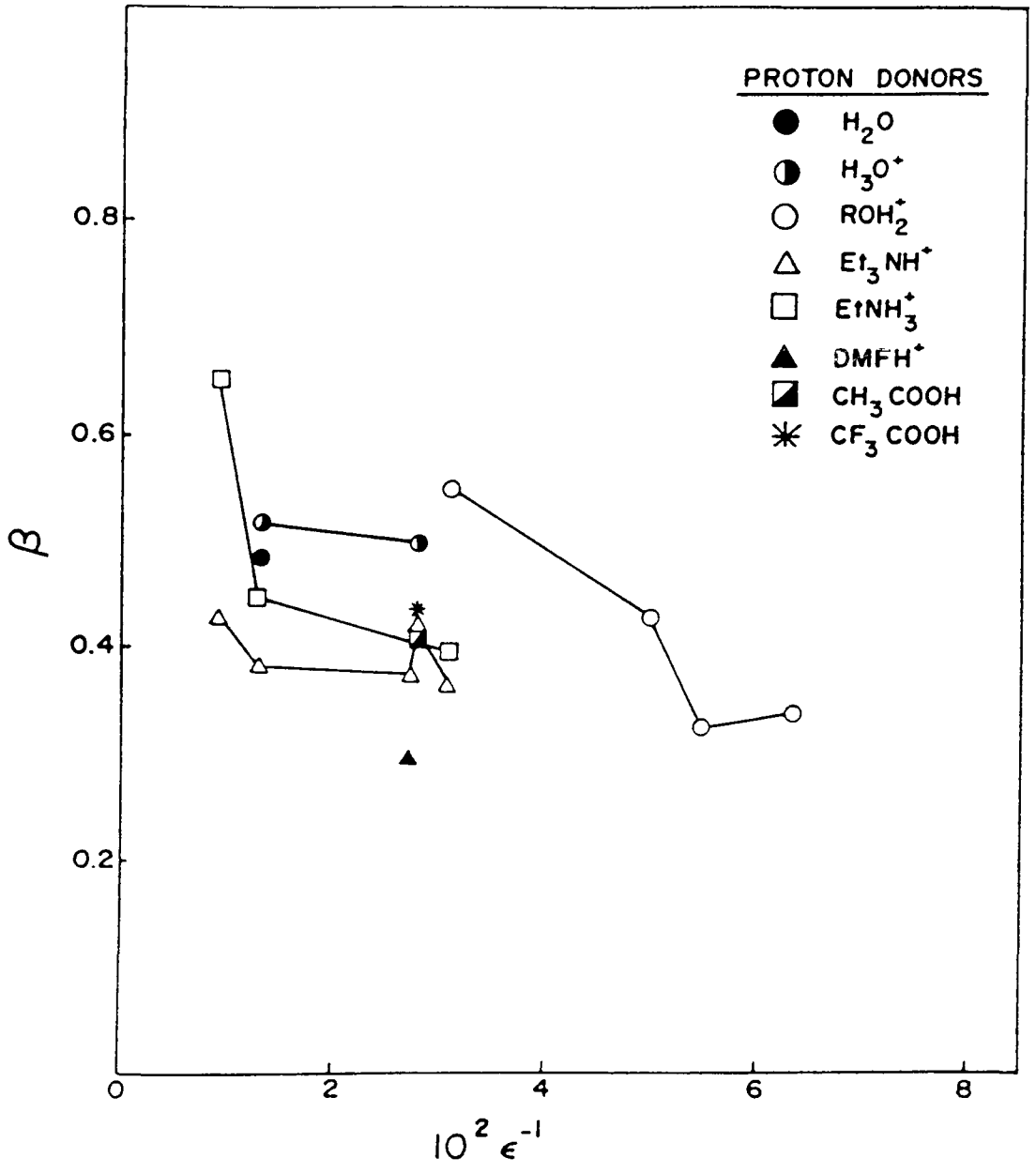

Fig. 64 β as a function of the reciprocal of the solvent dielectric constant (ϵ^{-1}) for the h e r at Hg from different proton donors at 298 K

diagram. Generally, the Gibbs energy of solvation will become less negative with decreasing dielectric constant (cf. the Born solvation energy expression) and this will increase the Gibbs energies of the initial and activated states with respect to that of the final state. The resultant distortion of the energy barrier will bring the activated state somewhat closer to the initial state while the distance between the initial and final states remains approximately the same and hence, from eqn.[84], β would be decreased.

8. Relation between β_H and β_S

A plot of β_H versus β_S for the h.e.r. at solid and liquid Hg from the data acquired for the systems studied here, is shown in Fig. 65. The two activation parameters evidently vary together in a systematic and compensatory way, so that the overall symmetry factor, β, given by equation[80] does not vary much in the series. This behaviour is thus similar to that of various "ΔH" and "$T\Delta S$" quantities for solution properties and solution processes where a "compensation effect" between these two types of quantities often arises. A linear relation between β_H and β_S is found,

$$\beta_H = -272\beta_S + 0.46 \qquad [87]$$

with a correlation coefficient of 0.87. The required restriction of $0 < \beta_H < 1$ gives the limiting values from eqn.[87] of; $\beta_S = +16.9 \times 10^{-4}K^{-1}$ at $\beta_H = 0$, with $\beta_S = 19.8 \times 10^{-4}K^{-1}$ at $\beta_H = 1$. These limiting values correspond to an overall

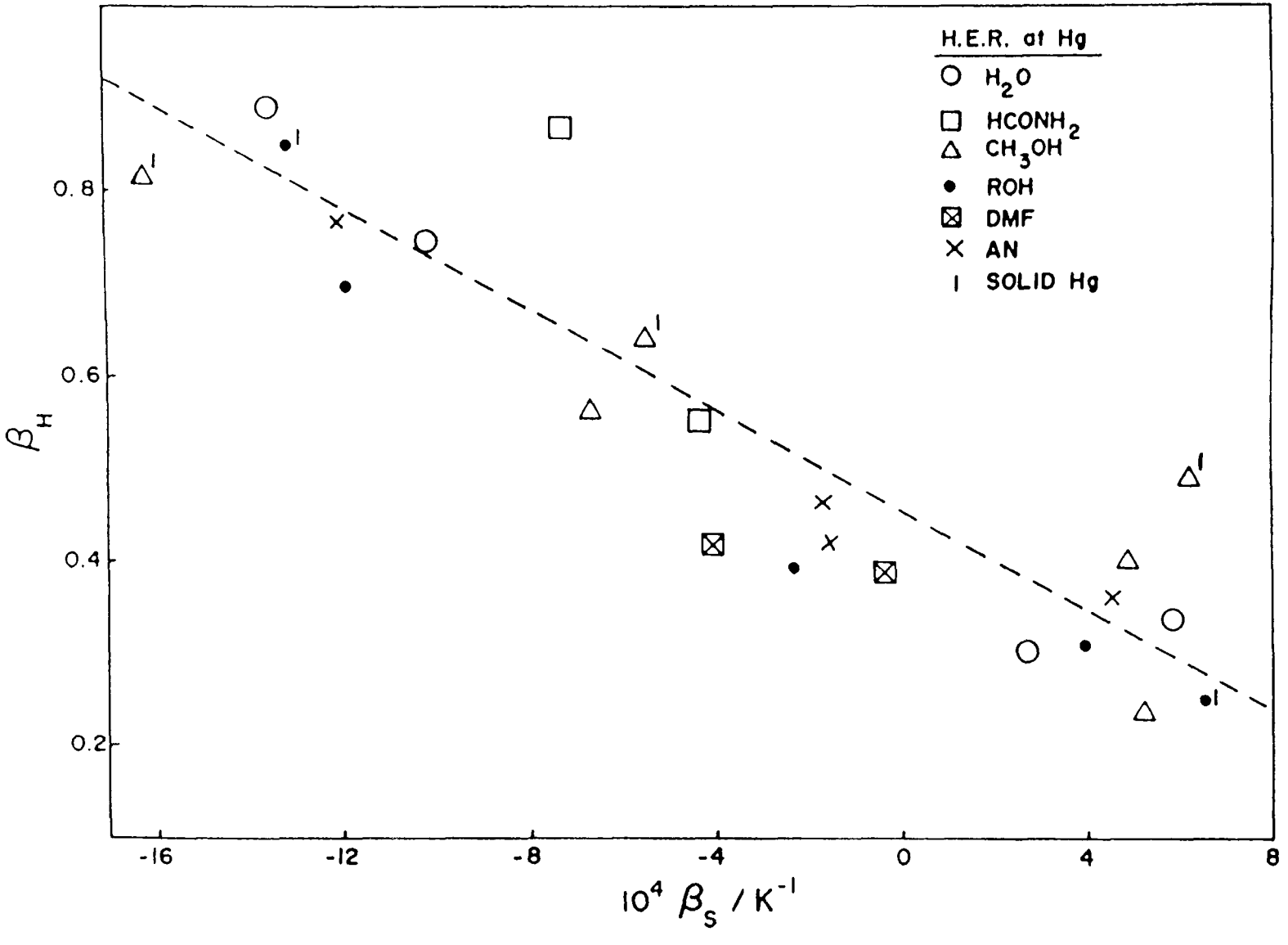

Fig 65 Compensation plot of β_H versus β_S for the h e.r at Hg from different proton donors in several solvents.

symmetry factor range of $0.41 < \beta < 0.50$ at 298 K, so that β is, in a relative way, approximately constant even though β_H and β_S vary considerably. It is significant that when $\beta_S = 0$ (i.e., $\Delta\bar{S}^{\ddagger}_{\phi}$ is independent of electrode potential), β is temperature independent and $\beta \approx 0.5$, so that classical behaviour is observed.

Compensation effects are a widely observed phenomenon in a number of kinetic and thermodynamic processes (103,149) such as heats and entropies of solution, activation quantities in heterogeneous catalysis, etc. An advanced statistical mechanical theory for the compensation effect between the log of the frequency factor (proportional to $\Delta S^{\ddagger}$) and the heat of activation, $\Delta H^{\ddagger}$, for kinetic processes has been discussed by Ruetschi (150). He showed that the compensation effect was caused by a relative invariance of the shape of the potential energy surfaces and particularly of their anharmonicity for a series of processes involving similar bonds. This is a result of the relation between force constant or frequency, and dissociation energy of similar bonds. It is of interest, but not unexpected, that the potential dependence of the frequency factor or $\Delta\bar{S}^{\ddagger}_{\phi}$ and the potential dependence of $\Delta\bar{H}^{\ddagger}_{\phi}$ also show a compensation effect for the h.e.r. which involves similar bonds, i.e.,

$$d(\Delta\bar{H}^{\ddagger}_{\phi})/Fd\phi = C\ d(\Delta\bar{S}^{\ddagger}_{\phi})/Fd\phi + K \qquad [88]$$

where C and K are constants For the b e.r. very different bonding from that for the h e r is involved, and the

relationship between values of β_H and β_S for this reaction at vitreous carbon and pyrolytic graphite (Table 13) is appreciably different from the compensation plot of Fig. 65 for the h.e.r. case.

9. Correlation of β_S with $\Delta\bar{S}^{\ddagger}_{\phi}$ and β_H with $\Delta\bar{H}^{\ddagger}_{\phi}$ for the H.E.R. from Different Systems

All kinetic data were referred to the metal-solution potential difference, ϕ_R, of the reversible hydrogen electrode in 0.1M aqueous HCl at 298 K, i.e., $\phi = \phi_R$. Values of $\Delta\bar{H}^{\ddagger}_{\phi}$ and the logarithm of the frequency factor, log A_{ϕ} (proportional to $\Delta\bar{S}^{\ddagger}_{\phi}$) are taken from Tables 17 and 18; values of β_H and β_S are taken from Tables 14 and 15.

A plot of β_S versus log A_{ϕ} for the h.e.r. at solid and liquid Hg from the data acquired for the systems studied here is shown in Fig. 66 and an approximate linear relation is found:

$$\beta_S = 1.4 \times 10^{-4} \log A_{\phi} + 6.4 \times 10^{-4} \quad [89]$$

with a correlation coefficient of 0.89. Rearrangement of the expression for $\Delta\bar{S}^{\ddagger}_{\phi}$ (eqn.[133], this chapter) in terms of log A_{ϕ} gives,

$$\log A_{\phi} = \Delta\bar{S}^{\ddagger}_{\phi}/2\ 3R + \ln [zFc_{H+}\ (1 \quad \theta)\tilde{k}T/h]/2\ 3 \quad [90]$$

which can be substituted into eqn. [89] with appropriate values of $c_{H+} = 10^{-4}$ moles cm ^{3}, $z = 2$, and $1-\theta \approx 1$ (for Hg), to give

$$\beta_S = 7.3 \times 10^{-6} \Delta\bar{S}^{\ddagger}_{\phi} \quad 1.33 \times 10^{-3} \quad [91]$$

At $\beta_S = 0$ in eqn.[91], $\Delta\bar{S}^{\ddagger}_{\phi} = 180$ J mole $^{1}K^{1}$, corresponding to the "chemical" entropy of activation unaffected by potential. This type of behaviour is found for outer-sphere redox reactions

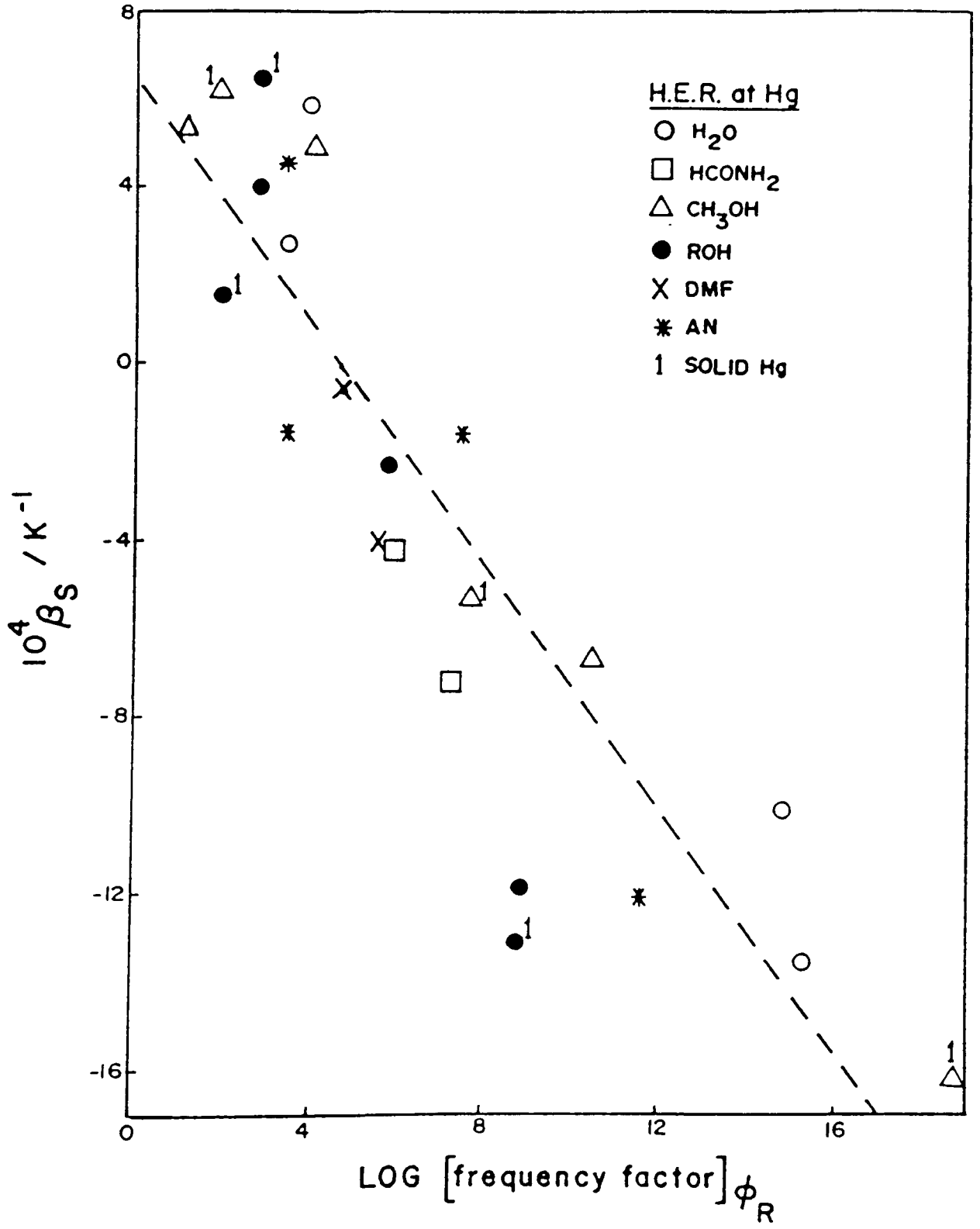

Fig 66 Plot of β_S versus log [frequency factor]$_\phi$ (proportional to $\Delta\bar{S}^{\ddagger}_{\phi}$) for the h.e r at Hg from different proton

at Hg (77), where $\Delta\bar{S}^{\ddagger}_{\phi}$ quantities are independent of potential but are ligand sensitive. In the present study, results for the h.e.r. from 0.1M $Et_3NHCF_3SO_3$ in DMF come closest to achieving the $\beta_S = 0$ condition, i.e., $\beta_S = -0.36 \times 10^{-4} K^{-1}$ (or $T\beta_S$ at 298 K = -0.01).

When the kinetic data are divided into groups involving a particular type of "active-bond" centre the correlation between β_S and log A_ϕ (or $\Delta\bar{S}^{\ddagger}_{\phi}$) is much better (see Fig. 67). For the "O-H^+" active-bond centre a linear relation is found:

$$\beta_S = -2.7 \times 10^{-4} \log A_\phi + 12.4 \times 10^{-4} \quad [92]$$
$$= 1.41 \times 10^{-5} \Delta\bar{S}^{\ddagger}_{\phi} - 2.56 \times 10^{-3}$$

with a correlation coefficient of 0.93 and for $\beta_S = 0$, $\Delta\bar{S}^{\ddagger}_{\phi}$ = 182 J mole $^{1}K^{-1}$. For the "N-H^+" active-bond centre a linear relation is also found:

$$\beta_S = -1.1 \times 10^{-4} \log A_\phi + 4.3 \times 10^{-4} \quad [93]$$
$$= 5.74 \times 10^{-6} \Delta\bar{S}^{\ddagger}_{\phi} \quad 1.12 \times 10^{-3}$$

with a correlation coefficient of 0.94 and for $\beta_S = 0$, $\Delta\bar{S}^{\ddagger}_{\phi}$ = 195 J mole $^{1}K^{-1}$.

A plot of β_H versus $\Delta\bar{H}^{\ddagger}_{\phi}$ for the h e r at solid and liquid Hg from the data acquired for the systems studied here is shown in Fig. 68 and an approximate linear relation is found:

$$\beta_H = 4.4 \times 10^{-3} \Delta\bar{H}^{\ddagger}_{\phi} + 0.07 \quad [94]$$

with a poor correlation coefficient of 0 78. No example of a system for the h.e.r. at Hg was found in the present work for which $\beta_H = 0$, i e , an entirely entropy-controlled reaction. At $\beta_H = 0$ in eqn [94], the "chemical" enthalpy of activation

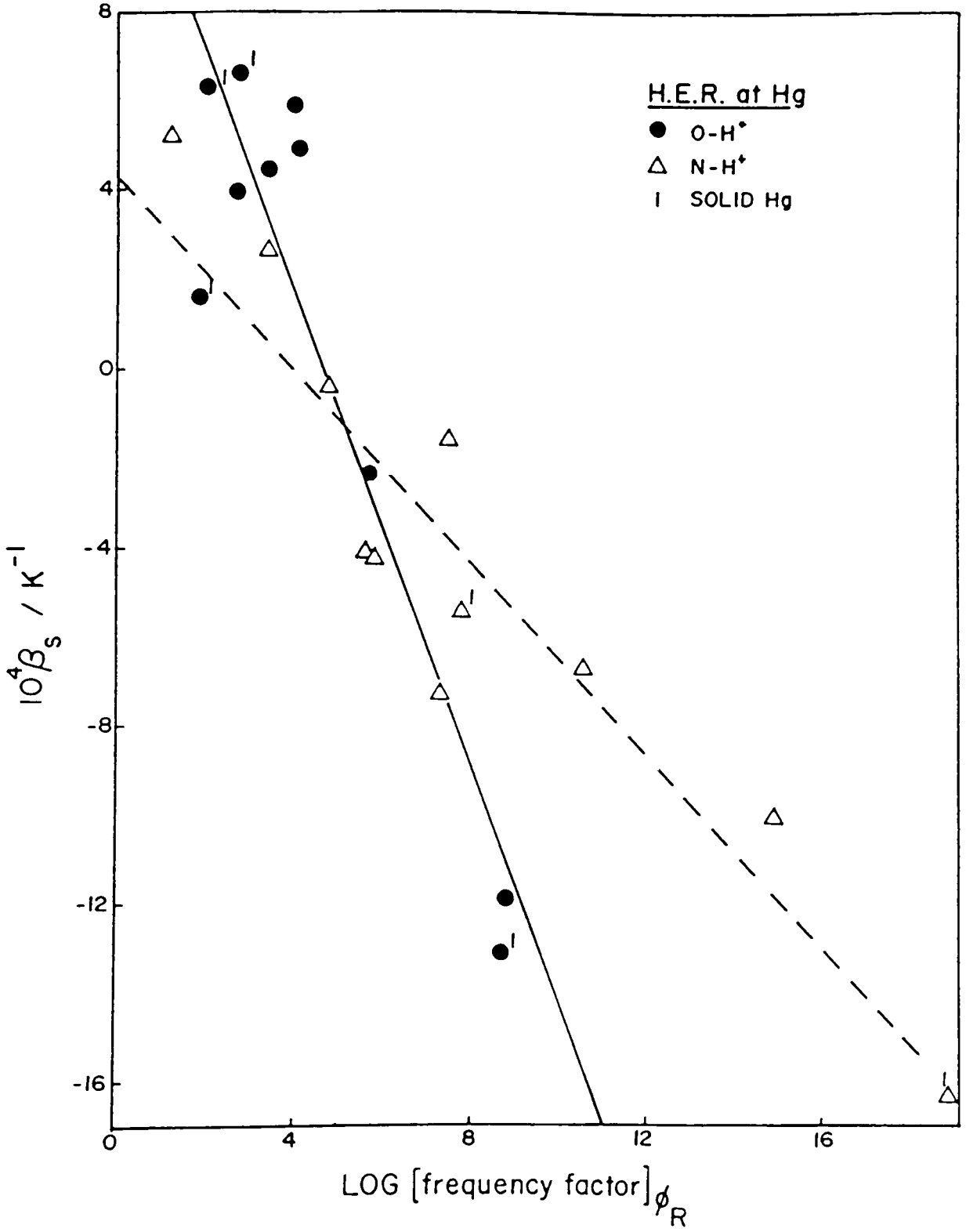

Fig. 67 Plot of β_S versus log [frequency factor]$_\phi$ (proportional to $\Delta\bar{S}^{\ddagger}_{\phi}$) for the h.e r. at Hg from proton donors with the same active-bond centre in several solvents: O-H^+

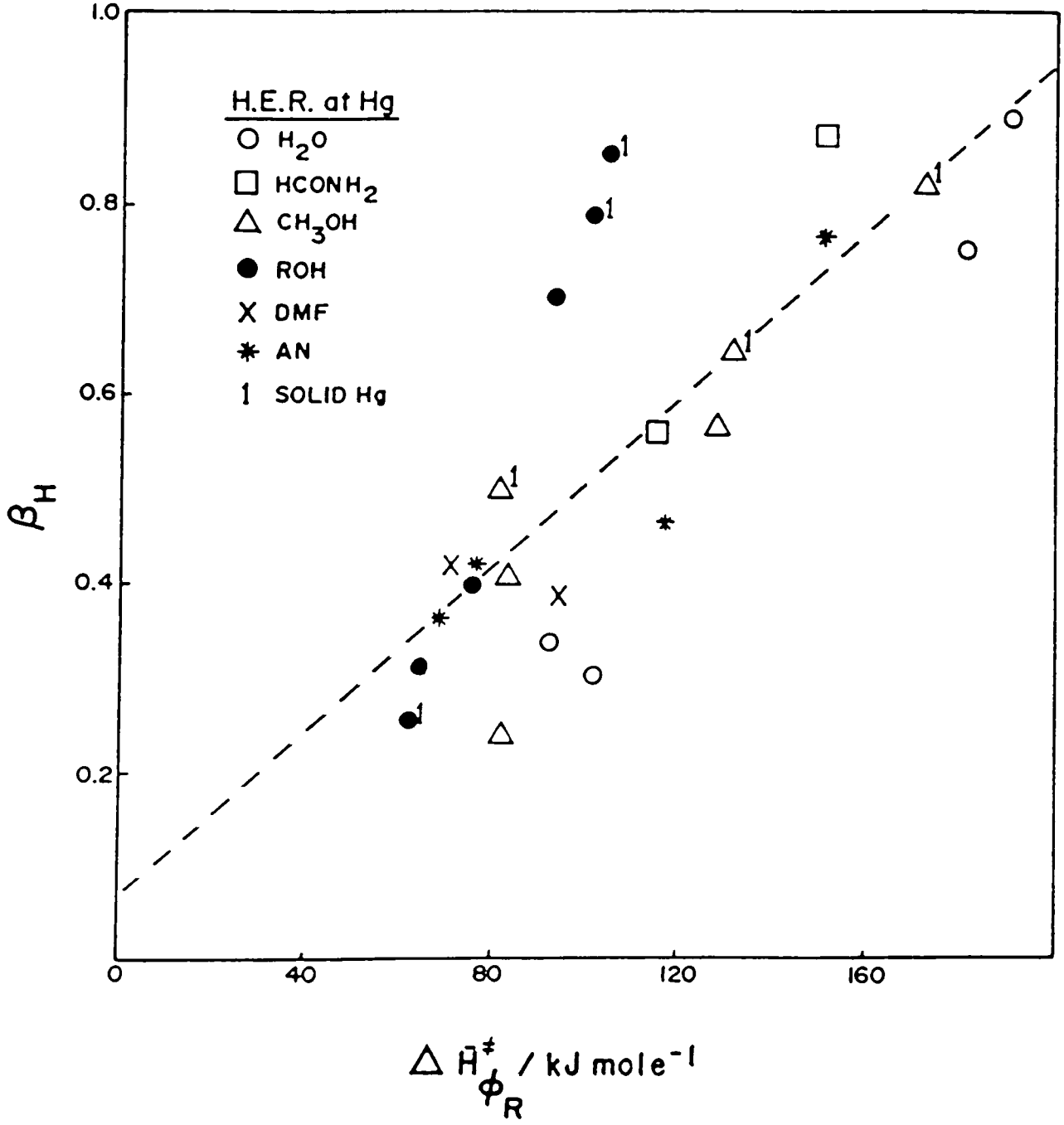

Fig. 68 Plot of β_H versus $\Delta\bar{H}^{\ddagger}_{\phi}$ for the h e r at Hg from different proton donors in several solvents.

unaffected by potential, would be $\Delta\bar{H}^{\ddagger}_{\phi}$ = 16 kJ mole^{-1}, i.e, such a system would have a negative enthalpy of activation which is very difficult to understand. However, when the kinetic data are divided into groups (oxonium and ammonium-type proton donors) involving a particular type of "active-bond" centre the correlation between β_H and $\Delta\bar{H}^{\ddagger}_{\phi}$ (Fig. 69) is substantially better and at $\beta_H = 0$, the "chemical" enthalpies of activation are then found to be positive as might be expected. For the "O-H$^+$" active-bond centre a linear relation is found:

$$\beta_H = 1.3 \times 10^{-2}\Delta\bar{H}^{\ddagger}_{\phi} \quad 0.54 \qquad [95]$$

with a correlation coefficient of 0.86 and for $\beta_H = 0$, $\Delta\bar{H}^{\ddagger}_{\phi}$ = +43.0 kJ mole^{-1}. For the "N-H$^+$" active-bond centre a linear relation is also found:

$$\beta_H = 5.2 \times 10^{-3}\Delta\bar{H}^{\ddagger}_{\phi} \; -0.09 \qquad [96]$$

with a correlation coefficient of 0.88 and for $\beta_H = 0$, $\Delta\bar{H}^{\ddagger}_{\phi}$ = $^{+}$17.1 kJ mole^{-1}.

The much better correlations found when proton sources with the same proton donor centre are treated as separate groups implies that the specific bond-type is important in the activation process The effect of bond-type on the entropy of activation, $\Delta\bar{S}^{\ddagger}_{\phi}$, and its potential-dependence, β_S, indicates specific bond effects are involved in the solvation of the reactant ion and transition state in the double-layer of the electrode interphase. Similarly, for the enthalpy of activation, $\Delta\bar{H}^{\ddagger}_{\phi}$, and its potential dependence, β_H, the above effects may also be important, but the major effect of bond-type

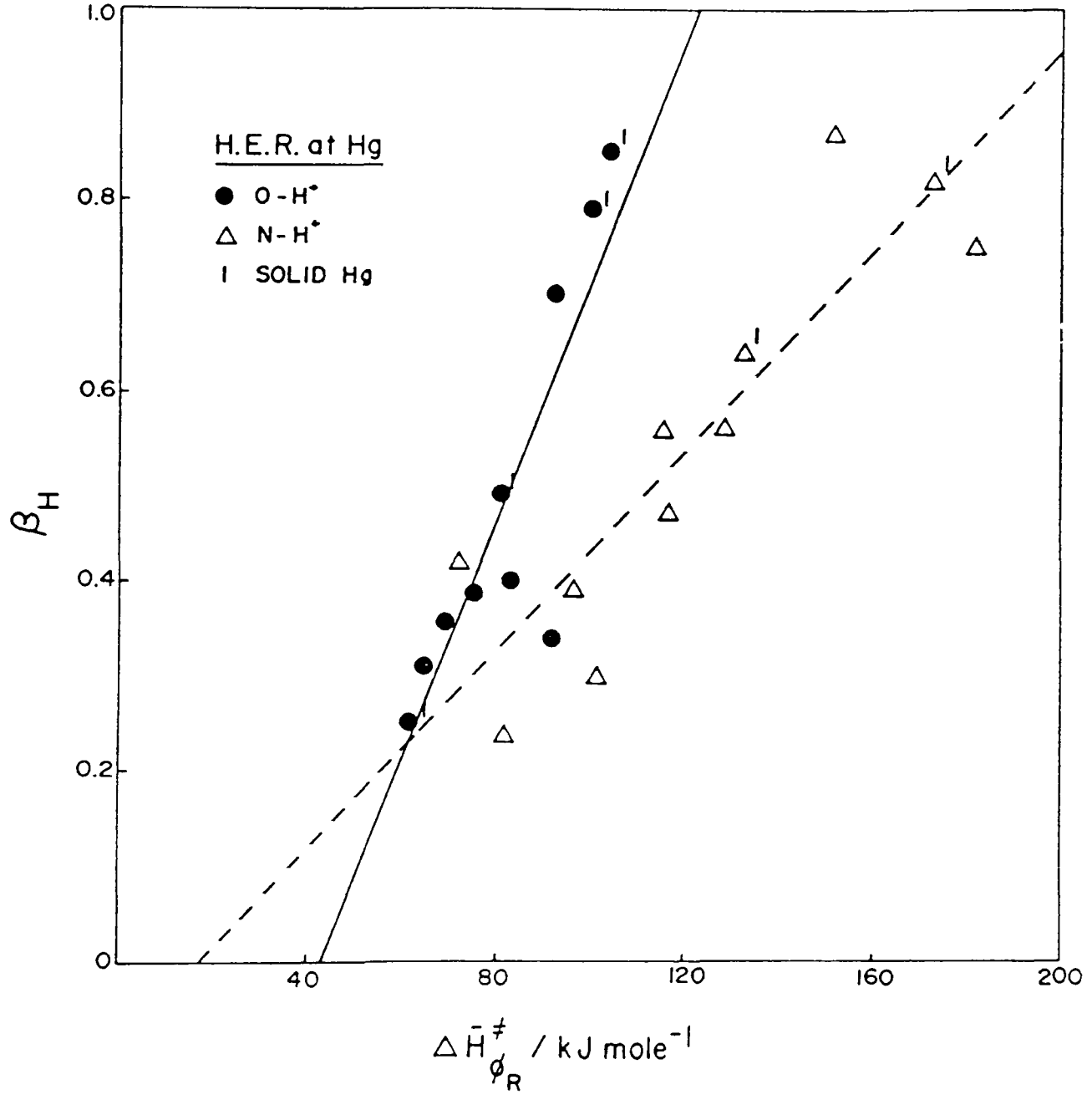

Fig 69 Plot of β_H versus $\Delta \bar{H}^{\neq}_{\phi}$ for the h.e r at Hg from proton donors with the same active bond centre in several solvents: O-H$^+$ (————); N-H$^+$ ( )

on the enthalpy parameters is probably due to different bond strengths, i.e., different force constants.

The observations of specificity of the correlation of kinetic parameters to the specific bond-type indicate that a more molecular picture of the activation process must be adopted, involving short-range effects rather than, or in addition to, long-range polarization effects (cf. the treatments of Dogonandze et al., section 5, chapter 1). A similar type of observation was made by Weaver et al. (77) for ionic redox reactions, where the entropy of activation was found to be both large and sensitive to the "ligand structure" around the metal ion.

10. Evaluation of the Entropy and Enthalpy of Activation when β is Temperature-Dependent

Generally, in the evaluation of "apparent" heats of activation and frequency factors, i.e., for constant overpotential, and those measured at a "fixed" metal-solution potential, ϕ_R, the temperature-dependence of β has been neglected. However, it is clear from eqns.[35], [37], [41] and [42] in chapter 4 that if β is a f(T), its temperature coefficient, $\partial\beta/\partial T$, must be taken into account in any evaluation of $\Delta H^{\ddagger}_{\phi=0}$ and $\Delta S^{\ddagger}_{\phi=0}$ from the experimentally determined heat of activation and frequency factor

Conway and MacKinnon (72,151) first examined the effect of a nonconventional Tafel relation on the apparent heat of activation ($\Delta H^{\ddagger}_{\phi=0} \pm \beta\Delta H_R$) evaluated at various overpotentials,

using the empirical relation that Conway et al. (132) used to represent $\beta(T)$, viz. $b = \pm 2.3RT/\beta' F + c$, where β' is a constant symmetry factor and c another constant.

The fundamentally more significant and general form of the Tafel relation $b = \pm 2.3RT/\beta F$, but with $\beta = \beta_H + \beta_S T$, which arises from the experimental potential-dependence of the enthalpy and entropy of activation is used here to examine the relation between $\Delta H^{\ddagger}_{\phi=o}$ and $\Delta S^{\ddagger}_{\phi=o}$ and the heats of activation and frequency factors measured at constant overpotential and at a fixed metal-solution potential difference, ϕ.

Case 1: Apparent Activation Parameters (Constant Overpotential)

Substitution of $\beta = \beta_H + \beta_S T$ into eqn.[35] gives

$$\Delta \bar{H}^{\ddagger}_{\eta} = \Delta H^{\ddagger}_{\phi=o} \pm \beta_H \Delta H_R \pm \beta_S T^2 \Delta S_R \mp \beta_H nF\eta \qquad [97]$$

Then for $\beta_H = 0$

$$\Delta \bar{H}^{\ddagger}_{\eta} = \Delta H^{\ddagger}_{\phi=o} \pm \beta_S T^2 \Delta S_R \qquad [98]$$

while for $\beta_S = 0$

$$\Delta \bar{H}^{\ddagger}_{\eta} = \Delta H^{\ddagger}_{\phi=o} \pm \beta_H \Delta H_R \mp \beta_H nF\eta \qquad [99]$$

Substitution of $\beta = \beta_H + \beta_S T$ into eqn.[37] gives

$$\ln A_{\eta} = \ln C + \frac{(\Delta S^{\ddagger}_{\phi=o} \pm \beta_H \Delta S_R)}{R} \pm \frac{\beta_S 2T\Delta S_R}{R} + \frac{\beta_S \Delta H_R}{R} \pm \frac{\beta_S nF\eta}{R} \qquad [100]$$

where $C = zFcf(\theta)\kappa kT/h$. Then for $\beta_H = 0$

$$\ln A_{\eta} = \ln C + \frac{\Delta S^{\ddagger}_{\phi=o}}{R} \pm \frac{\beta_S 2T\Delta S_R}{R} \mp \frac{\beta_S \Delta H_R}{R} \pm \frac{\beta_S nF\eta}{R} \qquad [101]$$

while for $\beta_S = 0$

$$\ln A_{\eta} = \ln C + \frac{(\Delta S^{\ddagger}_{\phi=o} \pm \beta_H \Delta S_R)}{R} \qquad [102]$$

Case 2: Activation Parameters Measured at Constant ϕ

Substitution of $\beta = \beta_H + \beta_S T$ into eqn.[41] gives

$$\Delta\bar{H}^{\ddagger}_{\phi} = \Delta H^{\ddagger}_{\phi=o} \mp \beta_H nF\phi \qquad [103]$$

Then for $\beta_H = 0$

$$\Delta\bar{H}^{\ddagger}_{\phi} = \Delta H^{\ddagger}_{\phi=o} \qquad [104]$$

But for $\beta_S = 0$, no simplification of eqn.[103] results.

Substitution of $\beta = \beta_H + \beta_S T$ into eqn.[42] gives

$$\ln A_{\phi} = \ln C + \frac{\Delta S^{\ddagger}_{\phi=o}}{R} \pm \frac{\beta_S nF\phi}{R} \qquad [105]$$

where $C = zFcf(\theta)\kappa\tilde{k}T/h$. Then for $\beta_S = 0$

$$\ln A_{\phi} = \ln C + \frac{\Delta S^{\ddagger}_{\phi=o}}{R} \qquad [106]$$

but for $\beta_H = 0$, no simplification of eqn.[105] results.

In the previous equations, the ΔH_R, ΔS_R and ϕ quantities refer to the reference electrode single half-cell reaction whereas the activation parameters β_H, β_S, $\Delta H^{\ddagger}_{\phi=o}$ and $\Delta S^{\ddagger}_{\phi=o}$ refer to the activation behaviour of the electrode reaction at the working electrode. This raises the subtle but important point that, for a given electrode reaction conducted under various defined conditions, β_H and β_S will probably be different for each experimental condition. For such a case, the difference of heats of activation and the ratio of frequency factors will not simply give the difference of "true" $\Delta H^{\ddagger}_{\phi=o}$ values and the ratio of "true" frequency factors, i.e., at ϕ=0, respectively, as is usually assumed. For example, for eqn [103] the difference of the measurable heats of activation at a fixed metal-solution potential ϕ for two systems (e.g., the same reaction in two media or for two proton sources in the same medium) gives

$$\Delta\bar{H}^{\ddagger}_{\phi}(2) \quad \Delta\bar{H}^{\ddagger}_{\phi}(1) = \Delta H^{\ddagger}_{\phi=0}(2) \quad \Delta H^{\ddagger}_{\phi=0}(1) \pm [\beta_H(1)-\beta_H(2)]nF\phi \qquad [10$$

for which the term $[\beta_H(1) \quad \beta_H(2)]nF\phi$ may be quite large Although the two β_H values can be obtained for each of the experimental conditions, the single metal-solution potential ϕ can only be estimated (see section C-12, this chapter).

When β=f(T), i.e., $\beta_S \neq 0$, the measurable apparent heat of activation will contain a T^2 term, as in eqns. [97] and [98], so that the electrochemical Arrhenius plots would have curvature which may be in either direction depending on the sign of β_S and ΔS_R. This curvature is not associated with such effects as proton tunneling, temperature-dependent solvent structure changes and solvent orientation at the electrode interface but arises from a non-zero β_S and the variation of the reference electrode potential with temperature when the reference electrode is at the same, but varied, temperature as the working electrode (constant η conditions).

The apparent heat of activation in eqn.[98] for the limiting case of $\beta(T) = \beta_S T$, i.e., β_H=0, has been examined by Conway (128) with regard to the evaluation of the true enthalpy of activation, $\Delta H^{\ddagger}_{\phi=0}$. For this case and for the evaluation of the true entropy of activation, $\Delta S^{\ddagger}_{\phi=0}$ from the logarithm of the apparent frequency factor of eqn.[102] for the limiting case of $\beta = \beta_H$, it is seen that only the overall entropy, ΔS_R, of the reference half-cell reaction is required. As discussed in section 3, chapter 5, ΔS_R for a half-cell reaction can be estimated much more reliably (i e , to within $\pm$ 4 0 J K^{-1}mole ^{1})

than the corresponding ΔH_R, so that $\Delta H^{\ddagger}_{\phi=o}$ and $\Delta S^{\ddagger}_{\phi=o}$ for the above cases can evidently be reliably determined.

For the activation parameters measured at constant metal solution potential-difference, as in the work reported here, simpler expressions involving $\Delta H^{\ddagger}_{\phi=o}$ and $\Delta S^{\ddagger}_{\phi=o}$ are obtained than for the apparent activation parameters. The heat of activation, $\Delta \bar{H}^{\ddagger}_{\phi}$, of eqn.[104] for the limiting case of $\beta(T) = \beta_S T$, i.e., $\beta_H = 0$, gives $\Delta H^{\ddagger}_{\phi=o}$ directly while the logarithm of the frequency factor, log A_ϕ of eqn.[106] for the limiting case of $\beta = \beta_H$, i.e., $\beta_S = 0$, gives $\Delta S^{\ddagger}_{\phi=o}$ directly.

Thus, under certain conditions (i.e., eqns.[98], [102], [104] and [106]) the "true" enthalpy and entropy of activation at zero metal-solution potential-difference can be determined from experimental measurements to a much greater level of reliability than has hitherto been commonly supposed.

11. Effects of Potential on Molecular Bond Energy and Configuration

Some fraction, β_H, of the applied potential, ϕ, can be considered to modify the enthalpy of activation for the electrode reaction, through a change of ϕF in the Fermi level of the electrons in the metal. This direct effect of potential on the Fermi level of electrons has been observed in the red shift of the voltage threshold for photoelectron emission into solution by Heyrovsky and Norrish (152) for Hg under cathodic polarization.

In addition to the direct effect of potential on the Fermi level, it is important to know to what extent the chemical bond energy (e.g., for H chemisorbed on an electrode metal or the solvation energy of the reacting ion) is dependent on the local electrode field in which the bond is situated. An estimate of this effect can be made from polarizability data for polar diatomic molecules involving H given by Moelwyn-Hughes (153). The polarization energy of an "M-H" bond in the double-layer in a field of 10^5 e.s.u. which corresponds approximately to a rational potential of 1 V at Hg, will be only 0.09 kJ mole ^{1} for HF with $\alpha_p = 0.30 \times 10^{-24}$ cm^3 and 0.52 kJ mole ^{1} for HCl with $\alpha_p = 1.74 \times 10^{-24}$ cm^3. This negligible effect corresponds with recent observations from <u>in situ</u> infrared studies that chemisorption bond vibrational frequencies, e.g., for CO on Pt(154,155), vary with potential only by about 10 $cm^{-1}V^{-1}$, i.e., 0 1 kJ mole $^1V^{-1}$.

The electronegativity, χ, of a metal, M, will tend to become smaller with increasing cathodic potential and the resultant increase in electrode surface charge For example, a charge density of 20 μC cm^{-2} corresponds to a change of about 0 1 in electron density per atom on the surface relative to the situation at the p.z.c. The change of the electronegativity of a metal with potential should only have a small effect on the M-H bond energy because the $(\chi_M \quad \chi_H)^2$ term in the Eley-Pauling relation (156) for chemisorption bonds itself constitutes only about 10% of the total bond energy Thus, it is unlikely that

direct potential or field effects on the chemical bond energy will be significant compared to the direct effect of potential on the Fermi level of the reacting electrons.

However, the effect of electrode potential on the solvent structure in the double-layer of the electrode interphase may have an appreciable indirect effect on the chemical bond energy. This external effect of potential on the enthalpy of activation in addition to the internal effect of potential on the Fermi level of electrons in the metal

$$\beta_H = (\Delta\bar{H}^{\ddagger}_{\phi}/Fd\phi)_{total} = (d\Delta\bar{H}^{\ddagger}_{\phi}/Fd\phi)_{internal} + (d\Delta\bar{H}^{\ddagger}_{\phi}/Fd\phi)_{external} \quad [108]$$

may account for the variation of β_H for different systems (e.g., see Table 14). The effect of potential on the Fermi level must always be present (cf. the photoelectron emission result of Heyrovsky and Norrish) so that when $\beta_H \approx 0$, the external effect must be opposite to this internal effect.

12. Models for the Potential-Dependence of $\Delta\bar{S}^{\ddagger}_{\phi}$

The location of the proton in the act of discharge is probably in or near the inner solvent layer (19,23) so that the local orientation of neighboring solvent molecules might be expected to influence the discharge kinetics, especially through the entropy of activation since it is closely associated with a changing state of solvation in formation of the transition state. Entropy effects will be largest for those electrode reactions involving a change of state of H-bonding and/or complete elimination or creation of charge, e g., as in the

h.e.r. The large effect of potential on $\Delta\bar{S}^{\ddagger}_{\phi}$ for the h.e.r. and b.e.r. is therefore most likely due to the potential-dependence of the local solvent structure environment of the reactant ion (initial state) and the transition state complex in the interphase. However, it is very difficult, even qualitatively, to predict how such effects would differently affect the entropy of the transition state, $S^{\ddagger}$, in relation to the entropy of the initial state, S_i, i.e., $\Delta\bar{S}^{\ddagger}_{\phi} = S^{\ddagger} \quad S_i$.

a) Effect of Potential on Solvent Dipole Orientation

One of the most useful theories of changing solvent polarization in the double-layer with electrode potential has been that of Mott and Watts-Tobin (157), and its further development by Bockris, Devanathan and Muller (158) in their treatment of double-layer capacitance, i.e., the BDM "two-state" model. This model treats solvent dipoles in terms of two states of orientation, parallel and antiparallel to the electrode field, i.e., ↑ or ↓. The net orientation of dipoles is given by

$$\frac{N\uparrow - N\downarrow}{N_T} = \tanh\left[(-Uc/\tilde{k}T)(N\uparrow \quad N\downarrow)/N_T + \mu E/\tilde{k}T\right] \qquad [109]$$

while the dipole polarization, expressed as a surface potential contribution, χ_d, is given by

$$\chi_d = (4\pi\mu N_T/\epsilon_s)\ (N\uparrow \quad N\downarrow)/N_T \qquad [110]$$

where N_T is the total number of dipoles per cm^2 ($N_T = 10^{15}$ water dipoles cm^{-2}); U is the lateral dipole-dipole interaction energy (3-4 kcal mole ^{1} for -OH dipoles); c is half of the two-dimensional effective coordination number for the solvent; μ is

the solvent dipole moment; E is the field; and ϵ_s is the dielectric constant in the interphase which will be smaller than in the bulk because of dielectric saturation (for H_2O, $\epsilon_s = 6$ whereas $\epsilon = 78$ in the bulk). More recently, the BDM model has been modified to account for three states of dipole orientation, flat (→←), as well as up (↑) and down (↓), (159), and clusters of dipoles (160).

Conway, MacKinnon and Tilak (132) examined the effect of potential and temperature-dependent solvent dipole orientation on the entropy of activation of electrode processes in terms of the BDM two-state model. Normally, over the experimentally accessible range of surface charge density, q_m (20 to 20 μC cm ^{2}), χ_d will be much less than the orientational saturation value of ca. ± 1.2 V, but it can constitute an appreciable fraction of the metal-solution potential difference. The temperature-dependence of χ_d is determined by the magnitude of the lateral interactions between solvent molecules in the double-layer; thus, for small values of U, χ_d decreases with increasing T but for large values of U, χ_d increases with increasing T.

Solvent dipole orientation in the double-layer field is known to be temperature-, and potential-dependent in a correlated way (158, 161). For example, the volume fractions of oriented water dipoles and hydrated protons in the double-layer can be shown to be of comparable magnitude and both are dependent on electrode potential (158). Hence, these results

show how the solvent environment of a discharging ion in the interphase can be substantially modified by surface charge (or electrode potential) and temperature. Elsewhere, Conway et al (162,163) have shown that the decrease of librational entropy of oriented solvent dipoles in the double-layer with increasing electrode potential can be appreciable, especially at lower temperatures where this effect can be greater. The surface dipole potential, χ_d (and the orientation distribution function) varies approximately linearly with electrode potential and changes of librational entropy of oriented solvent molecules, so that the entropy of activation might be expected to vary in a linear way with electrode potential. Thus, it can be seen, at least qualitatively, how the effect of potential on solvent dipole orientation in the interphase can result in a potential effect on the entropy of activation.

b) Energy and Entropy Change along a Reaction Coordinate

For homogeneous reactions, the entropy and configuration of the transition state is considered to be intermediate between the entropy and configuration of the initial and final states. Hence, for a series of similar reactions, the initial state entropy, S_i, and final state entropy, S_f, will be approximately constant and the transition state entropy will move along a reaction coordinate connecting them, as ΔG_R for the reaction changes. As ΔG_R becomes more negative, the transition state "crossing region" becomes nearer to the initial state

configuration and the entropy of the transition state is considered to become increasingly similar to that of the initial state.

A similar model could be applied to heterogeneous electrode reactions in which the Gibbs energy is changed by applied potential (analogous to changing the pK's of reactants in the homogeneous case) and the entropy of activation is found to be potential-dependent, e.g., as found for the h.e.r. Such an effect of potential on the entropy of activation is illustrated schematically in Fig. 70, where $S_f > S_i$, and potential-dependent double-layer effects, e.g., solvent dipole orientation, are not considered.

It is reasonable to take $S_f > S_i$, because in electrode reactions involving extinction of charge, the entropy change is considered to be dominated by electrostrictive factors and hence positive. For example, the half-cell reaction entropies of the hydrogen reference electrode (i.e., $H^+ + e \rightarrow 1/2\ H_2$) in several solvents are positive (see Table 9, section A-3). By analogy with the homogeneous case, this simple model predicts a decrease in $\Delta\bar{S}^{\ddagger}_{\phi}$ with increasing potential, i.e., β_S is negative. However, some cases are observed where $\Delta\bar{S}^{\ddagger}_{\phi}$ increases with increasing potential, i.e., β_S is positive, and this is probably because of potential-dependent double-layer effects which affect S_i and $S^{\ddagger}$ to different extents.

c) Potential-Dependent Double-Layer Effects on S_i and $S^{\ddagger}$

A simple qualitative account of potential-dependent double-

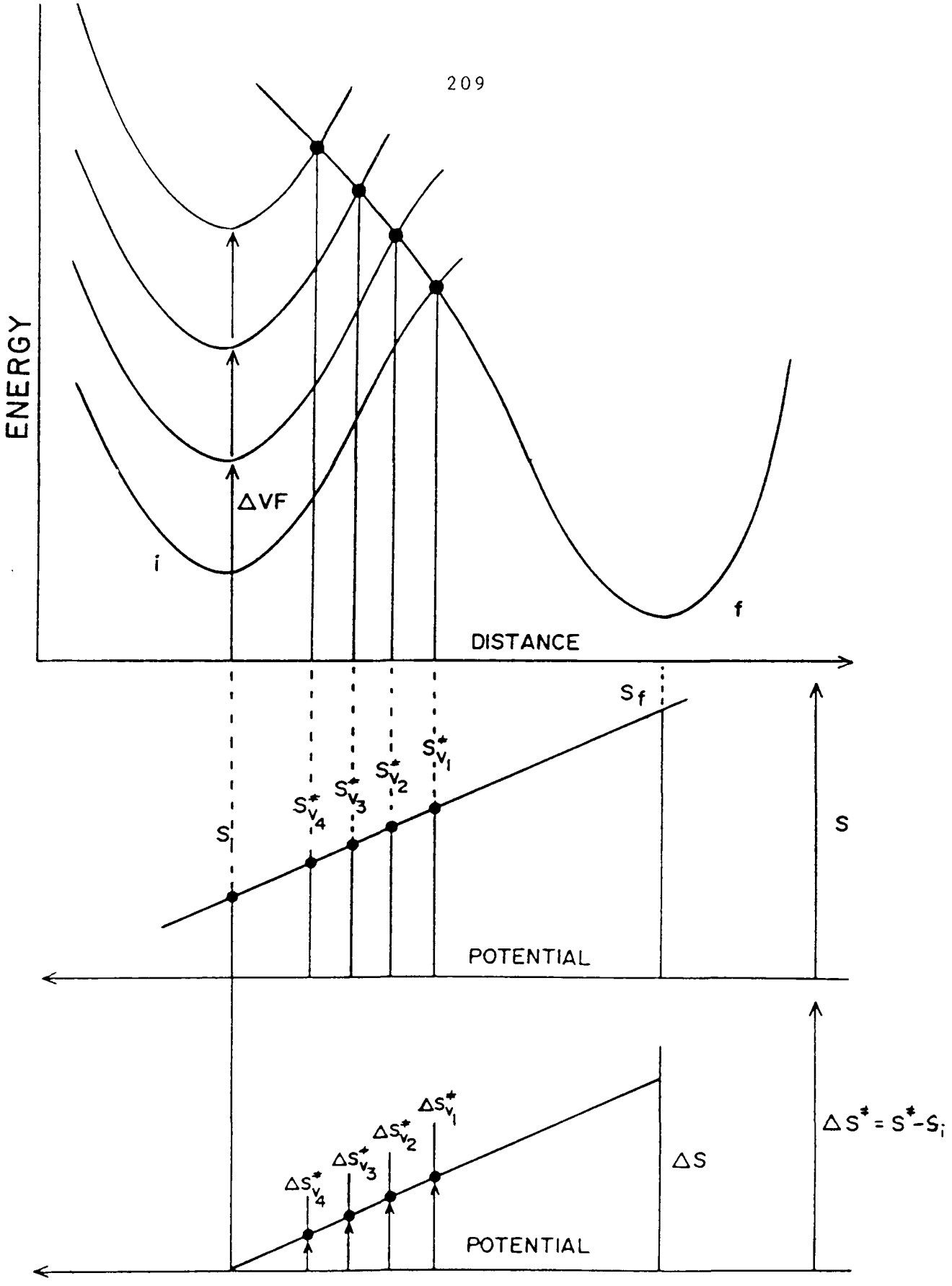

Fig 70 Model of the effect of applied potential on the energy and entropy of activation in an heterogeneous electrode reaction.

layer effects on S_i and $S^{\ddagger}$ can be given by the state of interaction of an ion being discharged with polarized solvent dipoles in the double layer. Near the potential of zero charge at Hg or at the potential (or charge) for zero solvent dipole orientation (e.g., for H_2O at Hg, $q \approx 2\ \mu C\ cm^{-2}$) reactant ions in the double-layer can experience maximum electrostatic interaction with the surrounding medium adjacent to the electrode and hence acquire minimum entropy of solvation. Dipole polarization in the inner region of the double-layer will increase with increasing electrode potential (158,164), and the entropy of solvation of ions in the double-layer will tend to become more positive because part of their solvation co-spheres will already be polarized by the electrode field (see Fig. 71). The partially charged transition state will be affected in the same way as reactant ions in the double-layer, but to a lesser extent because it is usually considered to be less charged. In this way such a differential effect on S_i and $S^{\ddagger}$ might be expected to decrease $\Delta\bar{S}^{\ddagger}_{\phi}$ with increasing potential.

It is of interest that the only systems studied here which show an increase of $\Delta\bar{S}^{\ddagger}_{\phi}$ with increasing potential, i.e , β_S positive, were ones which involve hydrogen-bonded solvents, i.e., H_2O, methanol and 1-propanol to a lesser extent Although simple models predict a decrease of $\Delta\bar{S}^{\ddagger}_{\phi}$ with increasing potential, i e., β_S negative, it is obvious that for more structured solvents other specific effects would have to be included to account for their behaviour.

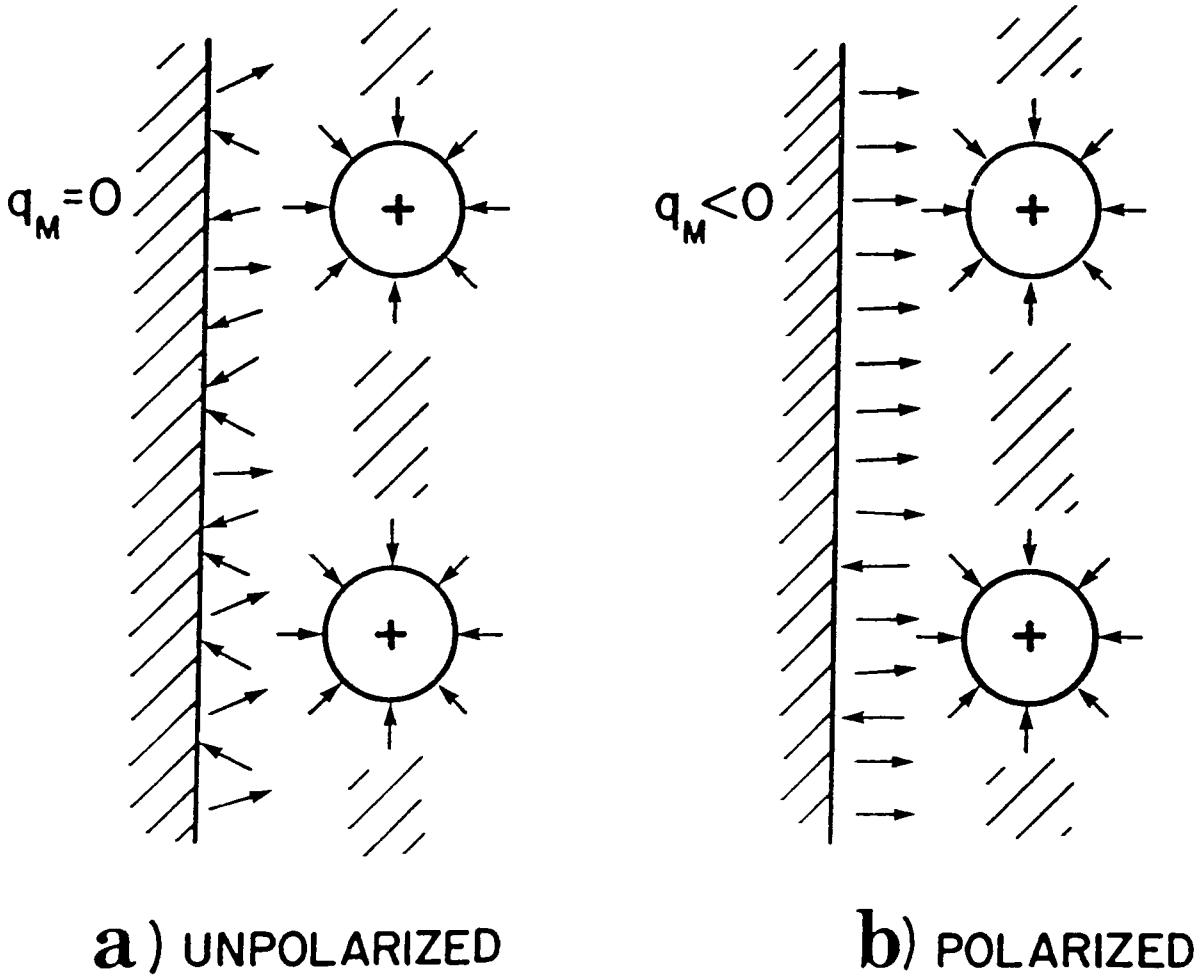

Fig 71 Model of the effect of applied potential on solvent dielectric polarization at an electrode surface

C. The Effect of Proton Source and its Environment on the Kinetic Behaviour of Electrochemical Proton Discharge

1. Introduction

The electrochemical hydrogen evolution reaction is regarded as a useful model for the kinetic study of simple and other complex multistep electrode reactions (1,2), especially at Hg where it can be studied without the complication of any significant potential-dependent coverage of the electrode by adsorbed H. The mechanism of the activation process in such a coupled atom/electron transfer process is still not understood well, despite many papers on h.e.r. kinetics published in earlier years. A comparison of the free energy of activation, and its enthalpic and entropic components for the h.e.r from different proton sources in various solvent media, should therefore lead to an improved understanding of the nature of activation and the medium effect in the elementary act of coupled electron and atom transfer.

It is useful to interpret the electrochemical kinetics of proton discharge (19) and the homogeneous kinetics of proton transfer (22,42) in terms of potential energy diagrams that represent the energy course of the reaction, as discussed in chapter 1. Changes in proton donor or solvent for electrochemical proton discharge at constant metal solution potential, ϕ, can be considered to be exactly analogous to changes in acid or base strength in homogeneous proton transfer processes. In the electrochemical case, the metal-solution

potential, ϕ, can be considered to affect the Fermi energy level of the electrons in the metal (in the usually assumed way) and, in some cases also the entropy of activation as observed in the present work (section B); however, the shape of the potential energy profile of the proton donor will not change appreciably over a wide range of potential, i.e., for the h.e.r. at Hg, β has been found to be constant over 1.2 V (28).

The symmetry factor β and the Brϕnsted coefficient α have been associated with the relative slopes of the reactant and product energy profiles (9,19) at their region of intersection, i.e., where the activated or transition state arises, and therefore will reflect any changes in their shape in that region.

A change of solvent is usually considered to change the initial state energy of the proton donor by the change in solvation energy, $\pm\Delta G_s$, and to change indirectly the energy of the transition state by $\pm$ $(1-\beta)\Delta G_s$, to give a change of energy of activation of $\mp$ $\beta\Delta G_s$ (See Fig. 8) In recent studies of medium effects (113, 114) the energy of the activated complex has been considered not to change with solvent, so that in this case a change of energy of activation of $\pm$ ΔG_s would result. Although this assumption is said (113) to involve less error than those caused through experimental errors and extrathermodynamic assumptions in the study of medium effects, it is highly unlikely , if only for electrostatic reasons (cf ref. 103), that a polar transition state will not be affected by

change of solvent

For a change of proton donor in the same solvent, there will be a change both of solvation energy and bond-strength to the H which will result in a shift of the initial state energy of the reference proton donor, and probably a different energy surface or potential energy profile. In practice, for changes of proton donor or solvent, changes in the energy of the transition state can occur other than those predicted by Brønsted effects based on shifting the same initial state energy curve up or down. A more detailed model of the transition state, which includes coordination by solvent molecules, its geometry in relation to the initial state, any specific interactions of the transition complex with oriented solvent dipoles and other ions in the double-layer, would be required to give a more realistic model of the change in activation energy resulting from a change in proton donor or solvent.

2 The Problem of Comparing Measurements at "Constant Overpotential"

In general, most electrochemical measurements are compared at constant overpotential or current density, using a reference electrode reversible to the reaction being studied. In this case, the solvation energy and the bond energy of the proton donor are also involved in the thermodynamic energy cycle which determines the equilibrium Gibbs energy of the reference electrode half-cell reaction (cf. energy cycle of page 107)

Hence, a change in activation energy due to a change in energy of the initial state, i.e., for a change of proton donor or solvent, will be partially or completely compensated for by a corresponding change in the reference electrode metal-solution potential difference, so that the electrochemical Gibbs energy of activation will remain approximately constant. For example, for a particular reference system (1) i.e., proton donor and solvent, the electrochemical Gibbs energy of activation at constant overpotential will be given by

$$\Delta\bar{G}^{\ddagger}_{\eta}(1) =$$

$$\Delta G^{\ddagger}_{\phi=o}(1) \mp \beta(1)\phi_R(1)nF \mp \beta(1)nF\eta = \Delta G^{\ddagger}_{\phi=o}(1) \pm \beta(1)\Delta G_R(1) \mp \beta(1)nF\eta \quad [111]$$

so that for a change of energy of the initial state of $\pm \Delta G_t$ and a corresponding change of energy of the transition state of $\pm(1-\beta)\Delta G_t$, the electrochemical Gibbs energy of activation for the new system (2) at constant overpotential will be given by

$$\Delta\bar{G}^{\ddagger}_{\eta}(2) = \Delta G^{\ddagger}_{\phi=o}(2) \pm \beta(2)\Delta G_R(2) \mp \beta(2)nF\eta$$

$$= \Delta G^{\ddagger}_{\phi=o}(1) \mp \beta(2)\Delta G_t \pm \beta(2)(\Delta G_R(1) \mp \Delta G_t) \mp \beta(2)nF\eta \quad [112]$$

so that the difference in the electrochemical Gibbs energy of activation will now be given by

$$\Delta\bar{G}^{\ddagger}_{\eta}(2) \quad \Delta\bar{G}^{\ddagger}_{\eta}(1) = \pm [\beta(2)-\beta(1)]\Delta G_R(1) \mp [\beta(2)-\beta(1)]nF\eta \quad [113]$$

If the shape of the potential energy profile of the initial state remains approximately constant for the system, i.e., $\beta(1) \approx \beta(2)$, then no effect on the electrochemical Gibbs energy of activation will be observed for the second, relative to the first system, i.e., $\Delta\bar{G}^{\ddagger}_{\eta}(2) - \Delta\bar{G}^{\ddagger}_{\eta}(1) \approx 0$. However, changes in

shape of the potential energy profile usually occur, especially for changes in proton donor (D) where a change of D-H bond strength and associated force constant are involved. For these cases, β can vary significantly (see Table 14) just as the exactly analogous Brønsted α factor has been found to vary appreciably over a range of $\Delta \log K$ for a number of systems (5), and this will result in a non-zero value of the Gibbs energy difference in eqn.[113].

Hickling and Salt (165) in an early paper made the first comprehensive investigation of the effect of solvent on hydrogen overpotential for different metals in solutions of HCl in H_2O, ethylene glycol, ethanol and cyclohexanol. They found, in general, that the shapes, slopes and positions of the overvoltage-log [current density] plots for the nonaqueous solvents were not substantially different from those for aqueous solutions and concluded that the environment of the hydrogen ion is not a primary factor in hydrogen overvoltage. Bockris et al (166,167) studied the steady-state current vs hydrogen overpotential behaviour of the h.e.r at various metals in HCl solutions of H_2O, methanol, ethanol, ethylene glycol, acetic and formic acids, diethyl ether and dioxane, and their solvent mixtures with H_2O. Although the solvation effects were complex and, in the solvent mixtures, reflected the selective solvation of the proton, they concluded that the properties of the solvent have a considerable effect on the hydrogen overpotential at high current densities. More recently, Krishtalik (168) has shown

that hydrogen overpotentials in a number of nonaqueous solvents differ very little, and that no simple quantitative relation exists between these values and the corresponding proton solvation energies in these media.

All the previous investigations of solvent effects were made using a reversible hydrogen reference electrode in the system under study, so that the results of these works can be explained qualitatively in terms of eqn.[113]

If the shape of the potential energy profile of the initial state remains approximately constant with changing solvent, i.e., $\beta \approx$ constant, then the change in activation energy will be exactly compensated for by the change in the metal-solution potential, so that no net primary effect is observed, e.g., as in Krishtalik's work. For changes in the shape of the potential energy profile of the initial state, i.e., $\beta \neq$ constant, a solvent effect <u>will</u> be observed which increases with increasing overpotential or current-density

3 <u>Comparison of "Constant Potential" Measurements</u>

In the present work, the rates and kinetic parameters for proton discharge from different proton donors and solvents were compared at the constant metal-solution potential ϕ_R of the reference electrode $Pt|H_2$, 0.1M $HCl(H_2O)$ In this case, for a particular reference system (1), i.e., proton donor and solvent, the electrochemical Gibbs energy of activation is given by

$$\Delta\bar{G}^{\ddagger}_{\phi}(1) = \Delta G^{\ddagger}_{\phi=0}(1) \mp \beta(1)\phi nF \qquad [114]$$

so that for a change of energy of the initial state by $\pm\Delta G_t$ and

a corresponding change of energy of the transition state by $\pm(1-\beta)\Delta G_t$, the electrochemical Gibbs energy of activation for the new system (2) will be given by

$$\Delta\bar{G}^{\ddagger}_{\phi}(2) = \Delta G^{\ddagger}_{\phi=o}(2) \mp \beta(2)\phi nF = \Delta G^{\ddagger}_{\phi=o}(1) \mp \beta(2)\Delta G_t \mp \beta(2)\phi nF \quad [115]$$

Then the difference in the electrochemical Gibbs energy of activation will be given for this case by

$$\Delta\bar{G}^{\ddagger}_{\phi}(2) \quad \Delta\bar{G}^{\ddagger}_{\phi}(1) = \mp\beta(2)\Delta G_t \mp [\beta(2)-\beta(1)]\phi nF \quad [116]$$

which will reflect any changes in the initial state energy, i.e., solvational state and D-H bond strength.

The corresponding relations for the differences of the enthalpic and entropic components of the electrochemical Gibbs energy of activation are given by

$$\Delta\bar{H}^{\ddagger}_{\phi}(2) \quad \Delta\bar{H}^{\ddagger}_{\phi}(1) = \mp\beta_H(2)\Delta H_t \mp [\beta_H(2) - \beta_H(1)]\phi nF \quad [117]$$

$$\Delta\bar{S}^{\ddagger}_{\phi}(2) - \Delta\bar{S}^{\ddagger}_{\phi}(1) = \mp\beta_S(2)\Delta S_t \mp [\beta_S(1) - \beta_S(2)]\phi nF \quad [118]$$

where ΔH_t and ΔS_t are the respective enthalpy and entropy changes of the initial state for a change of proton donor or solvent. If the transition state energy had been assumed not to change, i.e. $\Delta\bar{G}^{\ddagger}_t = 0$, then similar relations would result, except the ΔG_t, ΔH_t, and ΔS_t quantities would not be multiplied by their respective "β" factors. Of course, any experimental evaluation of eqn.[116], eqn.[117] and eqn.[118] will involve differences in double-layer effects (see section C-5), and possible junction potential effects which are considered to be minimized in the present work by use of the experimental procedures described in section A, this chapter.

4 Experimental Results

The kinetic parameters ($\Delta\bar{H}^{\ddagger}_{\phi}$, $\Delta\bar{S}^{\ddagger}_{\phi}$, $\Delta\bar{G}^{\ddagger}_{\phi}$, log A_{ϕ} and i_{ϕ}) determined at the metal solution potential, ϕ_R, of the reference electrode, Pt|H_2, 0.1M HCl (H_2O) at 298K, are shown in Tables 17 and 18 for the h.e.r. on liquid and solid Hg, respectively. The kinetic parameters for liquid Hg are illustrated comparatively in solvent groups, in the histograms of Figs. 72 to 75. Although different kinetic behaviour was found on liquid and solid Hg, no curvature was found in the low temperature (down to ca. 185 K) Arrhenius plots of log i_{ϕ} versus T^{-1}, indicating the absence of significant proton tunneling in the h.e.r. This is consistent with the low temperature studies (down to ca. 163 K) of Conway and Salomon (37,38,169) on the h.e.r. and d.e.r. on Hg, from HCl|CH_3OH and DCl|CH_3OD, respectively, which did not show any of the characteristics indicative of significant proton tunneling, and for which isotope effects could be explained satisfactorily from a consideration of zero-point energy difference effects.

The data for the b.e.r from 0 4M (n Pr)$_4$NBr, 0.2M Br_2 in AN at vitreous carbon are also included in Table 17 in order to provide comparative information on an anodic atom/electron transfer reaction. The kinetic parameters for this system were determined at the metal-solution potential, ϕ_R, of the reference electrode, C|Br_2, 0.4M (n-Pr)$_4$NBr, 0 2M Br_2 (AN) at 298 K (reversible reaction $1/2Br_2 + e = Br^-$), so that the results are, of course, on a different potential scale from that for the

TABLE 17

Kinetic Parameters* at Constant ϕ for the H.E.R. at Liquid Hg, from Different Proton Donors in Several Solvents

Proton Donor	Solvent	$\Delta\bar{H}^{\ddagger}_{\phi}$ kJmole^{-1}	**$\Delta\bar{S}^{\ddagger}_{\phi}$ JK^{-1}mole^{-1}	***$\Delta\bar{G}^{\ddagger}_{\phi}$ (298 K) kJmole^{-1}	log [A]$_{\phi}$ A in Acm^{-2}	i_{ϕ} (298K) Acm^{-2}	pK_d (298K)
H_3O^+	H_2O	91.2	-202	151.4	3.9	9.1×10^{-13}	-1.74[b]
$EtNH_3^+$	H_2O	181.5	+ 15	177.0	14.9	1.1×10^{-17}	10.63[b]
Et_3NH^+	H_2O	101.3	-203	161.8	3.4	4.9×10^{-15}	10.87[b]
H_2O	H_2O	190.5	+ 24	183.3	15.3	$9\ 4\times10^{-19}$	14.00[b]
$EtNH_3^+$	$HCONH_2$	150.8	-130	189.5	7.3	7.0×10^{-20}	≈10.41(i)
Et_3NH^+	$HCONH_2$	114.3	-158	161.4	5.8	6.1×10^{-15}	9.99[c]
$EtNH_3^+$	CH_3OH	81.8	-248	155.7	1.1	5.7×10^{-14}	≈12.1(ii)
Et_3NH^+	CH_3OH	127.2	69	147.8	10.5	1.6×10^{-12}	--
$MeOH_2^+$	CH_3OH	82.5	-194	140.3	3.9	3.0×10^{-11}	-2[a]
			(-193)	(140.1)	(4.0)	(3.3×10^{-11})	
$PrOH_2^+$	1-Propanol	64.6	-223	131.0	2.4	1.3×10^{-9}	--
			(-219)	(130.0)	(2.6)	(2.0×10^{-9})	
$CH_3C(OH_2^+)HCH_3$	2-Propanol	74.8	-167	124.6	5.4	1.9×10^{-8}	--
			(-162)	(123.1)	(5.6)	(3.2×10^{-8})	
$(CH_3)_2CHCH_2OH_2^+$	Isobutanol	91.8	-110	124.6	8.4	1.8×10^{-8}	--
			(-103)	(122.5)	(8.7)	(4.0×10^{-8})	
$DMFH^+$	DMF	71.8	-163	120.4	5.6	9.3×10^{-8}	-1.5[e]
Et_3NH^+	DMF	95.5	-180	149.1	4.7	8.5×10^{-13}	9.25[d]
Et_3NH^+	AN	116.7	-128	154.9	7.4	9.0×10^{-14}	18.46[e]
H_3O^+	AN	68.2	-206	129.6	3.3	2.4×10^{-9}	3.67[g]
CH_3COOH	AN	150.8	48	165.1	11.6	1.4×10^{-15}	22.4[f]
CF_3COOH	AN	76.9	-203	137 4	3.5	9.4×10^{-11}	14.2(iii)
Br^-(b.e.r·)****	AN	40.9	-232	110.0	2.4	1.9×10^{-5}	--

* All parameters are determined at the metal-solution potential ϕ_R of the reference electrode, $Pt|H_2$, 0.1M $HCl(H_2O)$ at 298 K, and for a 0.1M proton donor concentration. Corrections are made for ionic association (see Table 1) according to $[d\log i/d\log c_{DH^+}]_{\phi} = 1-\beta$, and corrected parameters are shown in parenthesis.

** $\Delta\bar{S}^{\ddagger}_{\phi} = R\{2.303\log A_{\phi} - \ln[zFc_{DH^+}(1-\theta)kT/h]$

*** $\Delta\bar{G}^{\ddagger}_{\phi} = \Delta\bar{H}^{\ddagger}_{\phi} - T\Delta\bar{S}^{\ddagger}_{\phi}$

**** Kinetic parameters for the b.e.r. from 0.4M $(n\text{-}Pr)_4NBr$, 0.2M Br_2(AN) determined at the metal-solution potential ϕ_R of the reference electrode, C/Br_2, 0.4M $(n\text{-}Pr)_4NBr$, 0.2M Br_2(AN) at 298 K.

(i) $pK(HCONH_2)$ $pK(H_2O) \approx -0.6$ (ref. 5); pK $EtNH_3^+(H_2O)$-11.01

(ii) $pK(CH_3OH)$ $pK(H_2O) \approx 1.1$ (ref. 5); pK $EtNH_3^+(H_2O)$-11.01

(iii) $pK(AN)$ $pK(H_2O) \approx 14$ (ref. 5); pK $CF_3COOH(H_2O)$-0.25

a. ref. 149; b. ref. 220; c. ref. 213; d. ref. 214; e. ref. 215; f. ref.216 g. ref. 217

TABLE 18

Kinetic Parameters* at Constant ϕ for the H.E.R. at Solid Hg, from Different Proton Donors in Several Solvents

Proton Donor	Solvent	$\Delta\bar{H}^{\ddagger}_{\phi}$ kJmole^{-1}	**$\Delta\bar{S}^{\ddagger}_{\phi}$ JK^{-1}mole^{-1}	***$\Delta\bar{G}^{\ddagger}_{\phi}$ (233 K) kJmole^{-1}	log $[A]_{\phi}$ A in Acm^{-2}	i_{ϕ} (233K) Acm^{-2}
$EtNH_3^+$	CH_3OH	172.3	95	150.2	18.9	1.4×10^{-20}
Et_3NH^+	CH_3OH	131.6	-120	159.6	7.7	1.7×10^{-24}
$MeOH_2^+$	CH_3OH	80.5	-232 (-231)	134.5 (134.3)	1.9 (1.9)	6.9×10^{-17} (7.5×10^{-17})
$PrOH_2^+$	1-Propanol	102.9	-105 (-102)	127 4 (126.7)	8.5 (8.6)	2.6×10^{-15} (3.7×10^{-15})
$CH_3C(OH_2^+)HCH_3$	2-Propanol	99.7	-238 (-237)	155.2 (155.0)	1.5 (1.6)	1.5×10^{-21} (1.7×10^{-21})
$(CH_3)_2CHCH_2OH_2^+$	Isobutanol	61.3	-225 (-219)	113 7 (112.2)	2.2 (2.6)	3.2×10^{-12} (6.6×10^{-12})
$DMFH^+$	DMF	--	--	--	--	2.1×10^{-17}
Et_3NH^+	DMF	--	--	--	--	2.0×10^{-25}
Et_3NH^+	AN	--	--	--	--	$\approx3.3\times10^{-20}$

* All parameters are determined at the metal-solution potential ϕ_R of the reference electrode $Pt|H_2$, 0.1M $HCl(H_2O)$ at 298 K, and for a 0.1M proton donor concentration. Corrections are made for ionic association (see Table 1), according to $[d\log i/d\log c_{DH^+}]_{\phi} = 1-\beta$, and corrected parameters are shown in parenthesis.

** $\Delta\bar{S}^{\ddagger}_{\phi} = R(2.303\log A_{\phi} \quad \ln[zFc_{DH^+}(1-\theta)kT/h]$

*** $\Delta\bar{G}^{\ddagger}_{\phi} = \Delta\bar{H}^{\ddagger}_{\phi} \quad T\Delta\bar{S}^{\ddagger}_{\phi}$

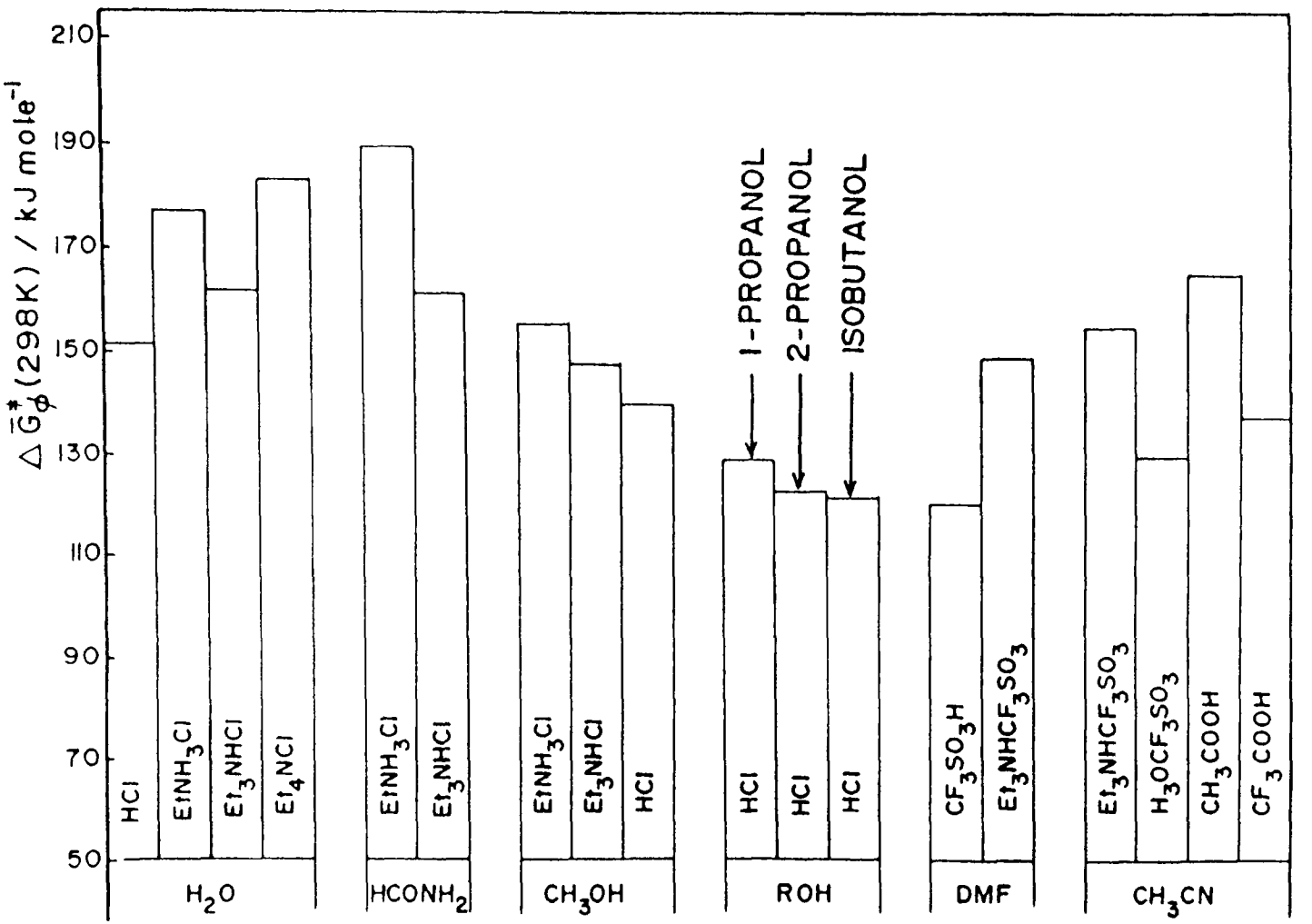

Fig 72 Histogram showing relative values of $\Delta \bar{G}^{\ddagger}_{\phi}$ for proton discharge at Hg from different proton donors in several solvents.

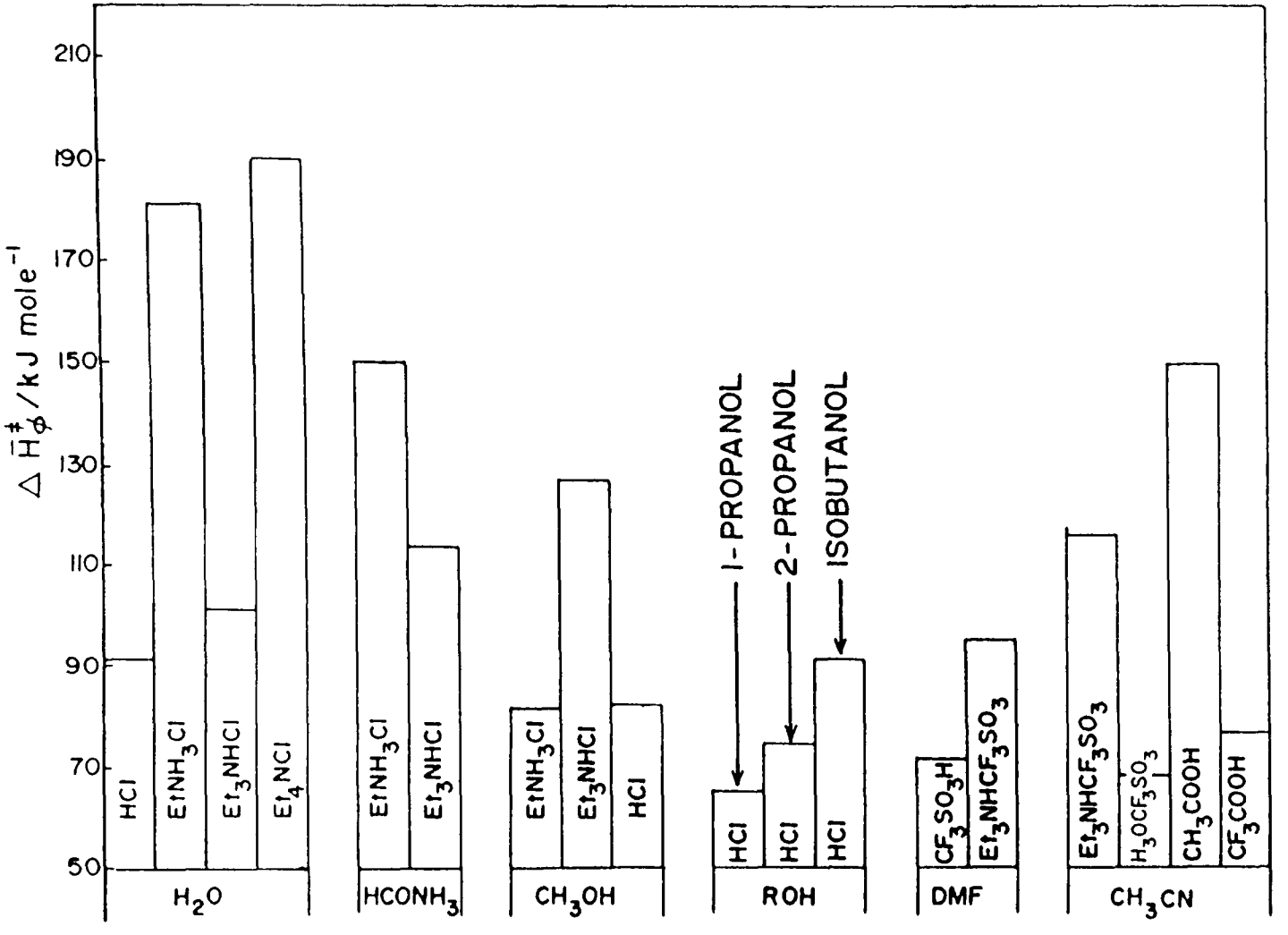

Fig 73 Histogram showing relative values of $\Delta \bar{H}^{\ddagger}_{\phi}$ for proton discharge at Hg from different proton donors in several solvents.

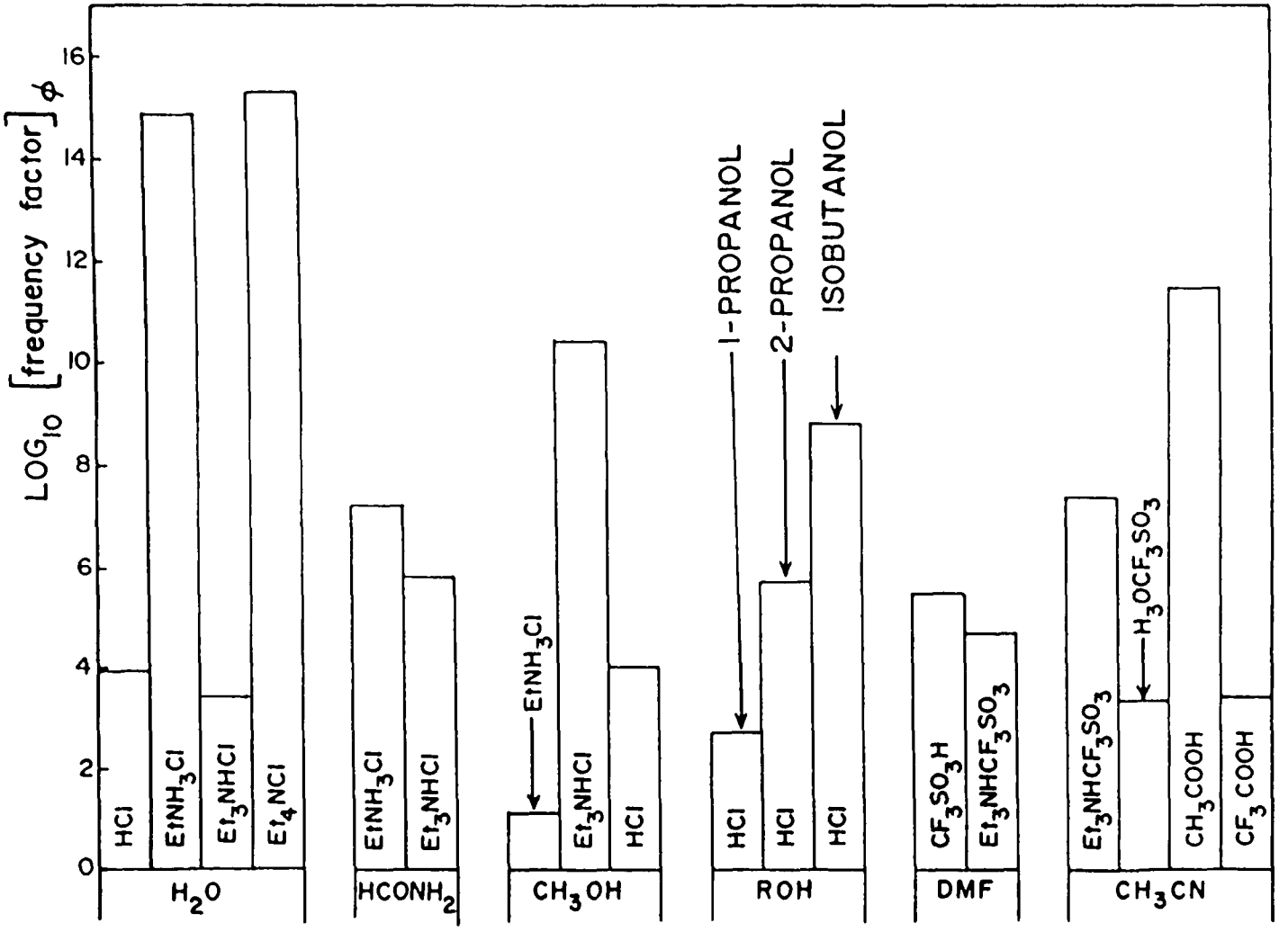

Fig. 74 Histogram showing relative values of log [frequency factor] for proton discharge at Hg from different proton donors in several solvents.

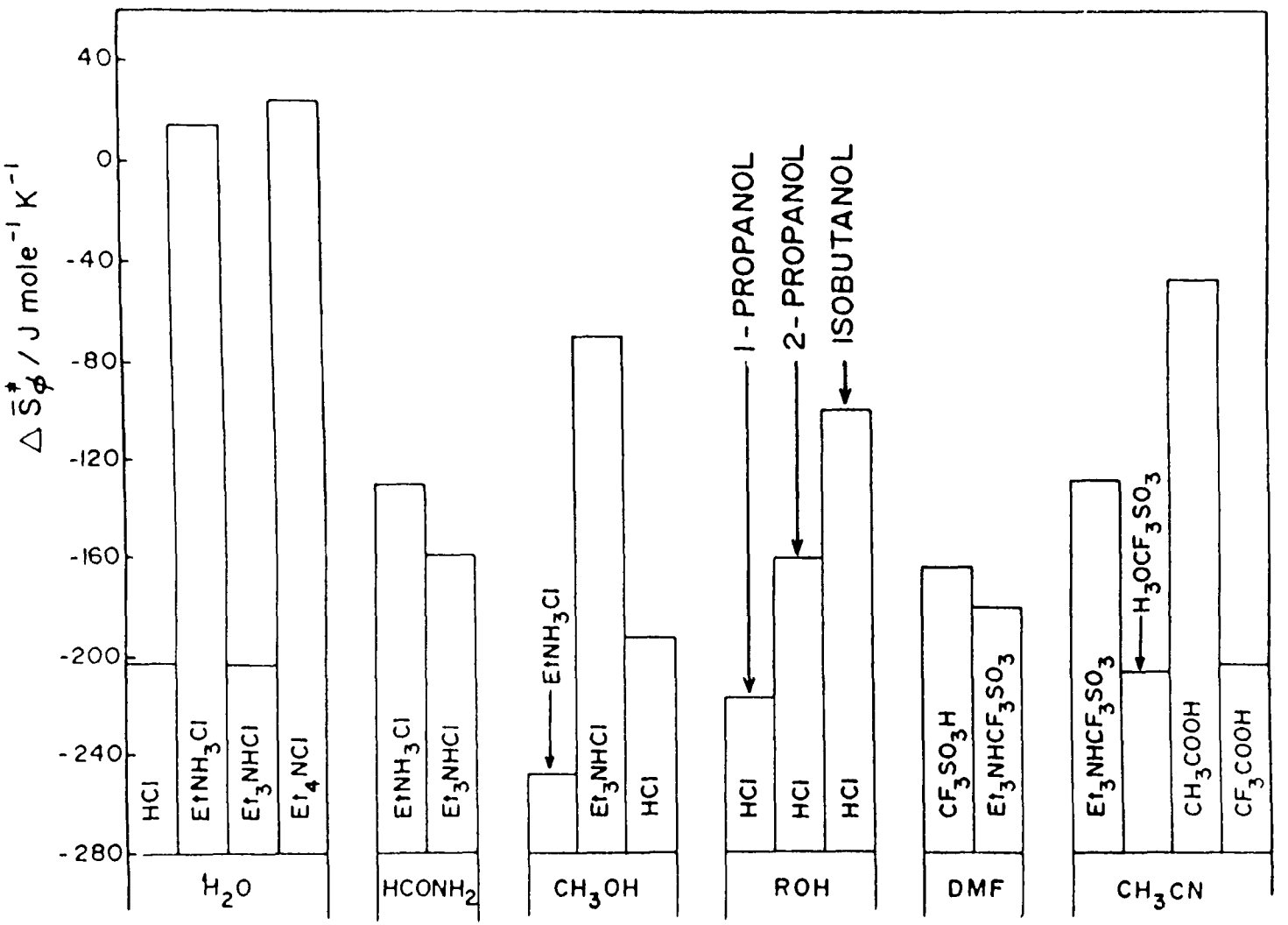

Fig 15 Histogram showing relative values of $\Delta\bar{S}^{\ddagger}_{\phi}$ for proton discharge at Hg from different proton donors in several solvents

h e r referred to above

a) Correction for Proton Donor Association

The concentration of all the proton donors was 0 1M in their respective solvents. However, for the alcohols where HCl is only partially dissociated (see Table 1), a concentration correction has to be made to allow for the extent to which the ROH_2^+ ion, as proton source, is actually present. Considering double-layer effects (1,170,171), the log i_ϕ at constant ϕ should increase with an increase of proton donor concentration by the reaction order factor

$$[\text{dlog } i/\text{dlog } C_{H+}]_\phi = 1-\beta \qquad [119]$$

so that substitution of the ROH_2^+ concentrations and β values (Tables 14 and 15) for each system into eqn.[119] gives the corrected rate for a 0.1M proton donor concentration. It is found that these corrected rates and corresponding activation parameters shown in parenthesis in Tables 17 and 18, do not differ much from the uncorrected results

b) Experimental Errors in the Activation Parameters

An upper limit of the errors in determination of the activation parameters can be estimated if maximum junction potentials are taken to be ca. 100 mV for the H_2O, $HCONH_2$ and alcohol systems, and ca. 200 mV for the AN and DMF systems (see page 125; in reality these junction potentials may be much less). Taking a maximum value for the temperature coefficient of the thermal liquid junction potential of $d\phi_{t\,l\,j}/dT = 50$ μVK^{-1} (see page 127) and substituting this value together with

the junction potentials into eqn.[43] and eqn.[44], gives the error in $\Delta\bar{H}^{\ddagger}_{\phi}$ and log A_{ϕ} (or $\Delta\bar{S}^{\ddagger}_{\phi}$) resulting from isothermal and non-isothermal reference cell corrections. When these errors are combined with the maximum experimental errors in the raw polarization data of $\pm$ 2 kJ mole^{-1} for $\Delta\bar{H}^{\ddagger}_{\phi}$ and $\pm$ 0.3 for log A_{ϕ} (or $\pm$ 6 JK^{-1} mole ^{1} for $\Delta\bar{S}^{\ddagger}_{\phi}$), the upper limit estimates of the error in the activation parameters for systems involving H_2O, $HCONH_2$ and alcohols are as follows: $\Delta\bar{H}^{\ddagger}_{\phi}$ $\pm$ 6 kJ mole^{-1}, log A_{ϕ} $\pm$ 1 (or $\Delta\bar{S}^{\ddagger}_{\phi}$ $\pm$ 19 J K^{-1}mole^{-1}) and for systems involving AN and DMF they are: $\Delta\bar{H}^{\ddagger}_{\phi}$ $\pm$ 11 kJ mole ^{1}, log A_{ϕ} $\pm$ 1.8 (or $\Delta\bar{S}^{\ddagger}_{\phi}$ $\pm$ 34 J K^{-1}mole ^{1}). It is emphasized again that these figures are upper limits and the actual errors are probably substantially smaller.

c) Activation Parameters Determined in Previous Work

Although the h.e.r. has been studied extensively at Hg in aqueous solutions, very few reliable investigations have been made in nonaqueous media other than methanol. In all of these investigations a reversible hydrogen reference electrode was used at the same temperature and in a solution of the same composition as that for the working electrode, so that only the "apparent" activation parameters determined in the present work should be compared with those results.

The polarization data of Post and Hiskey (143) for aqueous 0.1M HCl and of Bockris et al. (27,141) for 0.1N HCl in CH_3OH compare well with the polarization results found in the present work (see Figs. 19 and 23). The apparent activation parameters

derived by these authors are shown in Table 19, along with those in the present work for comparison.

The results of Krishtalik et al. (137,138) for 0.1M $HClO_4$, in AN and the less well defined system 0.01M $HClO_4$, 0.085M H_2O in AN, are also shown in Table 19. Unfortunately, apparent activation parameters could not be determined in the present work for the similar systems, 0.1M CF_3SO_3H in DMF and 0.1M $CF_3SO_3^-H_3O^+$ in AN, because the $H^+|H_2$ reference electrode is unreliable in such solvents so that the reliable $Ag^+|Ag$ reference electrode had to be used instead.

TABLE 19

Apparent Heat of Activation and log [frequency factor] for the H.E.R. at Hg from Various Media

System	Other Studies		Present Work	
	$\Delta\bar{H}^{\ddagger}_{\eta=o}$ kJ mole^{-1}	log $A_{\eta=o}$	$\Delta\bar{H}^{\ddagger}_{\eta=o}$ kJ mole^{-1}	log $A_{\eta=o}$
$H_3O^+|H_2O$	90.8 ± 1.0 (ref. 143)	3.4	86.0 ± 2.0	3.0 ± 0.3
$CH_3OH_2^+|CH_3OH$ (liquid Hg)	86.2 ± 2.5 (refs. 27,141)	3.6	79.8 ± 3.0	2.7 ± 0.5
$CH_3OH_2^+|CH_3OH$ (solid Hg)	80.3 ± 2.5 (ref. 141)	1.5	77.0 ± 3.0	0.4 ± 0.5
$H_3O^+|CH_3CN$	76.1 ± 1.7 (ref. 138)	3.2 ± 0.3		
$CH_3CNH^+|CH_3CN$	76.1 ± 1.7 (ref. 138)	2.1 ± 0.3	---	

5. Double-Layer Effects

An electrode reaction occurs within the double layer and therefore either a prior knowledge of the double-layer capacitance and electrocapillary behaviour, or the elimination of its effects on the reaction rate is essential in any study in which the behaviour of one system with another is to be compared. At higher solute concentrations and higher electrode potentials, the effects of the diffuse double layer diminish substantially and one can neglect the variation of the diffuse double-layer potential with the total metal-solution potential difference (172). The presence of adsorbed ions in the double layer changes the structure and potential profile across the double-layer where the transition state is established. The specific adsorption of an ion on an electrode surface is mainly determined by its electrostatic attraction or repulsion with the electrode, its solvation energy and solvent interaction with the electrode.

Based on interfacial tension measurements (136), water is easier to displace from Hg than most nonaqueous solvents, so that this effect will favour stronger ion adsorption from aqueous solutions. However, most ions are less strongly solvated in nonaqueous solvents than in water, so that this effect will favour stronger adsorption from nonaqueous solutions

The specific adsorption of anions has been shown to lower hydrogen overpotential because of a shift of the inner Helmoltz

potential to more negative values (172,173) This effect will result in departure from the Tafel relationship, which ceases at sufficiently negative electrode potentials where the anions are desorbed. It is unlikely that anion adsorption is significant in the present work where relatively low electrolyte concentrations (≈0.1M) were used and only the linear Tafel region at high overpotentials was considered.

Specific adsorption of Cl^- in dilute aqueous HCl at Hg, is indicated by electrocapillary and capacitance studies, but at the high overpotentials required to attain appreciable rates of hydrogen evolution, e.g., $> 10^{-6}$ A cm^{-2}, Cl^- is known to be desorbed (172,174). Similarly, in alcoholic solutions of HCl, specific adsorption of Cl^- is not significant at higher overpotentials (132,37,38), although nearer the p.z.c., specific adsorption of Cl^- is greater than in aqueous medium for the same concentration (175). Formamide, with its unsubstituted N-hydrogen, is able to solvate anions through a hydrogen-bonding mechanism and consequently specific adsorption of Cl^- would be expected to be similar to that in water (176) Solvation in aprotic solvents depends on the polarizability of the anion which increases with size of the anion (176,177) Specific adsorption of the $CF_3SO_3^-$ anion at Hg in DMF and AN is similar to that of perchlorate and is not significant (176,69)

The specific adsorption of quaternary ammonium cations has been shown to increase hydrogen overpotential, because of a positive shift of the inner Helmholtz potential and blocking of

the electrode surface (172,173). In aqueous solutions, these effects result in a departure from linear Tafel behaviour only at sufficiently negative electrode potentials where there is a decrease in free energy when small inorganic cations and water molecules displace the adsorbed quaternary ammonium cations, so that an increase of capacity results (172). Similar behaviour might be expected in nonaqueous solvents at least for H-bonded associated ones, and for partially substituted alkylammonium salts, although such effects were not observed in the present work.

Conway and Rocheleau (218) have shown that adsorption of $(n\text{-}Pr)_{4-n}NH_n^+$ ions at Hg in water decreases as n increases from 0 to 3, which is consistent with a view of decreasing hydrophobicity and increasing solvent accessibility to the N^+ charge centre. The kinetic situation of a specifically adsorbed reactant such as Et_3NH^+, located at the inner Helmholtz layer, is more favorable than if it is solvated and located at the less negative potential of the outer Helmholtz layer. This is probably the situation in the present work for proton discharge from Et_3NH^+ and $EtNH_3^+$ in different solvents.

A comprehensive review of the properties of the electrical double-layer in nonaqueous solutions has been given by Payne (136), but capacity and electrocapillary studies on $R_{4-n}\ NH_n^+$ ions ($0 \leq n \leq 4$) in such media are practically nonexistant. There is some evidence to suggest specific adsorption of NH_4^+ ions from CH_3OH (178) but the concentration dependence of the capacity in NH_4^+ solutions has not been measured. Some indication of

specific adsorption of NH_4^+ is suggested by capacity measurements for NH_4NO_3 solutions in DMF (179).

From a treatment of Parsons (180), and following the procedure of Conway et al. (132,13), it is possible to show approximately the effect of adsorption of a reactant cation on the symmetry factor β, the heat of activation and the frequency factor. If the interaction between the activated complex of the electrode reaction and the adsorbed ions is expressed through the activity coefficient of the activated complex (180) then the relative change of rate constant k with coverage θ by the cations can be given by

$$\ln(k/k_o) = +2B'\theta \qquad [120]$$

where k_o is the rate constant in the absence of adsorption of cations and resulting interactions with the activated complex, and B' is the second virial coefficient in the equation of state for the adsorbed species. If the coverage, θ, is approximately linear in potential, ϕ, (constant inner-layer capacity contribution C' per cm^2) then

$$\ln(k/k_o) = +2B'C'\phi \qquad [121]$$

The electrode reaction current-density i_η at a given overpotential of eqn.[33], measured in the presence of specific reactant cation adsorption will now be given by

$$i_{\eta,ads.} = (zFcf(\theta)\kappa\tilde{k}T/h)\exp(\Delta S^{\ddagger}_{\phi=o}/R)\exp(-\Delta H^{\ddagger}_{\phi=o}/RT)$$
$$\exp(\pm \beta\phi nF/RT)\exp(2B'C'\phi) \qquad [122]$$

where c is the concentration in mole cm^{-2} of specifically adsorbed reactant cations at the electrode surface, i.e., $c=C'\phi/F$, and the potential ϕ is the potential difference across the inner Helmholtz plane, i.e., $\phi = \phi_{m-s} - \phi_{ihp} = \eta + \phi_R - \phi_{ihp}$.

Combining the exponential factors in ϕ of eqn.[122] gives

$$\exp(\pm\beta\phi nF/RT)\exp(2B'C'\phi)=$$

$$\exp(\pm\phi nF/RT)(\beta \pm 2B'C'RT/nF) = \exp(\pm\beta'\phi nF/RT) \quad [123]$$

so that the apparent symmetry factor, $\beta' = \beta \pm 2B'C'RT/nF$, consists of the normal β plus a temperature-dependent term involving the interaction parameter B' and the capacity term C' characterizing the potential-dependence of coverage of the adsorbed cations.

The heat of activation measured at constant overpotential and in the presence of specific reactant cation adsorption will now be given by

$$\Delta\bar{H}^{\ddagger}_{\eta,ads.} = -R\,[\partial \ln i_{\eta,ads.}/\partial(1/T)]_{\eta,c} = \Delta\bar{H}^{\ddagger}_{app} + 2B'C'\partial\phi/\partial(1/T) \quad [124]$$

and the logarithm of the frequency factor by

$$\ln A_{\eta,ads.} = \ln i_{\eta,ads.} + \Delta\bar{H}^{\ddagger}_{\eta,ads.}/RT \quad [125]$$

$$= \ln A_{app.} + 2B'C'\phi + (2B'C'/RT)\partial\phi/\partial(1/T)$$

where $\Delta\bar{H}^{\ddagger}_{app.}$ and $\ln A_{app.}$ are the apparent activation quantities of eqn.[35] and eqn.[37], respectively, measured in the absence of any specific adsorption effects. A similar result for the heat of activation, when specific adsorption is significant, was derived by Parsons et al. (181), i.e.

$$\Delta\bar{H}^{\ddagger}_{\eta,ads.} = \Delta\bar{H}^{\ddagger}_{app.} + \text{constant}[\partial(\phi_a/T)/\partial(1/T)]_{\eta,c} \quad [126]$$

where ϕ_a is the potential at the reactant layer and depends on the extent of specific adsorption. They considered Frumkin double-layer corrections only (170) and did not include the effect on the activity coefficient of the activated complex as is done in the present derivation. If the potential at the

reactant layer is approximately independent of temperature, i.e., for specific reactant cation adsorption, $\phi_{ihp} \neq f(T)$, then for a fixed reference electrode potential, ϕ_R, such as used in the present work, the effect of specific adsorption on the heat of activation (eqn.[124] and the form of eqn.[126]) can be ignored, but not for the frequency factor, i.e., eqn.[125]. Expressions similar to eqn.[124] and eqn.[125] for the heat of activation and the frequency factor will result for other cases involving specific ion adsorption such as anion or cation adsorption with the reactant located at the outer Helmholtz plane. In these cases the expressions for the reactant layer concentration c and the potential difference, ϕ, affecting the reaction rate will be different (181). Double-layer effects at Hg for the systems studied here are expected to be similar except for specific adsorption of the alkylammonium ions, so that some caution should be exercised in comparing activation parameters, especially those involving the frequency factor from which $\Delta\bar{S}^{\ddagger}_{\phi}$ is derived.

6. H.E.R. at Solid Hg

In the present work, a discontinuous change was found in the Tafel behaviour (see Table 16) and the Arrhenius plots of log i_ϕ versus T^{-1} as temperature was raised or lowered through the melting point of Hg, for the h.e.r. from several different systems. Differences in the kinetic parameters ($\Delta\bar{H}^{\ddagger}_{\phi}$, $\Delta\bar{S}^{\ddagger}_{\phi}$, $\Delta\bar{G}^{\ddagger}_{\phi}$, log A_ϕ and i_ϕ) determined for solid Hg and liquid Hg, at the melting point of Hg are shown in Table 20.

TABLE 20

Change in Kinetic Parameters* at the Freezing Point of Hg (234.16 K) for the H.E.R from Various Proton Sources

Electrolyte (0.1M)	Solvent	$\Delta(\Delta\bar{H}^{\ddagger}_{\phi})$ kJmole^{-1}	$\Delta(\Delta\bar{S}^{\ddagger}_{\phi})$ JK^{-1}mole^{-1}	$\Delta(\Delta\bar{G}^{\ddagger}_{\phi})$ (234 K) kJmole^{-1}	$\Delta\log A_{\phi}$ A in Acm^{-2}	$\frac{i_{\phi}(\text{solid Hg})}{i_{\phi}(\text{liquid Hg})}$ (234 K)
$EtNH_3Cl$	CH_3OH	90.5	343	10.2	17.8	4.2×10^{-3}
Et_3NHCl	CH_3OH	4.4	51	16.3	-2.8	1.8×10^{-4}
HCl	CH_3OH	-2.0	38	6.9	-2.1	2.5×10^{-2}
HCl	1-Propanol	38.3	119	10.5	6.0	3.1×10^{-3}
HCl	2-Propanol	24.9	75	42.5	-4.0	4.0×10^{-10}
HCl	Isobutanol	-30.5	-116	-3.4	-6.1	5.2
CF_3SO_3H	DMF	--	--	--	--	7.3×10^{-7}
$Et_3NHCF_3SO_3$	DMF	--	--	--	--	1.1×10^{-8}
$Et_3NHCF_3SO_3$	AN	--	--	--	--	$\approx4.4\times10^{-1}$

* $\Delta(\Delta X)$ = ΔX(solid Hg) ΔX(liquid Hg); kinetic parameters, $\Delta X = \Delta\bar{H}^{\ddagger}_{\phi}$, $\Delta\bar{S}^{\ddagger}_{\phi}$, $\Delta\bar{G}^{\ddagger}_{\phi}$ and $\log A_{\phi}$, are from the data of Tables 1 and 2.

In all cases except for 0.1M HCl in isobutanol, there is an increase in the electrochemical Gibbs energy of activation and a corresponding decrease in current on going from liquid to solid Hg. The differences in the activation parameters measured at solid Hg(S) and liquid Hg(L) at some constant metal-solution potential ϕ are given by

$$\Delta(\Delta\bar{G}^{\ddagger}_{\phi}) = \Delta\bar{G}^{\ddagger}_{\phi}(S) - \Delta\bar{G}^{\ddagger}_{\phi}(L) = \Delta G^{\ddagger}_{\phi=0}(S) - \Delta G^{\ddagger}_{\phi=0}(L) \mp [\beta(S) - \beta(L)]nF\phi \quad [127]$$

$$\Delta(\Delta\bar{H}^{\ddagger}_{\phi}) = \Delta\bar{H}^{\ddagger}_{\phi}(S) - \Delta\bar{H}^{\ddagger}_{\phi}(L) = \Delta H^{\ddagger}_{\phi=0}(S) - \Delta H^{\ddagger}_{\phi=0}(L) \mp [\beta_H(S) - \beta_H(L)]nF\phi \quad [128]$$

$$\Delta(\Delta\bar{S}^{\ddagger}_{\phi}) = \Delta\bar{S}^{\ddagger}_{\phi}(S)\ \Delta\bar{S}^{\ddagger}_{\phi}(L) = \Delta S^{\ddagger}_{\phi=0}(S)\ \Delta S^{\ddagger}_{\phi=0}(L) \pm [\beta_S(S) - \beta_S(L)]nF\phi \quad [129]$$

where β, β_H, and β_S were all found to be different at solid and liquid Hg; hence, through the last terms of each of the above equations, the differences in the kinetic parameters will depend on the particular ϕ used, but should reflect any systematic differences in the true "chemical" activation quantities, i e., for $\phi = 0$.

The decrease in apparent surface area of the Hg by contraction upon solidification can be estimated to be about 15% (170), but is counter-balanced by an increase in real surface area by at least 10% due to crystallization (173). Clearly, such a small change in the Hg surface area cannot account for the appreciable difference in i_ϕ at solid and liquid Hg. However, the double-layer at solid Hg might be expected to be quite different from that at liquid Hg, because of the inhomogeneity of the solid surface producing nonequivalent surface sites with different adsorption energies for ions and solvent molecules. However, double-layer studies (182,183) in a 50% supersaturated aqueous solution of K_2CO_3 at solid and liquid Hg resulted in the same capacity-potential curves and, in the presence of ethanol, the capacity peaks for its adsorption were also identical for solid and liquid Hg. Double-layer studies (184) at gallium, a similar metal to Hg, also indicate no difference in the capacity behaviour at liquid and solid gallium in an aqueous solution of 0.5M Na_2SO_4 + 0 01M HCl, even in the presence of n-hexyl alcohol Although these results would

indicate that anion and solvent adsorption are not significantly different at solid and liquid Hg, the situation may be quite different for specifically adsorbed reactant cations, such as Et_3NH^+ and $EtNH_3^+$ used in some parts of the present work, but no double-layer results are available.

The kinetic results obtained for 0.1M HCl in CH_3OH at solid and liquid Hg are similar to those obtained by Bockris et al. (141) for the same system. They considered the principal cause for the difference in the exchange current, i_o, to be restriction of the translational motion of the activated complex upon freezing of the Hg, which results in a more negative entropy of activation.

It has been shown elsewhere (23) that the entropy of activation for a discharge reaction calculated on the assumption of an immobile activated complex, is as expected more negative than the observed value. While this entropy effect may be important, the entropy of activation for the h.e.r. from two of the present systems, 0.1M $EtNH_3Cl$ in CH_3OH and 0.1M HCl in 1 propanol, becomes more positive upon freezing of the Hg, so that other important entropy effects must evidently be involved. With the exception of two of the present systems, 0 1M Et_3NHCl in CH_3OH and 0 1M HCl in CH_3OH, enthalpy effects, $\Delta(\Delta\bar{H}_\phi^\ddagger)$, are of equal or greater significance than the entropy effects, $T\Delta(\Delta\bar{S}_\phi^\ddagger)$ These enthalpy effects most probably result from a different energy of H-adsorption on the solid Hg surface, which will affect the enthalpy of the final and activated states

7 Proton Discharge from the Solvent

The question of whether proton discharge from the solvent molecules is significant in comparison to proton discharge from the proton donor is important for a meaningful interpretation of the kinetic parameters and has to be considered. The protic solvent H_2O has the highest autoprotolysis constant of the solvents used in the study reported here, i.e., $pK_s = 14$, and therefore would be the most likely solvent to be involved in proton discharge. The possibility exists, in principle, of a parallel reduction process involving the H_2O solvent molecule and the proton donor DH^+,

$$DH^+ + e \rightarrow 1/2\ H_2 + D \qquad [130]$$

$$H_2O + e \rightarrow 1/2\ H_2 + OH^- \qquad [131]$$

Recently a new method, the sinusoidal hydrodynamic modulation technique at a rotating disk electrode, has been used for separation of the partial currents for reduction of the hydronium ion and water in aqueous acid solutions (185). Results at Pt and Au indicate a negligible current contribution for the reaction of H_2O in dilute strong acid solutions, but a larger contribution is found in weak acid solutions, e g., CH_3COOH.

The partial current for proton discharge from H_2O may be significant for aqueous solutions of the undissociated proton donors Et_3NH^+ ($pK_d = 10.87$) and $EtNH_3^+$ ($pK_d = 10.63$) used in the present work. In order to examine this question, the kinetics of proton discharge from H_2O was studied directly from a

solution of 0.1M Et_4NCl in H_2O (pH ≈ 5.5 6) which was selected as an analogue of Et_3NH^+ but having no dischargeable proton. This quaternary ammonium salt was chosen as the supporting electrolyte because i) the structure of the double-layer at Hg for contact adsorbed Et_4N^+ is probably similar to that for $EtNH_3^+$ and Et_3NH^+ and ii) R_4N^+ cations have the greatest stability to reduction (high potential for discharge). Thus, the half-wave potential for reduction of aqueous Et_4N^+ at Hg to form an onium amalgam is -2.6 V vs. SCE (186):

$$Et_4N^+ + e + Hg \rightarrow Et_4N/Hg \qquad [132]$$

However, the highest potentials used in the present kinetic studies were at least 0.4 V below this potential and no change in the colour of the Hg surface was observed.

The current density and Tafel slope for proton discharge from H_2O (i_ϕ = 9.4 x 10^{-19} A cm^{-2}, b=0.123 V) are appreciably smaller than for aqueous Et_3NH^+ (i_ϕ = 4.9 x 10^{-15} A cm^{-2}, b=0.155 V) and aqueous $EtNH_3^+$ (i_ϕ=1.1x10^{-17}A cm^{-2}, b=0.133 V) when compared at 298 K at the potential, ϕ_R, of the reference electrode, Pt/H_2, 0.1M HCl (H_2O) In a parallel reaction sequence involving proton discharge from H_2O and either $EtNH_3^+$ or Et_3NH^+, the proton discharge from H_2O will eventually be the dominant reaction at some higher potential because it has the lower Tafel slope ($\Delta\phi/\Delta\log i$) , and this will result in non-linear Tafel behaviour. However, the present results show linear Tafel behaviour for proton discharge from aqueous Et_3NH^+ and aqueous $EtNH_3^+$ over the entire potential range studied,

indicating negligible proton discharge from H_2O.

The latter behaviour, and the corresponding large activation energy for proton discharge from H_2O in the presence of Et_4N^+, i.e., $\Delta\bar{G}^{\ddagger}_{\phi}$=183.3 kJ mole ^{1}, may be due, in part, to blocking of the electrode surface by the hydrophobically adsorbed alkyl ammonium ions. Further evidence for this comes from the work of Parry and Parsons (187) who showed that for reduction of the neutral molecule H_2O_2 in water at Hg, the rate of hydrogen evolution is retarded in the presence of specifically adsorbed tetraalkylammonium ions. They postulated a blocking effect due to increase in dimensions of the inner part of the double-layer, causing an increase in the energy of activation of the reaction.

8. <u>The Sign and Magnitude of $\Delta\bar{S}^{\ddagger}_{\phi}$</u>

The entropies of activation, $\Delta\bar{S}^{\ddagger}_{\phi}$, were derived in the present work from $1/T \rightarrow 0$ intercepts, viz. log A_{ϕ}, of electrochemical Arrhenius plots at constant metal solution potential difference, ϕ; the log A_{ϕ} values can be related to $\Delta\bar{S}^{\ddagger}_{\phi}$ by transition state theory (cf. eqn [42]) to give

$$\Delta\bar{S}^{\ddagger}_{\phi} = R\{2.303\log A_{\phi} \quad \ln [zFc_{H^+}(1\ \theta)kT/h]\} \qquad [133]$$

where A_{ϕ} is the "frequency factor" in A cm^{-2}; z is the total number of electrons transferred in the overall process, i.e., z=2 for the h.e r., c_{H^+} is an appropriate reactant surface concentration, which, in the present work, is taken to be the bulk concentration in mole cm^{3} and θ is the surface coverage by H, assumed $<<1$ for Hg, so that $1\ \theta \approx 1$; the other terms have

their usual significance.

It is seen from Tables 17 and 18 that most of the $\Delta\bar{S}^{\ddagger}_{\phi}$ values for the h.e.r (and b.e.r.) are relatively large and negative. Parsons and Bockris (23) also found a large negative value for the apparent entropy of activation, $\Delta\bar{S}^{\ddagger}_{\eta=o}$ for the h.e.r. at Hg from aqueous HCl. These results are at first sight unexpected since for a reaction involving loss of net charge, as in ion neutralization, e.g., h.e.r., the entropy change would be expected to be dominated by elimination of electrostrictive effects and hence be positive. In fact the "overall" reaction entropy, ΔS°_{R}, for the hydrogen reference electrode in water and several alcohols is found to be positive in the present work (see Table 9). A positive overall reaction entropy was also found by Conway et al. (188) for deposition of adsorbed H at Pt from H_3O^+ in acid solution.

Normally, in homogeneous reactions involving extinction of charge, both the reaction entropy ΔS_R, and the activation entropy, $\Delta S^{\ddagger}$, are positive. For a possible comparison with the homogeneous proton transfer case, an estimate was made of the "true" chemical entropy of activation at zero metal-solution potential for the h.e r at Hg from aq H_3O^+ (see section C-12). This entropy, i.e., $\Delta\bar{S}^{\ddagger}_{\phi=o}$ = 181 J K^{-1}mole ^{1}, is still very negative and not much different from the corresponding entropy of activation at the fixed metal-solution potential, i.e., $\Delta\bar{S}^{\ddagger}_{\phi}$ = -202 J K^{-1} mole ^{1}. Therefore the situation here with respect to the h.e.r is unexpected in terms of electrostatic effects

that are likely to be involved.

Conway and Currie (189) found a corresponding anomalously negative volume of activation, $\Delta V^{\ddagger}$, for the h.e.r., and have suggested that this behaviour originates from a localization of the proton in the $H_9O_4^+$ complex at the moment of proton transfer and neutralization, so that electrostriction is enhanced. This type of effect may cause $\Delta\bar{S}_{\phi}^{\ddagger}$ to be negative, but a negative value of $\Delta\bar{S}_{\phi}^{\ddagger}$ is not specific to the proton in H_2O. Negative values of $\Delta\bar{S}_{\phi}^{\ddagger}$ are also found for the proton in non-hydrogen bonded solvents (cf. $DMFH^+$, $\Delta\bar{S}_{\phi}^{\ddagger}$ = 163 J K^{-1} mole ^{1}); for specifically adsorbed proton donors which are only partially solvated (cf. Et_3NH^+ in H_2O, $\Delta\bar{S}_{\phi}^{\ddagger}$ = 203 J K^{-1} mole ^{1}); and for a different atom transfer reaction (cf. Br^- discharge at C in CH_3CN, $\Delta\bar{S}_{\eta=0}^{\ddagger}$ = -232 J K^{-1}mole ^{1}). These results indicate that the negative $\Delta\bar{S}_{\phi}^{\ddagger}$ may be characteristic of the atom/electron transfer process itself. Factors which determine the entropy of activation of complex-ion redox reactions and relation to inner- and outer-sphere routes (190), have been examined in various papers by Weaver et al. (77, 125, 126, 127) but the situation is probably quite different for the h.e.r where atom, as well as electron transfer, is involved.

In considering the significance of the magnitude and sign of $\Delta\bar{S}_{\phi}^{\ddagger}$ quantitites it is necessary to take into account the choice of standard state (191, 192) and the units of concentration (23, 193, 194) for the reactant and activated complex, in addition to chemically significant factors For electrode processes, the

rate in terms of current-density, is expressed as (mole $s^{1}cm^{2}$) x (coulombs $mole^{1}$), implying a standard state of 1 mole cm^{-2}, but in the derivation of $\Delta\bar{S}_{\phi}^{\ddagger}$ values in the present work a reactant concentration expressed in mole cm^{3} is used. The reactant concentration can be normalized to a nominal two-dimensional surface concentration by multiplying it by the thickness, λ, of the reaction layer at the electrode (23, 193). This procedure eliminates the arbitrary difference between current-densities or rates expressed per cm^2 and concentrations per cm^3, but the values of $\Delta\bar{S}_{\phi}^{\ddagger}$ will still depend on the particular value chosen for λ. The value of λ has been identified with the width of the Helmholtz layer, i.e., $\lambda \approx 0.3$ nm (23), so that introducing this value into eqn.[19] will make the resulting $\Delta\bar{S}_{\phi}^{\ddagger}$ values more positive by an amount R ln (3×10^{-8}cm) = 144 J $K^{-1}mole^{1}$.

Although a different standard state from that of the reactant is implied in eqn.[133] for the unoccupied metal sites (the $1-\theta$ term), it may be better for consistency to identify the quantity $1-\theta$ with the concentration of bare metal sites in mole cm^{2}. For Hg where $1-\theta \approx 1$, $c_m \approx 1\times10^{15}$ sites $cm^{-2}/6.02\times10^{23}$ sites $mole^{-1}$ = 1.66×10^{-9} moles cm^{-2}, so that introducing this value into eqn. [133] for $(1\ \theta)$, and ignoring activity coefficient effects, the resulting $\Delta\bar{S}_{\phi}^{\ddagger}$ values will be more positive by an amount -R ln (1.66×10^{-9} mole cm^{-2}) = 168 J $K^{-1}mole^{1}$.

When these corrections for reactant and metal site concentration are applied to the results in Tables 17 and 18 all the $\Delta\bar{S}_{\phi}^{\ddagger}$ values become positive. In fact there is surprising

agreement between the corrected entropy of activation for the h.e.r. at Hg from aq.H_3O^+, i.e., $\Delta\bar{S}^{\ddagger}_{\phi}$ = +110 ± 20 J K^{-1}mole ^{1} and its overall reaction entropy, i.e., ΔS_R = +85 ± 3 J K^{-1} mole ^{1} (see Table 9). It is seen that considerable caution is required in interpreting the sign or magnitude of these entropies of activation, but comparison of corrected or uncorrected $\Delta\bar{S}^{\ddagger}_{\phi}$ values may allow useful conclusions to be made.

9. Relation between $\Delta\bar{H}^{\ddagger}_{\phi}$ and $\Delta\bar{S}^{\ddagger}_{\phi}$

A plot of $\Delta\bar{H}^{\ddagger}_{\phi}$ versus the logarithm of the frequency factor (proportional to $\Delta\bar{S}^{\ddagger}_{\phi}$) for the h.e.r. at solid and liquid Hg from the data acquired for the systems studied here, is shown in Fig. 76. Similar to the relationship found between β_H and β_S (Fig. 65), $\Delta\bar{H}^{\ddagger}_{\phi}$ and $\Delta\bar{S}^{\ddagger}_{\phi}$ evidently also vary together in a systematic and compensatory way to give a linear relation

$$\Delta\bar{H}^{\ddagger}_{\phi} = 7.0 \log A_{\phi} + 60 \qquad [134]$$

with a correlation coefficient of 0.87. Substitution of the expression for $\Delta\bar{S}^{\ddagger}_{\phi}$ (eqn.[133]) in terms of log A_{ϕ} into eqn.[134] with appropriate values of $c_{H+} = 10^{-4}$ mole cm ^{3}, z=2, and $1-\theta \approx 1$ (for Hg) gives

$$\Delta\bar{H}^{\ddagger}_{\phi} = 0.37\ \Delta\bar{S}^{\ddagger}_{\phi} + 159 \qquad [135]$$

The above behaviour is similar to that of various "ΔH" and "ΔS" quantities for solution properties and processes in solution where a "compensation effect" between these two types of quantities often arises (see section B-8, this chapter). Thus, in view of the relation between activation quantities and corresponding initial-state solution properties (cf.

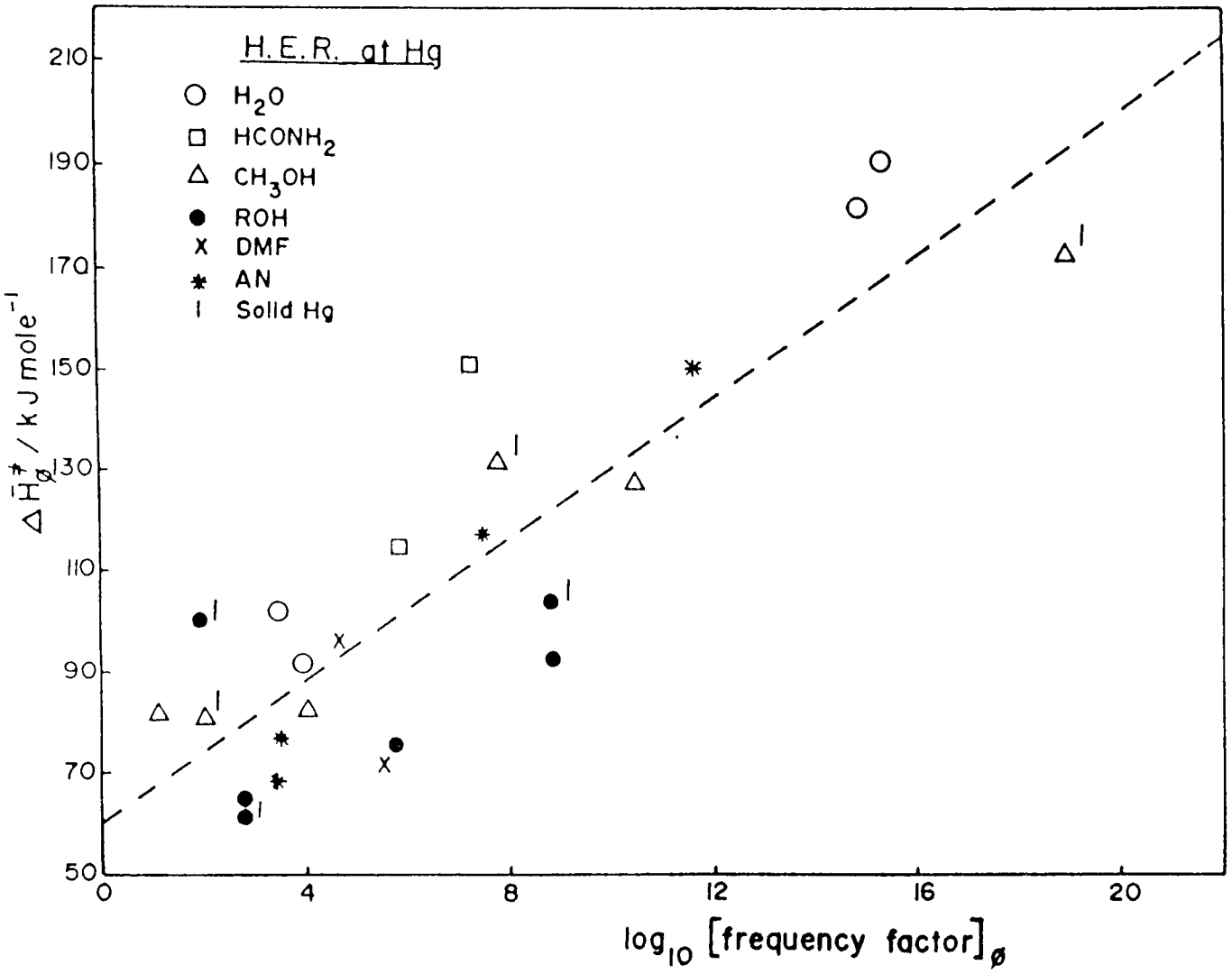

Fig. 76 Compensation plot of $\Delta \bar{H}_{\phi}^{\ddagger}$ versus log [frequency factor] (proportional to $\Delta \bar{S}_{\phi}^{\ddagger}$) for the h.e.r at Hg from different proton donors in several solvents.

eqns [117] and [118]), a compensation effect might be expected.

The general basis of these "ΔH" / "ΔS" compensation effects is that factors which lead to larger exoenergetic energies of interaction (ΔH negative) cause increased frequencies in the interaction complex, some local compression and often more configurational order; these are factors which tend to diminish the entropy of the system in proportion to the negative ΔH for the interaction. Similar behaviour applies to the $\Delta H^{\ddagger}$ and $\Delta S^{\ddagger}$ quantities for activation. Compensation effects of this kind are well established, especially for structured solvent media like water.

10. Medium and Proton Donor Effects

The relation between electrochemical activation quantities measured at fixed ϕ and the medium effect on the initial state energy and entropy (cf. eqns [116], [117], and [118]) would suggest that $\Delta\bar{G}^{\ddagger}_{\phi}$, $\Delta\bar{H}^{\ddagger}_{\phi}$ and $\Delta\bar{S}^{\ddagger}_{\phi}$, should be compared with their respective single ion chemical transfer functions, i e , ΔG_t, ΔH_t and ΔS_t for transfer from one solvent to another Virtually no studies have been made on the medium effect for electrochemical proton transfer with the exception of the work of Salomon (113,195) who has discussed the medium effect on proton discharge in H_2O and CH_3OH in terms of ionic Gibbs energies of transfer.

When values of $\Delta\bar{G}^{\ddagger}_{\phi}$ for discharge from the proton in hydroxylic solvents (i e , $H\text{-}OH^{+}$ and $R\text{-}OH_2^{+}$ which have the same

active proton donor centre) are plotted against the Gibbs energy of transfer of H^+ from H_2O to ROH, a linear relation is found. (see Fig. 77) The behaviour of the proton in DMF ($\Delta\bar{G}_{\phi}^{\ddagger}$ = 120 4 kJ mole ^{1}, ΔG_t (H^+, $H_2O \rightarrow$ DMF) = 18 kJ mole ^{1}) diverges substantially from this linear relation but this is not unexpected since a different active bond centre is involved, i.e. $\rightarrow NH^+$.

Unfortunately, no other reliable transfer values could be found for the proton donors used in the present work, so that other parameters have to be used to rationalize medium effects For example, a plot of $\Delta\bar{G}_{\phi}^{\ddagger}$ with respect to $1/\epsilon$ for the various proton donors used here, shows a decrease of $\Delta\bar{G}_{\phi}^{\ddagger}$ with decreasing ϵ for the same proton donor, i.e., for constant ionic radius (see Fig. 78). This is consistent with the Born relation

$$\Delta G_{I-S} = -N_A \frac{(ze)^2}{2r_i} (1\ 1/\epsilon) \qquad [136]$$

which predicts a decrease in the Gibbs energy of solvation with a decrease in ϵ and hence a lower energy of activation.

Schmid (196) has recently indicated that the macroscopic dielectric constant can be considered to reflect a combination of specific solvent parameters characterizing nucleophilic properties, i.e., donor number, and the electrophilic properties, i.e., acceptor number of the solvent: however, for highly structured solvents, attempts at correlation with any solvent property fails. Thus plots of $\Delta\bar{G}_{\phi}^{\ddagger}$ with respect to the solvent dipole moment (Fig 79) and the solvent donor number (Fig. 80) show no correlation, indicating that these specific

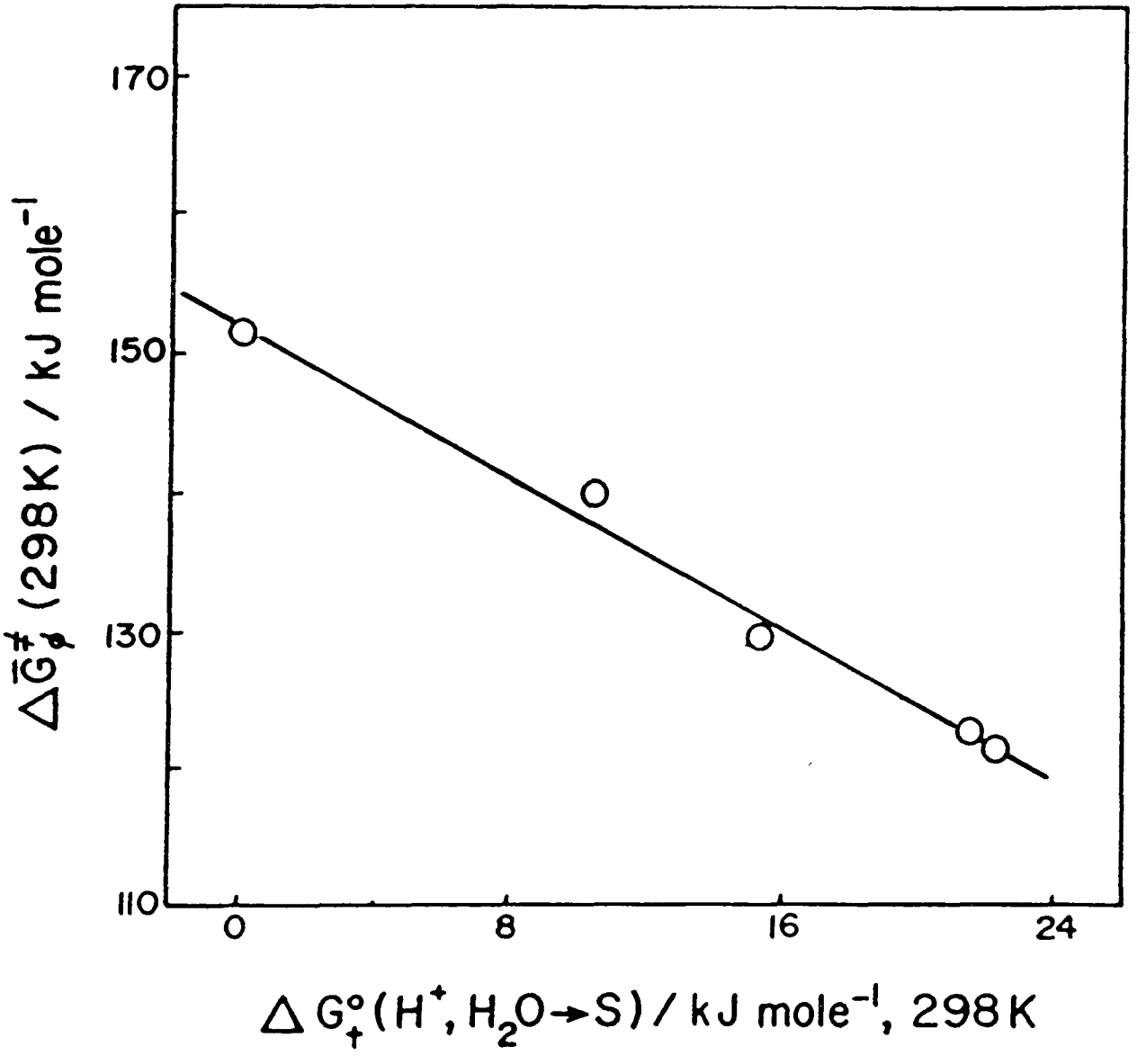

Fig 77 $\Delta \bar{G}_\phi^{\ddagger}$ for the h.e r at Hg from ROH_2^+ as a function of the Gibbs energy of transfer of H^+ from H_2O to ROH (transfer values from ref 111)

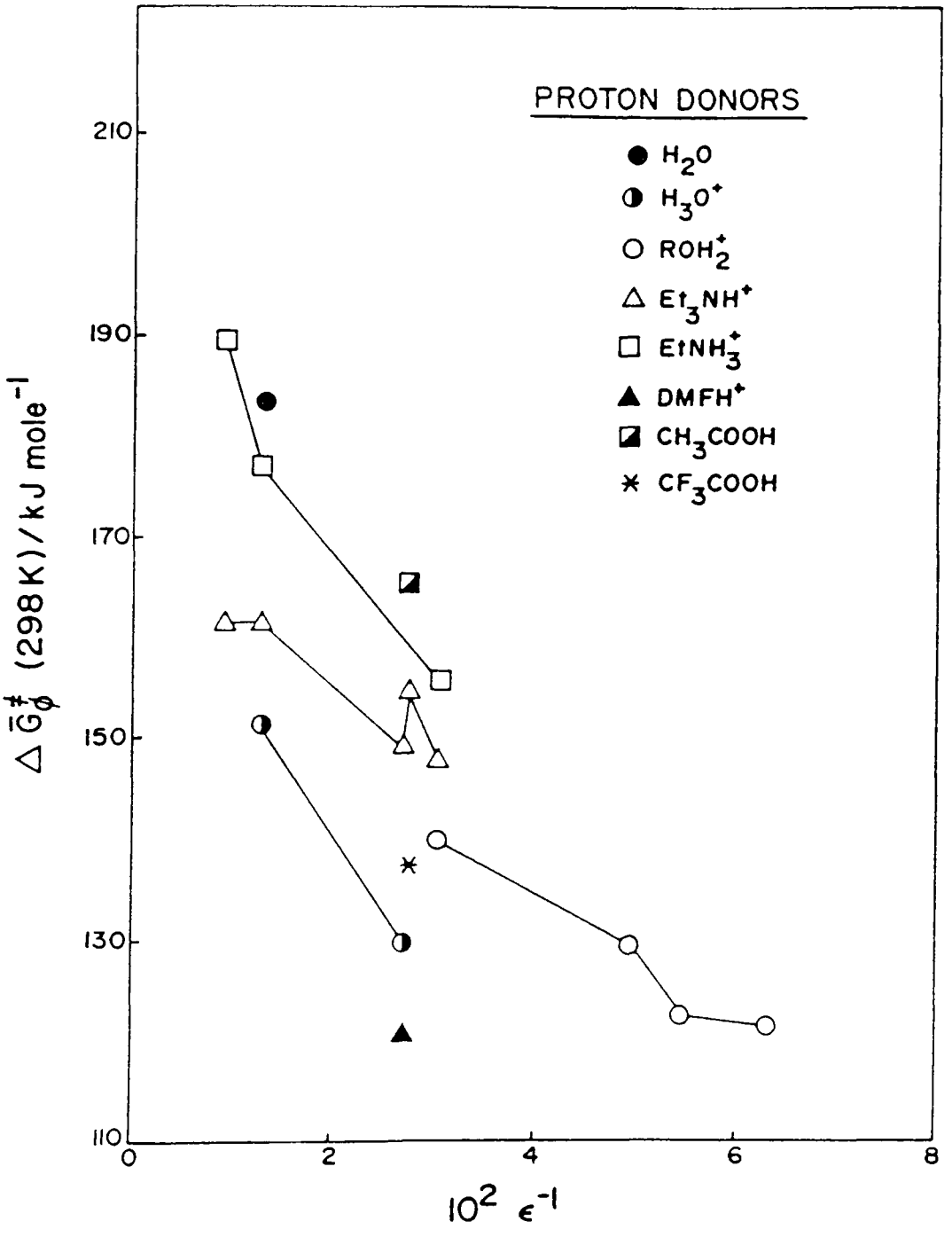

Fig. 78 $\Delta \bar{G}_\phi^\ddagger$ as a function of the reciprocal of the solvent dielectric constant for the h.e.r. at Hg from different proton donors at 298 K.

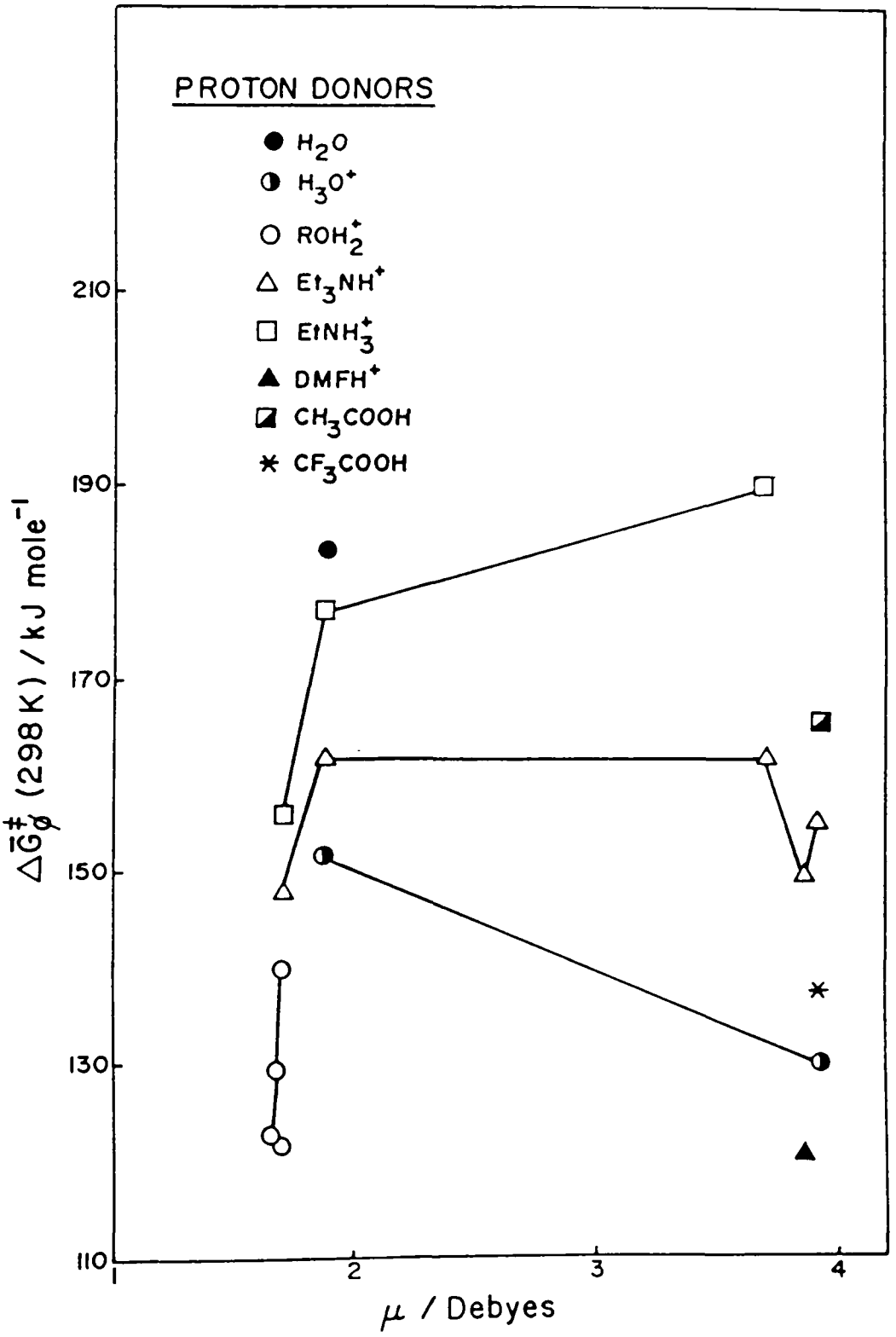

Fig. 79 $\Delta\bar{G}_\phi^\ddagger$ as a function of solvent dipole moment for the h e.r. at Hg from different proton donors at 298 K.

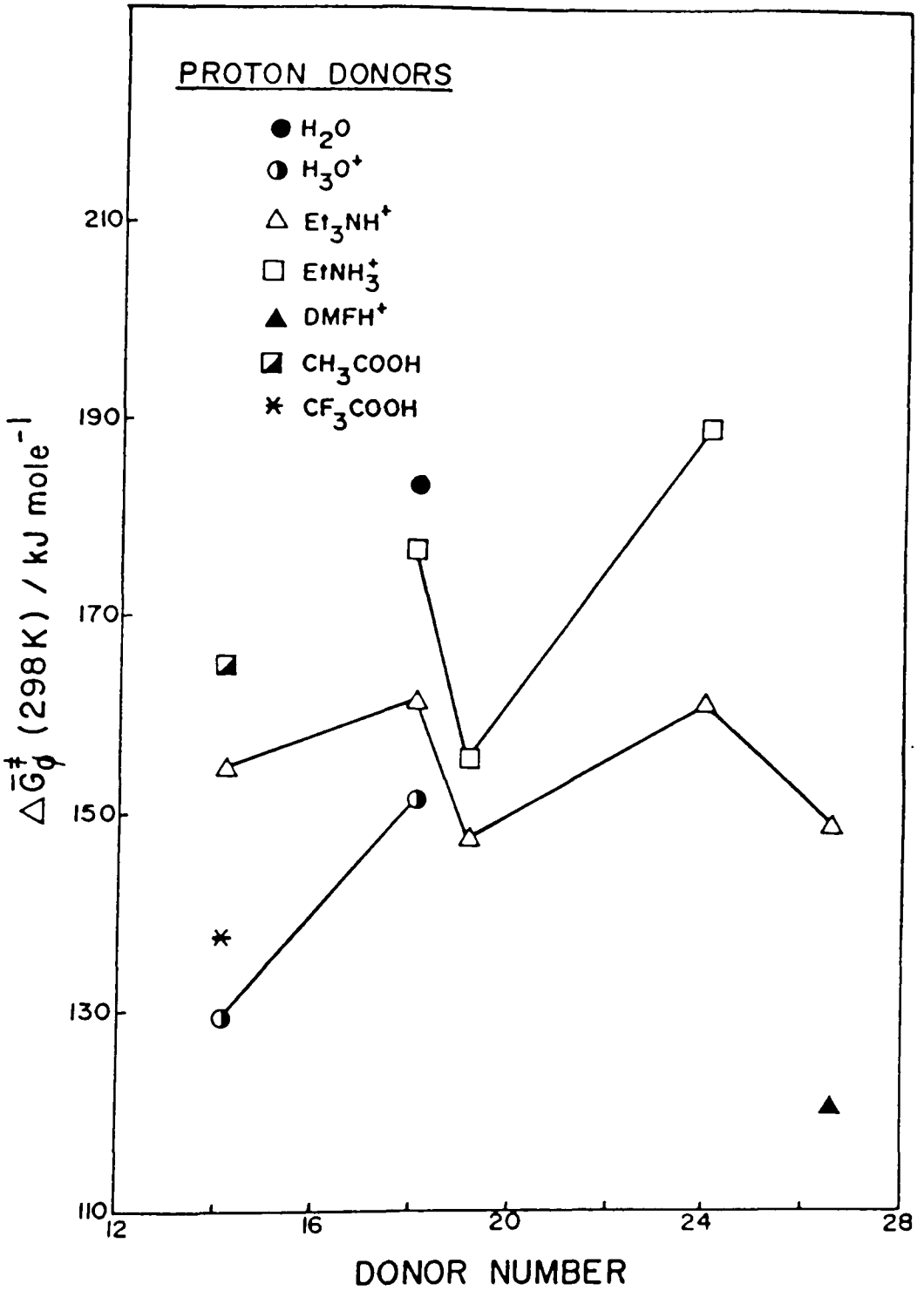

Fig. 80 $\Delta\bar{G}_\phi^{\ddagger}$ as a function of solvent donor number for the h.e r. at Hg from different proton donors at 298 K.

electrical and chemical effects are not significant compared to the "Born-type" interactions. Plots of $\Delta\bar{H}^{\ddagger}_{\phi}$ and log [frequency factor]$_{\phi}$ (proportional to $\Delta\bar{S}^{\ddagger}_{\phi}$) with respect to $1/\epsilon$, solvent dipole moment and solvent donor number are shown in Figs. 81 86 These relations evidently behave in an erratic manner, most likely reflecting specific solvational effects other than the above, e.g., solvent-specific structural effects.

The $\Delta\bar{G}^{\ddagger}_{\phi}$ values in Table 17 for the alkylammonium cations Et_3NH^+ and $EtNH_3^+$ in H_2O, CH_3OH, and $HCONH_2$ show a well known specific solute-solvent interaction of an "hydrophobic" kind related to H bonding between solvent molecules. Several authors (197,198) agree that the (gas phase) proton affinities of amines follow the sequence: $R_3N > R_2NH > RNH_2 > NH_3$ because an increase in size and number of alkyl substituents stabilizes the cation. However, in aqueous solution, the sequence of acid strengths does not follow the steady rise in base strength as would be expected, i.e., $NH_4^+ > Et_3NH^+ \approx EtNH_3^+ > Et_2NH_2^+$, but in aprotic solvents it does (199,200,201). These results have been explained by the degree of hydrogen bonding with the solvent, which depends upon the number of hydrogen atoms in the cation (202) and by steric effects of the alkyl groups which prevent the solvent molecules from close interaction with the positive charge centre (203). The activation energies reflect these specific solvation effects in that $\Delta\bar{G}^{\ddagger}_{\phi}$ ($EtNH_3^+$) > $\Delta\bar{G}^{\ddagger}_{\phi}$ (Et_3NH^+), and the difference between these activation energies decreases as the solvent become less hydrogen bonded, i e. $\Delta(\Delta\bar{G}^{\ddagger}_{\phi})_{HCONH_2} > \Delta(\Delta\bar{G}^{\ddagger}_{\phi})_{H_2O} > \Delta\ (\Delta\bar{G}^{\ddagger}_{\phi})_{CH_3OH}$.

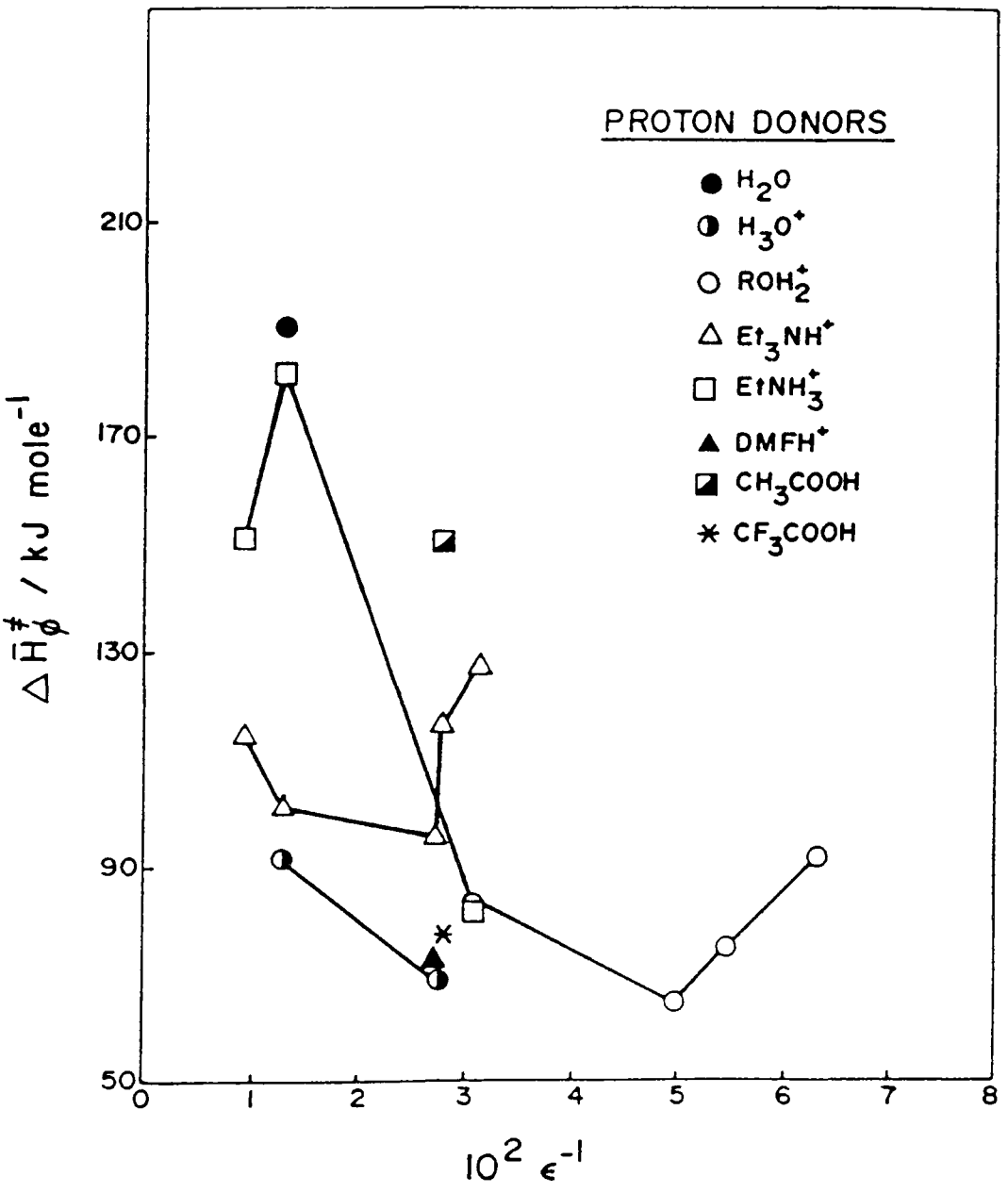

Fig. 81 $\Delta \bar{H}_\phi^\ddagger$ as a function of the reciprocal of the solvent dielectric constant for the h e.r at Hg from different proton donors at 298 K.

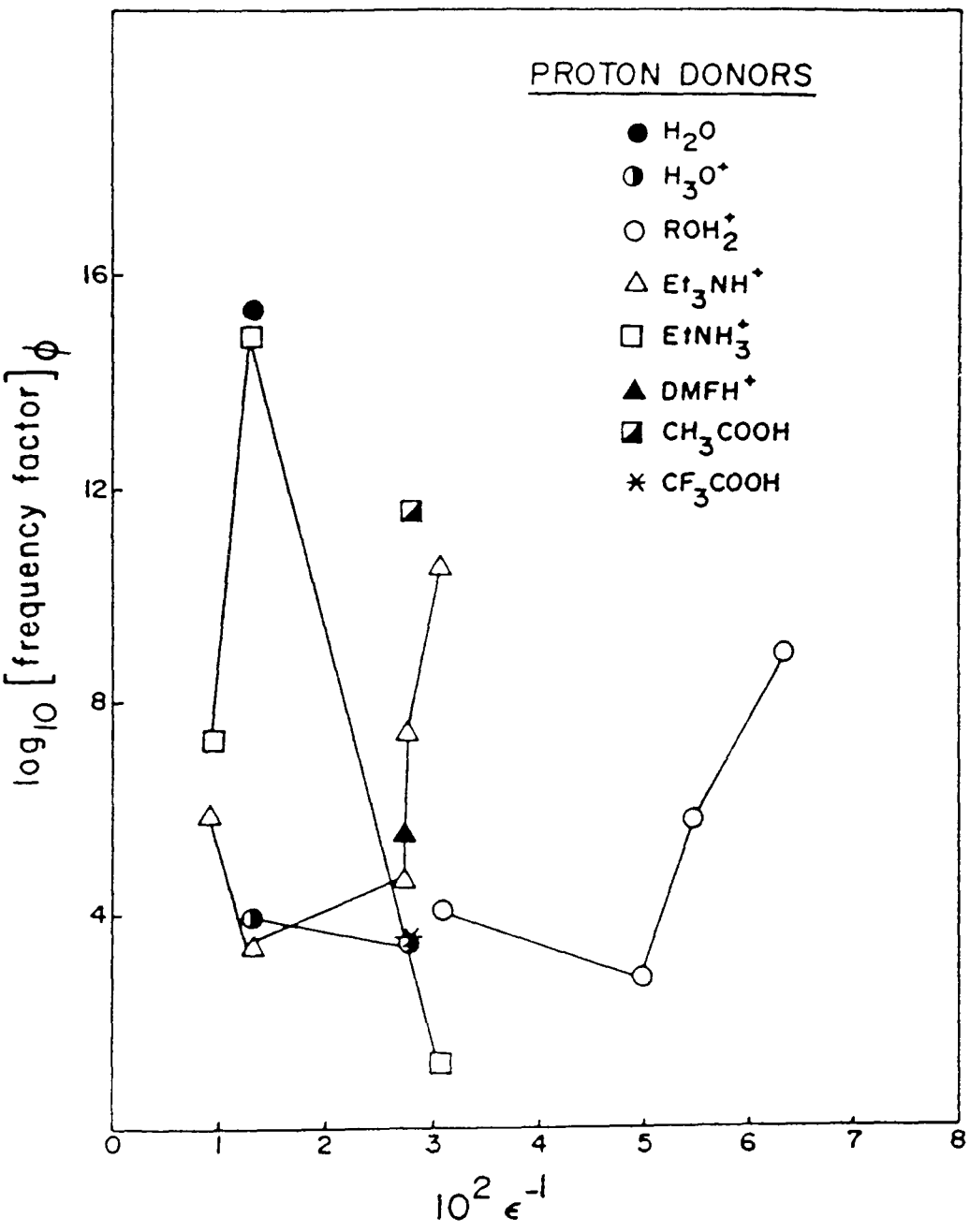

Fig. 82 Log [frequency factor]$_\phi$ as a function of the reciprocal of the solvent dielectric constant for the h e r. at Hg from different proton donors at 298 K.

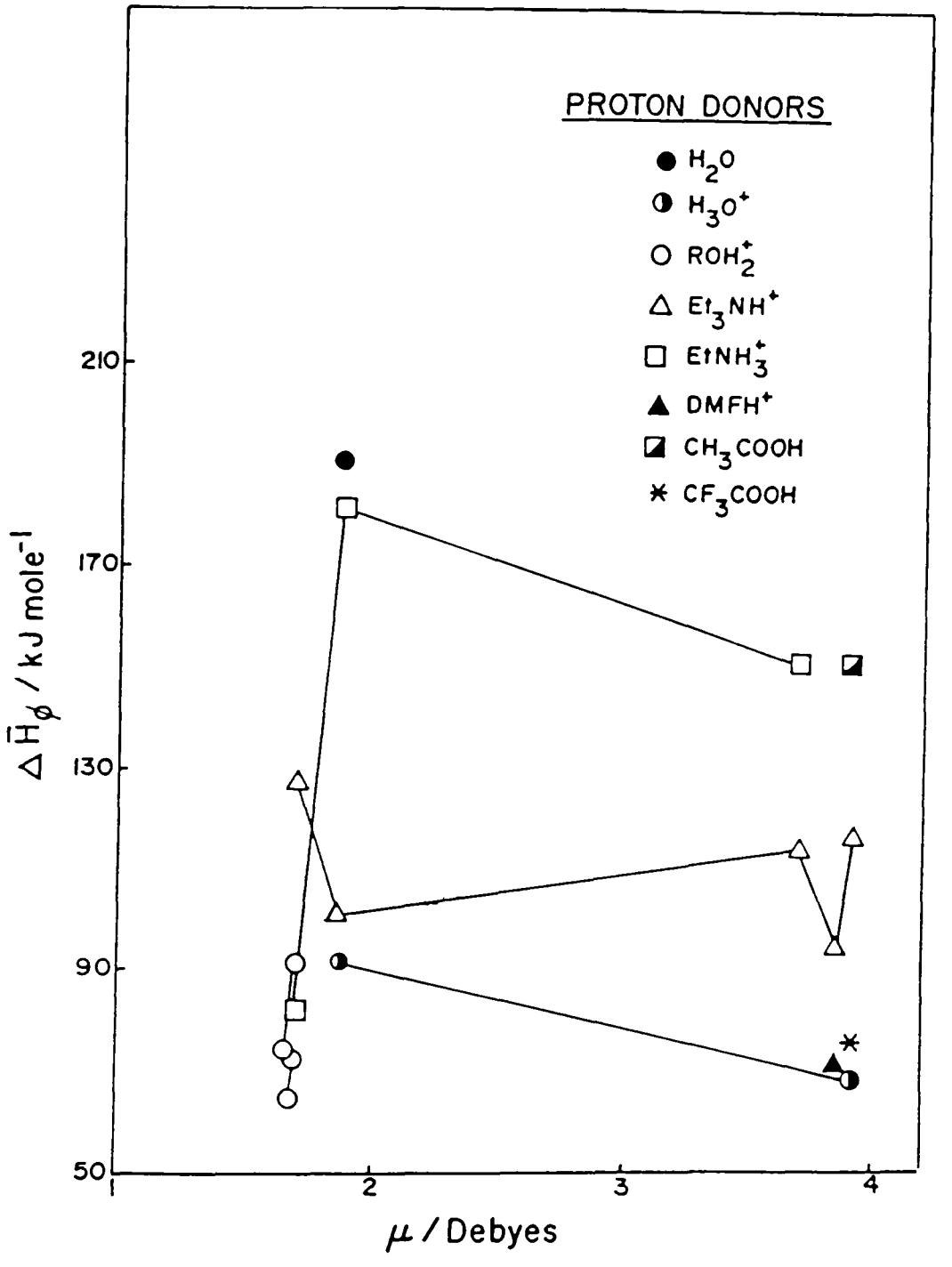

Fig. 83 $\Delta \bar{H}_\phi^\ddagger$ as a function of solvent dipole moment for the h.e.r. at Hg from different proton donors at 298 K.

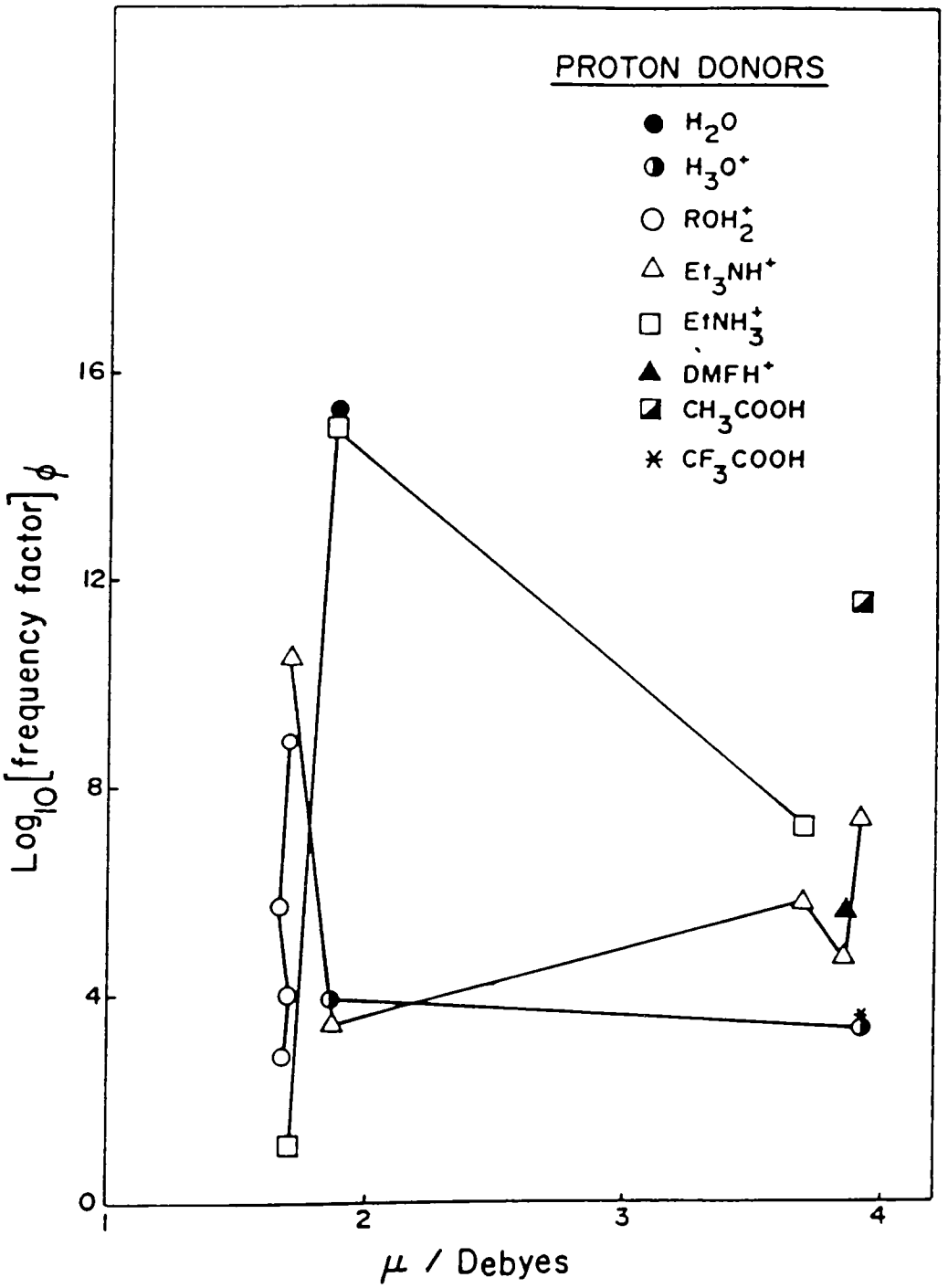

Fig. 84 Log [frequency factor]$_\phi$ as a function of solvent dipole moment for the h.e.r. at Hg from different proton donors at 298 K.

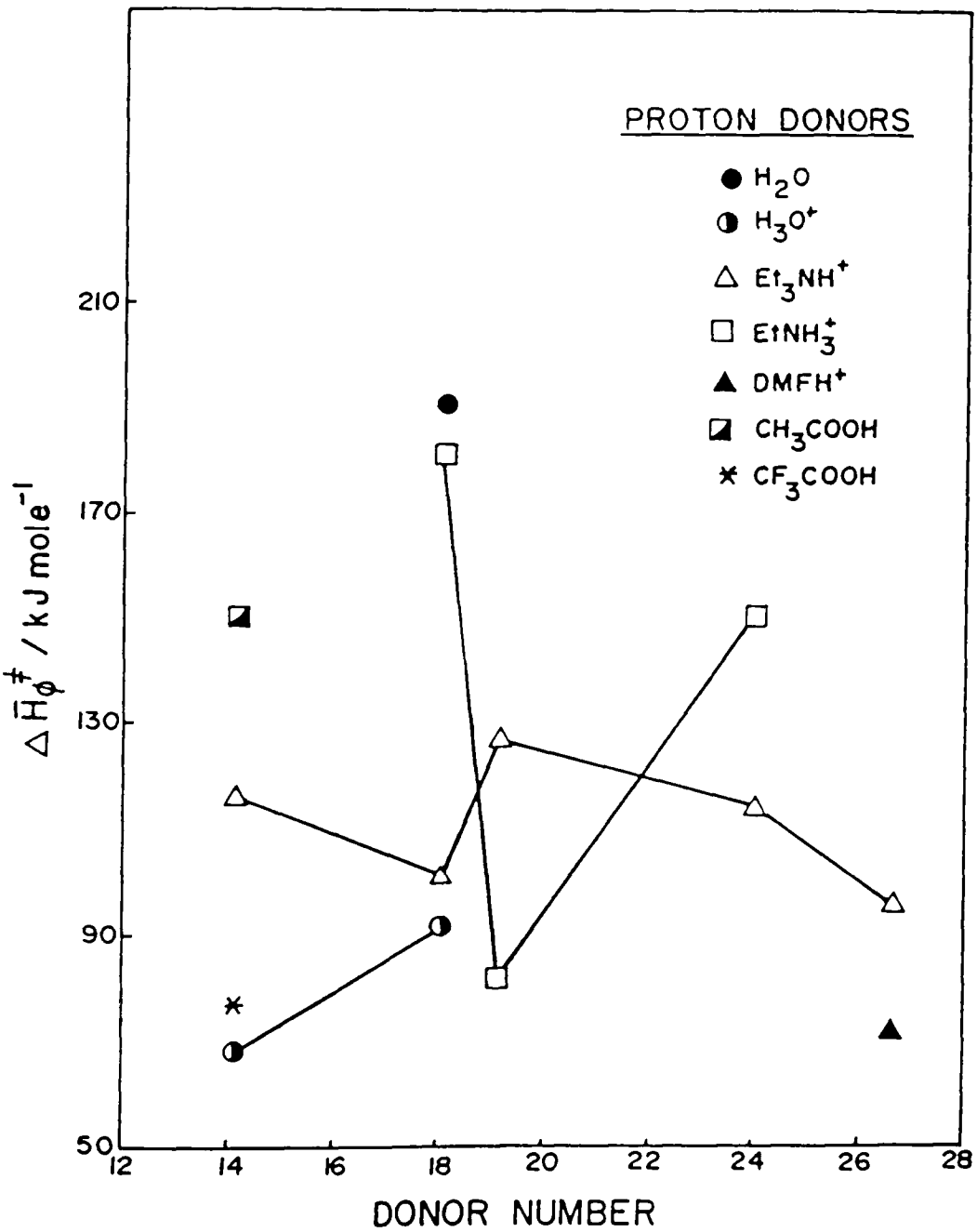

Fig 85 $\Delta \bar{H}_\phi^\ddagger$ as a function of solvent donor number for the h e.r at Hg from different proton donors at 298 K

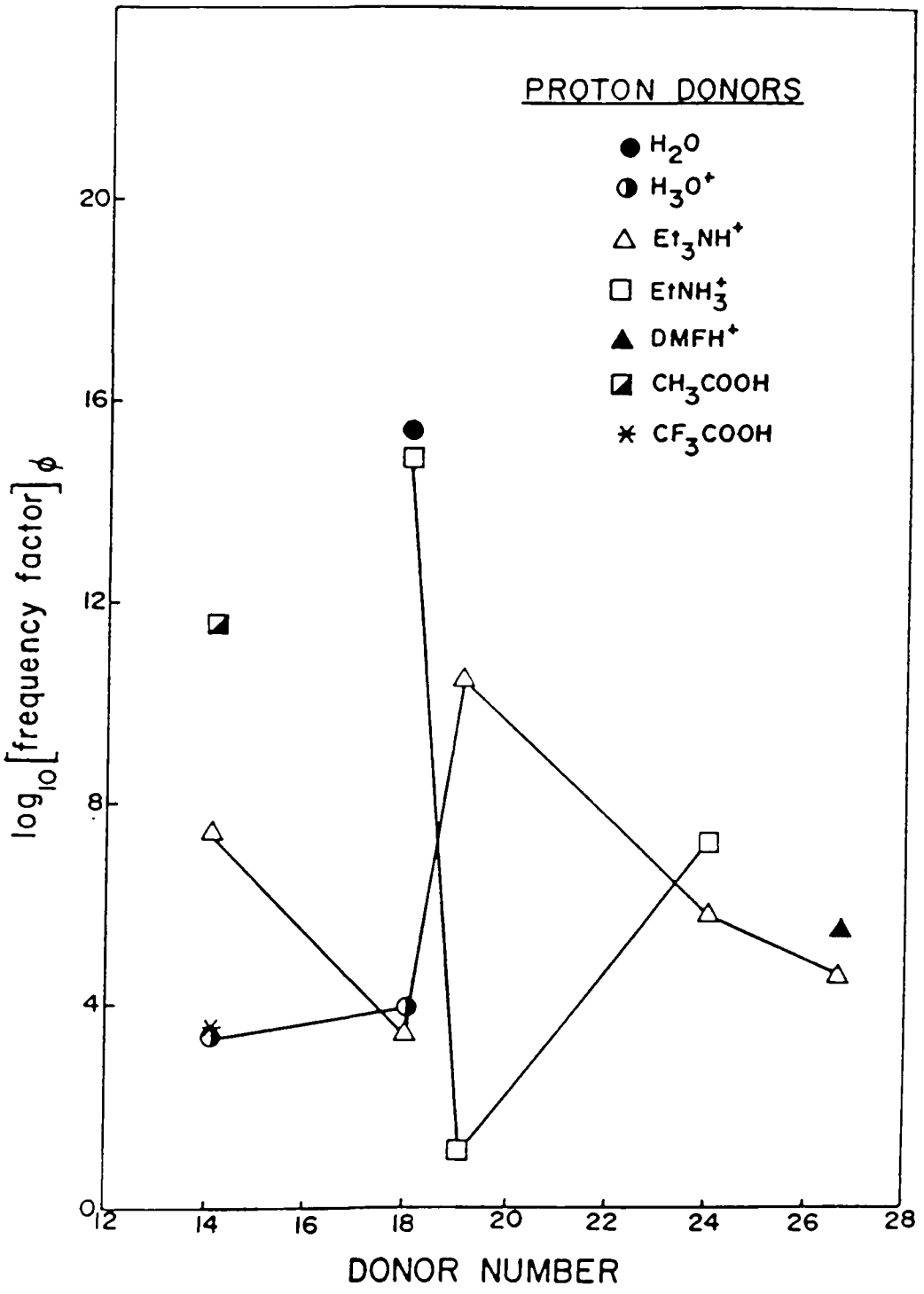

Fig 86 Log [frequency factor]$_\phi$ as a function of solvent donor number for the h.e r. at Hg from different proton donors at 298 K.

11 Brønsted Relation for Heterogeneous Processes

The Brønsted relation for direct homogeneous proton transfer reactions of the type

$$AH^+ + B \rightarrow A + BH^+ \qquad [137]$$

can be represented by

$$k_A = B_a K^{\alpha} = B_a e^{-\alpha \Delta G/RT} \qquad [138]$$

where k_A is the rate constant for proton transfer, K is acid dissociation constant related to the equilibrium Gibbs energy by $\Delta G = -RT \ln K$, and B_a and α are constant for a series of structurally similar acids donating a proton to a given base B in a given solvent at constant temperature. Although the connection between changes in acidity constant in homogeneous proton transfer and changes in electrode potential in electrochemical proton transfer has been well established (see section 4, chapter 1), no attempt has been made to study the effects of changes in acidity constant on heterogeneous proton transfer reactions of the type

$$DH^+ + M + e \rightarrow MH + D \qquad [139]$$

at a fixed metal(M)-solution potential difference.

However, for kinetic rate measurements made at a constant metal solution potential, ϕ, as in the present work, the heterogeneous rate constant will be given by

$$k_h = k_{\phi=o} e^{\pm \beta nF\phi/RT} \qquad [140]$$

where $k_{\phi=o}$ is the "true" chemical heterogeneous rate constant at zero metal solution potential difference for the reaction in eqn.[139] This chemical heterogeneous rate constant might be

expected to have the same relation to the acid dissociation constant as in eqn.[138] for the homogeneous proton transfer case but with different constants α' and B_a', so that the heterogeneous rate constant would then be given by

$$k_h = B_a' e^{\pm\beta nF\phi/RT} e^{-\alpha' \Delta G/RT} \qquad [141]$$

For the same solvent, and for constant temperature and electrode potential measured vs a common fixed reference potential, $C = B_a' e^{\pm\beta nF\phi/RT}$ will be approximately constant for structurally similar acids so that

$$k_h = Ce^{-\alpha' \Delta G/RT} \qquad [142]$$

The corresponding "linear free energy" relation will be

$$\ln k_h = -\alpha' \Delta G/RT + \ln C \qquad [143]$$
$$= \alpha' \ln K + \ln C$$

Since experimental rate measurements usually involve current density ($i = zFcf(\theta)\bar{k}_h$), double-layer effects may be important in the evaluation of eqn.[141] if they change appreciably for a series of acids.

Plots of log i_ϕ versus log K for several proton donors in three solvents (data from Table 17) are shown in Fig 87 for the h.e.r. at Hg at 298 K. The plots give values of α' of 0.33 $\pm$ 0.09, 0.47 (only 2 points), and 0.33 $\pm$ 0.06 in the solvents H_2O, DMF and AN, respectively; these values are similar to those found for the electrochemical symmetry factor (cf. Table 14). It is to be noted that for each solvent system, the same reference electrode is used, so that for each series of proton donors there are no differences of junction potentials involved

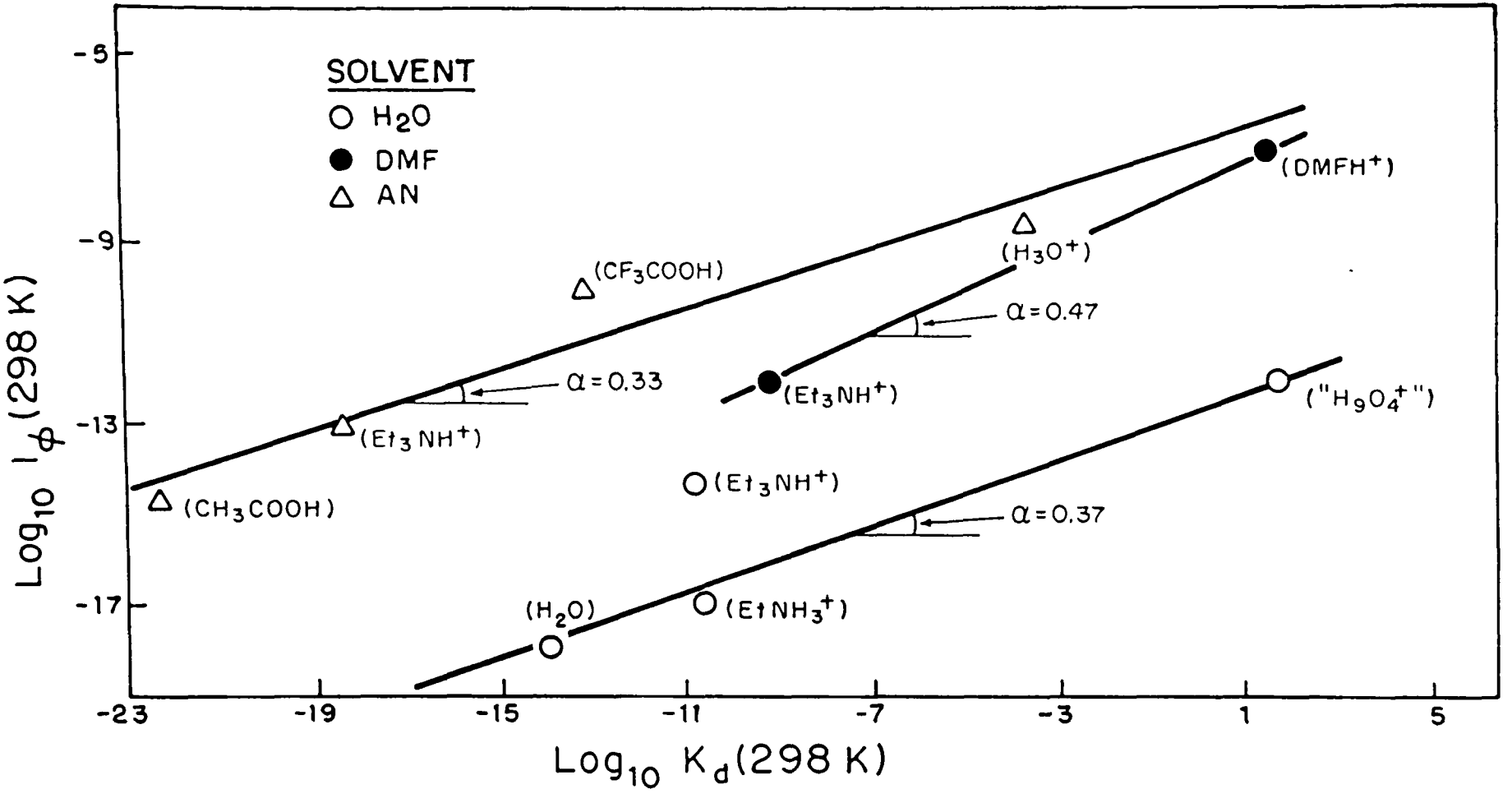

Fig. 87 Brønsted relation for the heterogeneous h.e.r at Hg from different proton donors in several solvents at 298 K.

in the measurements of log i_ϕ.

Values of log i_ϕ for the proton donors Et_3NH^+ and $EtNH_3^+$ are appreciably different in each of the solvents H_2O, $HCONH_2$ and CH_3OH (Table 17), even though their dissociation constants are nearly the same in each solvent. These proton donors exhibit specific steric effects and different double-layer effects, i.e., cation adsorption, and hence do not fit any Brønsted relation well. It is perhaps surprising that a heterogeneous Brønsted relation of the type in eqn.[143] is so clearly indicated, considering the wide range of pK values and the different double-layer effects and active bond sites that are involved for these proton donors investigated in the present work.

12. Estimation of "True" Activation Quantities

It is usually considered that evaluation of the "true" chemical activation quantities $\Delta H^{\ddagger}_{\phi=0}$ and log $A_{\phi=0}$ (which is linearly related to $\Delta S^{\ddagger}_{\phi=0}$) is not possible because the absolute "Galvani" metal-solution potential difference cannot be determined (142) Electrocapillary measurements at liquid Hg in an electrolyte solution enable the potential of zero charge (p z.c.) to be unambiguously measured but, in general, a residual metal-solution potential will still exist because of solvent dipole orientation, i.e., $(\Delta\chi)_{p.z\ c} \neq 0$, and an electron overspill potential difference However, Conway and Dhar (204) using the flat, non-dipolar molecule, 1,4-pyrazine, which itself

is not oriented, were able to establish the charge for zero H_2O dipole orientation at Hg in a 0 1M aq. $HClO_4$ electrolyte at about $q_m = -2\ \mu C\ cm^{-2}$, in the temperature range 293-323 K. Taking the double-layer capacity at Hg as 20 $\mu F\ cm^{-2}$ then gives the potential for zero net dipole orientation as 0 1 V negative to the p.z.c. and this will also correspond to the potential of zero field, i.e., for the condition $\phi=0$. Also, the potential drop due to oriented water dipoles at the potential of zero charge for Hg has been suggested by Trasatti (205,206), on the basis of a number of considerations and pieces of experimental evidence, to be about -0.08V.

The p.z.c. for 0.1M aq. HCl at Hg has been determined from electrocapillary measurements (207) to be ca. -0.17 V versus RHE*(298 K) so that the potential of zero field is ca. -0.27 V versus RHE (298 K). The potential dependence of $\Delta\bar{H}^{\ddagger}_{\phi}$ (Fig. 51) and log A_{ϕ} (Fig. 53) has been determined for this electrolyte system using a potential scale referred to the fixed metal solution potential of the reference electrode $Pt|H_2$, 0 1M HCl (H_2O) at 298 K, i.e , RHE (298 K). Hence, the zero field potential can be located on this potential scale and the corresponding "true" activation quantities are thence found to be $\Delta H^{\ddagger}_{\phi=0} = 82$ kJ mole ^{1} and log $A_{\phi=0} = 4\ 65$ (or $\Delta S^{\ddagger}_{\phi=0} = 181$ J K^{-1}mole ^{1}). In general, the above procedure can be applied to any electrolyte system provided electrocapillary data is

---

* The symbol RHE stands for a reversible hydrogen electrode immersed, not in a standard solution, but in the same electrolyte as the electrode under study

available and the potential dependence of the activation parameters is known. However, the only reliable data at present available are for the $Hg|H_2O$ interface.

13. Nature of Activation in Electrochemical Proton Transfer

In electrochemical proton transfer, there is a coupled electron and H-particle transfer with neutralization of the proton charge and elimination of the proton's solvation. The first meaningful treatment of this coupled process was given by Gurney (15) who recognized the role of quantum-mechanical tunneling of the electron. Soon after, Horiuti and Polanyi (22) and Butler (19) showed, in terms of potential energy diagram representations, how the state of hydration of the reactant H^+ ion and the energy of chemisorption of the H atom at the electrode metal could determine the proton transfer kinetics.

Following Bell's calculation (31), the contribution of proton tunneling in the proton discharge step of the h.e.r. was discussed by Bawn and Ogden (33) and Appelby and Ogden (34). Later, Conway (36), Christov (35), and Matthews and Bockris (208) gave diagnostic calculations for proton-tunneling and H/D isotope effects in the kinetics of the h.e.r. More detailed treatments of the classical activation process in proton transfer at electrodes were given by Parsons and Bockris (23) and by Conway and Bockris (87), following the Butler model. Conway, Bockris and Lovrecek (193, 194) took into account the contribution to the potential-dependent activation energy that arises from both the hydration shell and $O\text{-}H^+$ bond energy

changes in the hydrated H_3O^+ ion as the H entity is transferred to the metal In all these bond-stretching treatments of activation, which may involve varying degrees of proton tunneling (cf. the calculation of Bell, ref. 31), vibrational activation is considered to be achieved by a wide range of coupled oscillations between the proton and its primary solvation shell and surrounding solvent molecules which can take up energy in thermal fluctuations from the surroundings. The availability of such vibrational modes for the proton in H_2O, and in general for ions in liquids at ordinary temperatures, is demonstrated by their large heat capacity (56).

More recent treatments of proton discharge have been based on the general theories of electron transfer of Marcus (45, 46, 47) and Hush (44), but place little emphasis on the specific nature of the solvated proton in solution. The most developed approach of this kind was the DKL model given in 1969 by Dogonadze, Levich and Kuznetsov (48), in which they rejected classical "bond-stretching" activation, because the vibrational quantum $h\nu_{OH}$ for the O-H symmetrical mode in H_3O^+ or H_2O ($\approx$42 kJ mole ^{1}) is much greater than the thermal energy kT at ordinary temperatures so that transitions from vibrational excited states were found to be negligible They envisaged the OH bond in H_3O^+ as relatively unchanged because of the supposedly large quanta, $h\nu$, required for activation of its vibrations, so that only long-range fluctuations in solvent dielectric polarization in the proton's solvation cosphere were considered in the

activation process

Conway et al. (209,54,55) have pointed out that this approach treats $O\text{-}H^+$ bond activation in H_3O^+ as though it were an ion in the gas phase, and does not take into account the broad range of lower frequency hydration lattice modes, particularly those associated with the primary hydration shell, i.e., $H_9O_4^+$, which are available for activation. Also in the DKL model the Born polarization energy of the surrounding dielectric medium is considered to be the main ion-solvent interaction and no account is made of specific ion-solvent interactions which can be very large especially for the proton, i.e., the interaction energy of H_3O^+ with H_2O to form the primary hydration shell is ca. 320 kJ mole ^{1} (210).

Krishtalik and coworkers (137,138,139,140) have examined the question of medium and bond-nature effects in proton discharge in relation to the DLK model, where considerable emphasis is placed on the role of the solvent medium. In an interesting experimental approach (138), the observation of equal "apparent" heats of activation for CH_3CNH^+ and H_3O^+ in virtually anhydrous CH_3CN at Hg (see Table 19) and the significantly different "apparent" heats of activation for H_3O^+ in H_2O and CH_3CN, were taken to indicate that the activation energy is completely determined by the solvent medium and is independent of the nature of the bond ($N\text{-}H^+$ or $O\text{-}H^+$) being broken. This conclusion was based, however, on comparison of $\Delta H^{\ddagger}_{\eta=0}$ values, neglecting the influence of the $T\Delta S^{\ddagger}_{\eta=0}$ components of $\Delta G^{\ddagger}_{\eta=0}$ values although

the frequency factors were known to be different. Also, Khan (211) has pointed out that, even on the basis of the DKL approach, different Gibbs energies of activation would be expected because of the unequal radii of the H_3O^+ (0.14 nm) and CH_3CNH^+ (0.25 nm) ions. Also, according to the bond-stretching model, one would also expect a different Gibbs energy of activation on the basis of force constants alone, since the stretching frequencies of $CH_3CN\text{-}H^+$ and $H_2O\text{-}H^+$ bonds are different, i.e., the difference in $\tilde{\nu}_1$, is ≥ 200 cm^{-1}.

In another interesting contribution to the examination of the mechanism of proton discharge, Conway and Tessier (54) made a comparative study of the kinetics of the h.e.r. at Hg from the unhydrated H_3O^+ ion in pure $CF_3SO_3^-H_3O^+$ (a melt above 307 K) and the fully hydrated H^+ ion, i.e. $H_9O_4^+$, in 1M aqueous CF_3SO_3H. Significantly different "apparent" activation parameters were found for these media and the greater rate of proton discharge from $H_9O_4^+$ than from H_3O^+ was attributed to the many more HO-vibrational and librational modes that can be involved in the activation process with the aquo-H^+ ion.

In the previous experimental studies on the proton discharge mechanism, a comparison of "apparent" activation parameters (i.e., at constant overpotential) was made but, under these conditions as previously discussed, a quantitatively meaningful comparison of the proton discharge kinetics is difficult. In the present work, the kinetic parameters for different proton sources in different solvent media were determined at a constant

metal solution potential ϕ (constant field), so that a "chemically" more meaningful comparison could be made.

It is evident from a comparison of the kinetic parameters in Table 17, that there can be appreciable differences for the same proton donor in different solvent media, and for different proton donors in the same solvent. The following observations can be made:

i) In AN, for the proton donors CH_3COOH and CF_3COOH, which are of similar size and have the same active O-H bond, the kinetic parameters are appreciably different.

ii) The Gibbs energies of activation for the proton donor Et_3NH^+ in H_2O (ϵ=78) and in $HCONH_2$ (ϵ=110) are almost identical, i.e., $\Delta\bar{G}^{\ddagger}_{\phi} \approx 161 \pm 11$ kJ mole^{-1}, even though there is an appreciable difference in solvent dielectric constant.

iii) For the same proton donor, H_3O^+, in AN (ϵ=36) and in H_2O (ϵ=78), the entropies of activation are almost identical, i.e., $\Delta\bar{S}^{\ddagger}_{\phi} \approx -204 \pm 11$ J K^{-1}mole^{-1}, even though the solvent dielectric constant and the solvent structure are extremely different. It was also noted in section B-5-a, this chapter, that the entropic (β_S) and enthalpic (β_H) components of the symmetry factor (β) are almost the same in both media (see Table 14).

iv) For the proton donors Et_3NH^+ and $EtNH_3^+$ which have the same charge centre, i.e., $\geq N\text{-}H^+$, the activation parameters are appreciably different in each of the

solvents, H_2O, $HCONH_2$ and CH_3OH

The previous observations indicate that the nature of the ruptured bond and specific solvational and solvent-structure aspects, particularly those involved with the primary solvation shell, must be important in the activation process. Previously (see Figs. 81 and 82) it was shown that the $\Delta\bar{H}^{\ddagger}_{\phi}$ and log [frequency factor]$_{\phi}$ (proportional to $\Delta\bar{S}^{\ddagger}_{\phi}$) quantities have no correlation with the solvent dielectric constant, probably because of the specific, short-range solvational effects that are involved. However, the Gibbs energy of activation, $\Delta\bar{G}^{\ddagger}_{\phi}$, does show a "Born-type" correlation, i.e., with the reciprocal of the solvent dielectric constant (see Fig. 78) indicating the importance of the general solvent medium.

From the results recorded and described above, it is to be concluded that specific as well as general medium effects have to be included in any interpretation of the mechanism of proton discharge, and probably in other electrode processes too. In fact, more recent developments of the DKL model (60,212) which have accounted for specific effects through inclusion of excited vibrational levels and their associated anharmonicities in the initial-state H_3O^+ ion, are in better agreement with the experimentally found <u>linear</u> Tafel behaviour that does not arise from treatments based on activation models involving only harmonic oscillators.

CONTRIBUTIONS TO ORIGINAL RESEARCH

1. Reliable experimental data is required to provide a basis for characterizing the unconventional temperature-dependence of the Tafel slope and symmetry factor and for a better understanding of the nature of the activation process in the elementary act of complex electron and atom transfer. Published data on the electrode kinetics of charge-transfer processes in nonaqueous media are very scarce, particularly for the h.e r at Hg. In the present work, new current-potential relations were obtained for the h.e.r. at Hg from several proton sources (H_3O^+, ROH_2^+, $DMFH^+$, $EtNH_3^+$, Et_3NH^+, H_2O, CH_3COOH, CF_3COOH) in aqueous and nonaqueous media (CH_3OH, 1-propanol, 2-propanol, isobutanol, $HCONH_2$, DMF and AN). Polarization behaviour was examined over a wide range of temperature for each system, and in some cases, this approach allowed a comparison of the kinetic behaviour at liquid and solid Hg (F P = 234 2 K) to be made.

2 In order to make a quantitatively meaningful comparison of the proton donor discharge kinetics in the different systems it is necessary to compare activation parameters determined at constant metal solution potential (or field) rather than "apparent" activation parameters determined at constant overpotential Although kinetic activation parameters have been determined at a fixed metal-solution

potential, ϕ, by Weaver et al. (77,78) for ionic redox reactions, this approach has not been applied to an atom/electron transfer reaction. In the present work, the kinetic activation parameters for various proton sources in different solvent media were determined at a constant metal solution potential, ϕ, by means of isothermal and non-isothermal reference electrode cells which allow corrections to be made for variation of the reference electrode potential with temperature and solution composition. Comparison of these "chemically" more meaningful activation parameters indicates the importance of specific as well as general medium effects (e.g., relations between $\Delta\bar{G}^{\ddagger}_{\phi}$ and ϵ) in the activation process.

3 Non-isothermal reference cell measurements under conditions where the thermal junction potential is minimized, i.e., the Eastman thermocell (219), were used in the present work to fix the reference electrode potential with respect to temperature. These direct "electrochemical" measurements allowed the half-cell reaction entropies of the reference electrodes $H^+|H_2$, Ag|AgCl and $Ag^+|Ag$, and the corresponding single ion entropies of H^+, Cl^-, and Ag^+ to be determined in several nonaqueous media. Practically all previous attempts at dividing experimental partial molar entropies of electrolytes in nonaqueous solutions into there ionic components have used the "correspondence method" based

entirely on the ionic entropies of ions in aqueous solution Although there is excellent agreement in the values determined by the two methods in aqueous media, there are appreciable differences in nonaqueous media.

4. Although a temperature-dependence of the symmetry factor has been discussed in terms of a potential-dependent entropy of activation, experimental evidence for the potential dependence of the entropy of activation has not previously been demonstrated. For ionic redox reactions involving supposedly only outer-shell reorganization in the activation process, there is little or no dependence of the entropy of activation, $\Delta\bar{S}^{\ddagger}_{\phi}$, on potential. For atom/electron transfer reactions, the entropy of activation has been assumed to be constant with changes in potential in almost all earlier work. However, the present results for the h.e.r. at Hg and the b.e.r. at vitreous carbon show that $\Delta\bar{S}^{\ddagger}_{\phi}$ is substantially dependent on potential, so that the effect of electrode potential on electrochemical rates for a simple discharge process must now be considered as a combination of two effects:

   i) an "inner" effect on the Fermi level of electrons relative to "vacuum", and

   ii) an "outer" effect on the solvent structure and state of reactant ion and transition state solvation in the double-layer of the electrode

interphase.

This is a new and hitherto unsuspected effect in electrode kinetics, which results in a symmetry factor of the form, $\beta = \beta_H + T\beta_S$, where β_H and $T\beta_S$ are the enthalpic and entropic components of the symmetry factor corresponding to the potential-dependence of the enthalpy and entropy of activation, respectively. Contrary to conventional assumptions the Tafel slope is not given by the usual relation, $b = \pm 2.3RT/\beta F$ but rather by $b = \pm 2.3RT/(\beta_H + T\beta_S)F$ which can now account for the often observed "anomalous" temperature-dependence of the Tafel slope.

5. Although "compensation effects" are a widely observed phenomenon in a number of kinetic and thermodynamic processes, they have not been demonstrated for electrochemical kinetic activation quantities In the present work for the h.e r at Hg, an important compensation effect between various values of β_H and β_S is demonstrated that makes the overall symmetry factor, β, approximately constant and near 0 5 at 298 K, even though β_H and β_S vary considerably The enthalpy of activation, $\Delta\bar{H}_\phi^\ddagger$, and the entropy of activation, $\Delta\bar{S}_\phi^\ddagger$, also vary together in a systematic and compensatory way, i.e., factors which decrease $\Delta\bar{H}_\phi^\ddagger$ also decrease $\Delta\bar{S}_\phi^\ddagger$ for the system.

6. The linear free energy relationship, i e , Brønsted relation, between the rates of "homogeneous" proton transfer and acid/base strengths is well established (40), but has not been previously shown for "heterogeneous" proton transfer. In the present work, where kinetic rate measurements were made at a constant metal-solution potential, ϕ, an "heterogeneous" Brønsted relation between the rate of proton transfer (i_ϕ) and the acid dissociation constant of the proton donor (pK_d) is clearly demonstrated in several solvents.

REFERENCES

1. A.N. Frumkin, "Adv. Electrochem. and Electrochem. Eng." vol. 3, Eds., P. Delahay and C. Tobia, Wiley Interscience, N.Y., 1963, p. 287.

2. J.O'M. Bockris, in "Modern Aspects of Electrochemistry", vol. 1, Eds., J.O'M Bockris and B.E. Conway, Butterworths, London, 1954.

3. J.N. Brønsted and N.L. Ross-Kane, J. Amer. Chem. Soc., 53, 3624 (1931).

4. A.N. Frumkin, Zeit. Phys. Chem., 160, 116 (1932).

5. R.P. Bell, "The Proton in Chemistry", London, 1973; see also R.P. Bell and D. Goodall, Proc. Roy. Soc., London, A294, 273 (1966).

6. J. Horiuti, "Transactions Symposium on Electrode Processes", The Electrochemical Society, Wiley, N.Y., 1961, Chap. 2, p. 17.

7. T. Langmuir, J. Amer. Chem. Soc., 40, 1361 (1918); ibid, 54, 2798 (1932).

8. M.I. Temkin, Zhur. Fiz. Khim., 15, 296 (1941).

9. B.E. Conway and J.O'M. Bockris, J. Chem. Phys., 26, 532 (1957).

10. S. Trasatti, J. Electroanal. Chem., 39, 163 (1972).

11. D.C. Walker, Can. J. Chem., 45, 807 (1967); Anal. Chem., 39, 896 (1967).

12. T. Pyle and C. Roberts, J. Electrochem. Soc., 115, 247 (1968).

13. D.J. MacKinnon, Ph.D. Thesis, U. of Ottawa, (1969).

14. J. Tafel, Z. Phys. Chem., 50, 641 (1905).

15. R.W. Gurney, Proc. R. Soc. (London), A134, 137 (1932).

16. R.W. Gurney and R.H. Fowler, Proc. R. Soc. (London) A136, 378 (1932).

17. F.P. Bowden and R. Rideal, Proc. Roy. Soc. (London), A120, 59 (1928).

18. F.P. Bowden, Proc. R. Soc. (London), A125, 446 (1929); A126, 107 (1929).

19. J.A.V. Butler, Proc. Roy. Soc. (London), A157, 423 (1936).

20. T. Erdey-Gruz and M. Volmer, A. Phys. Chem., 150, 203 (1930); 162, 53 (1932).

21. J.A.V. Butler, Trans. Faraday Soc., 19, 729 (1924); 28, 379 (1932).

22. J. Horiuti and M. Polanyi, Acta Physicochim. SSSR, 2, 505 (1935).

23. R. Parsons and J.O'M. Bockris, Trans. Faraday Soc., 47, 914 (1951).

24. B.E. Conway and J.O'M. Bockris, Can. J. Chem., 35, 1124 (1957).

25. O.A. Essin and V. Kozheurov, Acta Physicochim., 16, 169 (1942).

26. A.R. Despic and J.O'M. Bockris, J. Chem. Phys., 32, 389 (1960).

27. J.O'M. Bockris and R. Parsons, Trans. Faraday Soc., 45, 916 (1949).

28. H. Nürnberg, Fortschitte Chem. Forsch., 8, 241 (1967); Zeit. Tech. Chem., 12, 713 (1967); Disc. Faraday Soc., 39, 52 (1965).

29. L. Young, "Anodic Oxide Films", Academic Press, N.Y., 1961.

30. E. Wigner, Z. Physik. Chem., B19, 203 (1933).

31. R.P. Bell, Proc. Roy. Soc. (London), A139, 436 (1933); A48, 241 (1935).

32. C. Eckart, Phys. Rev., 35, 1303 (1930).

33. C.E.H. Bawn and G. Ogden, Trans. Faraday Soc., 30, 432 (1934).

34. M.P. Appleby and G. Ogden, J. Chem. Soc., 163 (1936).

35. St. G. Christov, Electrochim. Acta, 4, 194 (1961); 4, 306 (1961); 9, 575 (1964).

36. B.E. Conway, Can. J. Chem., 37, 178 (1959).

37. M Salomon and B.E. Conway, Disc. Faraday Soc., 39, 223 (1965).

38. B.E. Conway and M. Salomon, J. Chem. Phys., 41, 3169 (1964).

39. J. O'M. Bockris and D.B. Matthews, J. Chem. Phys., 44, 298 (1966).

40. J.N. Brønsted and K.J. Pederson, Z. Phys. Chem., 108, 185 (1924).

41. M. Eigen, M.L. Ahrens, W. Kruse, and G. Maass, Ber. Bunsengesell. Phys. Chem., 74, 380 (1970).

42. R.P. Bell, Proc. Roy. Soc. (London), A154, 414 (1936).

43. J.N. Brønsted and N.L. Ross-Kane, J. Amer. Chem. Soc., 53, 3024 (1931).

44. N.S. Hush, J. Chem. Phys., 28, 962 (1958).

45. R.A. Marcus, J. Chem. Phys., 24, 966 (1956).

46. R.A. Marcus, J. Chem Phys., 26, 867 (1957).

47. R.A. Marcus, An. Rev. Phys. Chem., 15, 155 (1964).

48. R.R. Dogonadze, A.M. Kuznetsov, and V.G. Levich, Elektrokhimiya, 3, 739 (1967); Electrochim. Acta, 13, 1025 (1968); 15, 353 (1970).

49. J. Weiss, Discuss. Faraday Soc., 1, 68 (1947).

50. W. Libby, J. Phys. Chem., 56, 863 (1952).

51. R.J. Marcus, B.J. Zwolinski, and H. Eyring, J. Phys. Chem., 58, 432 (1954).

52. R.A. Marcus, J. Chem. Phys., 38, 1858 (1963); 39, 1734 (1963); Can. J. Chem., 37, 155 (1959); J. Phys. Chem., 67, 853 (1963).

53. R.A. Marcus, J. Chem. Phys., 43, 679 (1965).

54. B.E. Conway and D.F. Tessier, Int. J. of Chem. Kin., 13, 925 (1981).

55. A.J. Appleby, J.O'M. Bockris, R.K. Sen, and B.E. Conway, in "M.T.P. Int. Rev. Sci. (Electrochemistry)", vol. 6, Ed., J. O'M. Bockris, Butterworths, London, chap. 1.

56. T. Ackermann, Disc. Faraday Soc., 24, 180 (1957); Z. Phys. Chem., N.F., 27, 253 (1961).

57. L.I. Krishtalik, Elektrokhimiya, 2, 624 (1966); Electrochim. Acta, 13, 1045 (1968).

58. P.D. Tyma and M.J. Weaver, J. Electroanal. Chem., 111, 195 (1980).

59. J.M. Saveant and D. Tessier, J. Electroanal. Chem., 65, 57 (1975); J. Phys. Chem., 81, 2192 (1977); 82, 1723 (1978).

60. Y.I. Kharkats, and J. Ulstrup, J. Electroanal. Chem., 65, 555 (1975).

61. A.M. Kuznetsov, J. Electroanal, Chem., 159, 241 (1983).

62. J. Ulstrup, Electrochim. Acta, 29, 1377 (1984).

63. A.M. Kuznetsov, J. Electroanal. Chem., 180, 121 (1984).

64. B.E. Conway, Lijun Bai and D.F. Tessier, J. Electroanal. Chem., 161, 39 (1984).

65. Z.A. Jofa and V. Stepanova, Zh. fiz. Khim., 19, 125 (1945).

66. A.K. Covington and T. Dickinson, Eds., "Physical Chemistry of Organic Solvent Systems", Plenum Press, N.Y., 1973.

67. J.D. Littlehailes and B.J. Woodhall, Discuss. Faraday Soc., 45, 187 (1968).

68. T. Fujinaga and I. Sakamoto, Pure and Appl. Chem., 52, 1387 (1980).

69. T. Fujinaga and I. Sakamoto, J. Electroanal, Chem., 67, 201 (1976).

70. R. De Levie and J.C. Kreuser, J. Electroanal. Chem., 38, 239 (1972).

71. E.R. Gonzalez and S. Srinivasan, Electrochimica Acta, 27, 1425 (1982).

72. E.R. Gonzalez, R. Naranjo, K.-L. Hsueh and S. Srinivasan, Electrochim. Acta, 28, 165 (1983).

73. D.M. Novak and B.E. Conway, J. Chem. Soc., Faraday Tans. I, 77, 2341 (1981).

74. A. Inesi and L. Rampazzo, J. Electroanal. Chem. and Interfac. Electrochem., 44, 25 (1973).

75. A. Inesi and L. Rampazzo, J. Electroanal. Chem. and Interfac. Electrochem., 49, 85 (1974).

76. W. Gerrard, R.W. Madden and P. Tolcher, J. of Appl. Chem., 5, 28 (1955).

77. M.J. Weaver, J. Phys. Chem., 83, 1748 (1979).

78. E.L. Yee, R.J. Cave, K.L. Guyer, P.D. Tyma, and M.J. Weaver, J. Am. Chem. Soc., 101, 1131 (1979).

79. A.M. Azzam, J.O'M. Bockris, B.E. Conway and H. Rosenberg, Trans. Faraday Soc., 46, 918 (1950).

80. B.E. Conway, H. Angerstein-Kozlowska, W.B.A. Sharp, and E. Criddle, Anal. Chem., 45, 1331 (1973).

81. J.W. Vaughn, "The Chemistry of Nonaqueous Solvents", vol. 2, Ed., J.J. Lagowski, Plenum Press, N.Y., 1967, p. 191.

82. G.J. Janz and R.P.T. Tomkins, "Nonaqueous Electrolytes Handbook", vol. I and II., Academic Press, N.Y., 1972.

83. R. Corkum and J. Milne, Can. J. Chem., 56, 1832 (1978).

84. T. Gramstad and R.M. Haszeldine, J. Chem. Soc., 4069 (1957).

85. B.E. Conway and D.F. Tessier, Int. J. of Chem. Kin., 13, 925 (1981).

86. D.J. Ives and G.J. Janz, "Reference Electrodes, Theory and Practice", Academic Press, N.Y., 1961.

87. J.N. Butler, "Adv. Electrochem. and Electrochem. Eng.", vol. 7, Eds. P. Delahay and C.W. Tobias, 1970, p. 77.

88. Ksenofontov, Proskurnin and Gorodetzkaya, Acta Physicochim., 9, 45 (1938).

89. P. Rosenberg, Rev. Sci. Inst., 10, 131 (1939).

90. D.C. Grahame, J. Am. Chem. Soc., 68, 301 (1946); 71, 2975 (1949).

91. D.A.J. Rand and R. Woods, J. Electroanal. Chem., 35, 209 (1972).

92. P. Sears, R. Wolford and L. Dawson, J. Electrochem. Soc., 103, 633 (1956).

93. B.G. Cox, Annual Reports of the London Chemical Society, A249 (1973).

94. J. Solution Chem., 4, 485 (1975).

95. G.J. Janz and S.S. Danyluk, Chem. Reviews, 60, 209 (1960).

96. S. Glasstone, K.J. Laidler, and H. Eyring, J. Chem. Phys., 7, 1053 (1939).

97. M.J. Weaver, J. Phys. Chem., 80, 2645 (1976).

98. M.I. Temkin, Zh. Fiz. Khim., 22, 1081 (1948).

99. B.E. Conway, "Theory and Principles of Electrode Processes", Ronald Press Co., N.Y., 1964.

100. H.F. Halliwell and S.C. Nyburg, Trans. Faraday Soc., 59, 1126 (1963).

101. C. Herring and M.H. Nichols, Rev. Mod. Phys., 21, 185 (1949).

102. B.E. Conway, J. Solution Chem., 7, 721 (1978).

103. B.E. Conway, "Ionic Hydration in Chemistry and Biophysics", Elsevier Scientific Publ. Co., N.Y., 1981.

104. J.N. Agar in "Adv. Electrochem. and Electrochem. Eng.", vol. 3, Eds. P. Delahay and C.W. Tobias, Wiley Interscience, N.Y., 1963, p. 31.

105. A.J. deBethune, T.S. Licht, and N. Swendeman, J. Electrochem. Soc., 106, 616 (1959).

106. C.M. Criss and M. Salomon in "Physical Chemistry of Organic Solvent Systems", Eds., A.K. Covington and T. Dickinson, Plenum Press, N.Y., 1973.

107. R.N. Khuri in "Ion Selective Electrodes", Ed., R.A. Durst National Bureau of Standards, Special Publication 314, U.S. Govt. Printing Office, Washington, D.C., 1969.

108. B.G. Cox, A.J. Parker, and W.E. Waghorne, J. Am. Chem. Soc., 95, 1010 (1973).

109. E.A. Guggenheim, J. Phys. Chem., 34, 1758 (1930).

110. M. Spiro in "Physical Chemistry of Organic Solvent Systems", Eds., A.K. Covington and T. Dickinson, Plenum Press, N.Y., 1973.

111. Y. Marcus, Pure and Applied Chem., 55, 977 (1983).

112. M. Alfenaar, C.L. De Ligny, and A.G. Remijnse, Rec. Trav. Chim., 86, 986 (1967).

113. M. Salomon, J. Electrochem. Soc., 118, 1609 (1971).

114. J. Jorne and P.G. Pai, J. Electrochem. Soc., 132, 1612 (1985).

115. B. Case and R. Parsons, Trans. Faraday Soc., 63, 1224 (1967).

116. B.E. Conway in "Comprehensive Treatise of Electrochemistry", vol. 5, Eds., B.E. Conway, J.O'M. Bockris and E. Yeager, Plenum Press, N.Y. (1980), p. 116.

117. R.C. Reid, J.M. Prausnitz, T.K. Sherwood, "The Properties of Gases and Liquids", McGraw-Hill Book Co., N.Y., 1977.

118. C.M. Criss, R.P. Held and E. Luksha, J. Phys. Chem., 72, 2970 (1968).

119. H.A. Bernhardt and H.D. Crockford, J. Phys. Chem., 46, 473 (1942).

120. W.G. Breck and J. Lin, Trans. Faraday Soc., 61, 2223 (1965).

121. B. Kratochvil, E. Lorah and C. Garber, Anal. Chem., 41, 1793 (1969).

122. G. Nonhebel and H. Hartley, Phil. Mag., 50, 298, 729 (1925).

123. J.N. Brønsted and K.J. Pederson, Z. Physik. Chem., 108, 185 (1924).

124. J.N. Bronsted, Chem. Rev., 5, 322 (1928).

125. J.T. Hupp and M.J. Weaver, J. Phys. Chem., 88, 6128 (1984).

126. J.T. Hupp and M.J. Weaver, J. Phys. Chem., 88, 1860 (1984).

127. H.Y. Liu, J.T. Hupp and M.J. Weaver, J. Electroanal. Chem., 179, 219 (1984).

128. B.E. Conway in "Modern Aspects of Electrochemistry", Eds., B.E. Conway, J. O'M. Bockris and R. White, Plenum Press, N.Y. 1985.

129. J.N. Brønsted and N.L. Ross-Kane, J. Am. Chem. Soc., 53, 3024 (1931).

130. J.N. Agar, Trans. Faraday Soc., 1, 81 (1947).

131. R. Parsons and J.O'M. Bockris, Trans Faraday Soc., 47, 914 (1951).

132. B.E. Conway, D.J. MacKinnon and B.V. Tilak, Trans. Faraday Soc., 66, 1203 (1970).

133. B.E. Conway, D.F. Tessier and D.P. Wilkinson, J. Electroanal. Chem. (in course of publication).

134. E.M. Eyring, L.D. Rich, L.L. McCoy, R.C. Graham and N. Taylor, "Advances in Chemical Physics", vol. 21, Wiley Interscience, N.Y.

135. M.H. Miles, E.M. Eyring, W.W. Epstein and R.E. Ostlund, J. Phys. Chem., 69, 467 (1965).

136. R. Payne in "Advances in Electrochemistry and Electrochemical Engineering", vol. 7, Eds., P. Delahay and C. Tobias, Wiley Interscience, 1968, p. 1.

137. L.I. Krishtalik and G.E. Titova, Elektrokhimiya, 13, 1118 (1977).

138. G.E. Titova and L.I. Krishtalik, Elektrokhimiya, 13, 897 (1977).

139. L.I. Krishtalik, V.M. Tsionsky and G.E. Titova, J. Res. Inst. Catalysis, Hokaido Univ., 22, 101 (1974).

140. L.I. Krishtalik, Faraday Disc., Chem. Soc., 74, 205 (1982).

141. J.O'M. Bockris, R. Parsons, and H. Rosenberg, Trans. Faraday Soc., 47, 766 (1951).

142. J.O'M. Bockris and A.K.N. Reddy, "Modern Electrochemistry", vol. 2, Plenum Press, N.Y., 1977.

143. B. Post and C.F. Hiskey, J Am. Chem. Soc., 72, 4203 (1950); 73, 161 (1951).

144. L.I. Krishtalik, Elektrokhimiya, 6, 507 (1970).

145. A.J. Appleby, J. Electroanal. Chem., 27, 325 (1970); 27, 335 (1970); 27, 347 (1970).

146. E. Yeager, Proc. Symp. on Electrocatalysis, The Electrochemical Society, San Francisco meeting, 1983 (in press).

147. H.P. Stout, Trans. Faraday Soc., 41, 64 (1945).

148. J.A.V. Butler, Trans. Faraday Soc., 33, 229 (1937).

149. J.E. Gordon, "The Organic Chemistry of Electrolyte Solutions", Wiley Interscience, N.Y., 1975, p. 156.

150. P. Ruetschi, Zeit. Phys. Chem., N.F., 14, 277 (1958).

151. B.E. Conway and D.J. Mackinnon, J. Electrochem. Soc. (1969).

152. M. Heyrovsky and R.G. Norrish, Nature, 200, 880 (1963); M. Heyrovsky, ibid., 206, 1356 (1965); Proc. Roy. Soc. (London), A301, 880 (1963).

153. E.A. Moelwyn-Hughes, "Physical Chemistry", Cambridge University Press, 1947.

154. J.W. Russel, M. Severson, K. Scanlon, and J. Oversend, J. Phys. Chem., 87, 293 (1983).

155. W.G. Golden, K. Kunimatsu and H. Seki, J. Phys. Chem., 88, 1275 (1984).

156. D.D. Eley, Disc. Faraday Soc., 8, 34 (1950).

157. N.F. Mott and R.J. Watts-Tobin, Phil. Mag. 7, 483 (1962).

158. J. O'M. Bockris, M.A.V. Devanathan, and K. Muller, Proc. R. Soc. (London), A274, 55 (1963).

159. R.W. Fawcett, Isr. J. Chem., 18, 3 (1979).

160. R. Parsons, J. Electroanal. Chem., 59, 229 (1975).

161. K.J. Laidler and D.K. Banerjee, Can. J. Biochem., 61, 1201 (1983).

162. B.E. Conway and L.G.M. Gordon, J. Phys. Chem., 73, 3609 (1969).

163. B.E. Conway, Proc. Roy. Soc., A256, 128 (1960).

164. S.L. Marshall and B.E. Conway, J. Chem. Phys., 81, 923 (1984).

165. A. Hickling and F.W. Salt, Trans. Faraday Soc., 37, 224, (1941).

166. J. O'M. Bockris, Disc. Faraday Soc., 1, 95 (1947); 1, 229 (1947); J.O'M. Bockris and S. Ignatowicz, Trans. Faraday Soc., 44, 519 (1948).

167. J. O'M. Bockris and R. Parsons, Trans. Faraday Soc., 44, 860 (1948).

168. L.I. Krishtalik in "Comprehensive Treatise of Electrochemistry", vol. 7, B.E. Conway, J.O'M. Bockris, E. Yeager, S.U.M. Khan, and R.E. White, Eds., Plenum Press, N.Y., 1983, p. 107.

169. M. Salomon, Ph.D. Thesis, U. of Ottawa, 1964.

170. A.N. Frumkin, Z. Phys. Chem., A164, 121 (1933).

171. D.C. Grahame, Chem. Rev., 41, 441 (1947).

172. A.N. Frumkin in "Advances in Electrochemistry and Electrochemical Engineering", vol. 1, P. Delahay and C. Tobias, Eds., Wiley Interscience, N.Y., 1961.

173. S. Jofa, B. Kabanov, E. Kuchinsky, and F. Chistjakov, Acta Physicochim., U.R.S.S., 10, 317 (1939).

174. S. Jofa and A.N. Frumkin, Acta Physicochim., U.R.S.S., 10, 473 (1939).

175. R. Parsons and M.A.V. Devanathan, Trans. Faraday Soc., 49, 673 (1953).

176. R. Payne in "Physical Chemistry of Organic Solvent Systems", Eds. A.K. Covington and T. Dickinson, Plenum Press, N.Y., 1973, p. 733.

177. B. Tremillon, "Chemistry in Nonaqueous Solvents", Reidel Pub., Boston, 1974, p. 26.

178. D.C. Grahame, Z. Elektrochem., 59, 740 (1955).

179. R. Payne, Ph.D. Thesis, U. of London (1962).

180. R. Parsons, J. Electroanal. Chem., 21, 35 (1969).

181. R. Parsons, K.M. Joshi, and W. Mehl in "Transactions of the Symposium on Electrode Processes", Ed., E. Yeager, John Wiley and Sons, Inc., N.Y., 1962, p. 249.

182. A.V. Gorodetzkaja and M.A. Proskurnin, Zhur. Fiz. Khim., 12, 411 (1938).

183. V.L. Kheifets and B.S. Krasikov, Doklady Akad. Nauk. S.S.S.R., 94, 517 (1954).

184. D.I. Leikis and E.S. Sevastyanov, Doklady Akad. Nauk. S.S.S.R., 144, 1320 (1962).

185. S. Swathirajan and S. Bruckenstein, J. Electroanal. Chem., 163, 77 (1984).

186. L. Horner in "Organic Electrochemistry", Eds., M.M. Baizer and H. Lund, 2nd Ed., Marcel Dekker, Inc., 1983, p. 393.

187. J. Parry and R. Parsons, unpublished work; see ref. 43.

188. B.E. Conway, H. Angerstein-Kozlowska and W.B.A. Sharp, J. Chem. Soc., Faraday Trans. I, 74, 1373 (1978).

189. B.E. Conway and J.C. Currie, J. Electrochem. Soc., 125, 252 (1978).

190. H. Taube, "Electron Transfer Reactions of Complex Ions in Solution", Academic Press, N.Y., 1970.

191. S. Glasstone, K.J. Laidler and H. Eyring, "Theory of Rate Processes", McGraw-Hill, N.Y., 1941.

192. K.J. Laidler, "Theories of Chemical Reaction Rates", McGraw-Hill, N.Y., 1969.

193. B.E. Conway and J.O'M. Bockris, Can. J. Chem., 35, 1124 (1957).

194. B.E. Conway, J.O'M. Bockris and B. Lovrecek, Proc. C.I.T.C.E. Conference, Poitiers, (1954).

195. M. Salomon, J. Phys. Chem., 70, 3853 (1966).

196. R. Schmid, J. of Solution Chem., 12, 135 (1983).

197. M.S.B. Munson, J. Am. Chem. Soc., 87, 2332 (1965).

198. J.I. Braumann, J.M. Riveros, and L.K. Blair, J. Am. Chem. Soc., 93, 3914 (1971).

199. R.P. Bell and J.W. Bayles, J. Chem. Soc., 1518 (1952).

200. R.G. Pearson and D.C. Vogelsong, J. Am. Chem. Soc., 80, 1038 (1958).

201. J.W. Bayles and A. Chetwyn, J. Chem. Soc., 2328 (1958).

202. A.F. Trotman-Dickenson, J. Chem. Soc., 1293 (1949).

203. A.G. Evans and S.D. Hamann, Trans. Faraday Soc., 47, 34 (1951).

204. B.E. Conway and H.P. Dhar, Croat. Chem. Acta, 45, 173 (1973).

205. S. Trasatti, J. Chem. Soc. Faraday I, 70, 1752 (1974).

206. S. Trasatti, J. Electroanal. Chem., 33, 351 (1971); 54, 437 (1974); 64, 128 (1975); 82, 391 (1977).

207. S. Minc and M. Jurkiewicz-Herbich, J. Electroanal. Chem., 34, 351 (1972); also see Ref. 74, page 709.

208. J.O'M. Bockris and D.B. Matthews, Proc. Roy. Soc., London, A292, 479 (1966).

209. B.E. Conway, Faraday Discussion Chem. Soc. London, 74, 205 (1982).

210. J.O'M. Bockris, Quart. Rev., 3, 173, (1949).

211. S.U.M. Khan in "Modern Aspects of Electrochemistry", vol. 15, R.E. White, J. O'M Bockris and B.E. Conway, Eds., Plenum Press, N.Y., 1983, p. 336.

212. R.R. Dogonodze and A.M. Kuznetsov, Prog. Surf. Sci., 1, 1 (1975).

213. F.H. Verhoek, J. Amer. Chem. Soc., 58, 2577 (1936).

214. I.M. Kolthoff, M.K. Chantooni, Jr., and H. Smagowski, Anal. Chem., 42, 1622 (1970).

215. O. Popovych and R.P.T. Tomkins, "Nonaqueous Solution Chemistry", J. Wiley and Sons, Inc., N.Y., 1981, p. 63.

216. M.K. Chantooni and I.M. Kolthoff, J. Phys. Chem., 77, 527 (1973).

217. I.M. Kolthoff and S. Ikeda, J. Phys. Chem., 65, 1020 (1961).

218. B.E. Conway and F. Rocheleau, Can. J. Chem., 59, 1987 (1981).

219. E.D. Eastman, J. Am. Chem. Soc., 50, 292 (1928).

220. R.C. Weast, Ed., "Handbook of Chemistry and Physics", CRC Press, Inc., Cleveland, 1975, p. D-152.